

**UNDERSTANDING ADHESION TO MONITOR AND CONTROL ENVIRONMENT
PROCESSES: FROM VIRUS DETECTION TO MEMBRANE FOULING MITIGATION**

By

Xunhao Wang

A DISSERTATION

Submitted to
Michigan State University
in partial fulfillment of the requirements
for the degree of

Environmental Engineering – Doctor of Philosophy

2022

ABSTRACT

UNDERSTANDING ADHESION TO MONITOR AND CONTROL ENVIRONMENT PROCESSES: FROM VIRUS DETECTION TO MEMBRANE FOULING MITIGATION

By

Xunhao Wang

Adhesion is a physicochemical process of great importance for various environmental engineering technologies including those that are employed in water treatment facilities. Understanding adhesion is the key to elucidating separation mechanisms in unit processes and operations such as flocculation, granular media filtration, membrane separation. The likelihood of adhesion can be quantified in terms of the interfacial energy of interaction between two objects.

The first part of this dissertation is devoted to the study of virus adhesion to surfaces commonly encountered in various indoor settings. Fomites are inanimate surfaces, which can transfer the pathogens to a new human host. Fomite-based transfer is an important pathway of virus transmission, along with direct contact and transmission through aerosols. Adhesion of two viruses – one enveloped (human respiratory syncytial virus, HRSV) and one non-enveloped (human adenovirus 5, HAdV5) – to four fomites (silica, nylon, stainless steel, polypropylene) was quantified and interpreted based on physicochemical properties of viruses and fomites. Quartz Crystal Microbalance with Dissipation monitoring (QCM-D) is employed to quantify virus attachment to fomites. XDLVO modeling is applied to predict the virus-fomites interactions. It is found that for both HAdV5 and HRSV, the areal mass density of

deposited viruses correlated with the free energy of virus-fomite interfacial interaction in water, ΔG_{vwf} .

The second part of this dissertation describes the study of membrane filter aging as a result of membrane's intermittent exposure to foulants and cleaning agents. This study explores how the surface chemistry of polyvinylidene fluoride (PVDF) membranes evolves in challenge tests with humic acid (HA) fouling and sodium hypochlorite (NaClO) employed as a model foulant and cleaning agent, respectively. The evolution of physicochemical properties of the ageing membranes is characterized based on surface energy calculations. The results point to the formation of a chemically irreversible layer of foulants that is conditioned by consecutive exposures to foulants and is comprised of the adsorbed foulant fraction that is hard to oxidize further.

Copyright by
XUNHAO WANG
2022

ACKNOWLEDGEMENTS

First, I would like to express my sincere gratitude to my advisor Dr. Volodymyr Tarabara for the support of my PhD study, and for his patience and encouragement. I am particularly impressed by his enthusiasm and devotion to scientific research. Dr. Tarabara leads me to the world of scientific research. I am really grateful for his guide and support over this long journey.

Besides my advisor, I would like to thank the rest of my thesis committee: Dr. Irene Xagorarakis, Dr. Wei Zhang, and Dr. Rafael Auras, for their insightful comments and help.

I am also grateful to all my former and current lab members for their support and help. I also would like to thank Brijen Miyani for their help with biological experiments. I would like to thank all the specialists in Center of Advanced Microscopy Amy Albin, Carol Flegler, and Stanley Flegler for helping me with the SEM.

I also want to acknowledge all great staff members in the Department of Civil and Environmental Engineering. Many thanks to Lori Larner, Laura Post, Bailey Weber, the research administrator team in our department, and Joseph Nguyen, lab technician in our department.

Lastly, I would like to thank my parents for your unconditional love, support and care. I would like to thank all my friends who accompanied me walk through this long journey. Your support and encouragement are very precious to me.

TABLE OF CONTENTS

LIST OF TABLES	ix
LIST OF FIGURES	xi
CHAPTER ONE	1
Introduction and dissertation overview	1
1.1 The environmental importance of adhesion	1
1.2 Virus attachment to fomites.....	1
1.3 Virus adhesion to personal care products: PCPs as an important type of fomites	5
1.4 Membrane separation processes.....	6
1.5 Overview of adhesion measurements and data interpretation	8
1.5.1 Classical method	8
1.5.2 Graphical method	9
1.6 Dissertation overview	10
REFERENCES	12
CHAPTER TWO.....	20
Lip balm drying promotes virus attachment: Characterization of lip balm coatings and XDLVO modeling	20
2.1 Abstract.....	20
2.2 Introduction	21
2.3 Materials and Methods.....	25
2.3.1 Reagents	25
2.3.2 Preparation of lip balm surfaces	26
2.3.3 Characterization of the lip balm surface: Surface charge and morphology	27
2.3.4 Characterization of HAdV5 virions and SiO ₂ colloids: Size and charge	28
2.3.5 Quantifying hydrophobicity of HAdV5 and lip balm surfaces.....	29
2.3.6 QCM-D studies of SiO ₂ and HAdV5 attachment to lip balm surfaces	31
2.3.7 XDLVO modeling of colloid interactions with lip balm	32
2.4 Results and Discussion.....	34
2.4.1 Optimal coating protocol and coating morphology	34
2.4.2 Hydrophobicity and surface charge of lip balm-coated surfaces.....	36
2.4.3 Hydrodynamic size and surface charge of HAdV5 and SiO ₂ colloids	38
2.4.4 Attachment of viruses and SiO ₂ particles to lip balm-coated surfaces: XDLVO predictions	43
2.4.5 Attachment of SiO ₂ colloids and HAdV5 virions to lip balm-coated surfaces: Preliminary QCM-D study	49
2.4.6 Implications for virus control and public health protection.....	55
2.5 Conclusions	56
APPENDIX.....	59
REFERENCES	93

CHAPTER THREE	100
Virus adhesion to archetypal fomites: A study with human adenovirus and human respiratory syncytial virus	100
3.1 Abstract.....	100
3.2 Introduction	101
3.3 Materials and Methods.....	107
3.3.1 Reagents, fomites, viruses.....	107
3.3.2 Virion characterization: Hydrodynamic size, ζ -potential, concentration	108
3.3.3 Quantifying surface energy of viruses and fomites	109
3.3.3.1 Approach	109
3.3.3.2 Experiments.....	110
3.3.4 Modeling virus-fomite interactions. Extended Derjaguin-Landau-Verwey-Overbeek theory	111
3.3.5 QCM-D studies of HAdV5 and HRSV attachment to fomites	114
3.3.5.1 Approach: Quantifying virus-fomite attachment efficiency	114
3.3.5.2 QCM-D experiments.....	115
3.4 Results and Discussion.....	117
3.4.1 Virus concentration, size, charge and hydrophobicity.....	117
3.4.2 Fomite hydrophobicity.....	122
3.4.3 Quantifying virus-fomite interactions. Four archetypal fomites.....	123
3.4.4 Virus adhesion to fomites: QCM-D measurements.....	129
3.4.4.1 Model of mass transfer in QCM-D chamber. Assumptions.....	129
3.4.4.2 Quantifying mass transfer in QCM-D chamber: Mass transfer coefficients for HAdV5 and HRSV and size of depositing virions.	130
3.4.4.3 Virus deposition onto fomites. Virus-fomite attachment efficiency, avf	131
3.4.5 XDLVO predictions	137
3.5 Conclusions	141
APPENDIX	147
REFERENCES.....	178
CHAPTER FOUR.....	189
PVDF membrane ageing due to chemical cleaning: Understanding the evolution of membrane-foulant interactions.....	189
4.1 Abstract.....	189
4.2 Introduction	190
4.3 Experimental	192
4.3.1 Reagents and materials.....	192
4.3.2 Chemical cleaning study of membranes	192
4.3.3 Static fouling-cleaning test of membranes	193
4.3.4 Quantifying surface energy of PVDF membrane	193
4.3.5 Quantification of HA-membrane interactions.	194
4.4 Results.....	195
4.4.1 Impact of NaClO cleaning on membrane characteristics	195
4.4.2 Static fouling and cleaning cycles	197
4.5 Discussion.....	198

4.6 Conclusions	199
APPENDIX	200
REFERENCES.....	203
CHAPTER FIVE	206
Conclusions and future work	206
REFERENCES.....	209

LIST OF TABLES

<p>Table 1. Size, charge and hydrophobicity of colloids considered in this work. The three properties are quantified in terms of hydrodynamic diameter (d_h), zeta-potential (ζ), and free energy of interfacial interaction in water (ΔG_{sws}), respectively. Notes: A This study (see SM, Fig.); B Shi et al. [21]; C Shi and Tarabara [30]; D Calculated based on contact angle data reported by Zdziennicka et al. [60]. The error is not provided because the original contact angle values are reported as averages only; E This study (see SM, Table 5); F Dang and Tarabara [25]; G This study (see SM, Fig. 13); H This study (see Fig. 5)</p>	44
<p>Table 2. Values (in units of kT) of the primary maximum (E_{max}) and secondary minimum (E_{min}) in the XDLVO energy profile for colloid interaction with hydrated lip balms.</p>	46
<p>Table 3. Concentrations of various electrolytes in human saliva [9].....</p>	64
<p>Table 4. Composition of the four lip balms evaluated in this work.</p>	65
<p>Table 5. Contact angles (measured), surface energy parameters (calculated), and free interfacial energy of surface-surface interaction in water (calculated) for dry and hydrated lip balm samples and for human adenovirus 5. Lip balm coatings were prepared according to Protocol A (see Fig. 1).....</p>	66
<p>Table 6. Contact angles (measured), surface energy parameters (calculated), and free interfacial energy of surface-surface interaction in water (calculated) for three types of lip balm (dry) with four different preparation protocols (A, B, C, and D.) The protocols are described in Fig. 1. Values for protocol A duplicate corresponding values (protocol A) given for dry lip balms in Table 5.</p>	67
<p>Table 7. Guide to Figures with results of XDLVO modeling. Two of the 20 Figures are shown in the main manuscript while the other 18 are shown in the SM file.</p>	68
<p>Table 8. Contact angle of probe liquids, surface energy parameters (γ^{LW}, γ^+, γ^-, γ^{AB}, γ^{tot}) and the free energy of interfacial interaction in water ((ΔG_{sws})) of four fomites (clean, before use) and two viruses. Error estimates were obtained by propagating experimental errors in measured contact angles through the calculation of surface energy components (eqs (1) and (2)) and (ΔG_{sws}) (eq. (3)). Additional contact angle measurements were performed for the four fomites using 150 mM NaCl solution at pH 5.8; the contact angle data and calculated surface energy values are given in SM (Table 11).</p>	119
<p>Table 9. Free energy of virus-fomite interfacial interaction in water, ΔG_{vwf}, and its dispersive ($\Delta G_{d_0}^{LW}$) and polar ($\Delta G_{d_0}^{AB}$) components, for eight different</p>	

virus-fomite pairs. Standard deviations were obtained by propagating experimental errors in measured contact angles (Table 3) through the calculation of surface energy parameters (eqs. (1) and (2)) and ΔG_{vwf} (eqs. (8), (9), and (10)). 125

Table 10. ζ -potential values computed using Ohshima's expression (eq. (S1)) based on measured electrophoretic mobilities of HRSV as a function of pH. 173

Table 11. Contact angle of probe liquids, surface energy parameters (γ^{LW} , γ^+ , γ^- , γ^{AB} , γ^{tot}) and the free energy of interfacial interaction in water (ΔG_{sws}) of four fomites (clean, before use). Surface energies are calculated based on contact angles of 150 mM NaCl instead of DI water. Corresponding surface energy values calculated based on contact angles of DI water are given in Table 3. Error estimates were obtained by propagating experimental errors in measured contact angles through the calculation of γ (eq. (1)) and ΔG_{sws} (eq. (3)). 174

Table 12. Contact angle of probe liquids, surface energy parameters (γ^{LW} , γ^+ , γ^- , γ^{AB} , γ^{tot}) and the free energy of interfacial interaction in water (ΔG_{sws}) of four fomites (after use and subsequent cleaning; see section S4 for the description of cleaning protocols). Error estimates were obtained by propagating experimental errors in measured contact angles through the calculation of γ (eq. (1)) and (ΔG_{sws}) (eq. (3))..... 175

Table 13. Contact angle of probe liquids, surface energy parameters (γ^{LW} , γ^+ , γ^- , γ^{AB} , γ^{tot}) and the free energy of interfacial interaction in water (ΔG_{sws}) of four fomites (after use and subsequent cleaning; see section S4 for the description of cleaning protocols). Surface energies are calculated based on contact angles of 150 mM NaCl instead of DI water. Error estimates were obtained by propagating experimental errors in measured contact angles through the calculation of γ (eq. (1)) and (ΔG_{sws}) (eq. (3)). 176

Table 14. Contact angle of probe liquids, surface energy parameters (γ^{LW} , γ^+ , γ^- , γ^{AB} , γ^{tot}) and the free energy of interfacial interaction in water (ΔG_{sws}) of polypropylene at pH 4.1 and 3.8. 177

Table 15. The amount of each ingredient to make 50 g 15% solution of PVDF and PVDF/PVP in DMFA 201

LIST OF FIGURES

Figure 1. Lip balm coating protocols evaluated in this work. Of the three protocols (B, C, D) for preparing ultrathin coatings suitable for QCM-D measurements, protocol B yielded lip balm surface with the surface energy most closely matching that of a minimally processed sample (protocol A, baseline) and was, therefore, adopted for studying adhesion of colloids to such coatings. 28

Figure 2. Representative SEM images of a) Carmex b) ChapStick, c) Burt's Bees, and d) Vaseline coatings on a QCM-D sensor. 37

Figure 3. Free energy of interfacial interaction in water, ΔG_{sws} , of the Carmex lip balm as a function of the coating protocol (see Fig. 1). Measured contact angles of probe liquids and calculated surface energy parameters used to compute ΔG_{sws} values are given in Table 6. Each measurement was done in triplicate. Errors correspond to standard deviations. 40

Figure 4. Free energy of interfacial interaction in water, ΔG_{sws} , of the four lip balms coated using protocol B (see Fig. 1) in dry and hydrated states. Measured contact angles of probe liquids and calculated surface energy parameters used to compute ΔG_{sws} values are given in Table 5. Each measurement was done in triplicate. Errors correspond to standard deviations. 41

Figure 5. Surface charge of HAdV5 virions and lip balm surfaces as a function of pH. Vertical dashed lines indicate pH values (4.2 and 7.2) used in QCM-D measurements of HAdV5 attachment to lip balm surfaces. Lines connecting experimental data points are added to guide the eye. Average and standard deviations for lip balm samples are based on four independent measurements for each lip balm. Average and standard deviations for HAdV5 are based on three independent measurements. HAdV5 data is shown in both graphs to add data interpretation. 42

Figure 6. XDLVO energies of the interaction of human adenovirus 5 with Carmex lip balm at pH 4.2 (a, b) and pH 7.2 (c, d) in dry (a, c) and hydrated (b, d) states. DLVO and XDLVO energy profiles for HAdV5 interaction with the other three lip balms (Burt's Bees, ChapStick and Vaseline) are given in SM. DLVO total energy is provided for reference. 47

Figure 7. DLVO and XDLVO energies of the interaction of SiO₂ particles with Burt's Bees lip balm at pH 4.2 (a, b) and pH 7.2 (c, d) in dry (a, c) and hydrated (b, d) states. DLVO and XDLVO energy profiles for HAdV5 interaction with the other three lip balms (Carmex, ChapStick and Vaseline) are given in SM. DLVO total energy is provided for reference. 48

Figure 8. QCM-D measurements of the deposition of SiO₂ colloids onto hydrated Burt's Bees lip balm under conditions when SiO₂ loading is either a) constant (1.05 mg/ml) or b) increases stepwise from 0.52 mg/ml to 1.05 mg/ml. In both tests, deposition occurs from 150 mM NaCl electrolyte at pH 7.2. The mass values are calculated based on Sauerbrey equation (eq. (3)) with $n = 3$. The results for $n = 5$ are shown in SM (Fig. 32). 51

Figure 9. QCM-D measurements of the deposition of human adenovirus 5 onto hydrated Carmex lip balm from 150 mM NaCl electrolyte at pH 7.2. HAdV5 concentration in the QCM-D feed is ~109 GC/mL (~ 0.76 µg/mL). The mass values are calculated based on Sauerbrey equation (eq. (3)) with $n = 3$. The results for $n = 5$ are shown in SM (Fig. 33). 54

Figure 10. Particle size distribution in the stock HAdV5 and ST-ZL SiO₂ suspensions. Lines are added to guide the eye. 69

Figure 11. Free energy of interaction in water for three types of lip balm as a function of surface preparation method (see Fig. 1). 70

Figure 12. Free energy, ΔG_{sWS} , for four lip balms as a function of drying time: a) Carmex; b) Chapstick, c) Burt's Bees, d) Vaseline. Lip balms coatings were prepared using protocol B. In each graph, the solid line corresponds to the surface prepared using protocol A (melted lip balm with no dissolution and drying steps involved), which was used as the baseline: a) 65.03 mJ/m² for Carmex, b) -72.18 mJ/m² for Chapstick, c) -95.62 mJ/m² for Burt's Bees. d) -90.71 mJ/m² for Vaseline. Measured contact angles used to calculate ΔG_{sWS} values are given Table 6. 71

Figure 13. Surface charge of ST-ZL SiO₂ colloids as a function of pH. Vertical dashed lines indicate pH values (4.2 and 7.2) used in QCM-D measurements of SiO₂ attachment to lip balm surfaces. Lines connecting experimental data points are added to the guide the eye. 72

Figure 14. XDLVO energy of interaction of human adenovirus 5 with Burt's Bees lip balm at pH 4.2 (a, b) and pH 7.2 (c, d) in dry (a, c) and hydrated (b, d) states. DLVO total energy is provided for reference..... 73

Figure 15. XDLVO energy of interaction of human adenovirus 5 with ChapStick lip balm at pH 4.2 (a, b) and pH 7.2 (c, d) in dry (a, c) and hydrated (b, d) states. DLVO total energy is provided for reference..... 74

Figure 16. XDLVO energy of interaction of human adenovirus 5 with Vaseline lip balm at pH 4.2 (a, b) and pH 7.2 (c, d) in dry (a, c) and hydrated (b, d) states. DLVO total energy is provided for reference..... 75

Figure 17. XDLVO energy of interaction of human adenovirus 40 with Carmex lip balm at pH 4.2 (a, b) and pH 7.2 (c, d) in dry (a, c) and hydrated (b, d) states. DLVO total energy is provided for reference..... 76

Figure 18. XDLVO energy of interaction of human adenovirus 40 with Chapstick lip balm at pH 4.2 (a, b) and pH 7.2 (c, d) in dry (a, c) and hydrated (b, d) states. DLVO total energy is provided for reference.....	77
Figure 19. XDLVO energy of interaction of human adenovirus 40 with Burt's Bees lip balm at pH 4.2 (a, b) and pH 7.2 (c, d) in dry (a, c) and hydrated (b, d) states. DLVO total energy is provided for reference.....	78
Figure 20. XDLVO energy of interaction of human adenovirus 40 with Vaseline lip balm at pH 4.2 (a, b) and pH 7.2 (c, d) in dry (a, c) and hydrated (b, d) states. DLVO total energy is provided for reference.....	79
Figure 21. XDLVO energy of interaction of P22 with Carmex lip balm at pH 4.2 (a, b) and pH 7.2 (c, d) in dry (a, c) and hydrated (b, d) states. DLVO total energy is provided for reference.....	80
Figure 22. XDLVO energy of interaction of P22 with Chapstick lip balm at pH 4.2 (a, b) and pH 7.2 (c, d) in dry (a, c) and hydrated (b, d) states. DLVO total energy is provided for reference.....	81
Figure 23. XDLVO energy of interaction of P22 with Burt's Bees lip balm at pH 4.2 (a, b) and pH 7.2 (c, d) in dry (a, c) and hydrated (b, d) states. DLVO total energy is provided for reference.....	82
Figure 24. XDLVO energy of interaction of P22 with Vaseline lip balm at pH 4.2 (a, b) and pH 7.2 (c, d) in dry (a, c) and hydrated (b, d) states. DLVO total energy is provided for reference.....	83
Figure 25. XDLVO energies of interaction of MS2 with Carmex lip balm at pH 4.2 (a, b) and pH 7.2 (c, d) in dry (a, c) and hydrated (b, d) states. DLVO total energy is provided for reference.....	84
Figure 26. XDLVO energy of interaction of MS2 with Chapstick lip balm at pH 4.2 (a, b) and pH 7.2 (c, d) in dry (a, c) and hydrated (b, d) states. DLVO total energy is provided for reference.....	85
Figure 27. XDLVO energies of interaction of MS2 with Burt's Bees lip balm at pH 4.2 (a, b) and pH 7.2 (c, d) in dry (a, c) and hydrated (b, d) states. DLVO total energy is provided for reference.	86
Figure 28. XDLVO energy of interaction of MS2 with Vaseline lip balm at pH 4.2 (a, b) and pH 7.2 (c, d) in dry (a, c) and hydrated (b, d) states. DLVO total energy is provided for reference.....	87
Figure 29. XDLVO energies of interaction of SiO ₂ with Carmex lip balm at pH 4.2 (a, b) and pH 7.2 (c, d) in dry (a, c) and hydrated (b, d) states. DLVO total energy is provided for reference.....	88

Figure 30. XDLVO energy of interaction of SiO ₂ with Chapstick lip balm at pH 4.2 (a, b) and pH 7.2 (c, d) in dry (a, c) and hydrated (b, d) states. DLVO total energy is provided for reference.....	89
Figure 31. XDLVO energies of interaction of SiO ₂ with Vaseline lip balm at pH 4.2 (a, b) and pH 7.2 (c, d) in dry (a, c) and hydrated (b, d) states. DLVO total energy is provided for reference.....	90
Figure 32. Deposition of SiO ₂ colloids onto hydrated Burt's Bees lip balm under conditions when SiO ₂ loading is either a) constant (1.05 mg/ml) or b) increases stepwise from 0.52 mg/ml to 1.05 mg/ml. In both tests deposition occurs from 150 mM NaCl electrolyte at pH 7.2. The mass values are calculated based on Sauerbrey equation (eq. (3)) with $n = 5$. The results for $n = 3$ are similar and shown in the main manuscript (Fig. 8).....	91
Figure 33. QCM-D measurements of the deposition of human adenovirus 5 onto hydrated Carmex lip balm from 150 mM NaCl electrolyte at pH 7.2. HAdV5 concentration in the QCM-D feed is $\sim 10^9$ GC/mL (~ 0.76 μ g/mL). The mass values are calculated based on Sauerbrey equation (eq. (3)) with $n = 5$. The results for $n = 3$ are similar and shown in the main manuscript (Fig. 9).....	92
Figure 34. ζ -potential as a function of pH (A, D), size distribution (B, E), and TEM images (C, F, G) of HRSV (A-C) and HAdV5 (D-G). In A, B, D and E, lines are added to guide the eye. Charge and size values for HAdV5 (D, E) are adopted from our earlier report [36]. Additional TEM images are shown in SM, Figure 42.....	118
Figure 35. Free energy of interfacial interaction in water (ΔG_{fwf}) of four fomites as a function of pH. Depending on the type of aqueous solution used as a probe liquid, values are shown using either empty symbols (150 mM NaCl at pH 5.8; Table 10) or gray symbols (DI water at pH 5.8; Table 3) or black symbols (1 mM NaCl water at pH 3.8 and 4.1; Table 14).....	124
Figure 36. Free energy, ΔG_{vwf} , of interfacial interaction of HRSV with <i>monopolar</i> fomites ($\gamma_f^+ = 0$) in DI water. The solid line corresponds to $\Delta G_{vwf} = 0$ (i. e. solution of eq. (16)).	128
Figure 37. Example QCM-D data set: deposition of HRSV on stainless steel. Representative QCM-D data for all virus-fomite pairs and deposition conditions are given in SM (Figures 50 – 57). All calculations based on the QCM-D data were performed using the signal for the 5 th overtone ($n = 5$ in eq. (14)). The reason for choosing the 5 th harmonic was that the signals for the 3 rd and 1 st harmonics were unstable, likely due to their high sensitivity to mounting stress caused by the O-rings holding the sensor within the QCM-D chamber [96].	132

Figure 38. Virus-fomite attachment efficiency as a function of the free energy of virus-fomite interaction in water. Empty symbols correspond to tests with 150 mM NaCl electrolyte as the deposition solution. Filled symbols correspond to tests with virus deposition onto polypropylene from 1 mM NaCl at pH 4.1 for HAdV5 and at pH 3.8 for HRSV where virus-fomite electrostatic interaction is favorable and at its maximum absolute value. (See SM, section S6 for the algorithm used to select these pH values.)....	134
Figure 39. Mass and dissipation QCM-D data for the deposition of a) HRSV on polypropylene and b) HAdV5 on silica. Insets illustrate areal mass density values computed based on 5 th , 7 th , 9 th , and 11 th harmonics of the QCM-D signal.....	136
Figure 40. XDLVO total energy of interactions during virus deposition (a, c) and cleaning (b, d) stages of QCM-D experiments. The results are for HRSV interaction with polypropylene (a, b) and HAdV5 interaction with silica (c, d).....	139
Figure 41. Electrophoretic mobility of HRSV virions as a function of pH. Table 10 lists mobility and zeta potentials as functions of pH in a tabular format.	154
Figure 42. TEM images of (a, b) HAdV5 virions and (c, d) HRSV virions.....	156
Figure 43. Rate of HAdV5 deposition on stainless steel QCM-D sensors ($\frac{dm_v}{dt}$) as a function of HAdV5 concentration in the feed suspension (C_b). The intermediate value of C_b and deposition conditions are the same as in all other QCM-D tests. Solution is 150 mM NaCl. The observed linearity validates the assumption behind eq. (3): $\frac{dm_v}{dt} \approx \alpha_{vf} k C_b A$	157
Figure 44. Contact angle of four fomites: a) silica, b) nylon, c) stainless steel, d) polypropylene, as a function of pH. Depending on the type of aqueous solution used, values are shown using either empty symbols (150 mM NaCl at pH 5.8) or gray symbols (DI water at pH 5.8) or black symbols (1 mM NaCl at pH 3.8 and 4.1).	159
Figure 45. XDLVO total energy of interactions during virus deposition (a, c) and cleaning (b, d) stages of QCM-D experiments. The results are for HRSV interaction with polypropylene (a, b) and stainless steel (c, d).	160
Figure 46. XDLVO total energy of interactions during virus deposition (a, c) and cleaning (b, d) stages of QCM-D experiments. The results are for HRSV interaction with nylon (a, b) and silica (c, d).	161
Figure 47. XDLVO total energy of interactions during virus deposition (a, c) and cleaning (b, d) stages of QCM-D experiments. The results are for HAdV5 interaction with polypropylene (a, b) and stainless steel (c, d).	162

Figure 48. XDLVO total energy of interactions during virus deposition (a, c) and cleaning (b, d) stages of QCM-D experiments. The results are for HAdV5 interaction with nylon (a, b) and silica (c, d).	163
Figure 49. XDLVO total energy of interactions during virus deposition (a, c) and cleaning (b, d) stages of QCM-D experiments. The results are for HRSV (a, b) and HAdV5 (c, d) interaction with polypropylene Conditions correspond to to $\alpha_{vf} = 1$	164
Figure 50. Example QCM-D data set: deposition of HRSV on polypropylene. The data are based on the 5 th harmonic of the QCM-D signal.	165
Figure 51. Example QCM-D data set: deposition of HRSV on stainless steel. The data are based on the 5 th harmonic of the QCM-D signal.	166
Figure 52. Example QCM-D data set: deposition of HRSV on nylon. The data are based on the 5 th harmonic of the QCM-D signal.	167
Figure 53. Example QCM-D data set: deposition of HRSV on silica. The data are based on the 5 th harmonic of the QCM-D signal.	168
Figure 54. Example QCM-D data set: deposition of HAdV5 on polypropylene. The data are based on the 5 th harmonic of the QCM-D signal	169
Figure 55. Example QCM-D data set: deposition of HAdV5 on stainless steel. The data are based on the 5 th harmonic of the QCM-D signal.	170
Figure 56. Example QCM-D data set: deposition of HadV5 on nylon. The data are based on the 5 th harmonic of the QCM-D signal	171
Figure 57. Example QCM-D data set: deposition of HAdV5 on silica. The data are based on the 5 th harmonic of the QCM-D signal.	172
Figure 58. Free energy of interfacial interaction in water (ΔG_{sww}) of membrane as a function of cleaning time (cleaning agent: 1% NaClO)	195
Figure 59. Free energy of interfacial interactions (ΔG_{mwm}) of PVDF (red) and PVDF/PVP (blue) membrane as a function of fouling and cleaning cycles. The solid and empty symbols refer to replicated tests.	197

CHAPTER ONE

Introduction and dissertation overview

1.1 The environmental importance of adhesion

Adhesion processes are of great significance in many treatment processes and operations employed by engineers to cure contamination of water, air, and soil.

Common water treatment techniques, such as flocculation and sand filtration rely on adhesion. The efficiency of membrane separations, among many other processes, is often limited by fouling – a phenomenon that has adhesion as its basis. Understanding adhesion is critical for both gaining better mechanistic understanding of environmental separations and improving process performance. This dissertation considers several specific contexts where adhesion is of critical importance - virus adhesion to fomites, virus adhesion to personal care products, foulant adhesion to polymeric membranes – and combines experimental measurements with modeling of interfacial interactions to understand and predict adhesion in these contexts.

1.2 Virus attachment to fomites

Numerous studies have been conducted to explore virus adhesion to surfaces such as minerals [1-11], dissolved and particulate natural organic matter [12-14], activated carbon [15-18], granular media filters [19-21], ion exchange resins [22], membrane filters [20, 21, 23-28], vegetables and fruits [29-32], as well as human skin [33-41].

However, the relationship between the interaction forces and adhesion and how the adhesion is controlled by the physicochemical properties of the viruses and surfaces remain insufficiently understood [42].

Naturally, virus adhesion depends on the properties of the virus [43]. It has been suggested that differences in virus surface charge and hydrophobicity play a significant role in virus adhesion [27]. Most viruses have capsid composed of protein polypeptides that contain amino acids such as glutamic acid, aspartic acid, histidine, and tyrosine. These amino acids feature acidic and basic groups (i. e., carboxyl and amino groups) that, if ionized, give the viral capsid an electrical charge. The isoelectric point (IP) is the pH value at which a surface has a zero net charge; surfaces are positively charged at $\text{pH} < \text{pI}$ and negatively charged at $\text{pH} > \text{pI}$. Viruses with a lipid envelope tend to be hydrophobic, whereas viruses without a lipid envelope are generally hydrophilic [44].

Individuals across the globe spend most of their lives indoors, where they are constantly exposed to viruses residing on surfaces. The term “fomite” stands for any inanimate object that, when contaminated with infectious microorganisms, can act as a vector for transferring the disease-causing agents to a new human host. Most important fomites are those that humans contact frequently; examples include countertops, indoor walls, clothing, and furniture. Despite the already large and quickly growing knowledge base on the persistence of viruses on various surfaces, physicochemical bases of virus attachment to and removal from surfaces are not fully understood. can consider personal care products that human applies on their body as fomites. The study of

fomites has traditionally focused on determining whether there is presence of specific pathogenic organisms. Understanding virus-fomite interaction at the mechanistic level, in terms of specific interaction forces can help predict adhesion and identify most likely accumulation loci (“hot spots”) for viruses. Potentially, such knowledge can guide the selection and placement of materials and surface coatings as well as optimization of protocols of their cleaning with the ultimate goal of protecting human health.

Most viruses are colloids, which making colloidal stability theories applicable to viruses. Virus-surface interactions can be modeled using the XDLVO theory, which builds on the DLVO theory and takes hydrophobic interactions into consideration. XDLVO theory has been widely used to study virus-fomites interactions [26, 45-52]. XDLVO theory describes the total energy of interaction U_{vwf}^{XDLVO} between a spherical particle (representing a virus (v)) and a flat surface (representing a fomite (f)) in water (w) as a sum (see eq. (7)) of Lifshitz-van der Waals (LW), U_{vwf}^{LW} , electrostatic double layer (EL), U_{vwf}^{EL} , and Lewis acid-base (AB), U_{vwf}^{AB} , energies expressed as follows:

$$U_{vwf}^{LW}(d) = -\frac{Aa}{6d} = 2\pi d_0^2 \frac{a}{d} \Delta G_{d_0}^{LW} \quad (4)$$

$$U_{vwf}^{EL}(d) = \pi \varepsilon_r \varepsilon_0 a \left[2\psi_v \psi_f \ln \left(\frac{1 + e^{-\kappa d}}{1 - e^{-\kappa d}} \right) + (\psi_v^2 + \psi_f^2) \ln(1 - e^{-2\kappa d}) \right] \quad (5)$$

$$U_{vwf}^{AB}(d) = 2\pi a \lambda \Delta G_{d_0}^{AB} \exp \left(\frac{d_0 - d}{\lambda} \right) \quad (6)$$

$$U_{vwf}^{XDLVO} = U_{vwf}^{LW} + U_{vwf}^{EL} + U_{vwf}^{AB} \quad (7)$$

where a is the virus radius, d is the virus-fomite minimal interfacial separation distance, $A = -12\pi d_0^2 \Delta G_{d_0}^{LW}$ is the Hamaker constant, ϵ_r is the relative dielectric permittivity of water (for water at 25 °C, $\epsilon_r \approx 78.3$), ϵ_0 is the dielectric permittivity of vacuum ($\epsilon_0 = 8.854 \times 10^{12} \text{ C} \cdot \text{V}^{-1} \cdot \text{m}^{-1}$), ψ_v and ψ_s are surface potentials of the virus and fomite, respectively, κ is the inverse Debye screening length, λ is the characteristic delay length of AB interactions in water ($\lambda = 0.6 \text{ nm}$), and d_0 is the minimum separation distance ($d_0 = 0.158 \text{ nm}$) due to Born repulsion. Surface potentials ψ_v and ψ_f are commonly approximated by ζ -potentials (ζ_v and ζ_f). Values of $\Delta G_{d_0}^{LW}$ and $G_{d_0}^{AB}$ in eq. (4) and eq. (6) are given by:

$$\Delta G_{d_0}^{LW} = 2 \left(\sqrt{\gamma_v^{LW}} - \sqrt{\gamma_w^{LW}} \right) \left(\sqrt{\gamma_w^{LW}} - \sqrt{\gamma_f^{LW}} \right) \quad (8)$$

$$\begin{aligned} \Delta G_{d_0}^{AB} = & 2 \sqrt{\gamma_w^+} \left(\sqrt{\gamma_f^-} + \sqrt{\gamma_v^-} - \sqrt{\gamma_w^-} \right) + 2 \sqrt{\gamma_w^-} \left(\sqrt{\gamma_f^+} + \sqrt{\gamma_v^+} - \sqrt{\gamma_w^+} \right) \quad (9) \\ & - 2 \sqrt{\gamma_f^+ \gamma_v^-} - 2 \sqrt{\gamma_f^- \gamma_v^+} \end{aligned}$$

The free energy of virus-fomite interfacial interaction in water, ΔG_{vwf} , is

$$\Delta G_{vwf} = \Delta G_{d_0}^{LW} + \Delta G_{d_0}^{AB} \quad (10)$$

Quartz crystal microbalance with dissipation monitoring (QCM-D) is a measurement technique that makes it uniquely suitable for studies of virus adhesion. First, QCM-D is very sensitive and can measure deposited materials with mass density as small as 17.7 ng/cm² [53]. Second, the technique allows for real-time monitoring of the deposited

mass and, therefore, can be used to measure deposition kinetics. With long range transport of species to the QCM-D sensor factored out, mass vs time data can offer insights into adsorption (or, more generally, adhesion) kinetics. The deposition of virus particles on the quartz surface can lead to a decrease in the frequency of vibration. Since the wet mass deposited onto the sensor is proportional to the changes in resonance and overtone frequencies, the rate of wet mass deposition can be represented by the rate of frequency shift [13]. Third, this technique can also offer information about the viscoelastic behavior of the adsorbed layer by measuring dissipation shifts [54]. QCM-D has been broadly used to study attachment of viruses such as bacteriophage MS2 [11, 12, 42], norovirus virus-like particle (VLPs) [55, 56], adenovirus [57], and pathogenic plant viruses [58, 59] to various surfaces including bare QCM crystals [11, 55, 60] (most often gold or silica but sensors with other coating are available), natural organic matter [12, 13, 61], polyelectrolyte multilayers [46, 57, 58, 62, 63], or self-assembled monolayers [42, 56, 58, 59].

1.3 Virus adhesion to personal care products: PCPs as an important type of fomites

Microbial contamination of personal care products has been a significant problem for researchers and manufacturers worldwide [64]. Personal care products often include natural ingredients, including organic compounds. The raw material that these natural ingredients are sourced from is what often determines the potential of microbial contamination. Further, personal care products can be contaminated during use. Of

particular concern are products such as lipstick and lip balm, which can facilitate contagion through routes such as ingestion and inhalation.

1.4 Membrane separation processes

Membrane processes are being increasingly used in drinking water treatment and water reuse due to their effectiveness in removing a broad range of contaminants and relatively low cost. Microfiltration (MF) is suitable for reducing turbidity and removing microorganisms (bacteria, protozoans) while ultrafiltration (UF) can remove various waterborne viruses and most dissolved organic matter. Polyvinylidene fluoride (PVDF) is widely used as the base polymer for MF and UF membranes due to its chemical resistance and excellent mechanical strength. However, pure PVDF membranes are hydrophobic, making them more susceptible to fouling [65]. To mitigate this practical limitation, membranes made from hydrophobic polymers such as PVDF are often blended with hydrophilic additives.

Indeed, membrane fouling is one of the critical challenges in the successful application of membrane processes. Fouling arises from interactions between a membrane and various components present in the raw water [66]. Natural organic matter (NOM), such as humic acid, is ubiquitous in surface water – a common source of raw water for drinking water treatment plants. NOM is one of the major membrane foulants as documented in research literature and reports from professional practice community

[66-69]. Fouling by humic acid is a complex phenomenon which involves both reversible and irreversible processes [66].

Membrane cleaning is the primary approach to fouling mitigation and recovering the membrane performance. Membrane cleaning is defined as the action of removing substances that are not an integral part of the membrane surface or membrane bulk. Cleaning can be conducted either by using chemicals (chemical cleaning) or water flow (hydraulic cleaning) [70]. Other processes such as vibration and ultrasound [71, 72] are often used to supplement chemical and hydraulic cleaning. There are several categories of cleaning chemicals including surfactants, oxidants, acids, and chelating agents. Among them, sodium hypochlorite (NaClO) is one of the most commonly used cleaning reagents because of its chemical stability, low price, and effectiveness against organic foulants [73]. However, over an extended time, NaClO can impact the physicochemical characteristics of the membrane, affect membrane performance, and reduce the service life of the membrane [74]. NaClO can cause damage to membrane structure [75] and depth [76]. The membrane can also become more hydrophilic due to NaClO cleaning [77], which can result in a flux increase [78]. The zeta potential and the contact angle of the membrane can also be changed by NaClO.

1.5 Overview of adhesion measurements and data interpretation

1.5.1 Classical method

Hydrophobicity of a solid (s) can be quantified in terms of the free energy of its interfacial interaction with an identical material when immersed in water (w), ΔG_{sws} [79]. We applied this approach to evaluate hydrophobicity of viruses (v) and fomites (f) by computing ΔG_{vww} and ΔG_{fww} , respectively. The calculation relies on the knowledge of the solid's surface energy in terms of its three components: two Lewis acid-base (electron acceptor, γ_s^+ , and electron donor, γ_s^-) components and the Lifshitz-van der Waals component, γ_s^{LW} . The Lewis acid-base components are also described as *polar* while the Lifshitz-van der Waals component is often referred to as *dispersive* or *apolar*. The components can be determined by measuring contact angles (θ) of three probe liquids (l) with known γ_l^{LW} , γ_l^+ and γ_l^- on the surface of the solid and substituting these values into the Young-Dupré equation [80, 81]

$$(1 + \cos\theta)\gamma_l^{TOT} = 2 \left(\sqrt{\gamma_s^{LW}\gamma_l^{LW}} + \sqrt{\gamma_s^+\gamma_l^-} + \sqrt{\gamma_s^-\gamma_l^+} \right), \quad (1)$$

where γ_l^{TOT} is the total surface energy of the probe liquid:

$$\gamma^{tot} = \gamma^{LW} + \gamma^{AB} = \gamma^{LW} + 2\sqrt{\gamma^-\gamma^+}. \quad (2)$$

The free energy of solid-solid interfacial interaction in water is given by

$$\Delta G_{sws} = -2 \left(\sqrt{\gamma_s^{LW}} - \sqrt{\gamma_w^{LW}} \right)^2 - 4 \left(\sqrt{\gamma_s^+\gamma_s^-} + \sqrt{\gamma_w^+\gamma_w^-} - \sqrt{\gamma_s^+\gamma_w^-} - \sqrt{\gamma_s^-\gamma_w^+} \right) \quad (3)$$

where γ_w^{LW} , γ_w^+ and γ_w^- are surface energy components of water. A positive value of ΔG_{sws} indicates a hydrophilic surface, while negative ΔG_{sws} corresponds to a hydrophobic surface. The absolute value of ΔG_{sws} indicates the degree of hydrophilicity (or hydrophobicity, when $\Delta G_{sws} < 0$) of the surface. Contact angles of three probe liquids – DI water, glycerol, and diiodomethane (DID) – on target solids are measured using sessile drop method. Additional contact angle measurements with ethylene glycol (EG) as the fourth probe liquid are often performed to obtain additional data and improve the accuracy of the prediction; in such cases, the graphical method is used.

1.5.2 Graphical method

For some of surfaces, the “classical method” may give a small negative value of $\sqrt{\gamma_s^+}$; this is attributed to a limited accuracy of the method wherein the standard error around a small positive “true” average result in a prediction of a small negative average.

Therefore, a new approach – described herein as the “graphical method”, is used to solve $\sqrt{\gamma_s^+}$, $\sqrt{\gamma_s^-}$, and $\sqrt{\gamma_s^{LW}}$ of these types of surfaces.

Since γ_l^- and γ_l^+ of DID are both equal to zero, Eq. (1) can be simplified:

$$(1 + \cos\theta)\gamma_{DID}^{TOT} = 2\sqrt{\gamma_s^{LW}\gamma_{DID}^{LW}}, \quad (4)$$

where γ_{DID}^{TOT} and γ_{DID}^{LW} are the surface tension components of DID. Using Eq. (4), one can calculate γ_s^{LW} of solids by measuring their contact angles with DID only.

Eq. (1) can be recast as

$$\frac{(1 + \cos\theta)\gamma_l^{TOT} - 2\sqrt{\gamma_s^{LW}\gamma_l^{LW}}}{2\sqrt{\gamma_l^-}} = \sqrt{\gamma_s^+} + \sqrt{\frac{\gamma_l^+}{\gamma_l^-}}\sqrt{\gamma_s^-} \quad (5)$$

and γ_s^- can be determined from the slope of a linear dependence of the left-hand side of eq. (5) on $\sqrt{\gamma_l^+/\gamma_l^-}$ with the intercept ($\sqrt{\gamma_s^+}$) set to zero. To improve the reliability of the prediction, additional contact angle measurements with additional probe liquids can be performed. The calculation can be done using the LINEST function in Excel; other than the common availability of the software, the approach is also very useful in that LINEST calculation returns errors for each both parameters (slope and intercept) of the linear fit.

The methodology introduced in this section provides a brief introduction. A detailed discussion of the technique as applied in different adhesion contexts is provided in individual chapters of this dissertation.

1.6 Dissertation overview

The material presented in this dissertation is divided into Chapters where each Chapter is a manuscript either already published or in preparation for submission.

Chapter 2 presents the study of virus adhesion to archetypal fomites. In this chapter, adhesion of two viruses – one enveloped (human respiratory syncytial virus, HRSV) and one non-enveloped (human adenovirus 5, HAdV5) – to four fomites (silica, nylon,

stainless steel, polypropylene) was quantified and interpreted based on physicochemical properties of viruses and fomites. Virus-fomite interactions are predicted using the extended Derjaguin-Landau-Verwey-Overbeek (XDLVO) theory and are experimentally assessed in tests with quartz crystal microbalance with dissipation (QCM-D).

Chapter 3 tests the hypothesis that drying-induced decrease in lip balm surface energy can enhance virus adhesion due to the strong hydrophobic colloid-surface interactions. The surface properties of lip balm and human adenovirus 5 (HAdV5) were measured. Extended Derjaguin-Landau-Verwey-Overbeek (XDLVO) energy of interactions between lip balm coatings and HAdV5 as well as four other colloids: HAdV40, MS2 and P22 bacteriophages, and SiO₂, were calculated.

Chapter 4 describes a model of virus recovery by tangential flow filtration to guide the design of sample concentration process.

Chapter 5 focuses on the PVDF membrane ageing due to chemical cleaning. In this study, the effect of humic acid fouling and sodium hypochlorite cleaning on the physicochemical properties and surface energy of PVDF is investigated. The home-made PVDF membranes, with and without PVP additives, were treated by several cycles of humic acid fouling and sodium hypochlorite cleaning. The evolution of surface energy over this process is recorded. This study helps understand the evolution of membrane-foulant interactions when cleaned with sodium hypochlorite.

REFERENCES

REFERENCES

- [1] S. Chattopadhyay, R.W. Puls, Adsorption of bacteriophages on clay minerals, *Environmental science & technology* 33(20) (1999) 3609-3614.
- [2] G.W. Fuhs, M. Chen, L.S. Sturman, R.S. Moore, Virus adsorption to mineral surfaces is reduced by microbial overgrowth and organic coatings, *Microbial ecology* 11(1) (1985) 25-39.
- [3] S.M. Lipson, G. Stotzky, Adsorption of reovirus to clay minerals: effects of cation-exchange capacity, cation saturation, and surface area, *Appl. Environ. Microbiol.* 46(3) (1983) 673-682.
- [4] S.M. Lipson, G. Stotzky, Effect of proteins on reovirus adsorption to clay minerals, *Appl. Environ. Microbiol.* 48(3) (1984) 525-530.
- [5] S.H. Lo, O.J. Sproul, Polio-virus adsorption from water onto silicate minerals, *Water Research* 11(8) (1977) 653-658.
- [6] J.P. Loveland, J.N. Ryan, G.L. Amy, R.W. Harvey, The reversibility of virus attachment to mineral surfaces, *Colloids and Surfaces A: Physicochemical and Engineering Aspects* 107 (1996) 205-221.
- [7] R.S. Moore, D.H. Taylor, M.M. Reddy, L.S. Sturman, Adsorption of reovirus by minerals and soils, *Appl. Environ. Microbiol.* 44(4) (1982) 852-859.
- [8] R.S. Moore, D.H. Taylor, L.S. Sturman, M.M. Reddy, G.W. Fuhs, Poliovirus adsorption by 34 minerals and soils, *Appl. Environ. Microbiol.* 42(6) (1981) 963-975.
- [9] M. Schiffenbauer, G. Stotzky, Adsorption of coliphages T1 and T7 to clay minerals, *Appl. Environ. Microbiol.* 43(3) (1982) 590-596.
- [10] D.H. Taylor, R.S. Moore, L.S. Sturman, Influence of pH and electrolyte composition on adsorption of poliovirus by soils and minerals, *Appl. Environ. Microbiol.* 42(6) (1981) 976-984.
- [11] M. Tong, Y. Shen, H. Yang, H. Kim, Deposition kinetics of MS2 bacteriophages on clay mineral surfaces, *Colloids and Surfaces B: Biointerfaces* 92 (2012) 340-347.
- [12] B. Yuan, M. Pham, T.H. Nguyen, Deposition kinetics of bacteriophage MS2 on a silica surface coated with natural organic matter in a radial stagnation point flow cell, *Environmental science & technology* 42(20) (2008) 7628-7633.
- [13] M. Pham, E.A. Mintz, T.H. Nguyen, Deposition kinetics of bacteriophage MS2 to natural organic matter: Role of divalent cations, *Journal of colloid and interface science* 338(1) (2009) 1-9.

- [14] L. Gutierrez, X. Li, J. Wang, G. Nangmenyi, J. Economy, T.B. Kuhlenschmidt, M.S. Kuhlenschmidt, T.H. Nguyen, Adsorption of rotavirus and bacteriophage MS2 using glass fiber coated with hematite nanoparticles, *Water Research* 43(20) (2009) 5198-5208.
- [15] J.T. Cookson Jr, Mechanism of virus adsorption on activated carbon, *Journal-American Water Works Association* 61(1) (1969) 52-56.
- [16] J.T. Cookson, W.J. North, Adsorption of viruses on activated carbon. Equilibriums and kinetics of the attachment of Escherichia coli bacteriophage T4 on activated carbon, *Environmental science & technology* 1(1) (1967) 46-52.
- [17] T. Matsushita, H. Suzuki, N. Shirasaki, Y. Matsui, K. Ohno, Adsorptive virus removal with super-powdered activated carbon, *Separation and Purification Technology* 107 (2013) 79-84.
- [18] Q.L. Shimabuku, F.S. Arakawa, M. Fernandes Silva, P. Ferri Coldebella, T. Ueda-Nakamura, M.R. Fagundes-Klen, R. Bergamasco, Water treatment with exceptional virus inactivation using activated carbon modified with silver (Ag) and copper oxide (CuO) nanoparticles, *Environmental technology* 38(16) (2017) 2058-2069.
- [19] A.A. Torkelson, A.K. da Silva, D.C. Love, J.Y. Kim, J.P. Alper, B. Coox, J. Dahm, P. Kozodoy, R. Maboudian, K.L. Nelson, Investigation of quaternary ammonium silane-coated sand filter for the removal of bacteria and viruses from drinking water, *Journal of applied microbiology* 113(5) (2012) 1196-1207.
- [20] H. Wang, M. Li, K. Brockman, T.H. Nguyen, Reduction of MS2 bacteriophage and rotavirus in biosand filters, *Environmental Science: Water Research & Technology* 2(3) (2016) 483-491.
- [21] H. Wang, T. Narihiro, A.P. Straub, C.R. Pugh, H. Tamaki, J.F. Moor, I.M. Bradley, Y. Kamagata, W.-T. Liu, T.H. Nguyen, MS2 bacteriophage reduction and microbial communities in biosand filters, *Environmental science & technology* 48(12) (2014) 6702-6709.
- [22] P.S. Porter, M.J. Semmens, A review of virus and protein sorption by ion exchange resins, *Environment International* 3(4) (1980) 311-319.
- [23] A.M. ElHadidy, S. Peldszus, M.I. Van Dyke, An evaluation of virus removal mechanisms by ultrafiltration membranes using MS2 and ϕ X174 bacteriophage, *Separation and Purification Technology* 120 (2013) 215-223.
- [24] S.R. Farrah, Chemical factors influencing adsorption of bacteriophage MS2 to membrane filters, *Appl. Environ. Microbiol.* 43(3) (1982) 659-663.
- [25] J. Lukasik, T.M. Scott, D. Andryshak, S.R. Farrah, Influence of salts on virus adsorption to microporous filters, *Appl. Environ. Microbiol.* 66(7) (2000) 2914-2920.

- [26] B. Michen, F. Meder, A. Rust, J. Fritsch, C. Aneziris, T. Graule, Virus removal in ceramic depth filters based on diatomaceous earth, *Environmental science & technology* 46(2) (2012) 1170-1177.
- [27] P.A. Shields, S.R. Farrah, Influence of salts on electrostatic interactions between poliovirus and membrane filters, *Appl. Environ. Microbiol.* 45(2) (1983) 526-531.
- [28] K. Zodrow, L. Brunet, S. Mahendra, D. Li, A. Zhang, Q. Li, P.J.J. Alvarez, Polysulfone ultrafiltration membranes impregnated with silver nanoparticles show improved biofouling resistance and virus removal, *Water research* 43(3) (2009) 715-723.
- [29] M.A. Esseili, Q. Wang, L.J. Saif, Binding of human GII. 4 norovirus virus-like particles to carbohydrates of romaine lettuce leaf cell wall materials, *Appl. Environ. Microbiol.* 78(3) (2012) 786-794.
- [30] B.K. Ward, C.M. Chenoweth, L.G. Irving, Recovery of viruses from vegetable surfaces, *Appl. Environ. Microbiol.* 44(6) (1982) 1389-1394.
- [31] K. Verhaelen, M. Bouwknecht, A. Carratalà, F. Lodder-Verschoor, M. Diez-Valcarce, D. Rodríguez-Lázaro, A.M. de Roda Husman, S.A. Rutjes, Virus transfer proportions between gloved fingertips, soft berries, and lettuce, and associated health risks, *International journal of food microbiology* 166(3) (2013) 419-425.
- [32] E. Tuladhar, W.C. Hazeleger, M. Koopmans, M.H. Zwietering, E. Duizer, R.R. Beumer, Transfer of noroviruses between fingers and fomites and food products, *International journal of food microbiology* 167(3) (2013) 346-352.
- [33] S.A. Ansari, S.A. Sattar, V.S. Springthorpe, G.A. Wells, W. Tostowaryk, Rotavirus survival on human hands and transfer of infectious virus to animate and nonporous inanimate surfaces, *Journal of clinical microbiology* 26(8) (1988) 1513-1518.
- [34] S.A. Ansari, V.S. Springthorpe, S.A. Sattar, S. Rivard, M. Rahman, Potential role of hands in the spread of respiratory viral infections: studies with human parainfluenza virus 3 and rhinovirus 14, *Journal of Clinical Microbiology* 29(10) (1991) 2115-2119.
- [35] A. Elkhyat, P. Agache, H. Zahouani, P. Humbert, A new method to measure in vivo human skin hydrophobia, *International journal of cosmetic science* 23(6) (2001) 347-352.
- [36] M.L. Grayson, S. Melvani, J. Druce, I.G. Barr, S.A. Ballard, P.D.R. Johnson, T. Mastorakos, C. Birch, Efficacy of soap and water and alcohol-based hand-rub preparations against live H1N1 influenza virus on the hands of human volunteers, *Clinical Infectious Diseases* 48(3) (2009) 285-291.
- [37] T.R. Julian, J.O. Leckie, A.B. Boehm, Virus transfer between fingerpads and fomites, *Journal of applied microbiology* 109(6) (2010) 1868-1874.

- [38] J.N. Mbithi, V.S. Springthorpe, J.R. Boulet, S.A. Sattar, Survival of hepatitis A virus on human hands and its transfer on contact with animate and inanimate surfaces, *Journal of Clinical Microbiology* 30(4) (1992) 757-763.
- [39] A.K. Pitol, H.N. Bischel, A.B. Boehm, T. Kohn, T.R. Julian, Transfer of enteric viruses adenovirus and coxsackievirus and bacteriophage MS2 from liquid to human skin, *Appl. Environ. Microbiol.* 84(22) (2018) e01809-18.
- [40] A.K. Pitol, H.N. Bischel, T. Kohn, T.R. Julian, Virus Transfer at the Skin–Liquid Interface, *Environmental science & technology* 51(24) (2017) 14417-14425.
- [41] A.M. Wilson, K.A. Reynolds, M.P. Verhougstraete, R.A. Canales, Validation of a stochastic discrete event model predicting virus concentration on nurse hands, *Risk Analysis* (2019).
- [42] A. Armanious, M. Aeppli, R. Jacak, D. Refardt, T.r.s. Sigstam, T. Kohn, M. Sander, Viruses at solid–water interfaces: a systematic assessment of interactions driving adsorption, *Environmental science & technology* 50(2) (2015) 732-743.
- [43] C.P. Gerba, Applied and theoretical aspects of virus adsorption to surfaces, *Advances in applied microbiology*, Elsevier 1984, pp. 133-168.
- [44] A.K. Vidaver, R.K. Koski, J.L. Van Etten, Bacteriophage $\phi 6$: a lipid-containing virus of *Pseudomonas phaseolicola*, *Journal of Virology* 11(5) (1973) 799-805.
- [45] C.V. Chrysikopoulos, I.D. Manariotis, V.I. Syngouna, Virus inactivation by high frequency ultrasound in combination with visible light, *Colloids and Surfaces B: Biointerfaces* 107 (2013) 174-179.
- [46] H.T.T. Dang, V.V. Tarabara, Virus deposition onto polyelectrolyte-coated surfaces: A study with bacteriophage MS2, *Journal of colloid and interface science* 540 (2019) 155-166.
- [47] Z. Feng, R. Lu, B. Yuan, Z. Zhou, Q. Wu, T.H. Nguyen, Influence of solution chemistry on the inactivation of particle-associated viruses by UV irradiation, *Colloids and Surfaces B: Biointerfaces* 148 (2016) 622-628.
- [48] J.-A. Park, S.-B. Kim, DLVO and XDLVO calculations for bacteriophage MS2 adhesion to iron oxide particles, *Journal of contaminant hydrology* 181 (2015) 131-140.
- [49] V.I. Syngouna, C.V. Chrysikopoulos, Bacteriophage MS2 and titanium dioxide heteroaggregation: Effects of ambient light and the presence of quartz sand, *Colloids and Surfaces B: Biointerfaces* 180 (2019) 281-288.
- [50] K. Wong, B. Mukherjee, A.M. Kahler, R. Zepp, M. Molina, Influence of inorganic ions on aggregation and adsorption behaviors of human adenovirus, *Environmental science & technology* 46(20) (2012) 11145-11153.

- [51] X. Wu, Z. Feng, B. Yuan, Z. Zhou, F. Li, W. Sun, Effects of solution chemistry on the sunlight inactivation of particles-associated viruses MS2, *Colloids and Surfaces B: Biointerfaces* 162 (2018) 179-185.
- [52] S. Xu, R. Attinti, E. Adams, J. Wei, K. Kniel, J. Zhuang, Y. Jin, Mutually facilitated co-transport of two different viruses through reactive porous media, *Water research* 123 (2017) 40-48.
- [53] B. Becker, M.A. Cooper, A survey of the 2006–2009 quartz crystal microbalance biosensor literature, *Journal of Molecular Recognition* 24(5) (2011) 754-787.
- [54] M.C. Dixon, Quartz crystal microbalance with dissipation monitoring: enabling real-time characterization of biological materials and their interactions, *Journal of biomolecular techniques: JBT* 19(3) (2008) 151.
- [55] A.K. da Silva, O.V. Kavanagh, M.K. Estes, M. Elimelech, Adsorption and aggregation properties of norovirus GI and GII virus-like particles demonstrate differing responses to solution chemistry, *Environmental science & technology* 45(2) (2010) 520-526.
- [56] G.E. Rydell, A.B. Dahlin, F. Höök, G. Larson, QCM-D studies of human norovirus VLPs binding to glycosphingolipids in supported lipid bilayers reveal strain-specific characteristics, *Glycobiology* 19(11) (2009) 1176-1184.
- [57] M. Dimitrova, Y. Arntz, P. Lavalley, F. Meyer, M. Wolf, C. Schuster, Y. Haikel, J.C. Voegel, J. Ogier, Adenoviral gene delivery from multilayered polyelectrolyte architectures, *Advanced functional materials* 17(2) (2007) 233-245.
- [58] N.F. Steinmetz, E. Bock, R.P. Richter, J.P. Spatz, G.P. Lomonossoff, D.J. Evans, Assembly of multilayer arrays of viral nanoparticles via biospecific recognition: a quartz crystal microbalance with dissipation monitoring study, *Biomacromolecules* 9(2) (2008) 456-462.
- [59] X. Huang, J. Xu, H.-F. Ji, G. Li, H. Chen, Quartz crystal microbalance based biosensor for rapid and sensitive detection of maize chlorotic mottle virus, *Analytical Methods* 6(13) (2014) 4530-4536.
- [60] J. Lee, J. Jang, D. Akin, C.A. Savran, R. Bashir, Real-time detection of airborne viruses on a mass-sensitive device, *Applied physics letters* 93(1) (2008) 013901.
- [61] L. Gutierrez, S.E. Mylon, B. Nash, T.H. Nguyen, Deposition and aggregation kinetics of rotavirus in divalent cation solutions, *Environmental science & technology* 44(12) (2010) 4552-4557.
- [62] G. Tiliket, G. Ladam, Q.T. Nguyen, L. Lebrun, Polyethylenimine surface layer for enhanced virus immobilization on cellulose, *Applied Surface Science* 370 (2016) 193-200.

- [63] V. Curtis, S. Cairncross, R. Yonli, Domestic hygiene and diarrhoea—pinpointing the problem, *Tropical medicine & international health* 5(1) (2000) 22-32.
- [64] S.E. Stewart, M.D. Parker, A. Amézquita, T.L. Pitt, Microbiological risk assessment for personal care products, *Int. J. Cosmet. Sci.* 38(6) (2016) 634-645.
- [65] S.Z. Abdullah, P.R. Bérubé, Assessing the effects of sodium hypochlorite exposure on the characteristics of PVDF based membranes, *Water research* 47(14) (2013) 5392-5399.
- [66] W. Yuan, A.L. Zydney, Humic acid fouling during ultrafiltration, *Environmental Science & Technology* 34(23) (2000) 5043-5050.
- [67] I.H. Suffet, M. Patrick, *Aquatic humic substances: influence on fate and treatment of pollutants*, 1988.
- [68] V. Lahoussine-Turcaud, M.R. Wiesner, J.-Y. Bottero, Fouling in tangential-flow ultrafiltration: the effect of colloid size and coagulation pretreatment, *Journal of Membrane Science* 52(2) (1990) 173-190.
- [69] Y. Kaiya, Y. Itoh, K. Fujita, S. Takizawa, Study on fouling materials in the membrane treatment process for potable water, *Desalination* 106(1-3) (1996) 71-77.
- [70] H. Liang, W. Gong, J. Chen, G. Li, Cleaning of fouled ultrafiltration (UF) membrane by algae during reservoir water treatment, *Desalination* 220(1-3) (2008) 267-272.
- [71] S. Muthukumaran, K. Yang, A. Seuren, S. Kentish, M. Ashokkumar, G.W. Stevens, F. Grieser, The use of ultrasonic cleaning for ultrafiltration membranes in the dairy industry, *Separation and Purification Technology* 39(1-2) (2004) 99-107.
- [72] J. Wei, G. Wei, L. Xiaoping, H. Pingfang, W. Yanru, Effect of the ultrasound generated by flat plate transducer cleaning on polluted polyvinylidene fluoride hollow fiber ultrafiltration membrane, *Chinese Journal of Chemical Engineering* 16(5) (2008) 801-804.
- [73] Q. Wang, H. Zeng, Z. Wu, J. Cao, Impact of sodium hypochlorite cleaning on the surface properties and performance of PVDF membranes, *Applied Surface Science* 428 (2018) 289-295.
- [74] C. Regula, E. Carretier, Y. Wyart, G. Gésan-Guiziou, A. Vincent, D. Boudot, P. Moulin, Chemical cleaning/disinfection and ageing of organic UF membranes: A review, *Water research* 56 (2014) 325-365.
- [75] V. Gitis, R.C. Haught, R.M. Clark, J. Gun, O. Lev, Application of nanoscale probes for the evaluation of the integrity of ultrafiltration membranes, *Journal of membrane science* 276(1-2) (2006) 185-192.

[76] S.H. Wolff, A.L. Zydney, Effect of bleach on the transport characteristics of polysulfone hemodialyzers, *Journal of Membrane Science* 243(1-2) (2004) 389-399.

[77] T. Mohammadi, S. Madaeni, M. Moghadam, Investigation of membrane fouling, *Desalination* 153(1-3) (2003) 155-160.

[78] I. Wienk, E. Meuleman, Z. Borneman, T. Van Den Boomgaard, C. Smolders, Chemical treatment of membranes of a polymer blend: mechanism of the reaction of hypochlorite with poly (vinyl pyrrolidone), *Journal of Polymer Science Part A: Polymer Chemistry* 33(1) (1995) 49-54.

[79] C.J. Van Oss, *Interfacial forces in aqueous media*, CRC Press 2006.

[80] C.J. van Oss, M.K. Chaudhury, R.J. Good, Interfacial Lifshitz-van der Waals and polar interactions in macroscopic systems, *Chem. Rev.* 88(6) (1988) 927-941.
<https://doi.org/https://doi.org/10.1021/cr00088a006>.

[81] M.E. Schrader, Young-Dupre revisited, *Langmuir* 11 (1995) 3585-3589.
<https://doi.org/https://doi.org/10.1021/la00009a049>.

CHAPTER TWO

Lip balm drying promotes virus attachment: Characterization of lip balm coatings and XDLVO modeling

2.1 Abstract

Hypothesis

Drying-induced decrease in lip balm surface energy enhances virus adhesion due to the emergence of strong hydrophobic colloid-surface interactions.

Experiments

A protocol was developed for preparing lip balm coatings to enable physicochemical characterization and adhesion studies. Surface charge and hydrophobicity of four brands of lip balm (dry and hydrated) and human adenovirus 5 (HAdV5) were measured and used to calculate the extended Derjaguin-Landau-Verwey-Overbeek (XDLVO) energy of interactions between lip balm coatings and HAdV5 as well as four other colloids: HAdV40, MS2 and P22 bacteriophages, and SiO₂. Quartz crystal microbalance with dissipation monitoring (QCM-D) tests employed SiO₂ colloids, HAdV5 and hydrated lip balms.

Findings

Drying of lip balms results in a dramatic decrease of surface energy ($\delta(\Delta G_{sww}) \geq 83.0$ mJ/m²) making the surfaces highly hydrophobic. For dry lip balms, the interaction with all five colloids is attractive. For lip balms hydrated in 150 mM NaCl (ionic strength of human saliva), XDLVO calculations predict that hydrophilic colloids (MS2, P22, SiO₂) may attach into shallow secondary minima. Due to the relative hydrophobicity of human adenoviruses, primary maxima in XDLVO profiles are low or non-existent making irreversible deposition into primary energy minima possible. Preliminary QCM-D tests with SiO₂ colloids and HAdV5 confirm deposition on a hydrated lip balm.

Keywords: adenovirus, personal care products, lip balm, lipstick, adhesion, XDLVO, QCM-D, fomites, virus transfer, public health

2.2 Introduction¹

Environmental transmission via contaminated surfaces is an important pathway for pathogen transfer that can complement transfer with contaminated food or water, or via direct person-to-person contact. There is a growing body of literature on the pathogen adhesion to and resuspension from fomites [1]. Due to their smaller size, high infectivity, and resistance to disinfection, viruses are of special concern. Despite a clear need for

¹ Abbreviations: Extended Derjaguin-Landau-Verwey-Overbeek (XDLVO); quartz crystal microbalance with dissipation monitoring (QCM-D); human adenovirus 5 (HAdV5); human adenovirus 40 (HAdV40); American Type Culture Collection (ATCC); scanning electron microscopy (SEM). isoelectric point (IEP).

such data, relatively little is known about the propensity of viruses to attach to common surfaces. A number of studies have explored virus transfer to and from human body. [2-8]. Most but not all of these studies focused on unmodified human skin Julian et al. [5] showed that washing fingerpads reduced virus transfer; the trend was tentatively attributed to changes in the moisture level or pH of the skin [9] or to the presence of soap residuals pointing to the possible importance of skin coatings. In the two studies by Pitol et al. [6, 7], Vaseline was used to delimit the human skin area where bacteriophages were allowed to adhere to human skin. The approach was based on a viability assay, which showed that MS2 adsorption to Vaseline was at least one order of magnitude lower than to the skin. However, the duration of the longest test was 10 min and thus one can assume that Vaseline did not have time to dry.

Microbial contamination of personal care products has been a significant problem for researchers as well as manufacturers worldwide [10]. The presence of high numbers of pathogens poses a serious health threat to consumers, especially those who are already ill or in a weakened state [11]. According to the Rapid Alert System database, from January 2008 until week 26 of 2014 sixty-two cosmetic products were recalled because they were contaminated with pathogenic or potentially pathogenic microorganisms [12]. Although the use of preservatives, good manufacturing practices and quality control programs have improved product quality, cases of contaminated cosmetic products have been reported. For example, on December 7, 2010, there was an Import Alert regarding Alexia Lip gloss cosmetic contaminated by *Sphingomonas paucimobilis* and *P. aeruginosa*, manufactured by Maesa, Jinwan Zhuhai [13].

Legislation and introduction of good manufacturing practices have improved the microbiological standards, but contaminated cosmetics are still found [14] and consequences for end users can be grave. As an example, contaminated ocular cosmetics caused a *Pseudomonas* corneal ulcer after a woman sustained minor corneal trauma with a mascara applicator [15].

Cosmetics are designed and manufactured to ensure product stability and microbiological safety during normal and reasonably foreseeable product use. However, according to the U.S. Food and Drug Administration, personal care products intended for the general population are not intended to be sterile [10]. Personal care products often include natural ingredients, including organic compounds; the raw materials that these natural ingredients are sourced from are one of the main reasons for microbial contamination [16]. Further, cosmetic products can be contaminated during use. Of particular concerns are products such as lipstick and lip balm, which can facilitate contagion through common routes such as ingestion and inhalation. For example, sharing lipstick may increase the chance of infection of Epstein–Barr virus, an agent linked to systemic lupus erythematosus [17]. Lipstick-associated pathogens are most likely to enter the human body through the mouth when eating or drinking. This hypothesized route is of particular importance given the scale of lipstick usage. According to a study conducted by the Scientific Committee on Consumer Safety, the estimated daily amount applied lipstick is 0.057 g and the frequency of application is twice a day [18].

There are multiple studies on virus attachment to surfaces such as organic matter [19], soil [20], membrane filters [21], sand [22], polymers (e.g. polyvinylidene fluoride [23] and anion exchange resins [24]), and polyelectrolyte-coated surfaces [25]. Most of this work employed bacteriophages as human virus surrogates [19, 20]. To our knowledge, there has been no published work on the attachment of viruses to personal care products including lip balm and lipsticks. More broadly, to our knowledge, there have been no prior reports on the adhesion of particles of any kind to lip balm or lipstick surfaces. This is likely because of the absence of standard protocols for such measurements and difficulties of sample preparation. The present work aims at filling this knowledge gap.

This study began with developing a methodology for coating lip balms to prepare surfaces suitable for physicochemical characterization of lip balm as well as for testing adhesion of colloids to such materials. Both dry and hydrated lip balms were characterized in terms of charge and hydrophobicity. The data was used to predict the XDLVO energy of interfacial interactions between these surfaces and five colloids: human adenoviruses (serotypes 5 and 40) and two bacteriophages (P22 and MS2), and SiO₂ particles. The XDLVO modeling study was complemented with a preliminary experimental study of SiO₂ and HAdV5 deposition onto hydrated lip balm.

2.3 Materials and Methods

2.3.1 Reagents

All chemical reagents were of high purity (>99%). Petroleum distillate (Penetrol, PPG Industries) as well as ethyl acetate, isopropanol, methanol, pentane, and hexane (all – Sigma Aldrich) were used as solvents for lip balms. Aqueous solutions of KCl (Sigma Aldrich) were employed in measurements of particle size and electrophoretic mobility of SiO₂ colloids and HAdV5, streaming potential of lip balm surfaces, and colloid adhesion to lip balms. Eight different brands of over-the-counter lip balm, all purchased in the local supermarket (Meijer, Okemos, MI) were initially characterized in water contact angle tests. Based on contact angle values and manufacturer-supplied information on balm composition, four representative types of lip balm were selected for further characterization and colloid adhesion tests. While nanoparticles such as ZnO and TiO₂ are sometimes included in lip balm formulations for added UV protection, neither of the four lip balms selected for this study contained nanoparticles. The detailed composition of each lip balm is given in SM (Table 4). The stock of viable HAdV5 was purchased from American Type Culture Collection (ATCC) [26] (see SM, section S3). As described by the manufacturer, HAdV5 (ATCC VR-1516) was propagated by culturing on HEK 293 cells from the Working Cell Bank in Cell Cubes® and purified using a single-column chromatography with an anion exchange resin. The method was shown to give virus stock of the purity comparable to that achieved with CsCl gradient purification [27]. SiO₂ suspension (Snowtex ZL, 40-41 wt%, , SiO₂ density 2.3 g/cm³ [28]) was obtained from

Nissan Chemical Industries (Tokyo, Japan).

2.3.2 Preparation of lip balm surfaces

For contact angle and surface charge measurements, lip balms samples were melted and then spin coated into a relatively thick film on a surface of a glass slide (Protocol A, Fig. 1). Briefly, a solid lip balm sample was first melted on the heater and then pipetted on a glass slide positioned on the chuck of the spin coater operated at 3000 rpm. The deposition procedure was sufficiently fast (~ 5 s) to avoid premature on-contact solidification of the sample. The duration of spin-coating was 15 s.

For QCM-D measurements, the coating layer should be not only continuous but also very thin (a few microns at most) to avoid overloading the QCM-D sensor. To form such thin layers, melted lip balm samples were mixed with a solvent prior to being spin-coated on the QCM-D sensor surface. First, several solvents - ethyl acetate, isopropanol, methanol, pentane, hexane, and petroleum distillate were evaluated as alternatives for liquefying lip balm. The selection of solvents to test was partly based on the results of a study by Dasari and Goud, who extracted castor seed oil using polar and non-polar solvents [29]. Of the five solvents, petroleum distillate yielded the most homogenous lip balm solution. Then, three different protocols (B, C and D; Fig. 1) were assessed to select a method that gives a sufficiently thin coating with the surface energy most closely matching that of a solvent-free sample. Briefly, solid lip balm samples were melted in a glass vial using a heating plate and then dissolved in

petroleum distillate. The liquid sample was stirred (Multistirrer, Thomas Scientific) under 800 rpm and autoreverse (10 s) mode for 1 day and then sonicated overnight at 37 °C to break up larger, undissolved particles. The processed sample (~ 0.5 ml) was pipetted onto a clean support surface (glass slide or QCM-D sensor), spin-coated at 7500 rpm for 50 s, and left in the fume hood at room temperature for 5 days. After drying, the sample was heated on a heater at the minimum temperature of 100 °C for 2 min to evaporate residual solvents.

2.3.3 Characterization of the lip balm surface: Surface charge and morphology

Surface charge was determined using streaming current measurements (SurPASS electrokinetic analyzer, Anton Paar GmbH) performed on 20 mm x 10 mm lip balm-coated glass slides. Prior to measurements, each sample was immersed in 1 mM KCl solution overnight. Samples were fixed on sample holders and inserted into an adjustable gap cell with the gap height set at 145 μm . Measurements were done using KCl as the electrolyte and repeated four times for each sample. The homogeneity of the coating on the gold sensors was evaluated using scanning electron microscopy (SEM, JEOL 6610 LV microscope). Because of the concern that volatile components of lip balm samples may interfere with SEM imaging, microscopy was performed in the low vacuum mode (see SM, section S1).

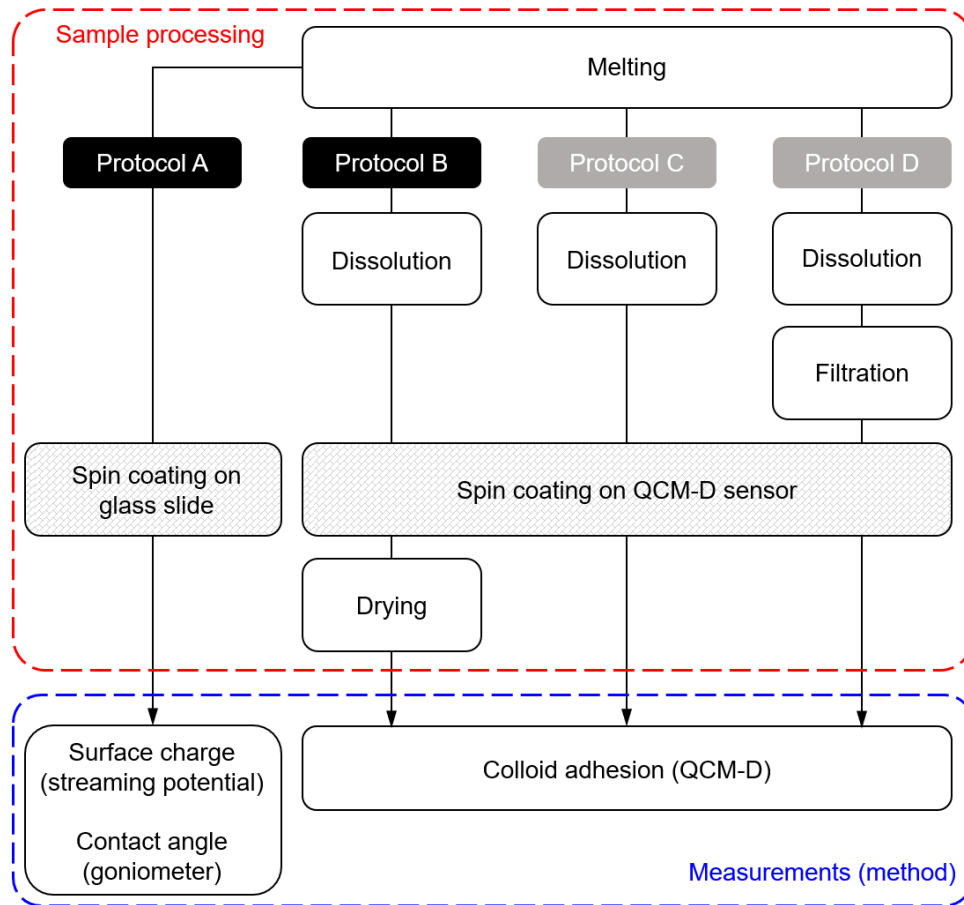


Figure 1. Lip balm coating protocols evaluated in this work. Of the three protocols (B, C, D) for preparing ultrathin coatings suitable for QCM-D measurements, protocol B yielded lip balm surface with the surface energy most closely matching that of a minimally processed sample (protocol A, baseline) and was, therefore, adopted for studying adhesion of colloids to such coatings.

2.3.4 Characterization of HAdV5 virions and SiO₂ colloids: Size and charge

Hydrodynamic diameter and electrophoretic mobility were measured by dynamic light scattering (ZetaPALS, Brookhaven Instruments) and laser doppler micro-electrophoresis (Zetasizer Nano ZS, Malvern), respectively. Zeta potential values were

calculated based on electrophoretic mobilities determined as a function of pH, which was adjusted using NaOH and HCl [30]. The particle size distribution in the SiO₂ stock (40.5 wt%) could not be measured because of high turbidity. Thus, the samples used to measure the particle size and ζ -potential were both diluted to 0.08 wt% in 1 mM KCl. Prior to use, the stock suspensions were sonicated (VWR ultrasonic cleaner, 35 kHz, 40 W, VWR International) for 20 min to ensure complete dispersion. Prior to measuring the hydrodynamic size and charge of colloids (virus or SiO₂), the suspensions were filtered through 0.22 μ m filter.

2.3.5 Quantifying hydrophobicity of HAdV5 and lip balm surfaces

While the hydrophobicity of a surface can be roughly evaluated based on its contact angle with water, a more accurate measure of surface hydrophobicity is given by the free energy of interfacial interaction (ΔG_{sws}) of two surfaces, identical to the one in question, when immersed in water [31]. The negative sign of ΔG_{sws} indicates that the surface is hydrophobic [32]. The absolute value of ΔG_{sws} indicates the degree of hydrophobicity (or hydrophilicity, when $\Delta G_{sws} > 0$) of the surface. To determine ΔG_{sws} for HAdV5 and lip balms (both dry and hydrated), contact angles of three probe liquids - DI water, glycerol, and diiodomethane - on virus lawn and on lip balm surface were determined using the sessile drop method (goniometer/tensiometer model 250, ramé-hart). Contact angle values were calculated by DROPimage Advanced software based on recorded droplets shapes. The droplet volume was in the 8 μ l to 10 μ l range. To prepare a virus lawn, purified virus stock was filtered through a 50 kDa ultrafiltration

membrane. The membrane coated with a multilayer cake of virions (> 4 monolayers) was dried until the water contact angle on the membrane stabilized (≥ 6 h across all samples) [21, 30, 33]. Lip balm surfaces were prepared by spin coating as described in section 2.2. To hydrate lip balm, coated glass slides were immersed for 30 min in NaCl solution with the ionic strength (150 mM) matching that of human saliva. The contact angle tests in air were performed at the ambient temperature of 22 °C and the relative humidity of 47 %.

Every contact angle measurement was repeated three times. Surface tension components of the surface (γ_s^{LW} , γ_s^+ , γ_s^-) were obtained by substituting measured contact angles and known surface tensions of probe liquids into the Young-Dupré equation (Eq. (1)) where θ is the contact angle of the probe liquid on the surface, γ_l^{TOT} is the total surface energy, while γ^{LW} , γ^+ and γ^- are Lifshitz-van der Waals (i.e. apolar), electron acceptor, and the electron donor components of surface energy. Subscripts l and s refer to the probe liquid and the surface, respectively [31].

$$(1 + \cos\theta)\gamma_l^{TOT} = 2(\sqrt{\gamma_s^{LW}\gamma_l^{LW}} + \sqrt{\gamma_s^+\gamma_l^-} + \sqrt{\gamma_s^-\gamma_l^+}) \quad (1)$$

The free energy of interfacial interaction in water, ΔG_{sWS} , was calculated based on the surface energy component of the solid (virus or lip balm) and the tabulated values of the surface energy components of water [31]:

$$\Delta G_{sWS} = -2\left(\sqrt{\gamma_s^{LW}} - \sqrt{\gamma_w^{LW}}\right)^2 - 4(\sqrt{\gamma_s^+\gamma_s^-} + \sqrt{\gamma_w^+\gamma_w^-} - \sqrt{\gamma_s^+\gamma_w^-} - \sqrt{\gamma_s^-\gamma_w^+}) \quad (2)$$

2.3.6 QCM-D studies of SiO₂ and HAdV5 attachment to lip balm surfaces

Colloidal deposition onto a surface can be quantified using quartz crystal microbalance with dissipation monitoring (QCM-D). This system allows real-time monitoring of the changes in vibrational frequency due to mass deposition onto the quartz crystal sensor. With the deposited mass proportional to the changes in resonance and overtone frequencies, the amount of mass deposited can be computed based on the frequency shift [34]. This technique can also offer information on the viscoelastic behavior of the adsorbed layer by measuring dissipation [35]. QCM-D has been used to study attachment of MS2 bacteriophage [19, 20, 36], human adenovirus [37] and pathogenic plant viruses [38, 39] onto various surfaces such as clays [20], natural organic matter [19, 34, 40], polyelectrolyte multilayers [25, 41], and household paints [37].

The QCM-D E4 system (Biolin Scientific) was used to quantify the deposition of colloids onto the lip balm-coated QCM sensor surfaces. Prior to measurement, gold QCM-D sensors were cleaned following the procedure recommended by the manufacturer (see SM, section S2) and then mounted into the flow chamber to determine their resonance frequency in air. This was followed by a 5-min measurement of resonance frequency to establish a stable baseline. QCM-D tests were carried out at 25 °C in a continuous flow mode (0.15 ml/min) using a digital peristaltic pump (IPC, four channels, ISMATEC). To acquire QCM resonances, lip balm-coated sensors were first contacted with 150 mM NaCl solution for at least 20 min until the baseline of the frequency signals was

stabilized using $\frac{\Delta f}{\Delta t} \leq 0.025$ Hz/min as the baseline criterion. The 150 mM solution matched the continuous phase of the colloidal suspension in the QCM-D measurement and had the ionic strength approximating that of human saliva (~ 136 mM; Table 3) [42]. In tests with SiO₂ colloids, the sensors were challenged with silica suspensions of one of two concentrations: 0.52 mg(SiO₂)/ml or 1.05 mg(SiO₂)/ml. In tests with HAdV5, the concentration of HAdV5 in the feed was ~ 10⁹ GC/mL. Based on the measured value of HAdV5 hydrodynamic size (103 nm, see section 3.3) and the approximate virion density (assumed 1.33 g/cm³ [43, 44]) the corresponding mass concentration of HAdV5 was estimated to be 0.76 µg/mL. QCM frequency and dissipation were recorded every 1 min. The frequency shifts were fitted into the Sauerbrey equation [45] to compute the mass change:

$$\Delta m = -C\Delta f/n \quad (3)$$

where $C = 17.7$ ng·Hz⁻¹·cm⁻² is the mass sensitivity constant, n is the overtone number and Δf is the frequency shift (Hz). Mass data were calculated based on 3rd 5th overtones.

2.3.7 XDLVO modeling of colloid interactions with lip balm

The interactions particles and surfaces include repulsive electrostatic interactions and attractive van der Waals forces, which can be described by the Derjaguin-Landau-Verwey-Overbeek (DLVO) theory of colloid stability [46, 47]. The classic DLVO theory, however, showed only limited ability to predict nanoparticle adhesion to surfaces [19, 34, 36, 48]. Extended DVLO (XDLVO) model [49] builds on the DLVO theory by taking

hydrophobic interactions into consideration. The XDLVO theory can predict interactions of dissolved and colloidal materials with various surfaces [50, 51] and has been applied to describe virus-surface interactions [21, 25, 33, 52]. The XDLVO theory describes the total energy of interaction $E_{S_1WS_2}^{XDLVO}$ between two surfaces in an aqueous medium as a sum of the Lifshitz-van der Waals, $E_{S_1WS_2}^{LW}$, electrostatic double layer, $E_{S_1WS_2}^{EL}$, an acid-base, $E_{S_1WS_2}^{AB}$, energies. When one of the surfaces is a virus:

$$E_{vws}^{XDLVO} = E_{vws}^{LW} + E_{vws}^{EL} + E_{vws}^{AB} \quad (4)$$

The XDLVO approach extends the DLVO theory by taking hydrophobic interactions ($E_{S_1WS_2}^{AB}$) into consideration. In the expression above,

$$E_{vws}^{LW} = -\frac{Aa}{6d} = 2\pi\frac{a}{d}d_0^2\Delta G_{y0}^{LW}, \quad (5)$$

where a is the virus radius, d is the separation distance, d_0 is the minimum separation distance ($d_0 = 0.158$ nm) [31, 53], and $A = -12\pi y_0^2\Delta G_{y0}^{LW}$ is Hamaker constant. Further,

$$E_{vws}^{EL} = \pi\epsilon_r\epsilon_0a \left[2\psi_v\psi_s \ln\left(\frac{1+e^{-k_Dd}}{1-e^{-k_Dd}}\right) \right] + (\psi_v^2 + \psi_s^2) \ln(1 - e^{-2k_Dd}) \quad (6)$$

$$E_{vws}^{AB} = 2\pi a\lambda\Delta G_{d_0}^{AB} \exp\left(\frac{d_0-d}{\lambda}\right) \quad (7)$$

where ϵ_r is the dielectric constant of water ($\epsilon_r = 79$), ϵ_0 is the relative permittivity in vacuum ($\epsilon_0 = 8.854 \cdot 10^{12}$ C·V⁻¹·m⁻¹), ψ_v and ψ_s are the surface potentials of the colloid and surface respectively, k_D is the reverse Debye length, λ is the characteristic delay length of the AB interaction ($\lambda = 0.6$ nm) [53].

$$\Delta G_{d_0}^{AB} = 2\sqrt{\gamma_s^+}(\sqrt{\gamma_s^-} + \sqrt{\gamma_v^-} - \sqrt{\gamma_w^-}) + 2\sqrt{\gamma_s^-}(\sqrt{\gamma_s^+} + \sqrt{\gamma_v^+} - \sqrt{\gamma_w^+}) - 2(\sqrt{\gamma_s^+ \gamma_v^-} + \sqrt{\gamma_s^- \gamma_v^+}) \quad (8)$$

$$\Delta G_{d_0}^{LW} = 2(\sqrt{\gamma_w^{LW}} - \sqrt{\gamma_s^{LW}})(\sqrt{\gamma_v^{LW}} - \sqrt{\gamma_w^{LW}}) \quad (9)$$

where γ^+ is the electron acceptor component, γ^- is the electron donor component and γ^{LW} is the apolar surface energy component. The surface energy components of the surface (γ_s^+ , γ_s^- , γ_s^{LW}) and the virus (γ_v^+ , γ_v^{LW} , γ_v^-) are calculated using the Young-Dupre equation and contact angle values of the probe liquids.

2.4 Results and Discussion

2.4.1 Optimal coating protocol and coating morphology

At each processing step, lip balm samples remained homogenous with no apparent changes other than in their flowability. While phase separation may occur in similar (e.g. recrystallization of cocoa butter leading to “fat blooms” on the surface of lip balms [54] and chocolate [55]), in our study no phase separation was observed at any point during sample preparation (melting, coating, drying). We attribute this to the relatively simple composition of the lip balms used in this work (see SM, Table 4). Detailed rheological studies would be necessary to explore possible structural and compositional changes in depth [56].

Lip balm film morphology was assessed using SEM (Fig. 2). The coating thickness was relatively constant across the coated area and had a homogeneous internal structure for all lip balms but Vaseline. The thickness was estimated to be $1.15 \pm 0.19 \mu\text{m}$, $2.03 \pm 0.12 \mu\text{m}$, $1.07 \pm 0.16 \mu\text{m}$, and $3.18 \pm 0.10 \mu\text{m}$ for Carmex, ChapStick, Burt's Bees, and Vaseline, respectively. The surface roughness of the coatings was not measured more accurately (e.g. with atomic force microscopy). However, how the roughness affected surface energy was captured by the measured values of apparent contact angles. (Surface roughness enhances apparent hydrophobicity of surfaces with water contact angle $> 90^\circ$ [57].) We also note that there may be a difference in the surface roughness (and, therefore, surface energy) between lip balm coatings on a relatively flat surface such as a glass slide, an SEM stub or a QCM-D sensor and that of a human lip. While outside of this study's scope, the effects of the morphology of the underlying surface on the adhesiveness of personal care products should be explored in future work.

Addition of petroleum distillate as a solvent enabled spin-coating of the lip balm sample but could also alter the physicochemical properties that affect adhesion. In this study, a change in the surface energy of lip balm was used as a composite indicator of solvent-induced alterations to the sample during the preparation process. The underlying assumption was that the deviation of the surface energy from its baseline value (measured for dry samples) was indicative of the presence of residual solvent. By extension, return of the surface energy value to that of the baseline (protocol A) was accepted as evidence of the removal of residual solvent. The optimal sample preparation procedure was selected in tests with Carmex lip balm coated onto a glass

slide surface. Based on measured values of contact angles of probe liquids, surface energies of Carmex coatings made using protocols B, C, and D were compared with that for a coating made using the “solvent-free” protocol A. Protocol B has ΔG_{sws} values matching those obtained by protocol A and, therefore, was selected as the coating method to prepare lip balm surfaces for adhesion studies (Fig. 3).

2.4.2 Hydrophobicity and surface charge of lip balm-coated surfaces

Lip balms hydrated in 150 mM NaCl (model human saliva) had the surface energy in the 15.2 mJ/m² to 38.4 mJ/m² range. The energy penalty associated with the replacement of the layer of water molecules bound at such hydrophilic surfaces makes them less adhesive. Drying had a dramatic effect on the surface energy of lip balms (Fig. 4)

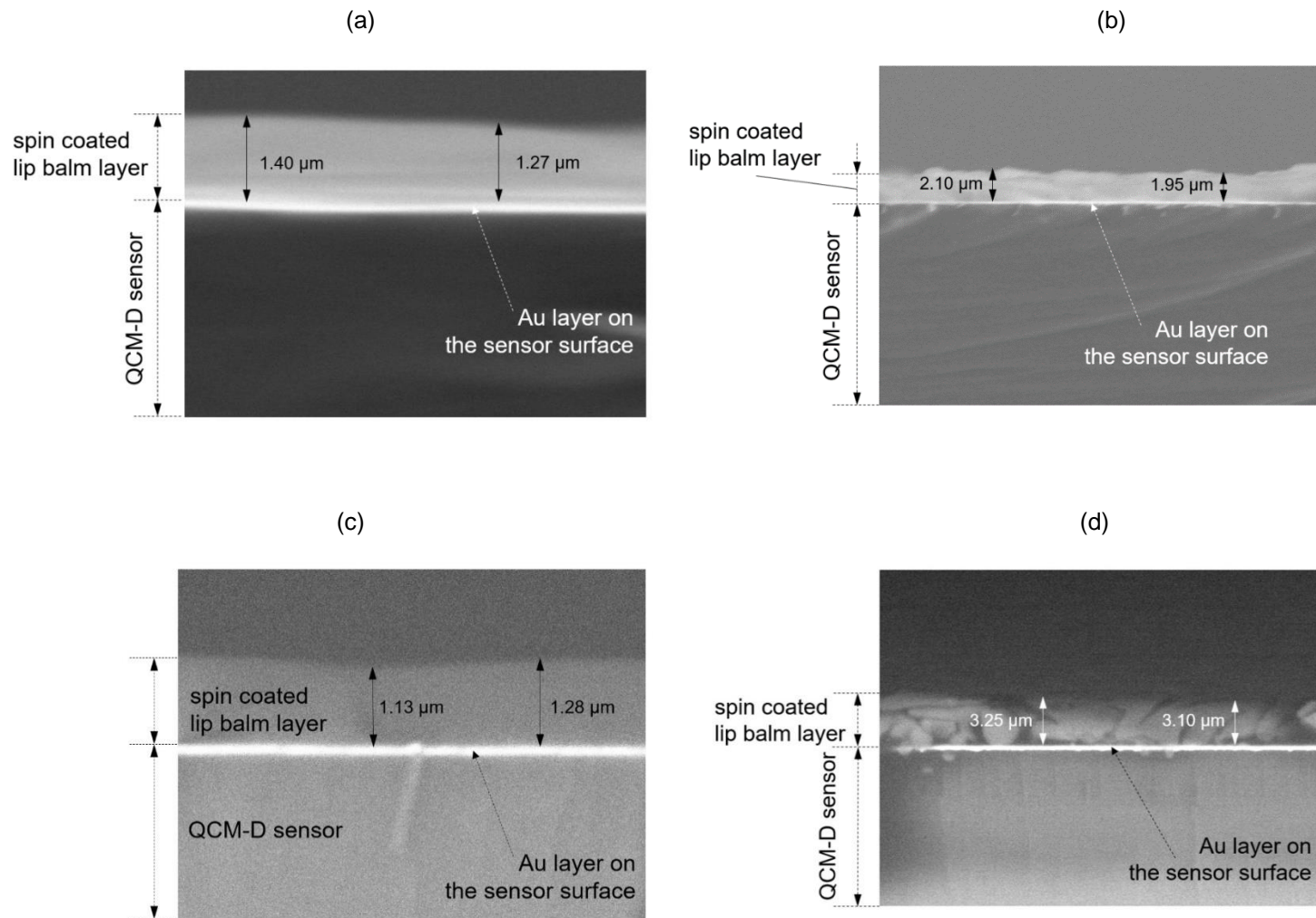


Figure 2. Representative SEM images of a) Carmex b) ChapStick, c) Burt's Bees, and d) Vaseline coatings on a QCM-D sensor.

converting them into strongly hydrophobic surfaces with G_{SWS} values ranging from - 65.0 mJ/m² to - 90.7 mJ/m². Such reversal of the surface energy from positive to highly negative should translate into a significant change in the adhesive properties of these surfaces.

All four lip balms had a pH-dependent charge indicating presence of ionizable surface groups. The ζ -potential of Carmex and Vaseline showed a steady decrease with an increase in pH (Fig. 5a). The isoelectric point (IEP) for Carmex and Vaseline lip balm samples were ~ 4.15 and ~ 4.0 , respectively. For ChapStick and Burt's Bees lip balms, the charge had a more complex dependence on pH (Fig. 5b) with two IEPs for each surface: 4.0 and 7.7 for ChapStick and 4.1 and 7.7 for Burt's Bees. The origin of the positive slope in the ζ vs pH dependence for ChapStick and Burt's Bees is unclear. We speculate that this non-monotonous nature of $\zeta(\text{pH})$ function is due to the presence of water-soluble compounds in the lip balms with a pH dependent charge and solubility. The observed increase ζ with an increase in pH can stem from leaching of negatively charged compounds at higher pH values. The irregular behavior was observed for only two out of four lip balms and should be explored further. This is particularly important given that the second IPE is close to the pH range of saliva.

2.4.3 Hydrodynamic size and surface charge of HAdV5 and SiO₂ colloids

The particle size distribution of HAdV5 suspension had a single narrow peak at $\sim 103 \pm 1$ nm (see SM, Fig. 10) indicating high purity of the stock [26, 27]. The ζ -potential of

HAdV5 continuously decreases with an increase in pH (Fig. 5). The IEP of HAdV 5 is ~ 4.5 consistent with the result reported by Trilisky and Lenhoff [58]. The ζ -potentials measured at pH < 4.5 and pH > 8 were different from the values reported in that earlier study likely due to differences in the background electrolyte (see SM, section S5).

The particle size distribution of ST-ZL (see SM, Fig. 10) features a single narrow peak at ~138 nm, which is above the manufacturer-provided size range (70 to 100 nm).

Earlier studies also reported larger sizes for ST-ZL silica (139 to 153 nm [28, 59]). The ζ -potential of ST-ZL decreased with an increase in pH (Fig. 13) and remained negative over the pH range measured in this study, which is consistent with the result reported by Kim et al. [59]. The ζ -potentials measured at pH < 4 and pH > 8 were different from the result reported by Kim et al. likely due to different background electrolytes used.

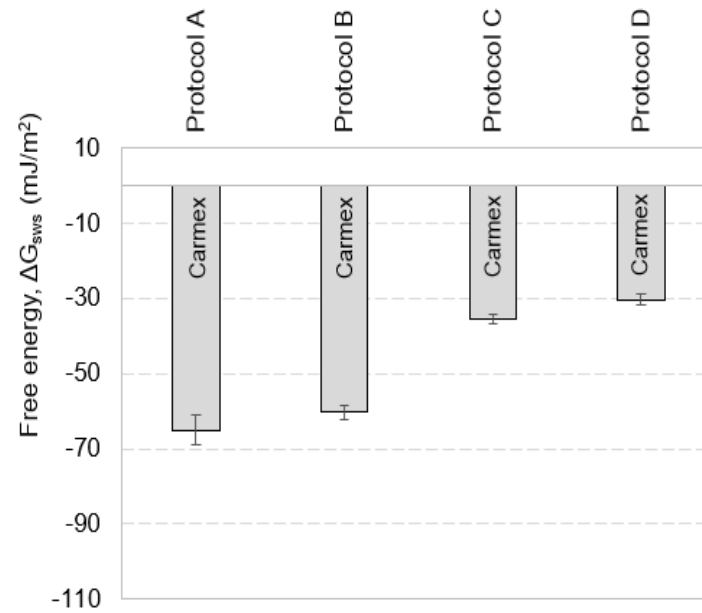


Figure 3. Free energy of interfacial interaction in water, ΔG_{sWS} , of the Carmex lip balm as a function of the coating protocol (see Fig. 1). Measured contact angles of probe liquids and calculated surface energy parameters used to compute ΔG_{sWS} values are given in Table 6. Each measurement was done in triplicate. Errors correspond to standard deviations.

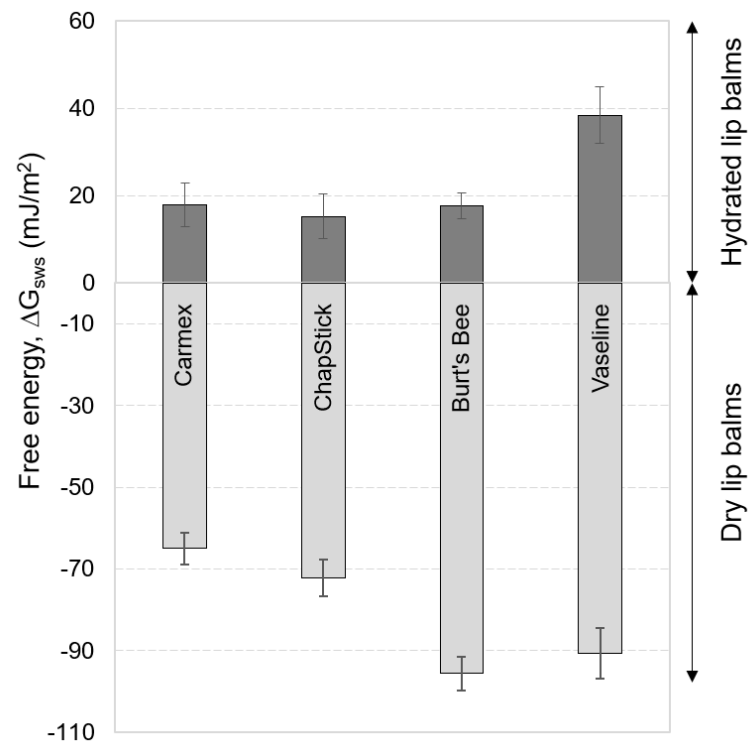


Figure 4. Free energy of interfacial interaction in water, ΔG_{sws} , of the four lip balms coated using protocol B (see Fig. 1) in dry and hydrated states. Measured contact angles of probe liquids and calculated surface energy parameters used to compute ΔG_{sws} values are given in Table 5. Each measurement was done in triplicate. Errors correspond to standard deviations.

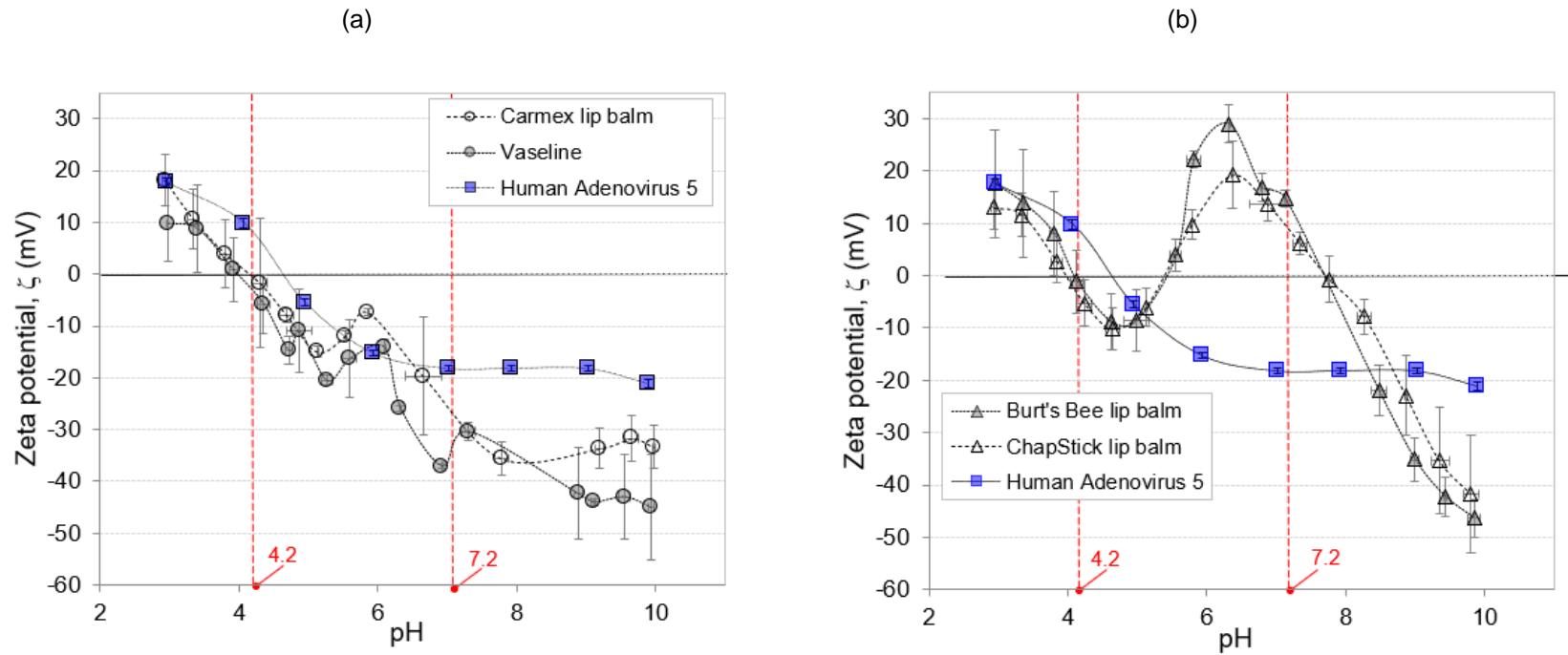


Figure 5. Surface charge of HAdV5 virions and lip balm surfaces as a function of pH. Vertical dashed lines indicate pH values (4.2 and 7.2) used in QCM-D measurements of HAdV5 attachment to lip balm surfaces. Lines connecting experimental data points are added to the guide the eye. Average and standard deviations for lip balm samples are based on four independent measurements for each lip balm. Average and standard deviations for HAdV5 are based on three independent measurements. HAdV5 data is shown in both graphs to add data interpretation.

2.4.4 Attachment of viruses and SiO₂ particles to lip balm-coated surfaces:

XDLVO predictions

XDLVO modeling of colloid-lip balm interaction was performed for five colloids: two human viruses (HAdV5, HAdV40), two bacteriophages (MS2, P22) and particulate SiO₂. Colloid properties required as inputs to XDLVO model included particle size, ζ -potential and surface energy. For HAdV5, all these characteristics were measured (section 4.3). To our knowledge, this is the first report of surface energy (or any other metric of hydrophobicity) for HAdV5. For SiO₂, size and charge were also determined in this study while the surface energy value was calculated based on contact angles of three probe liquids as reported by Zdziennicka et al. [60]. For HAdV40, P22 and MS2, the values were taken from the literature [21, 25, 30, 60] (Table 1).

Table 1. Size, charge and hydrophobicity of colloids considered in this work. The three properties are quantified in terms of hydrodynamic diameter (d_h), zeta-potential (ζ), and free energy of interfacial interaction in water (ΔG_{sws}), respectively.

Notes:

A This study (see SM, Fig.); B Shi et al. [21]; C Shi and Tarabara [30]; D Calculated based on contact angle data reported by Zdziennicka et al. [60]. The error is not provided because the original contact angle values are reported as averages only; E This study (see SM, Table 5); F Dang and Tarabara [25]; G This study (see SM, Fig. 13); H This study (see Fig. 5)

Property	Colloid type				
	SiO ₂	Human viruses		Bacteriophages	
	particles	HAdV5	HAdV40	P22	MS2
d_h , nm	137.9 ± 0.4 ^A (n=10)	103 ± 1.3 ^A (n=10)	98 ± 3.0 ^B (n=10)	54 ± 1.3 ^C (n=10)	27 ± 0.4 ^C (n=10)
ζ , mV (at pH 4.2)	-25 ± 2.9 ^G (n=10)	7 ± 0.8 ^H (n=30)	-8 ± 1.8 ^B (n=10)	-19 ± 1.3 ^C (n=10)	-31 ± 1.3 ^C (n=10)
ζ , mV (at pH 7.2)	-36 ± 2.8 ^G (n=10)	-18 ± 0.4 ^H (n=30)	-29 ± 4.7 ^B (n=10)	-47 ± 0.7 ^C (n=10)	-47 ± 0.9 ^C (n=10)
ΔG_{sws} , mJ/m ²	12.8 ^D	-27.7 ± 1.1 ^E (n=3)	-30.4 ± 6.5 ^B (n=3)	-6.3 ± 11.0 ^C (n=3)	48 ± 15.3 ^F (n=3)

Two pH values (4.2 and 7.2) were selected. pH 7.2 represented that of saliva of a healthy person (6.2 to 7.6 typical range [61]). pH 4.2 was chosen to explore HAdV5 deposition under different conditions of virus-balm electrostatic interaction (Fig.5). In what follows we present results of XDLVO modeling for two colloid/lip balm pairs (SiO₂/Burt's Bees and HAdV5/Carmex). Results for the other colloid/lip balm pairs are given in SM (Fig. 14 – 31).

Figure 6 shows XDLVO energy profiles for Burt's Bees-HAdV5 interaction. For dry lip balms, the XDLVO model indicates that at both pH values (4.2 and 7.2) the total energy of interaction is attractive: $E_{tot} \leq 0$ and $\frac{dE_{tot}}{dr} \geq 0$ (Fig. 6a, 6c). Figure 7 illustrates XDLVO energy profiles for Burt's Bees-SiO₂ interaction. For dry balms (Fig. 7a, 7c), the trends were the same as for HAdV5. In fact, for all five colloids and for both pH values, the overall interaction of colloids with *dry* lip balm is always attractive (Fig. 14 – 31). The main reason for the favorable interaction is the high hydrophobicity of dry lip balms (Fig. 4) and the resulting strong short-range hydrophobic attraction.

Table 2. Values (in units of kT) of the primary maximum (E_{max}) and secondary minimum (E_{min}) in the XDLVO energy profile for colloid interaction with hydrated lip balms.

Lip balm (hydrated)	pH	HAdV5		HAdV40		P22		MS2		SiO ₂	
		E_{max}	E_{min}	E_{max}	E_{min}	E_{max}	E_{min}	E_{ma}	E_{min}	E_{max}	E_{min}
Burt's Bees	4.2	-	-	10.9	-3.1	221.7	-1.1	381.4	-0.5	1099	-2.6
Burt's Bees	7.2	-	-	-	-	158.0	-1.3	378.4	-0.5	1191	-2.6
Carmex	4.2	13.7	-3.9	29.8	-2.9	262.5	-1.2	445.3	-0.5	1448	-2.6
Carmex	7.2	5.2	-3.1	68.6	-2.2	293.0	-1.0	451.0	-0.5	1337	-2.5
ChapStick	4.2	-	-	45.7	-1.9	257.0	-0.8	403.5	-0.4	1192	-1.8
ChapStick	7.2	13.4	-2.8	12.6	-2.3	139.5	-0.9	272.7	-0.4	922	-1.9
Vaseline	4.2	337.7	-2.2	433.3	-1.7	477.0	-0.9	447.0	-0.4	1562	-2.2
Vaseline	7.2	388.0	-2.0	488.0	-1.6	526.0	-0.8	493.0	-0.4	1673	-2.0

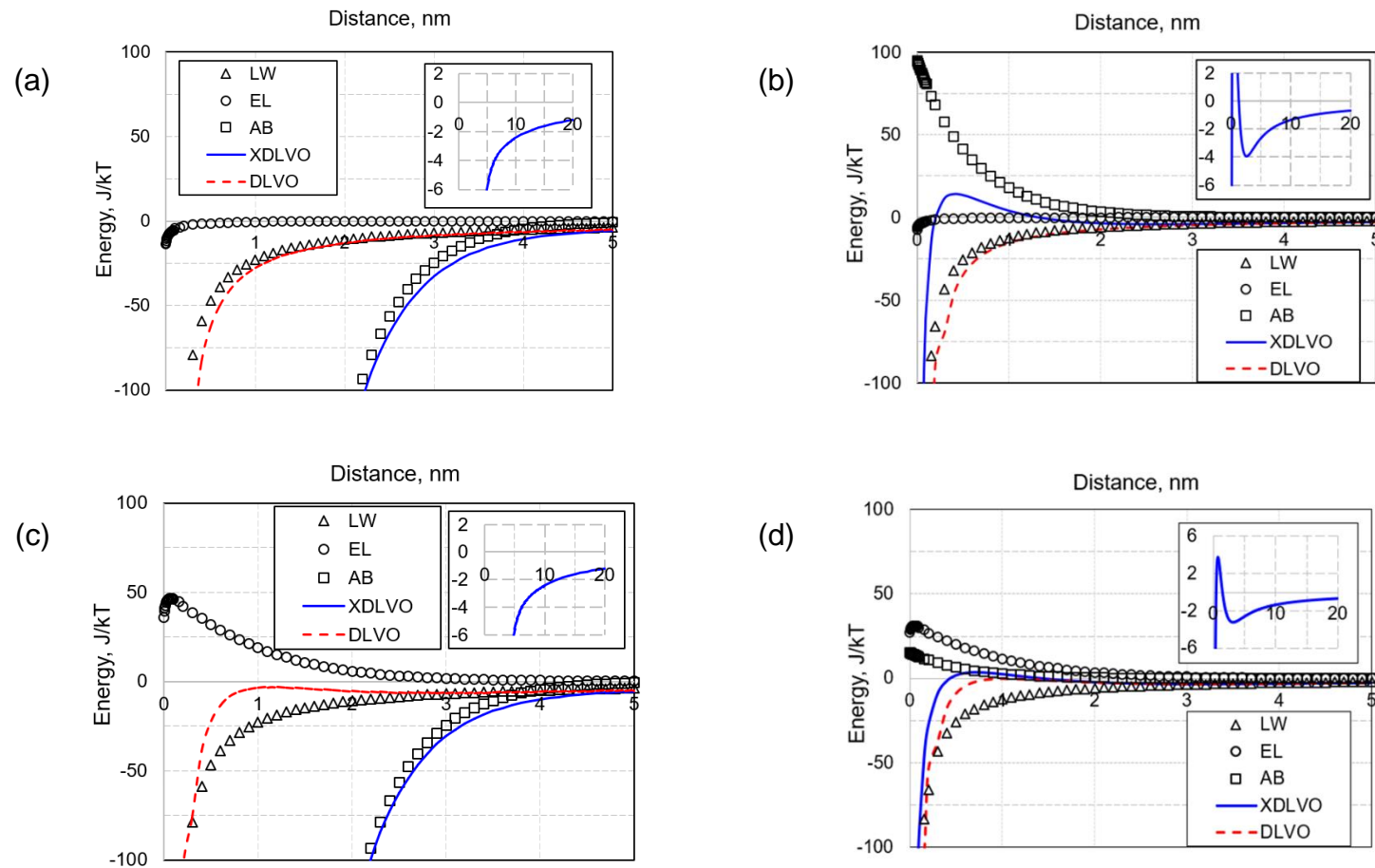


Figure 6. XDLVO energies of the interaction of human adenovirus 5 with Carmex lip balm at pH 4.2 (a, b) and pH 7.2 (c, d) in dry (a, c) and hydrated (b, d) states. DLVO and XDLVO energy profiles for HAdV5 interaction with the other three lip balms (Burt's Bees, ChapStick and Vaseline) are given in SM. DLVO total energy is provided for reference.

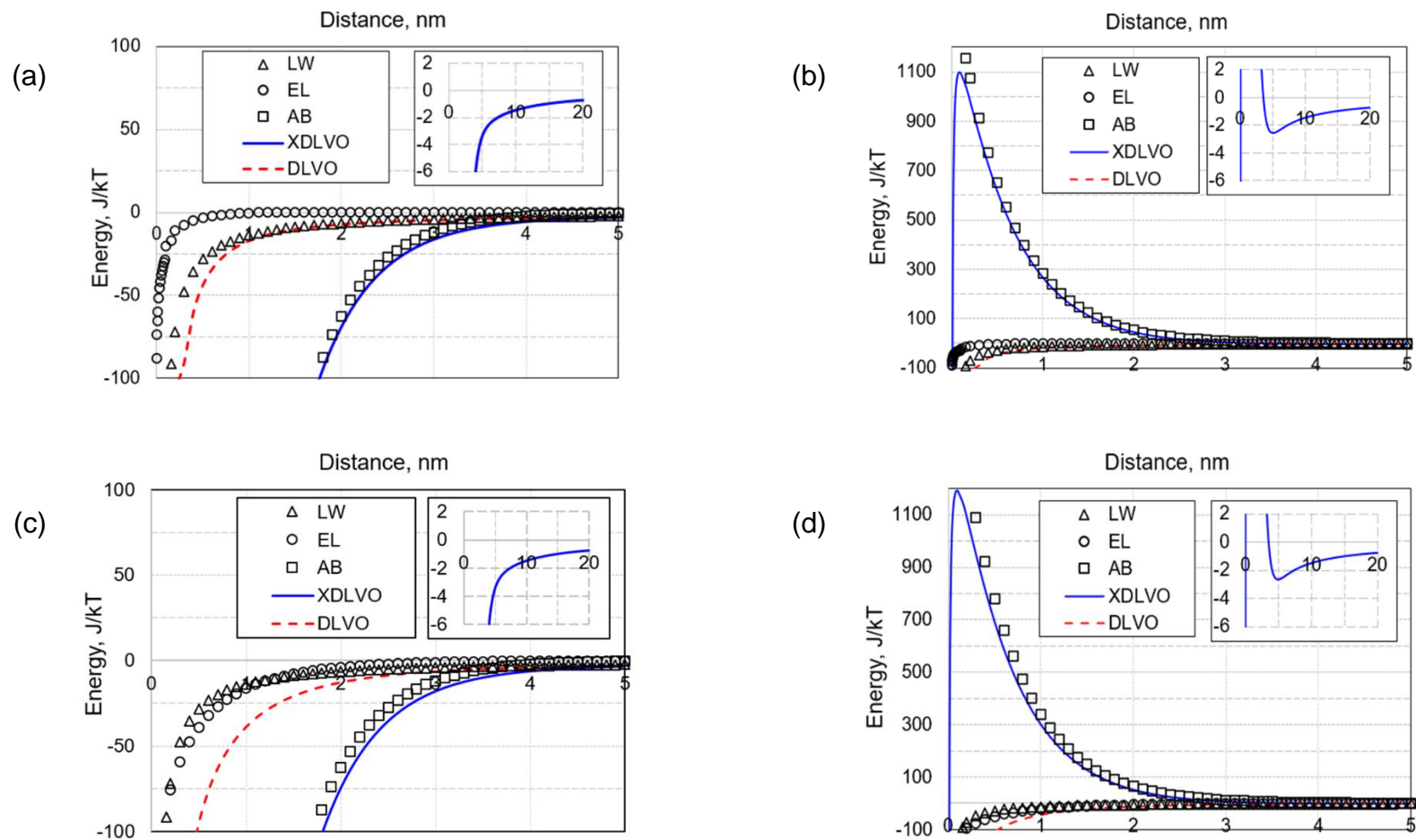


Figure 7. DLVO and XDLVO energies of the interaction of SiO₂ particles with Burt's Bees lip balm at pH 4.2 (a, b) and pH 7.2 (c, d) in dry (a, c) and hydrated (b, d) states. DLVO and XDLVO energy profiles for HAdV5 interaction with the other three lip balms (Carmex, ChapStick and Vaseline) are given in SM. DLVO total energy is provided for reference.

For *hydrated* lip balms, XDLVO modeling gives a more nuanced prediction. Across the 20 colloid/lip balm combinations evaluated in this work, interaction energy profiles covered a range E_{max} (zero to thousands kT) and E_{min} (zero to ~ 4 kT) values (Table 2; Fig. 6, Fig. 7, A14-A21). Low E_{max} (< several kT) or no primary energy barrier points to the likely irreversible attachment into the primary minimum. If the primary energy barrier (E_{max}) is high, deposition into the secondary minimum, provided it exists, is possible. Deposition into a secondary minimum is reversible and is stronger (or less reversible) for deeper minima. In the case of SiO₂, hydrating Burt's Bees lip balm flipped its short-range interaction with the colloids from strongly attractive to strongly repulsive (Fig. 7a vs Fig. 7b, Fig. 7c vs Fig. 7d). At the same time, hydration did not have the same dramatic effect on the lip balm's interaction with HAdV5 (Fig. 6a vs Fig. 6b, Fig. 6c vs Fig. 6d). The contrast in the predicted total energy of interaction with hydrated lip balm (attractive interaction with HAdV5 virions versus strongly repulsive interaction with SiO₂ colloids) underscores the importance of the physicochemical properties of the colloids.

2.4.5 Attachment of SiO₂ colloids and HAdV5 virions to lip balm-coated surfaces: Preliminary QCM-D study

To our knowledge, there have been no prior studies of particle adhesion to lip balms or other similar lipophilic personal care products. Establishing the experimental methodology for such measurements was one of the goals of this work. To study deposition onto dry lip balms one would need to work with aerosols and address the number of issues related to the transient processes of droplet evaporation and hydration

of the surface upon droplet deposition. The preliminary tests performed in this study were restricted to particle deposition from an aqueous solution onto hydrated lip balms. Longer term QCM-D deposition data were obtained for two colloid/lip balm pairs: SiO₂/Burt's Bees and HAdV5/Carmex.

Silica was selected to avoid any uncertainty related to any other suspended materials possibly present in the feed stock. The conditions of the QCM-D tests with SiO₂/Burt's Bees pair were not conducive to adhesion relative to other pairs (e.g. involving HAdV5 and 40) and could be viewed as a conservative estimate of the extent of particle adhesion to lip balms.

The first test was performed using a 1.05 mg(SiO₂)/ml suspension (Fig. 8a). QCM-D frequency data indicated significant deposition (Fig. 8). The monotonous increase in the dissipation signal was consistent with the deposition of colloids onto the lip balm.

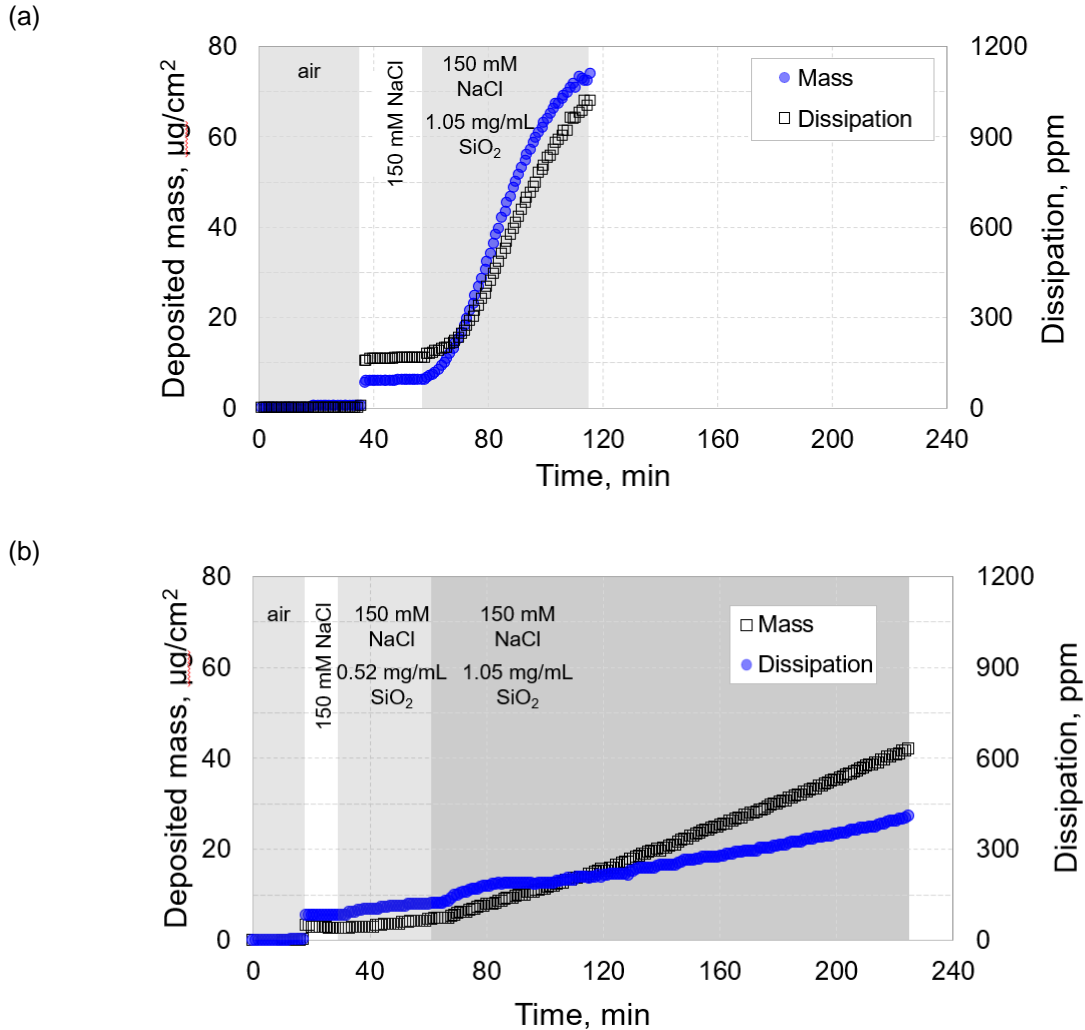


Figure 8. QCM-D measurements of the deposition of SiO₂ colloids onto hydrated Burt's Bees lip balm under conditions when SiO₂ loading is either a) constant (1.05 mg/ml) or b) increases stepwise from 0.52 mg/ml to 1.05 mg/ml. In both tests, deposition occurs from 150 mM NaCl electrolyte at pH 7.2. The mass values are calculated based on Sauerbrey equation (eq. (3)) with $n = 3$. The results for $n = 5$ are shown in SM (Fig. 32).

The total mass of deposited SiO₂ (65 μg) was $\sim 0.7\%$ of the mass flown (~ 9.4 mg) over the lip balm-coated sensor. In early stages of the experiment when the lip balm surface was relatively SiO₂-free, the deposition was determined by SiO₂-lip balm interactions. The surface loading of 74 $\mu\text{g}(\text{SiO}_2)/\text{cm}^2$ recorded ~ 1 h into QCM-D test (Fig. 8a) is equivalent to ~ 3 monolayers of colloids. We speculate that this relatively large amount

of SiO₂ deposited despite repulsive SiO₂-SiO₂ interactions can be due to the partial “burial” of SiO₂ in the soft hydrated surface of the lip balm. At pH 7.2, SiO₂ and Burt’s Bees balm have surface charges of opposite signs (-36 mV and 10 mV, respectively; Fig. 5b) so that electrostatic interactions between these surfaces are favorable. The hydrophobic interactions are strongly repulsive because SiO₂ and hydrated Burt’s Bees are both hydrophilic (Table 1, Fig. 4). As a result, XDLVO predicts a very high (> 1000 kT) primary barrier and a shallow (~ 2.6 kT) secondary minimum (Table 3, Fig. 7d). We conclude that SiO₂ deposition occurred into the secondary minimum and should be reversible.

In a companion test (Fig. 8b) on SiO₂ deposition, the lip balm-coated sensor was charged for 30 min with a two-times less concentrated SiO₂ suspension (0.52 mg(SiO₂)/ml) before reverting to the same feed as in test 1 (1.05 mg(SiO₂)/ml). A much weaker deposition was observed throughout the test. At the end of the first stage, the deposit was a submonolayer with the average distance between deposited particles of ~ 0.38 μm (~ 2 particle diameters). At the end of the long (160 min) second stage, the mass of deposited particles was smaller than in the first test even though the total mass of SiO₂ introduced into the QCM-D chamber in test 2 was higher. The total mass of SiO₂ deposited during test 2 (38 μg) was ~ 0.14% of the mass flown (27.5 mg) over the lip balm-coated sensor. We conclude that the deposition history is important and that the total mass load of colloids that a lip balm surface is exposed to cannot be a sole predictor of the extent of deposition.

QCM-D tests with HAdV5 were done using as-purchased highly purified stock with HAdV5 concentration of 10^9 GC/mL and Carmex lip balm. Even when undiluted, the mass concentration of HAdV5 stock (~ 0.76 $\mu\text{g/mL}$) was ~ 680 times smaller than that of the silica suspension in QCM-D tests with SiO_2 . Indeed, a much smaller deposited mass was measured for HAdV5, accompanied by a weaker dissipation signal (Fig. 9). The total mass of deposited HAdV5 (~ 2.4 μg) was ~ 10.6 % of the mass flown (~ 22.8 μg) over the lip balm-coated sensor. The % deposited value is significantly higher than that for SiO_2 colloids, which is consistent with the much smaller primary energy barrier, E_{max} : 5.2 kT for HAdV5/Carmex versus 1337 kT for SiO_2 /Burt's Bees (Table 2). The secondary minimum, E_{min} , was also deeper for HAdV5/Carmex (- 3.1 kT) than for SiO_2 /Burt's Bees (- 2.6 kT). We attribute the stronger (relative to the mass loading) deposition of HAdV5 to a more likely association with the lip balms surface through the secondary energy minimum and a possible irreversible attachment into the primary minimum.

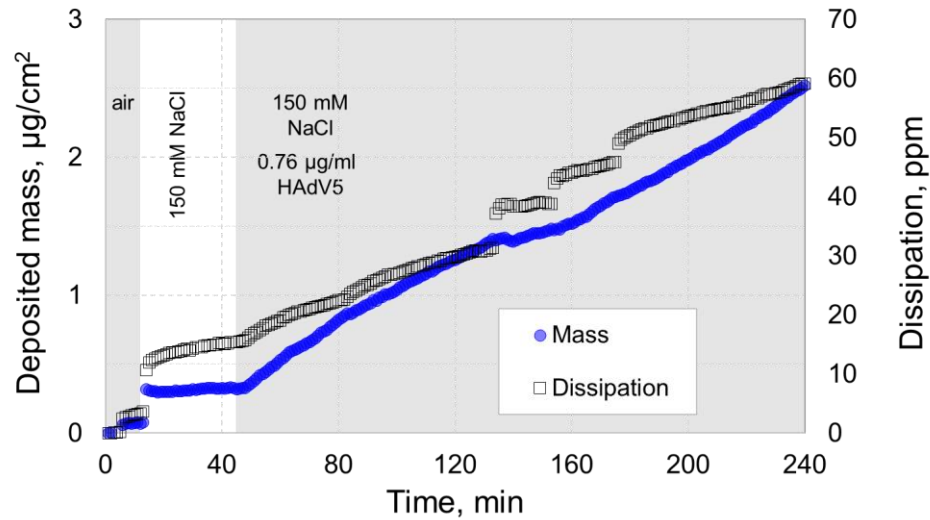


Figure 9. QCM-D measurements of the deposition of human adenovirus 5 onto hydrated Carmex lip balm from 150 mM NaCl electrolyte at pH 7.2. HAdV5 concentration in the QCM-D feed is ~ 109 GC/mL (~ 0.76 $\mu\text{g/mL}$). The mass values are calculated based on Sauerbrey equation (eq. (3)) with $n = 3$. The results for $n = 5$ are shown in SM (Fig. 33).

Higher mass concentrations in the feed are required for a higher QCM-D signal. To more accurately assess the mass flux towards the sensor surface for a given mass concentration in the feed, one would need to quantify the mass transfer of colloids to the depositional plane. This requires solving the Graetz problem of diffusion-limited transport to a surface from a crossflow [62, 63]. In the absence of such solution, the best approach is to employ virus stocks with as high virus titer as possible while still of high purity.

2.4.6 Implications for virus control and public health protection

The results reported in this work indicate that dry lip balm can serve as a “hot spot” for virus deposition. Given the intended application of lip balms, there is a clear risk to the health of individuals using these products. Low humidity environments (e.g. typical for long air travel) are of particular concern as they promote dehydration. Designing materials to retain surface moisture is one possible approach to staving off adhesion of colloids to lip balms and similar products. A multilayer design with a lipophilic core and a hydrophilic outer layer is one possible strategy.

Likely contagion scenarios should be identified and studied. Possible routes include ingestion of lip balm with associated viruses, ingestion of saliva laden with viruses detached from lip balm, and breathing in viruses resuspended from the lip balm surface into the flow of inhaled air. Given the importance of surface interactions, there is likely a difference between non-enveloped viruses (e.g., adenoviruses, coxsackieviruses, rotavirus) and enveloped viruses (influenza H1N1, human coronaviruses, herpesviruses, hepatitis C) in their propensity to adhere to a lipophilic surface. Future work should explore deposition from other relevant media (e.g. air, respiratory fluid) and onto other surfaces (face and hand creams) as well as virus resuspension into saliva, common drinks (e.g. low pH sodas, milk) and relevant fluid flows (e.g. breathed air).

2.5 Conclusions

The study reports a protocol for preparing lip balm coatings to enable charge and surface energy measurements as well as adhesion studies with these materials. Surface charge and hydrophobicity were determined for four brands of lip balms. Also measured were size, charge and hydrophobicity of human adenovirus 5. The measured values were used in XDLVO modeling of adenovirus adhesion to lip balms. Adhesion of four other colloids (HAdV40, MS2 and P22 bacteriophages and SiO₂) spanning a range of sizes, charges and surface energies was also evaluated.

The study tested the hypothesis that a drying-induced increase in lip balm hydrophobicity enhances virus adhesion due to strong hydrophobic colloid-surface interactions. Indeed, drying was shown to result in a dramatic decrease of surface energy ($\delta(\Delta G_{sws}) \geq 83.0 \text{ mJ/m}^2$) of lip balms making their surfaces highly hydrophobic. XDLVO modelling predicts that attachment to a dry lipstick ($\Delta G_{sws} < -65 \text{ mJ/m}^2$) is highly favorable as a result of strong short-range hydrophobic attraction. Lip balms hydrated in a solution with the ionic strength of human saliva are hydrophilic ($\Delta G_{sws} > 15 \text{ mJ/m}^2$) and resist colloid attachment. Physicochemical properties of colloids are also important. Adhesion occurs into shallow secondary minima for hydrophilic colloids such as SiO₂, MS2 and P22. Because of the hydrophobicity of adenoviruses, primary maxima in XDLVO profiles are low or non-existent making irreversible deposition into primary minima possible. Preliminary QCM-D tests with SiO₂ colloids and human adenovirus 5 confirm deposition even on a hydrated lip balm.

Prior work focused on virus adhesion to human skin [2-8], or, in two instances [6, 7], employed freshly applied Vaseline as a adhesion barrier for MS2. The present work extends these earlier investigations to study virus adhesion to lipophilic personal care products. The proposed methodology can help direct the compositional design of lip balms and similar materials and develop usage guidelines to minimize virus adhesion. Future work should explore deposition from other relevant media (e.g. air, respiratory fluid) and onto other surfaces (e. g. hand creams) as well as virus resuspension into saliva, common drinks (e.g. low pH sodas, milk) and relevant fluid flows (e.g. breathed air).

Acknowledgements

This material is based upon work supported in part by the National Science Foundation Partnerships for International Research and Education program under Grant IIA-1243433 and in part by the Center for European, Russian and Eurasian Studies at Michigan State University. We thank Dr. Hang Shi (CTI and Associates, Inc.), Dr. Irene Xagorarakis (Civil and Environmental Engineering, Michigan State University) and Dr. Kristin Parent (Biochemistry and Molecular Biology, Michigan State University) for useful discussions as well as to Dr. Wei Zhang (Department of Plant, Soil and Microbial Sciences, Michigan State University) for providing access to Malvern Zetasizer Nano ZS. We are also thankful to Mrs. Carol Flegler (Center for Advanced Microscopy, Michigan State University) for recording SEM images and advising on appropriate sample

preparation procedures.

APPENDIX

APPENDIX

A1. SEM imaging of lip balm coatings

The low vacuum (LV) mode enables examination of non-conducting samples or volatile samples up to a vapor pressure of 270 Pa [64]. While the main components of lip balm are petrolatum and petroleum, many other ingredients may be present (Table 4). The vapor pressure of petrolatum is 1.3 Pa, while for petroleum the value is in the 30 to 60 Pa range [65]. These values fall within the safety range of the JEOL 6610 LV operated in the LV mode. However, lip balm may contain components (e.g. volatile oils) with vapor pressures above the upper limit of the LV range. To avoid potential damage to the microscope, osmium tetroxide (OsO_4) vapor fixation was employed to stabilize lip balm samples. OsO_4 reacts with the double bonds of lipids and oils and increases their vapor pressure [66]. After 5 days of exposure to OsO_4 vapor, lip balm samples turned slightly darker, which indicated that the reaction did occur.

A2. QCM-D sensor cleaning procedure

QCM-D sensors were cleaned by following the procedure recommended by the manufacturer. After each experiment, the sensors were soaked in a 5:1:1 mixture (RCA-1 cleaning protocol [67]) of DI water, hydrogen peroxide (30 wt%) and ammonia (25 wt%) at 75 °C for 5 min, sonicated in DI water overnight, rinsed thoroughly with DI water, dried with high-purity N_2 and treated in a UV/ozone chamber (UV/ozone Procleaner™, Bioforce Nanosciences) for 60 min.

A3. Additional information on Human Adenovirus 5 (ATCC® VR-1516™)

The Adenovirus Reference Material [68] contains purified Adenovirus Type 5 formulated as a sterile liquid in 20 mM TRIS, 25 mM NaCl, 2.5% glycerol, pH 8.0 at room temperature, and stored frozen at -70 °C. The U.S. Food and Drug Administration has recommended using the Adenovirus Reference Material when characterizing adenoviral gene therapy products [69]. As stated by the supplier, the viability “is warranted for 30 days from the date of shipment” [70]. In all experiments described in this work, the virus was used within this time frame.

A4. Protocols of lip balm processing evaluated in the study

To produce a thin and homogenous layer of coating on sensors for QCM-D measurement, four different preparation protocols A, B, C, D were designed and evaluated. In protocol A (Fig. 1), a grain of lip balm was cut, put it in a vial, and melted on a heater. After the sample was liquified, it was coated on the QCM-D sensors. However, because of a very high viscosity of the melted sample it was difficult to produce a homogenous layer with a proper thickness for QCM-D measurement. Because of a high solidification point of the sample. it turned solid quickly upon contact with the sensor surface. It was also found that heating the sensor prior to the contact with the melted lip balm did not help achieve coatings of acceptable quality. In order to prepare a lip balm sample with appropriate viscosity for spin-coating, a solvent was

needed. Of the five solvents evaluated (ethyl acetate, isopropanol, methanol, pentane, hexane, and petroleum distillate), petroleum distillate yielded the most homogenous lip balm solution. After lip balm was melted and mixed with petroleum distillate, the mixture was stirred for 24 h (Protocol C, Fig. 1). Protocol C successfully produced lip balm solution with proper viscosity for spin-coating. However, the added material changed the surface free energy of lip balm sample (Fig. 11). To solve this, the mixture with lip balm and solvent was left in the fume hood for 5 days to remove the residual solvent. The comparison of surface free energy of samples processed with protocol A and B (Fig. 11) indicated that drying in the fume hood for 5 days can effectively remove the solvent. The impact of filtration was also evaluated. Filtration with 0.45 μm filter after dissolution was found to enhance the homogeneity of the sample-solvent mixture, which makes the sample layer on QCM-D sensors more homogenous (Protocol D). However, it was found that majority of the sample was rejected by the 0.45 μm filter, which indicated that filtration removed most of the components from the sample. Therefore, protocol D was not employed for the sample processing.

A5. ζ -potential measurements of HAdV5

In the study by Trilsky and Lenhoff [8], the following 20 mM buffers were used in measurements of ζ -potential and aggregation of HAdV5 as a function of pH: acetate buffer for pH 3.8, 4.5 and 5; MES for 5.5 < pH < 6.7; HEPES for pH 7.8 and for pH 7.5 and 8.5; ethanolamine for pH 8.5 and 10. In that study, no additional salt was employed in order to keep the ionic strength (I) minimal because ζ peaks widen with increasing I .

Also, at a lower I , the likelihood of electrolysis of the gold-plated electrodes of the folded capillary cell is lower. The gold plating from the electrodes tends to contaminate the sample at low pH and/or high. Trilsky and Lenhoff determined the ζ potential of HAdV5 using light scattering (Zetasizer Nano ZS particle analyzer, Malvern Instruments ZEN3600) and folded capillary cells (Malvern DTS1060). The ζ potential was found from the electrophoretic mobility using Henry's equation [71].

In contrast, our study employed 0.1 mM KCL as the background electrolyte. The pH of virus samples was adjusted by KOH and HCl. Firstly, 10 ml mixture of 0.1 mM KCl solution and HAdV5 sample were added into two sterile beakers. Both beakers had 10 ml mixture. Then the pH of the solution in the first beaker was adjusted to 7, 6, 5, 4, 3, and the pH in the second beaker was adjusted to 8, 9, 10 using KOH and HCl. The mobility and ζ -potential of the virus sample was measured (Zetasizer Nano ZS) immediately after each pH adjustment.

A6. XDLVO and DLVO modeling of colloid-lip balm interactions

The DLVO and XDLVO modeling was performed for each colloid/lip balm combination. Results for HAdV5/Burt's Bees and SiO₂/Burt's Bees are given in Figures 6 and 7 in the main manuscripts. Results for the other 18 combinations are given in Figures 13 – 30. Table 7 can be used as a guide to locate the Figures.

Table 3. Concentrations of various electrolytes in human saliva [9].

	$C_{min},$ mM	$C_{max},$ mM	$C_{ave},$ mM	Z	$C_{ave}Z^2,$ mM
Na ⁺	2	21	11.5	1	11.5
K ⁺	10	36	23	1	23
Ca ²⁺	1.2	2.8	2	2	8
Mg ²⁺	0.08	0.5	0.29	2	1.16
Cl ⁻	5	40	22.5	-1	22.5
HCO ₃ ⁻	25	25	25	-1	25
PO ₄ ³⁻	1.4	39	20.2	-3	181.8

Table 4. Composition of the four lip balms evaluated in this work.

Notes:

^A Components marked as “main ingredients” by lip balm manufacturers.

^B Burt Bees includes Lanolin, tocopherol, rosemary, limonene.

ChapStick includes jojoba esters, caprylic / capric triglyceride, tocopheryl acetate, shea butter, octyldodecanol, tocopherol, glyceryl stearate.

Carmex includes lanolin, cetyl esters, theobroma cacao seed butter, paraffinum liquidum, enthol, salicylic acid,

Lip balm	Components							
	Solvents		Oils ^A	Wax ^A	Camphor	Vitamin E	Flavor or fragrance	Other
	Petrolatum ^A	Petroleum ^A						
Burt's Bees			+	+		+		See notes ^B
ChapStick	+		+	+			+	
Carmex	+			+	+		+	
Vaseline		+						None

Table 5. Contact angles (measured), surface energy parameters (calculated), and free interfacial energy of surface-surface interaction in water (calculated) for dry and hydrated lip balm samples and for human adenovirus 5. Lip balm coatings were prepared according to Protocol A (see Fig. 1).

Surface		Contact angles, θ (°)			Surface energy parameters, γ (mJ/m ²)					ΔG_{sws} (mJ/m ²)
		H ₂ O	Glycerol	DID	γ^{LW}	γ^+	γ^-	γ^{AB}	γ^{tot}	
hydrated	Carmex	55.2±1.5	69.0±0.6	37.8±1.0	40.7±0.5	0	38.8±2.7	0	40.7±0.5	17.9±5.0
	ChapStick	60.0±1.5	72.3±0.6	49.5±0.7	34.6±0.4	0	35.4±2.7	0	34.6±0.4	15.3±5.1
	Burt's Bees	58.0±0.6	72.5±0.9	40.8±0.9	39.2±0.5	0	38.2±1.6	0	39.2±0.5	17.7±3.1
	Vaseline	55.5±1.7	78.4±0.5	45.2±0.7	36.9±0.4	0	51.1±3.5	0	36.9±0.4	38.5±6.5
dry	Carmex	77.3±1.3	57.1±0.7	26.4±0.7	45.6±0.3	0.8±0.2	2.8±0.8	2.9±1.3	48.6±1.3	- 65.0±4.0
	ChapStick	86.9±1.4	68.7±0.4	42.4±0.8	38.4±0.4	0.5±0.1	1.4±0.6	1.6±0.7	40.0±0.8	- 72.2±4.5
	Burt's Bees	96.7±1.1	77.0±0.6	40.8±1.7	39.2±0.9	0.1±0.1	0.1±0.1	0.2±0.0	39.4±0.9	- 94.7±4.2
	Vaseline	90.9±1.8	72.1±0.5	30.7±0.8	43.9±0.3	0.1±0.0	0.6±0.5	0.3±0.5	44.3±0.6	- 90.7±6.3
HAdV5		72.3±0.4	70.5±1.2	28.5±1.0	36.1±1.9	0	14.9±1.2	0	36.1±1.9	- 27.7±1.1

Table 6. Contact angles (measured), surface energy parameters (calculated), and free interfacial energy of surface-surface interaction in water (calculated) for three types of lip balm (dry) with four different preparation protocols (A, B, C, and D.) The protocols are described in Fig. 1. Values for protocol A duplicate corresponding values (protocol A) given for dry lip balms in Table 5.

Surface	Protocol	Contact angles, θ (°)			Surface energy parameters, γ (mJ/m ²)					ΔG_{sws} (mJ/m ²)
		H ₂ O	Glycerol	DID	γ^{LW}	γ^+	γ^-	γ^{AB}	γ^{tot}	
Carmex	A	77.3±1.3	57.1±0.7	26.4±0.7	45.6±0.3	0.8±0.2	2.8±0.8	2.9±1.3	48.6±1.3	-65.0±4.0
	B	70.8±1.0	59.1±0.5	32.6±0.8	54.1±1.3	0	7.7±1.0	0	54.1±1.3	-60.3±2.0
	C	73.2±0.5	69.3±1.1	25.1±1.0	38.7±1.8	0	12.5±1.1	0	38.7±1.8	-35.4±1.3
	D	70.5±0.6	67.6±1.4	25.1±0.5	39.4±2.3	0	14.5±1.5	0	39.4±2.3	-30.3±1.5
ChapStick	A	86.9±1.4	68.7±0.4	42.4±0.8	38.4±0.4	0.5±0.1	1.4±0.6	1.6±0.7	40.0±0.8	-72.2±4.5
	B	73.1±0.9	57.9±3.2	32.6±0.8	58.2±2.8	0	5.0±0.9	0	58.2±2.8	-74.2±3.1
	C	70.9±1.7	65.1±1.7	26.1±0.7	39.2±0.9	0	11.8±1.5	0	44.0±1.6	-40.3±1.7
	D	66.6±2.3	60.2±1.7	29.4±1.3	44.5±0.6	0.05±0.1	13.5±2.9	1.7±29.7	46.1±29.7	-34.5±7.5
Burts Bees	A	96.7±1.1	77.0±0.6	40.8±1.7	39.2±0.9	0.1±0.1	0.1±0.1	0.2±0.0	39.4±0.9	-94.7±4.2
	B	95.7±0.9	78.6±1.0	41.6±1.7	40.4±1.9	0	0.4±0.3	0	40.4±1.9	-95.3±3.9
	C	76.9±1.0	76.4±0.1	32.9±0.3	30.2±0.6	0	14.1±1.3	0	30.2±0.6	-27.4±1.0
	D	84.8±2.5	106±0.9	35.9±2.8	3.8±0.8	0	36.9±5.9	0	3.8±0.8	5.8±2.9
Vaseline	A	90.9±0.2	72.1±3.9	30.7±0.8	43.9±0.3	0.05±0.2	0.57±0.6	0.32±0.6	44.3±0.7	-90.7±9.7
	B	84.5±0.8	56.9±2.3	29.1±0.8	44.6±0.3	1.6±0.5	0.22±0.2	1.2±0.7	45.8±0.8	-77.5±5.1
	C	71.5±2.5	63.9±1.1	25.1±0.9	46.3±2.7	0	10.3±2.9	0	46.3±2.7	-46.4±3.7
	D	73.1±2.4	67.6±2.8	25.1±0.5	41.4±5.0	0	11.2±3.7	±	41.4±5.0	-40.5±4.6

Table 7. Guide to Figures with results of XDLVO modeling. Two of the 20 Figures are shown in the main manuscript while the other 18 are shown in the SM file.

		Lip balms			
		Carmex	ChapStick	Burt's Bees	Vaseline
Colloids	HAdV5	Figure 6	Figure 15	Figure 14	Figure 16
	HAdV40	Figure 17	Figure 18	Figure 19	Figure 20
	P22	Figure 21	Figure 22	Figure 23	Figure 24
	MS2	Figure 25	Figure 26	Figure 27	Figure 28
	SiO₂	Figure 29	Figure 30	Figure 7	Figure 31

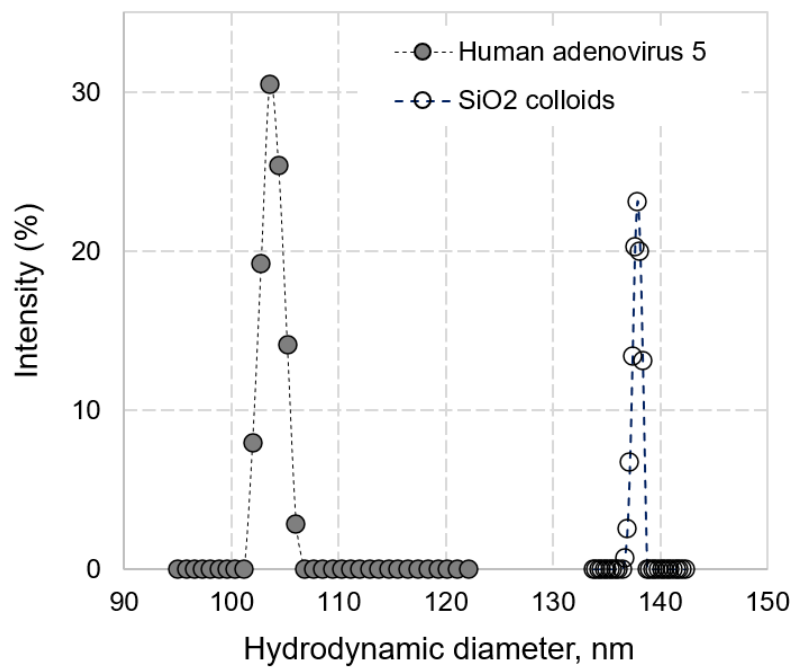


Figure 10. Particle size distribution in the stock HAdV5 and ST-ZL SiO₂ suspensions. Lines are added to guide the eye.

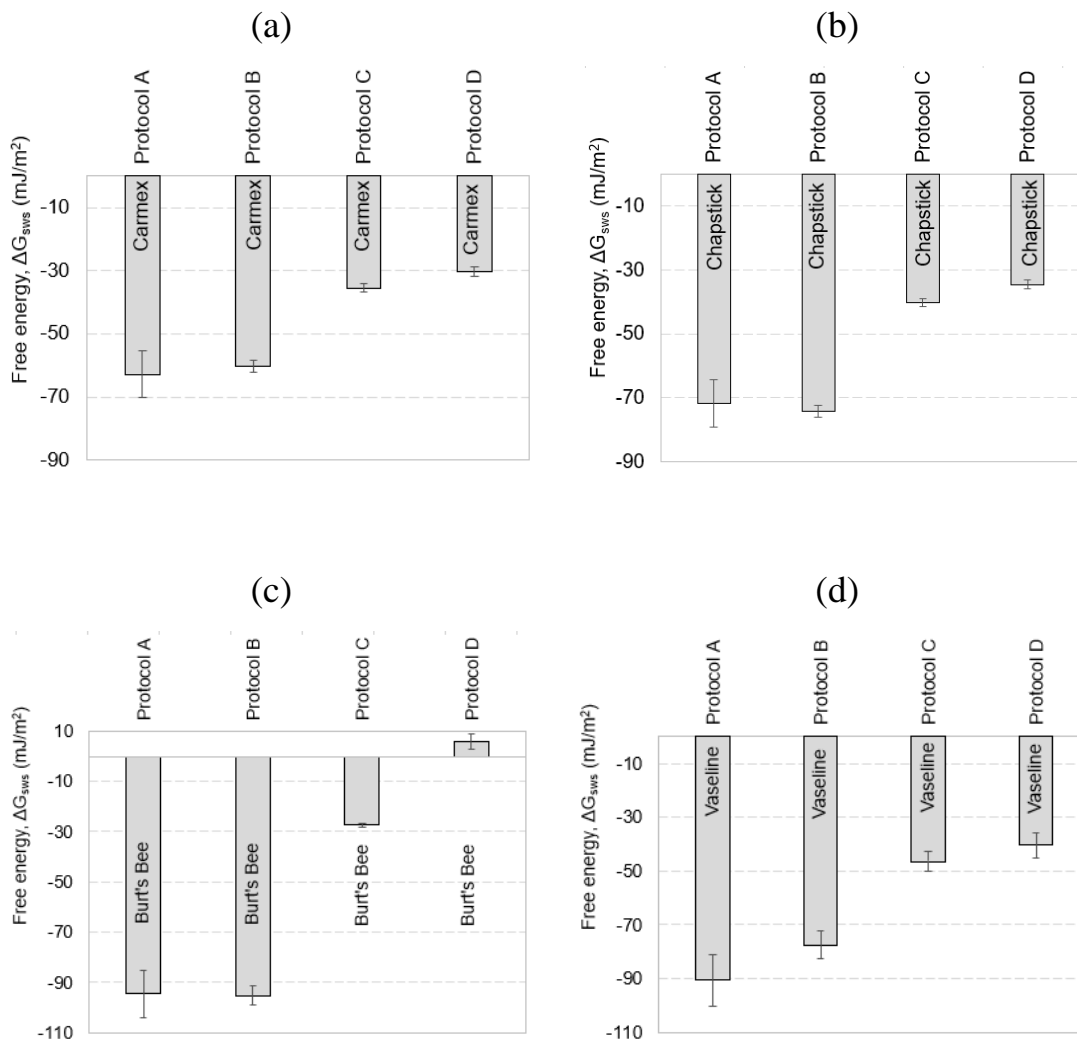


Figure 11. Free energy of interaction in water for three types of lip balm as a function of surface preparation method (see Fig. 1).

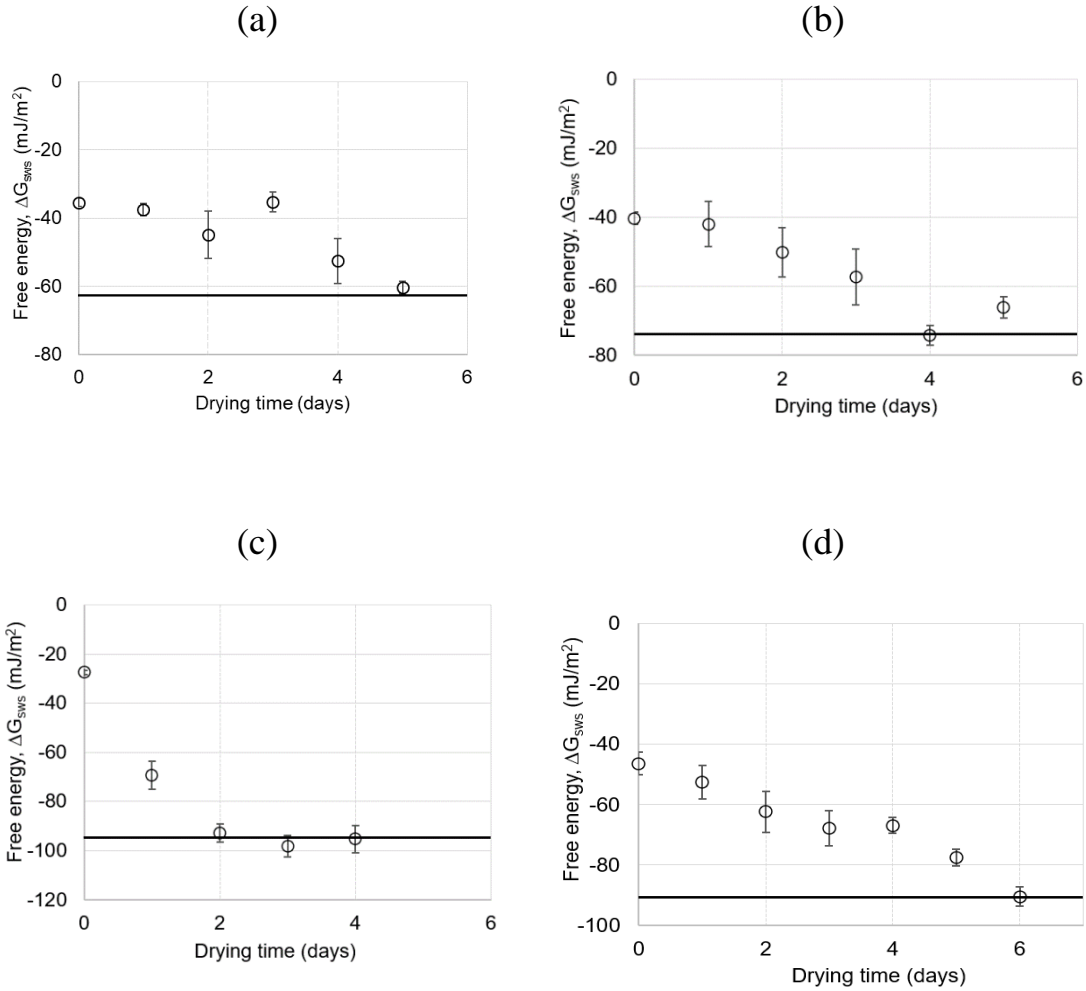


Figure 12. Free energy, ΔG_{sWS} , for four lip balms as a function of drying time: a) Carmex; b) Chapstick, c) Burt's Bees, d) Vaseline. Lip balms coatings were prepared using protocol B. In each graph, the solid line corresponds to the surface prepared using protocol A (melted lip balm with no dissolution and drying steps involved), which was used as the baseline: a) 65.03 mJ/m^2 for Carmex, b) -72.18 mJ/m^2 for Chapstick, c) -95.62 mJ/m^2 for Burt's Bees. d) -90.71 mJ/m^2 for Vaseline. Measured contact angles used to calculate ΔG_{sWS} values are given Table 6.

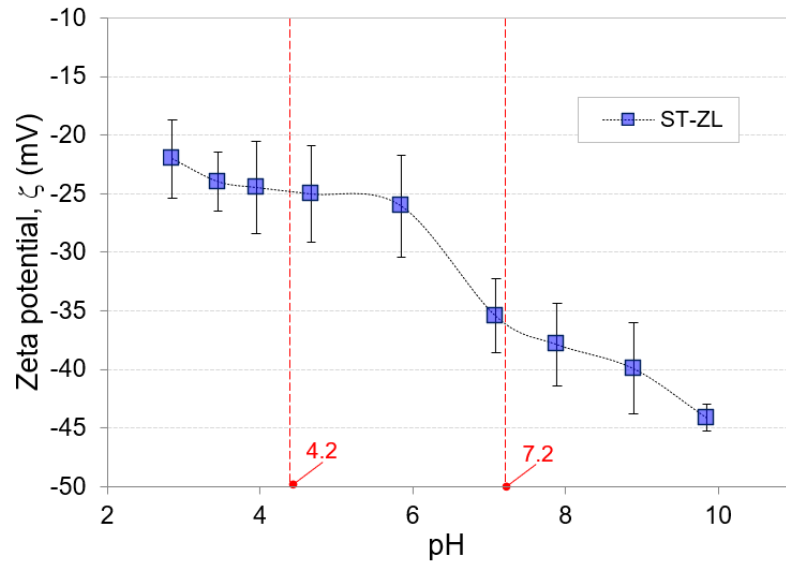


Figure 13. Surface charge of ST-ZL SiO₂ colloids as a function of pH. Vertical dashed lines indicate pH values (4.2 and 7.2) used in QCM-D measurements of SiO₂ attachment to lip balm surfaces. Lines connecting experimental data points are added to the guide the eye.

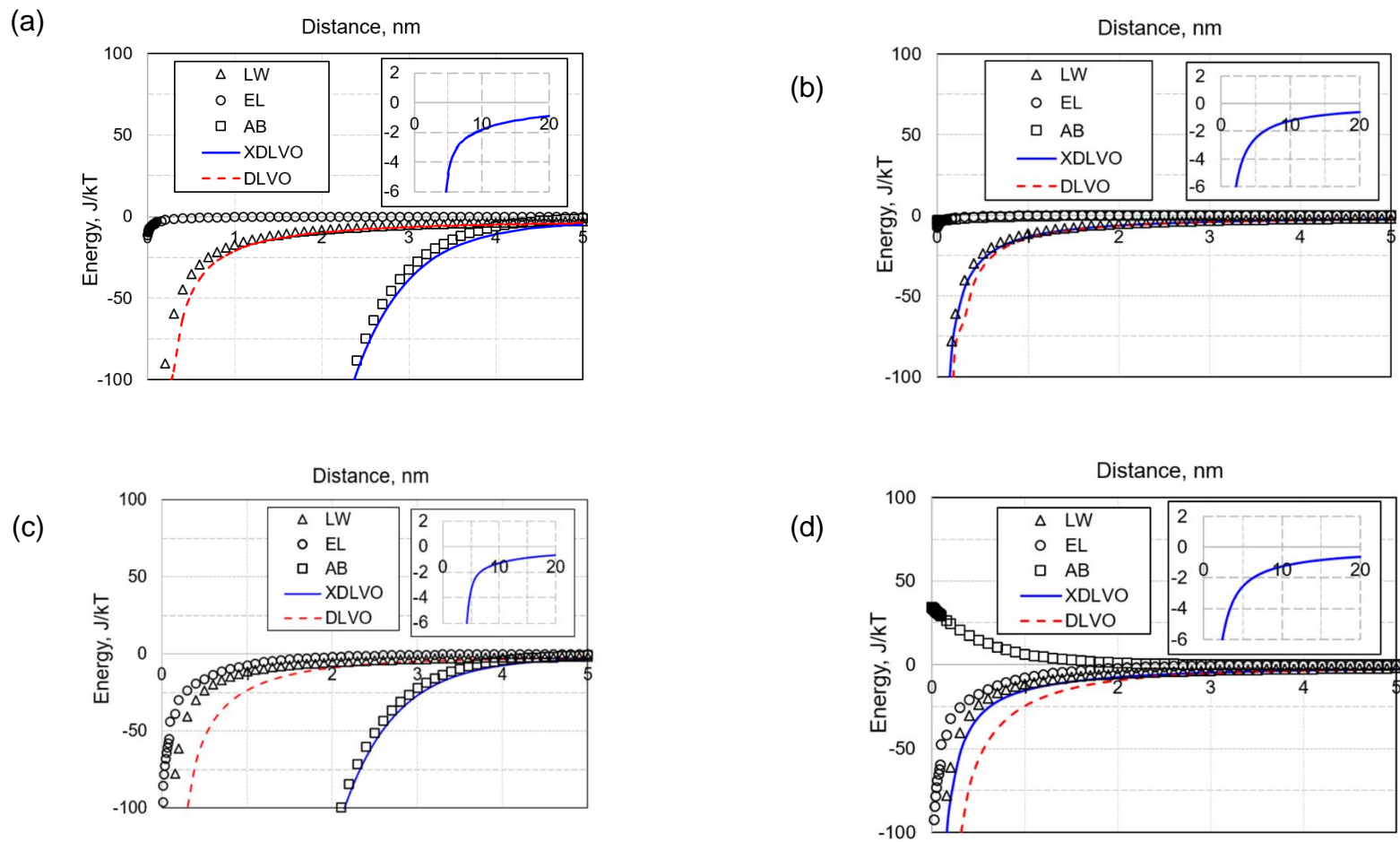


Figure 14. XDLVO energy of interaction of human adenovirus 5 with Burt's Bees lip balm at pH 4.2 (a, b) and pH 7.2 (c, d) in dry (a, c) and hydrated (b, d) states. DLVO total energy is provided for reference.

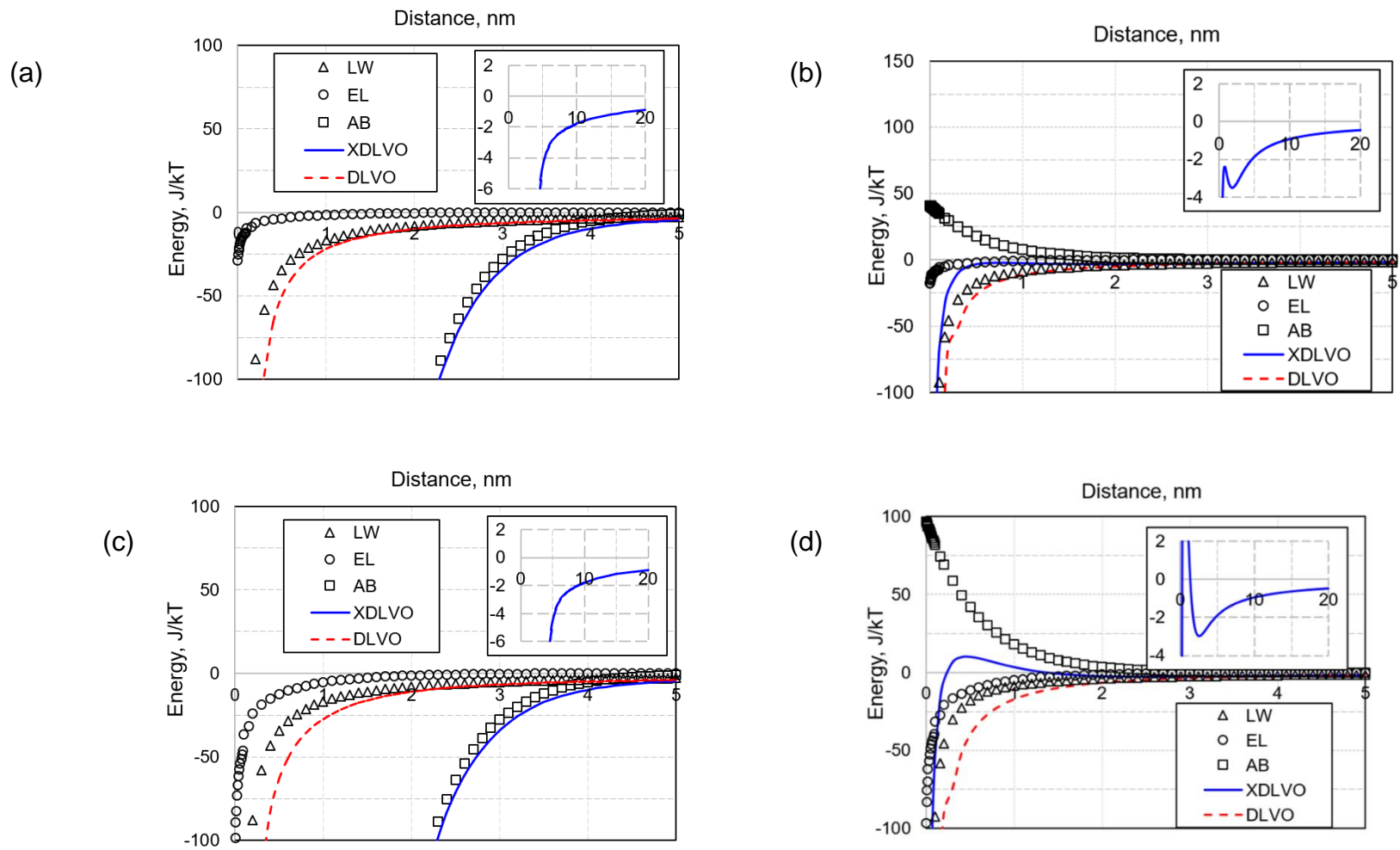


Figure 15. XDLVO energy of interaction of human adenovirus 5 with ChapStick lip balm at pH 4.2 (a, b) and pH 7.2 (c, d) in dry (a, c) and hydrated (b, d) states. DLVO total energy is provided for reference.

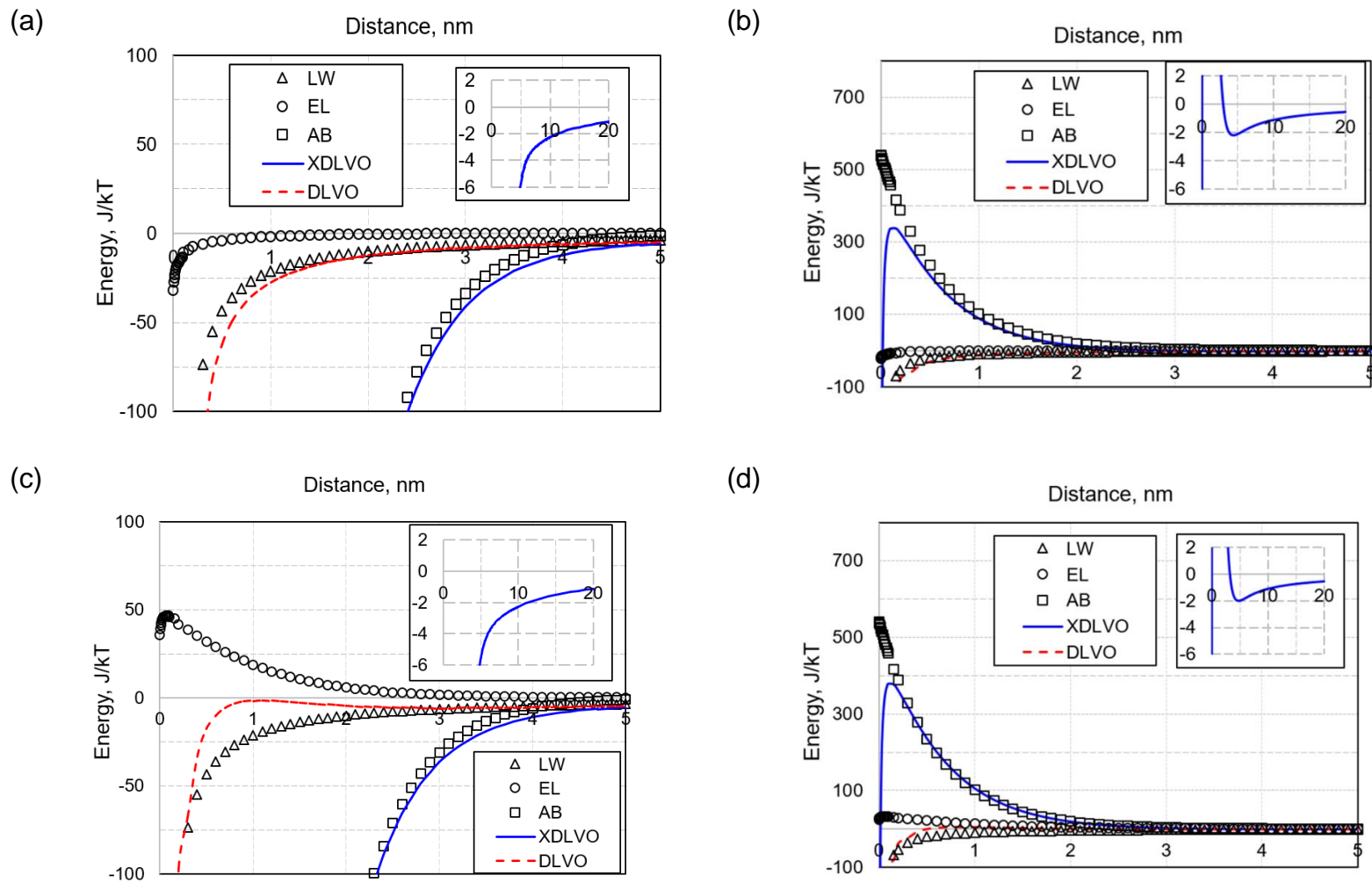


Figure 16. XDLVO energy of interaction of human adenovirus 5 with Vaseline lip balm at pH 4.2 (a, b) and pH 7.2 (c, d) in dry (a, c) and hydrated (b, d) states. DLVO total energy is provided for reference.

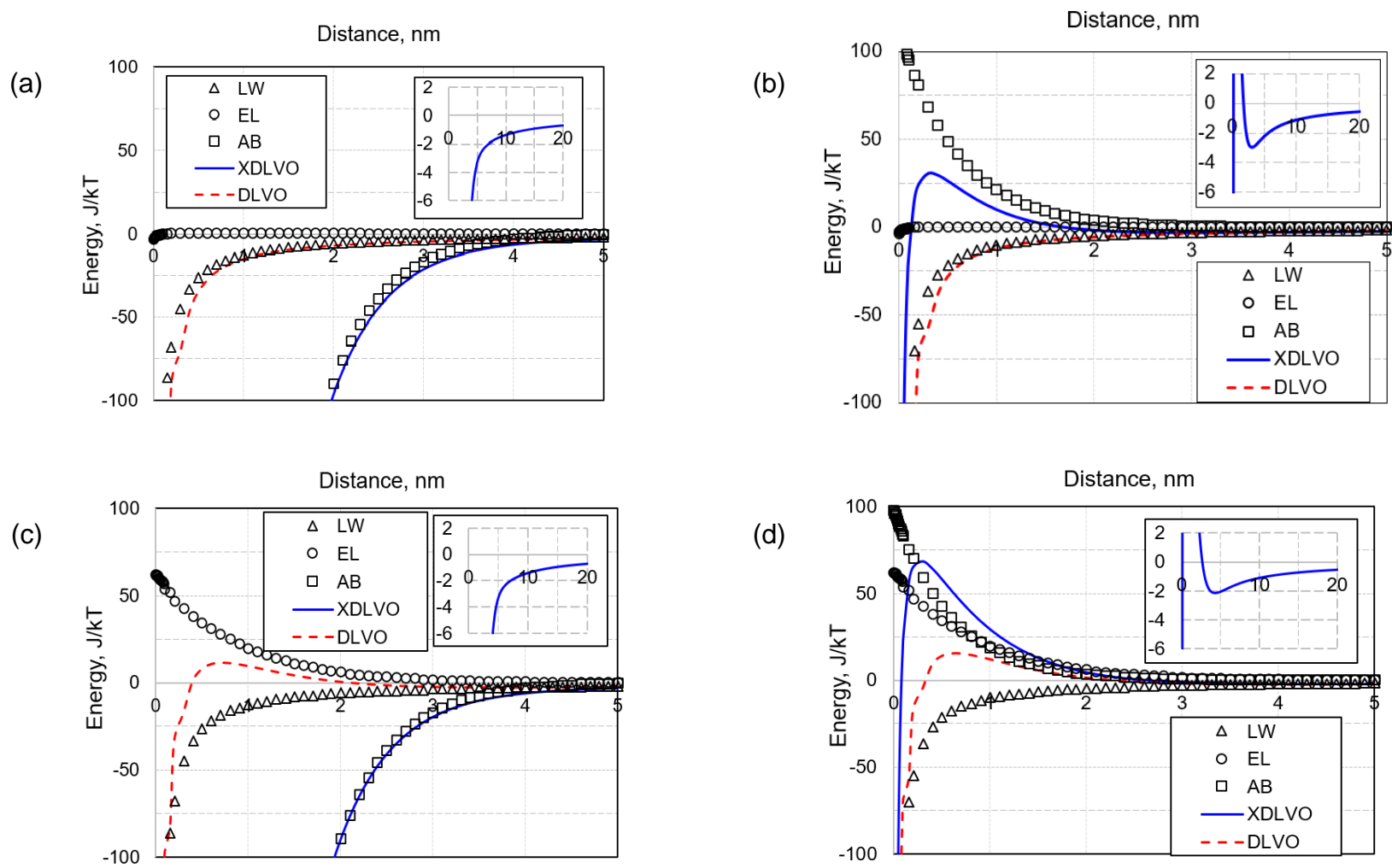


Figure 17. XDLVO energy of interaction of human adenovirus 40 with Carmex lip balm at pH 4.2 (a, b) and pH 7.2 (c, d) in dry (a, c) and hydrated (b, d) states. DLVO total energy is provided for reference.

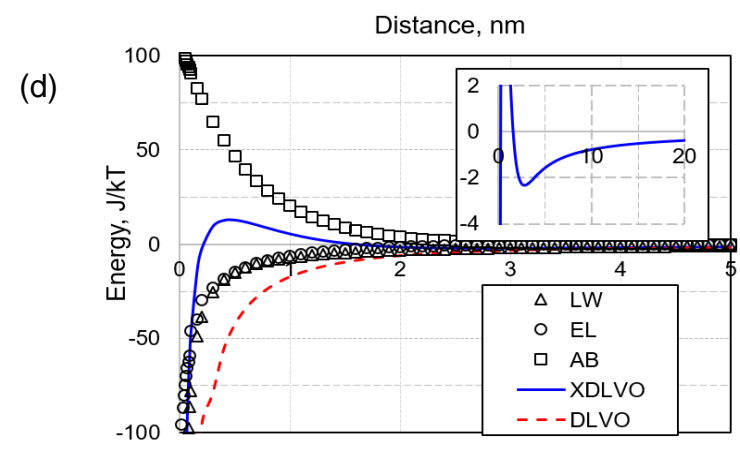
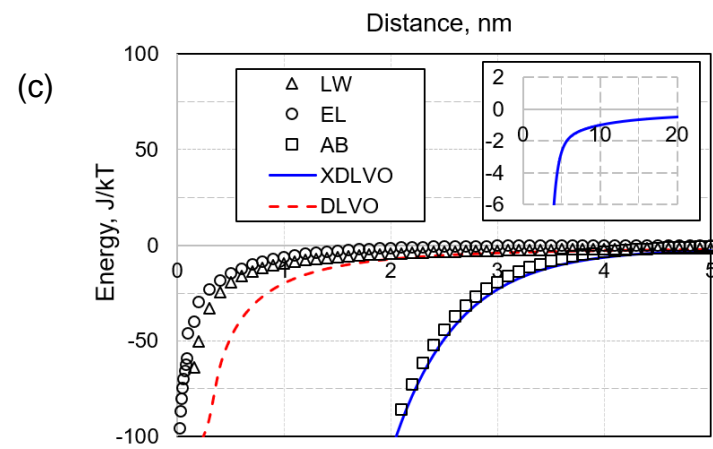
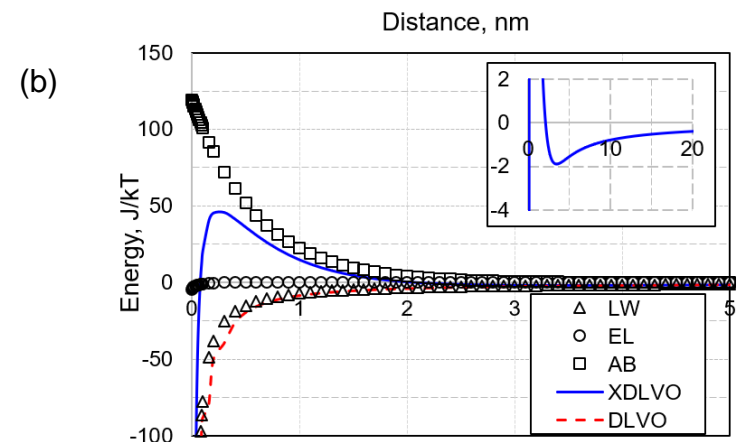
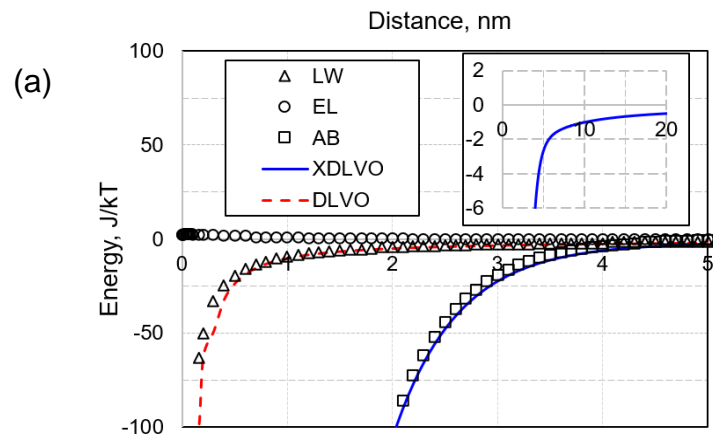


Figure 18. XDLVO energy of interaction of human adenovirus 40 with Chapstick lip balm at pH 4.2 (a, b) and pH 7.2 (c, d) in dry (a, c) and hydrated (b, d) states. DLVO total energy is provided for reference.

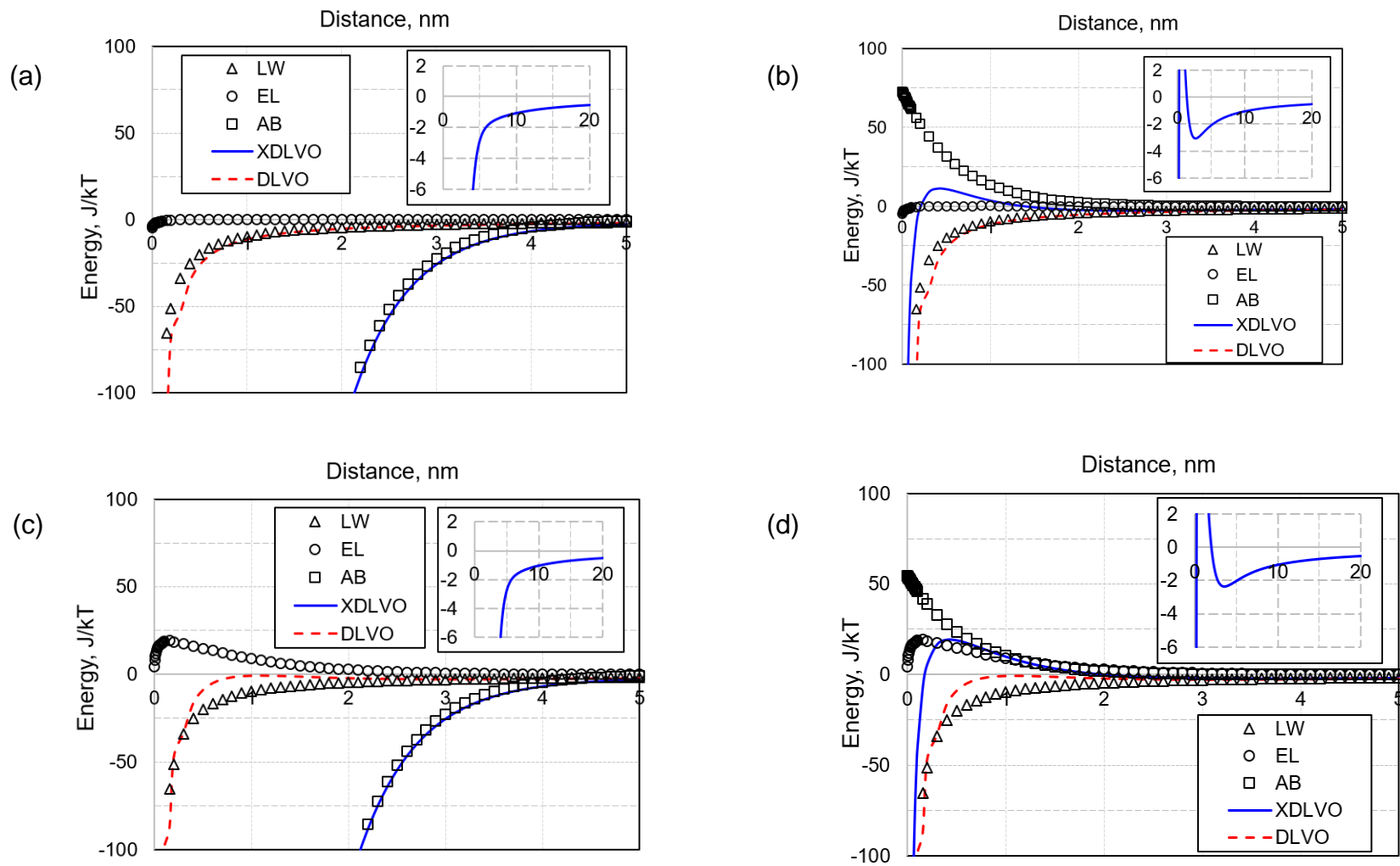


Figure 19. XDLVO energy of interaction of human adenovirus 40 with Burt's Bees lip balm at pH 4.2 (a, b) and pH 7.2 (c, d) in dry (a, c) and hydrated (b, d) states. DLVO total energy is provided for reference.

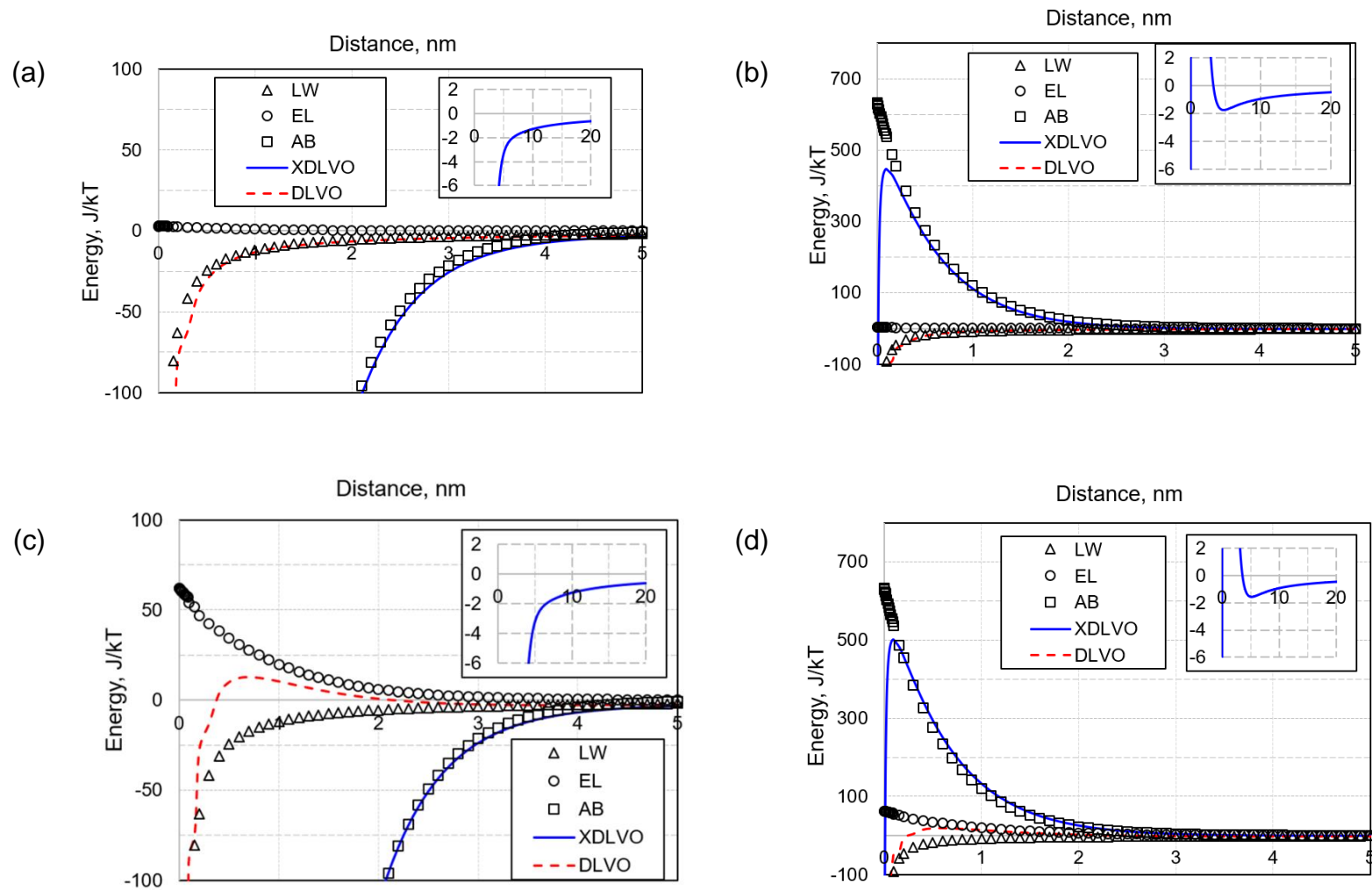


Figure 20. XDLVO energy of interaction of human adenovirus 40 with Vaseline lip balm at pH 4.2 (a, b) and pH 7.2 (c, d) in dry (a, c) and hydrated (b, d) states. DLVO total energy is provided for reference.

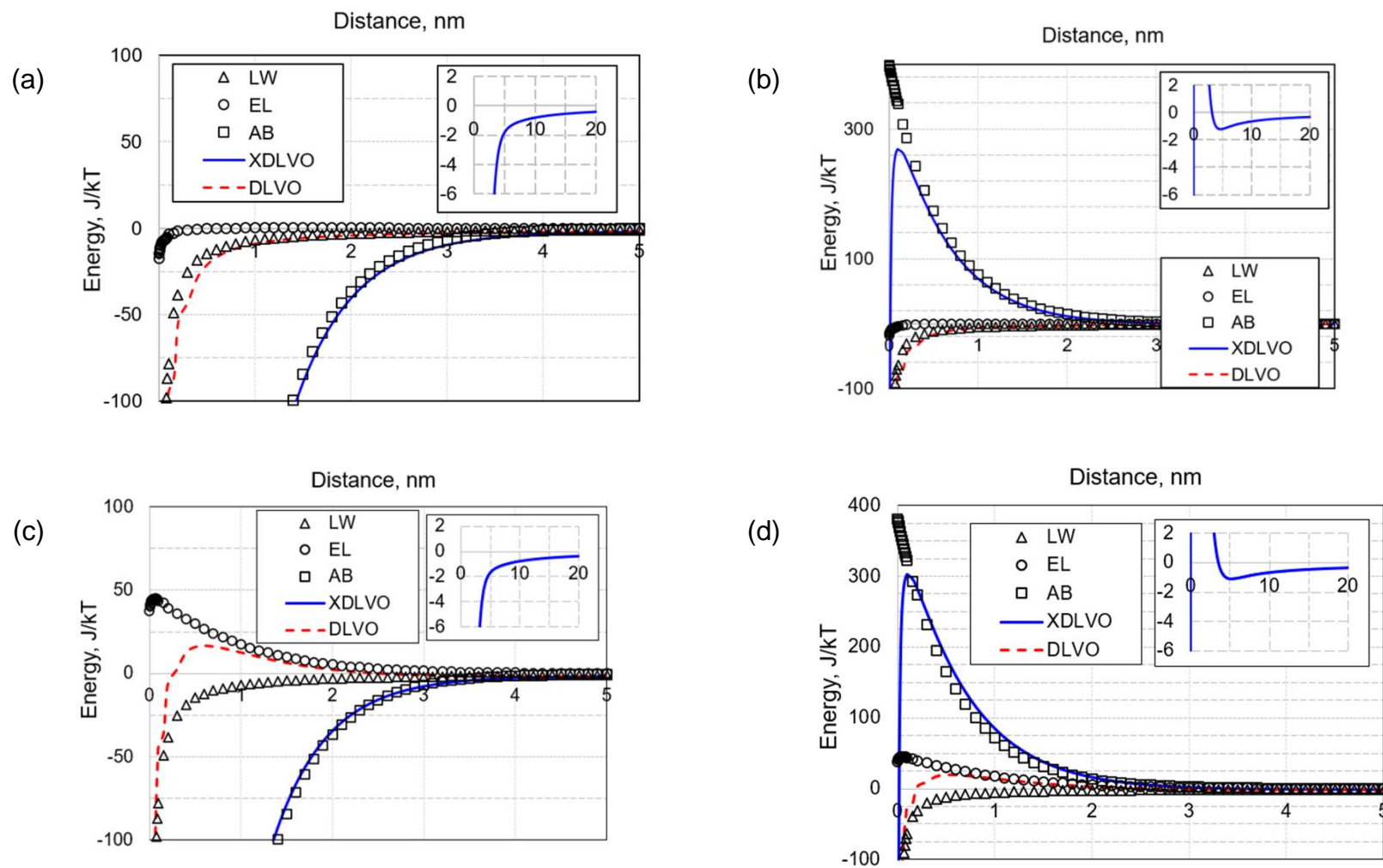


Figure 21. XDLVO energy of interaction of P22 with Carmex lip balm at pH 4.2 (a, b) and pH 7.2 (c, d) in dry (a, c) and hydrated (b, d) states. DLVO total energy is provided for reference.

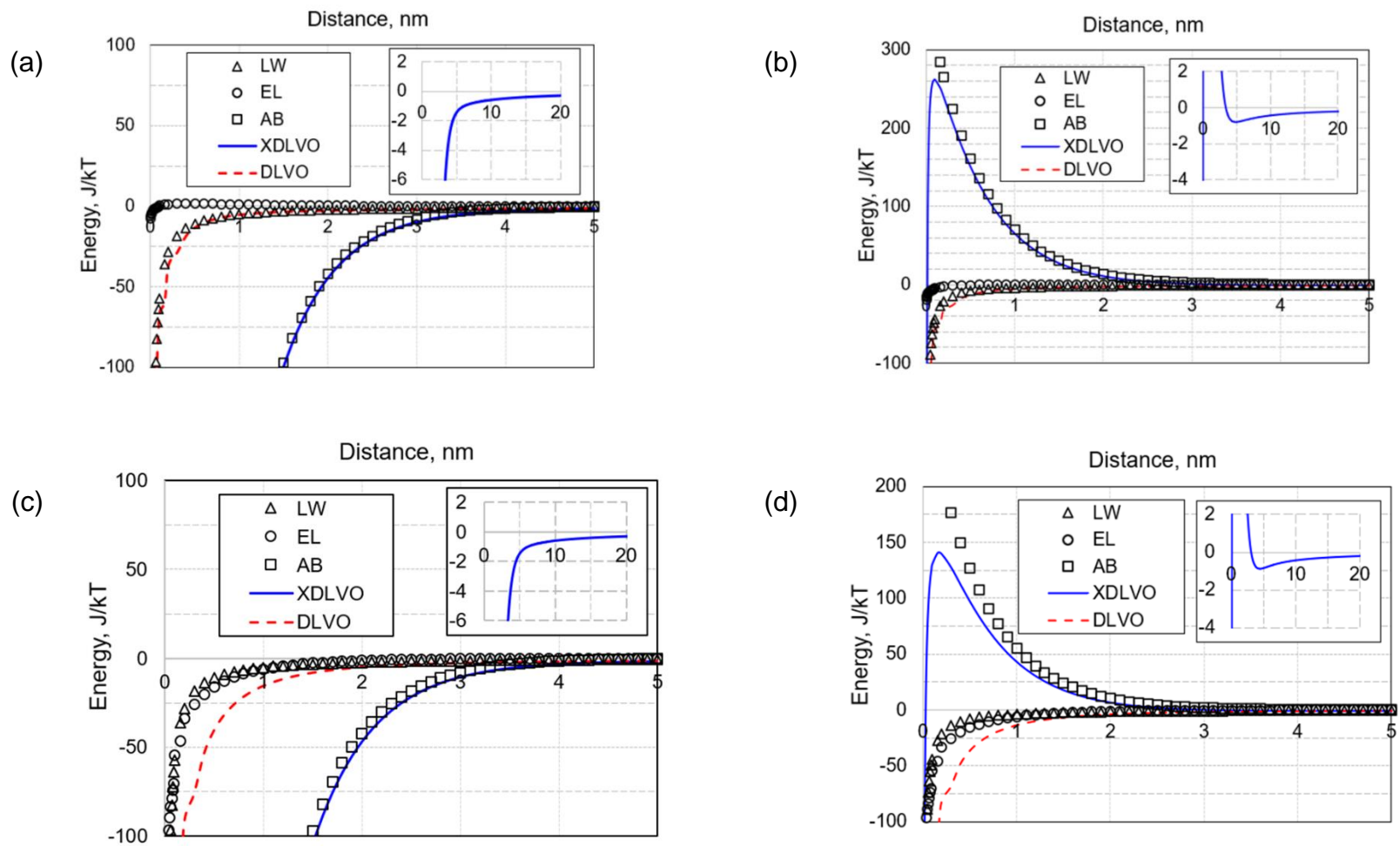


Figure 22. XDLVO energy of interaction of P22 with Chapstick lip balm at pH 4.2 (a, b) and pH 7.2 (c, d) in dry (a, c) and hydrated (b, d) states. DLVO total energy is provided for reference.

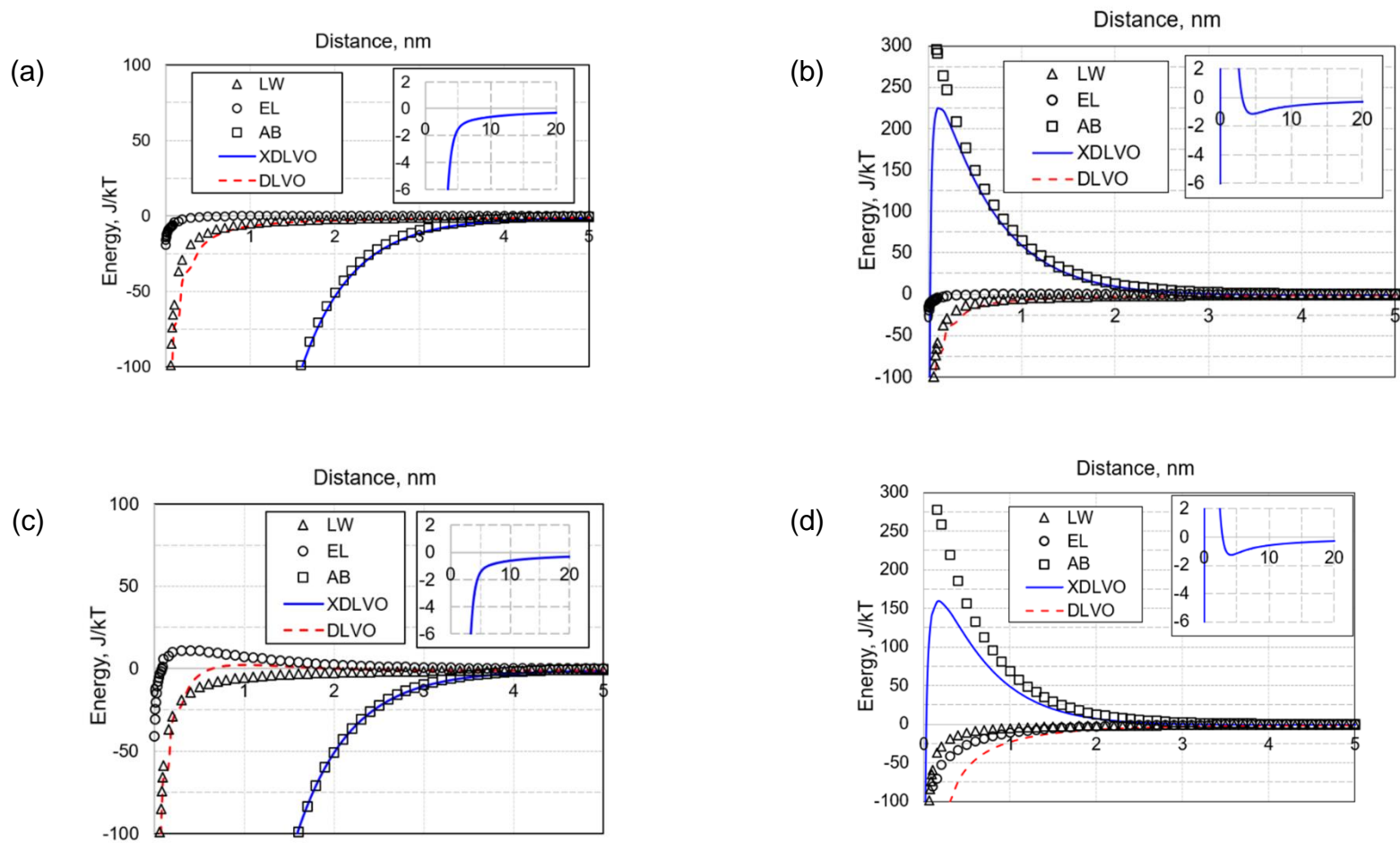


Figure 23. XDLVO energy of interaction of P22 with Burt's Bees lip balm at pH 4.2 (a, b) and pH 7.2 (c, d) in dry (a, c) and hydrated (b, d) states. DLVO total energy is provided for reference.

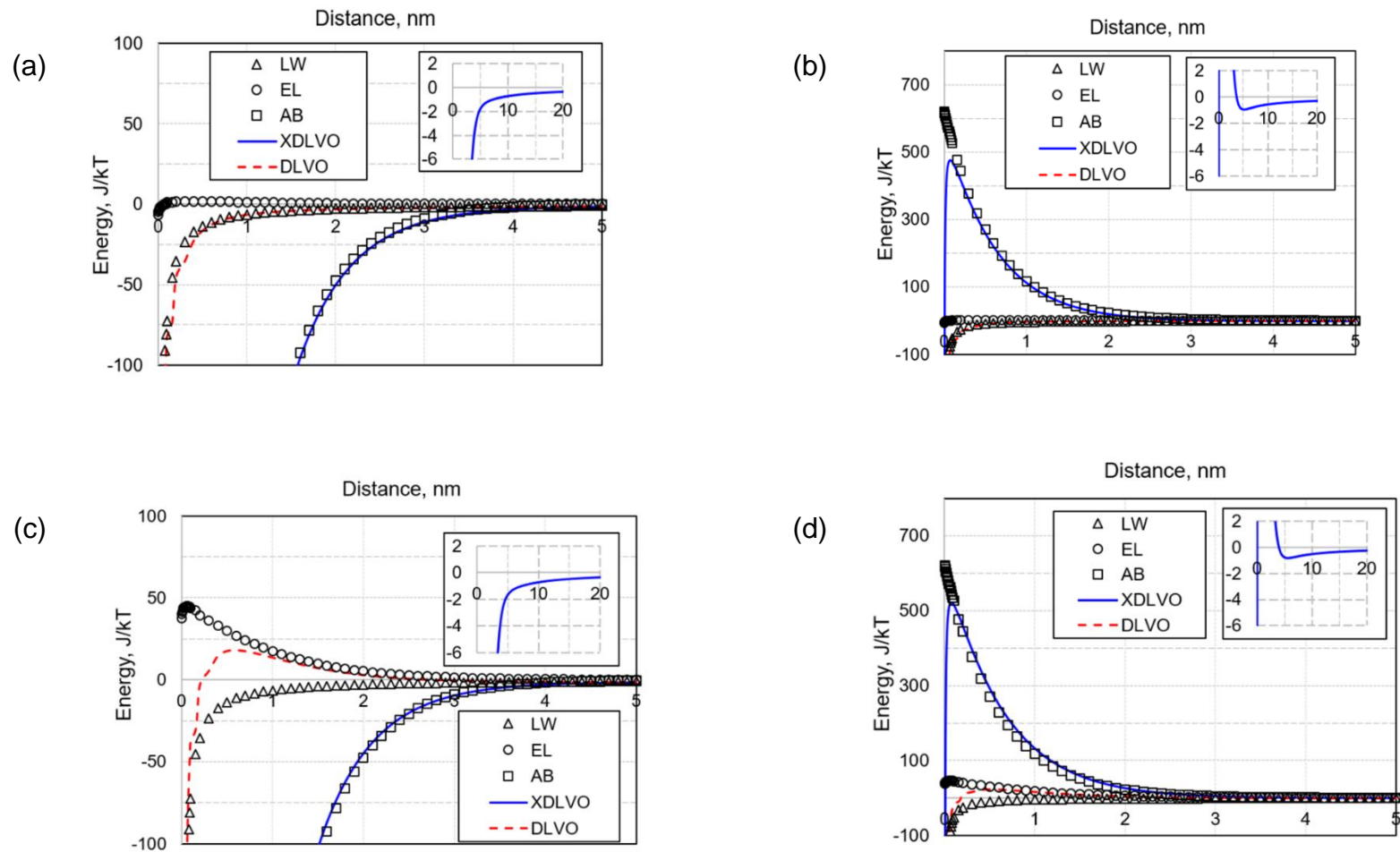


Figure 24. XDLVO energy of interaction of P22 with Vaseline lip balm at pH 4.2 (a, b) and pH 7.2 (c, d) in dry (a, c) and hydrated (b, d) states. DLVO total energy is provided for reference.

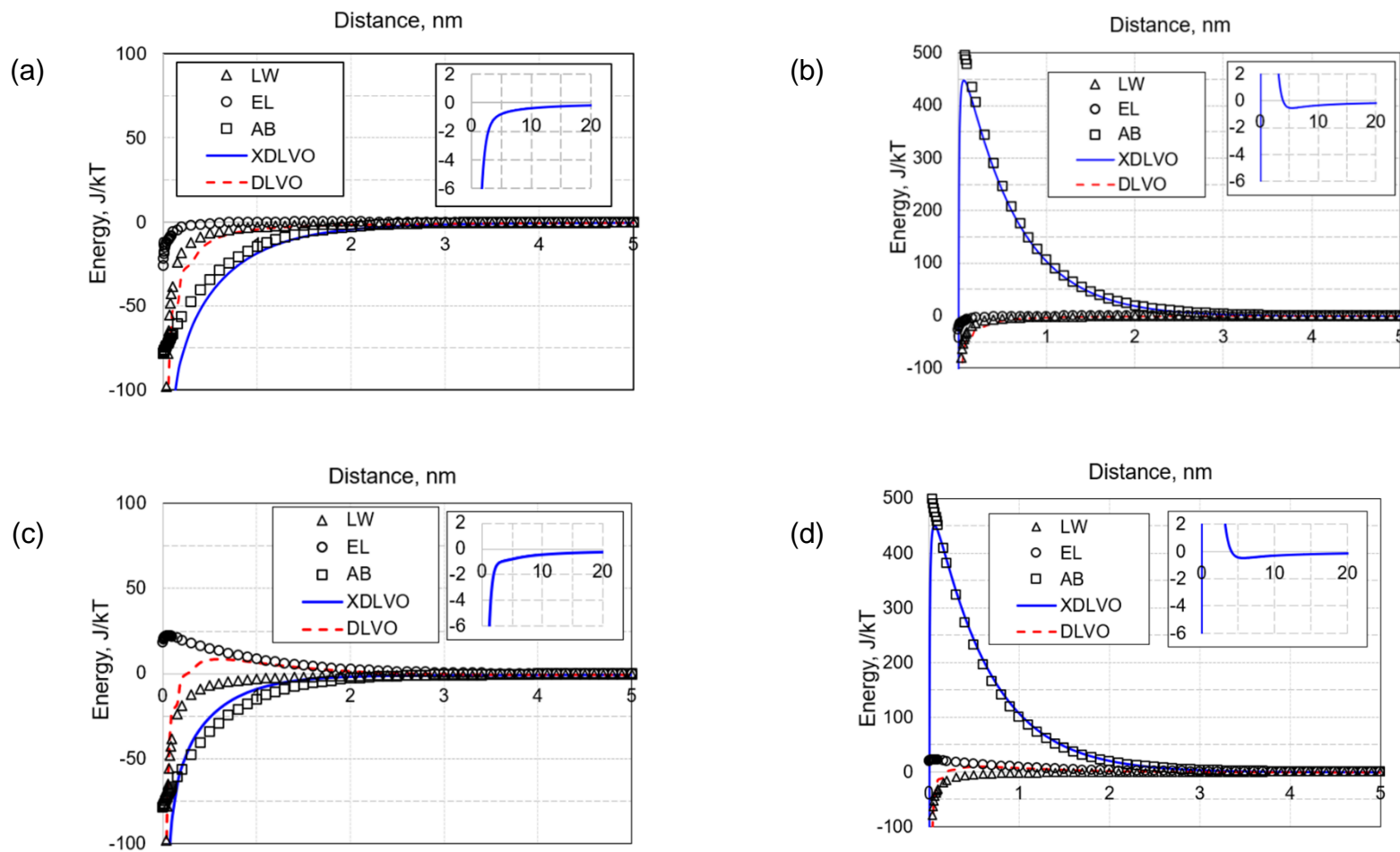


Figure 25. XDLVO energies of interaction of MS2 with Carmex lip balm at pH 4.2 (a, b) and pH 7.2 (c, d) in dry (a, c) and hydrated (b, d) states. DLVO total energy is provided for reference.

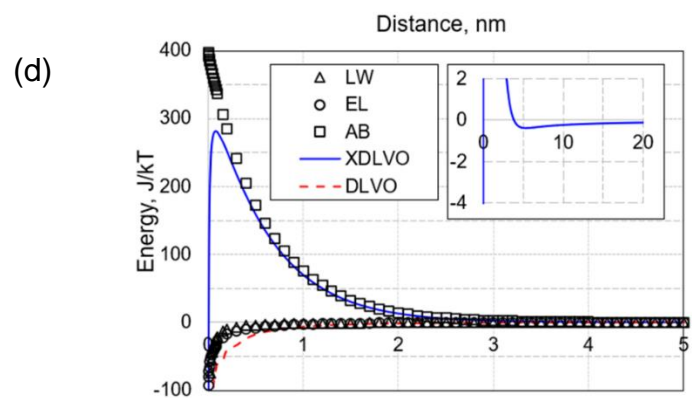
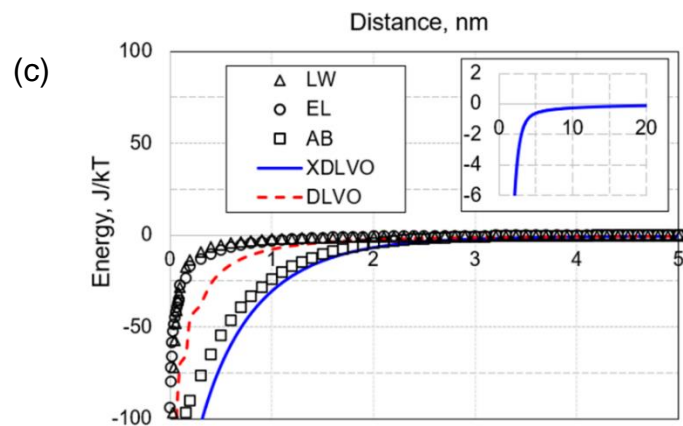
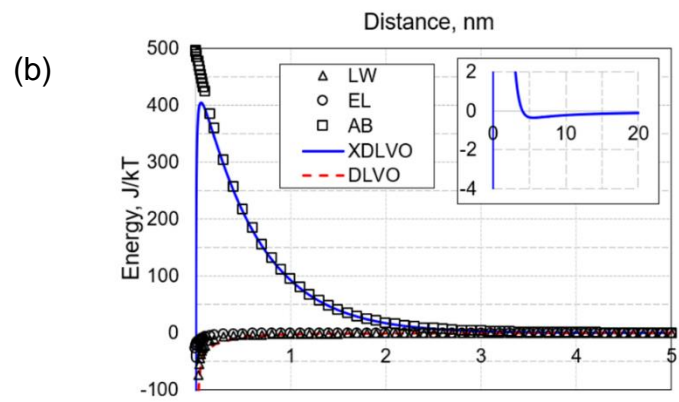
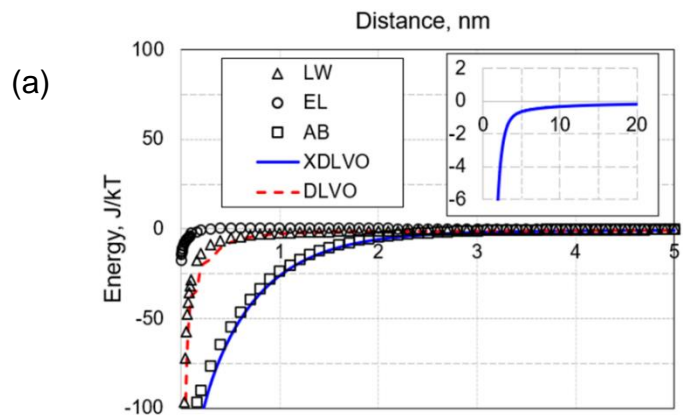


Figure 26. XDLVO energy of interaction of MS2 with Chapstick lip balm at pH 4.2 (a, b) and pH 7.2 (c, d) in dry (a, c) and hydrated (b, d) states. DLVO total energy is provided for reference.

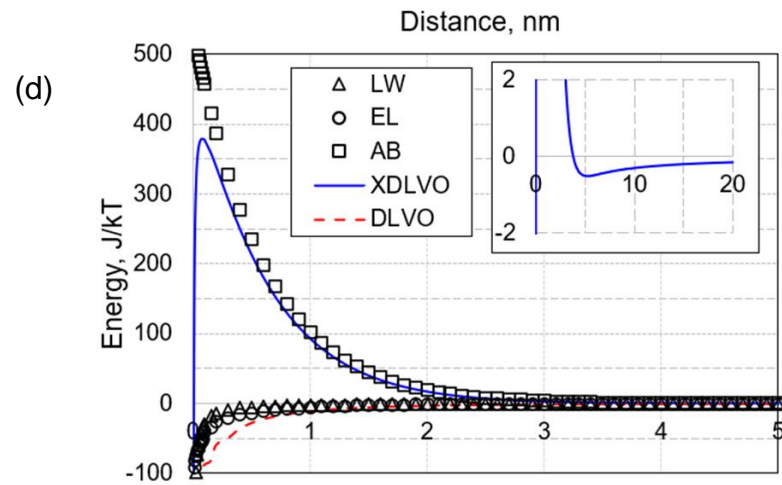
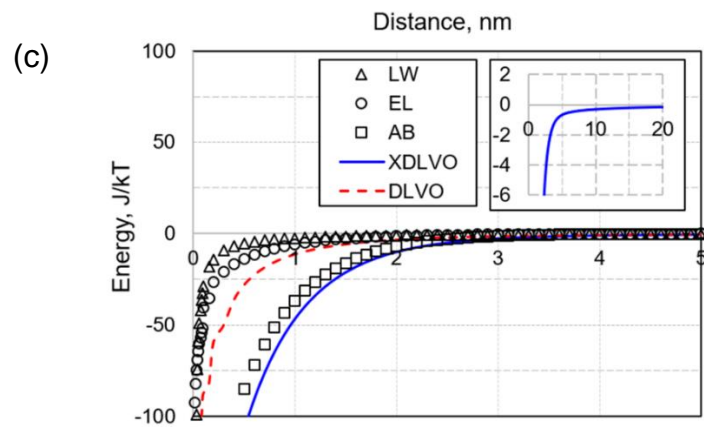
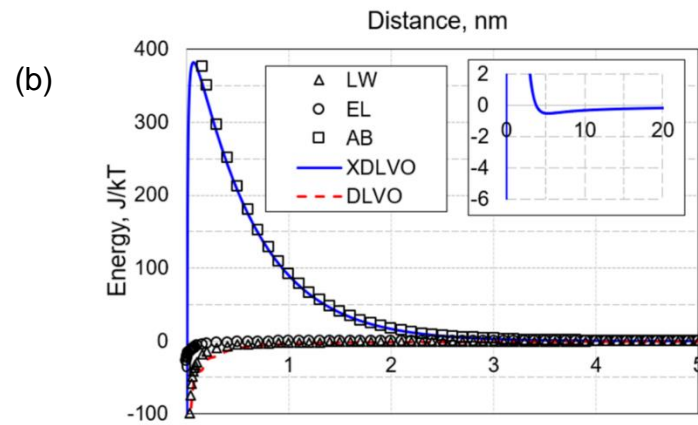
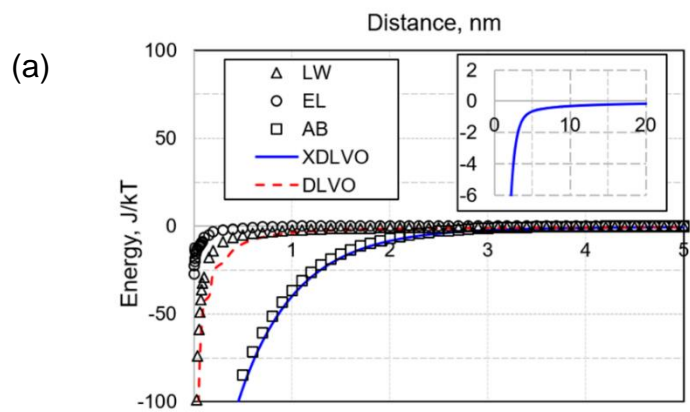


Figure 27. XDLVO energies of interaction of MS2 with Burt's Bees lip balm at pH 4.2 (a, b) and pH 7.2 (c, d) in dry (a, c) and hydrated (b, d) states. DLVO total energy is provided for reference.

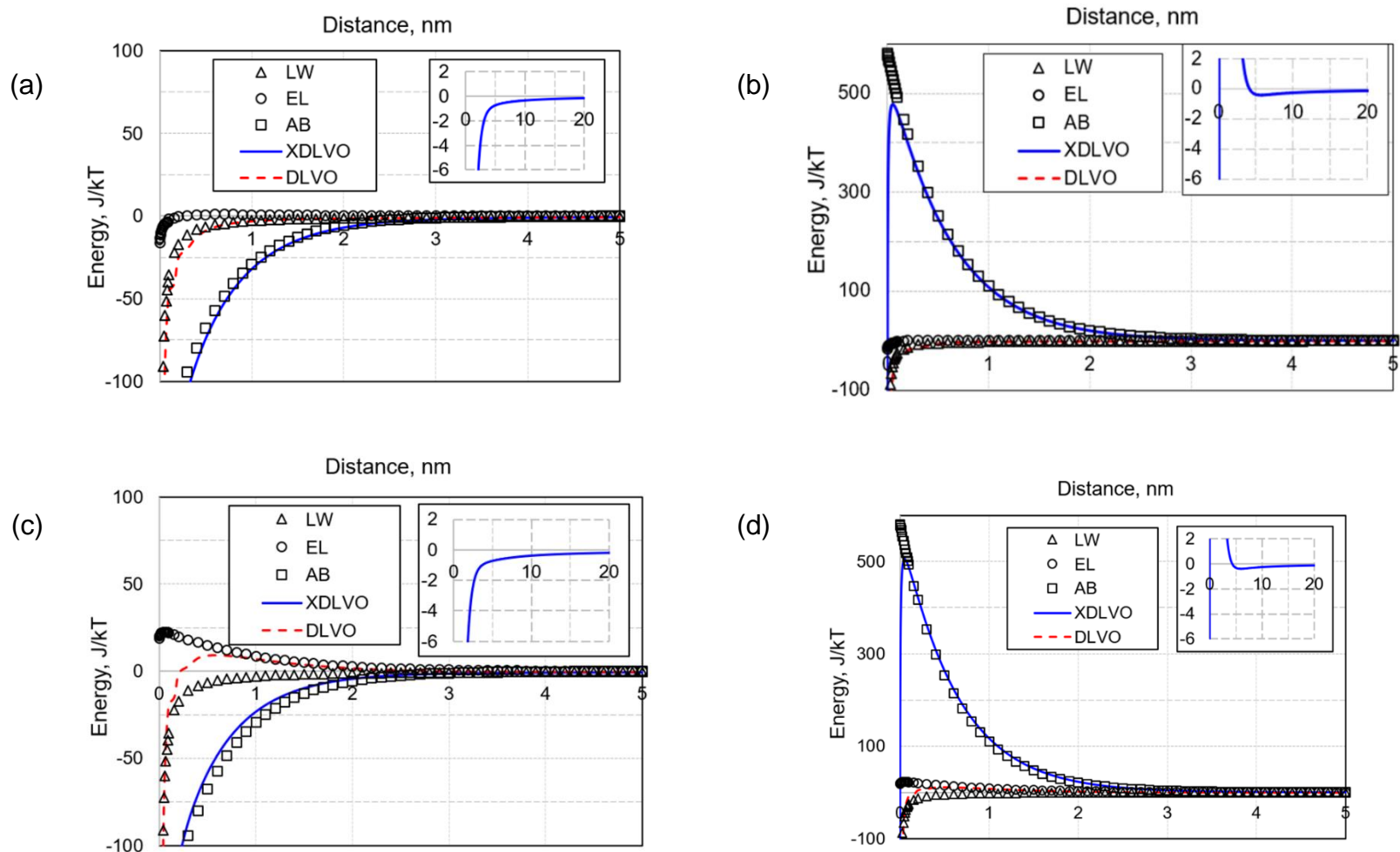


Figure 28. XDLVO energy of interaction of MS2 with Vaseline lip balm at pH 4.2 (a, b) and pH 7.2 (c, d) in dry (a, c) and hydrated (b, d) states. DLVO total energy is provided for reference.

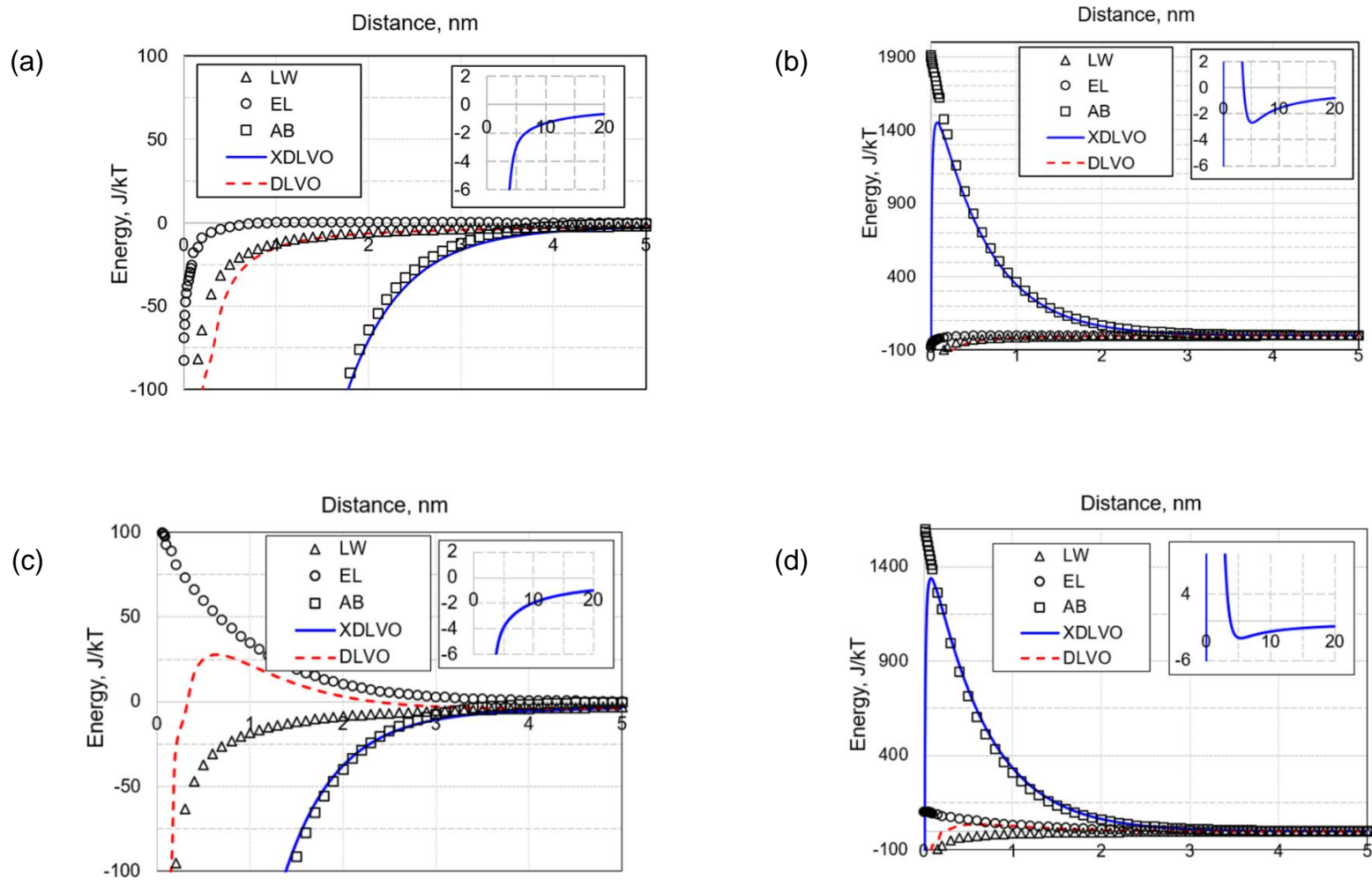


Figure 29. XDLVO energies of interaction of SiO₂ with Carmex lip balm at pH 4.2 (a, b) and pH 7.2 (c, d) in dry (a, c) and hydrated (b, d) states. DLVO total energy is provided for reference.

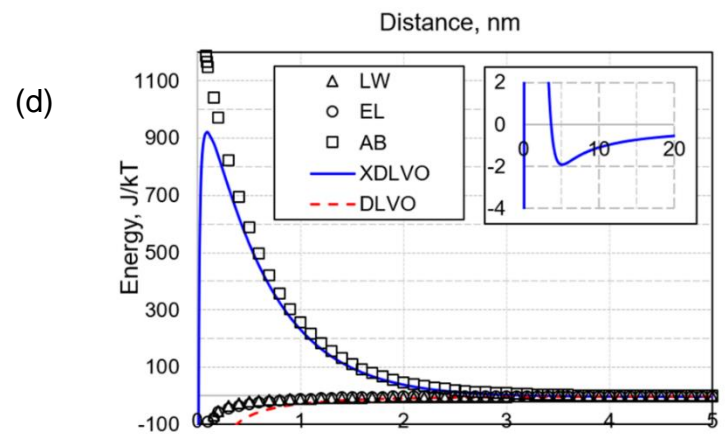
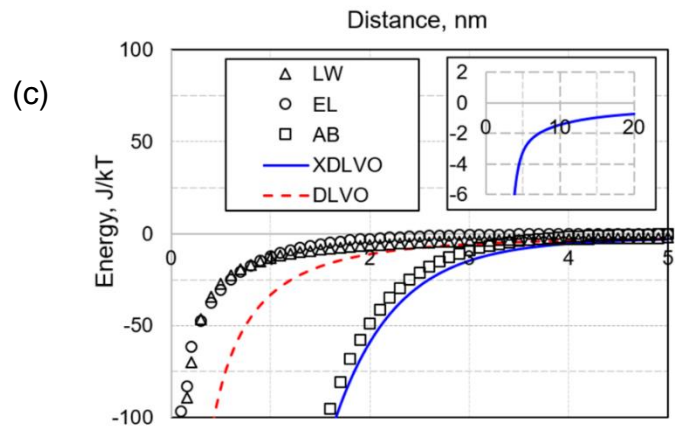
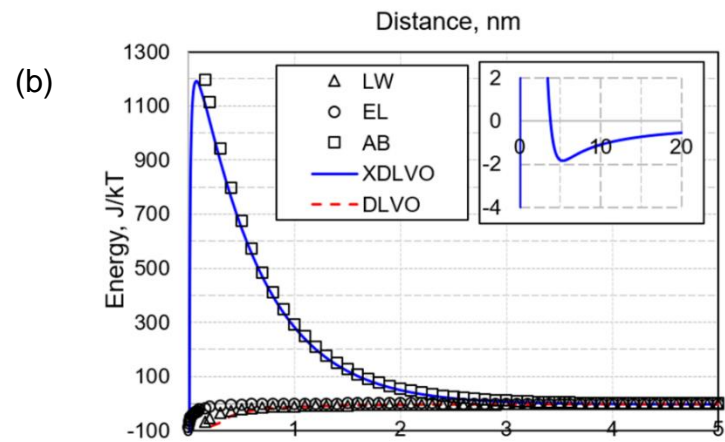
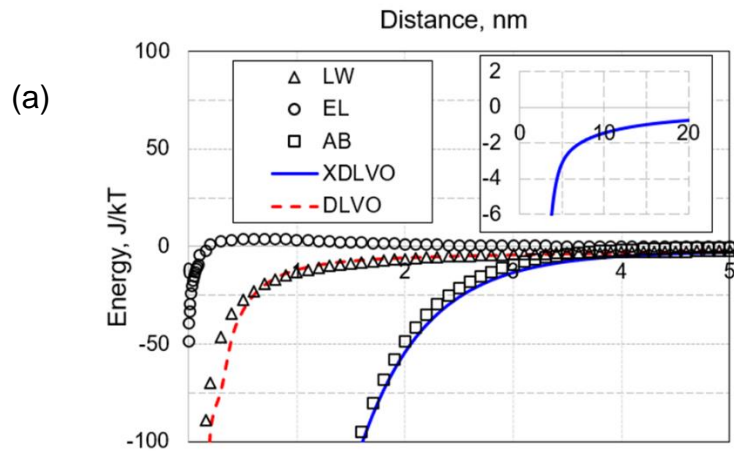


Figure 30. XDLVO energy of interaction of SiO_2 with Chapstick lip balm at pH 4.2 (a, b) and pH 7.2 (c, d) in dry (a, c) and hydrated (b, d) states. DLVO total energy is provided for reference.

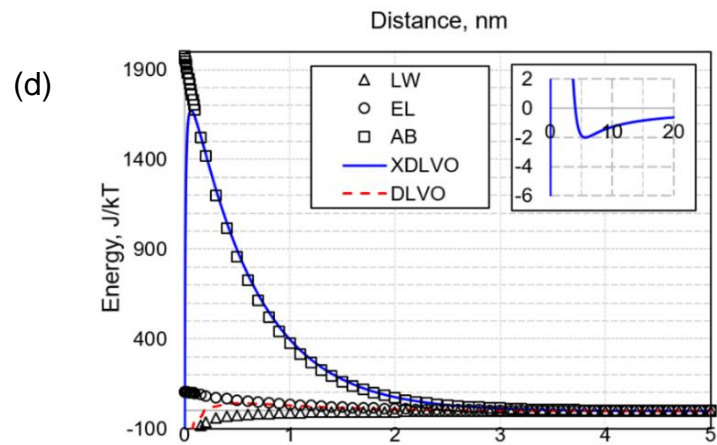
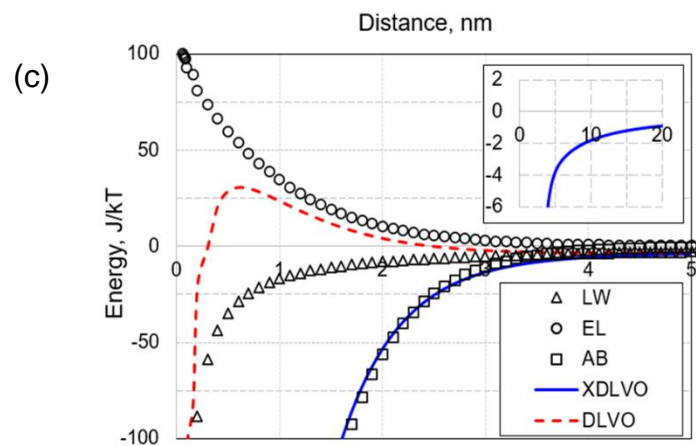
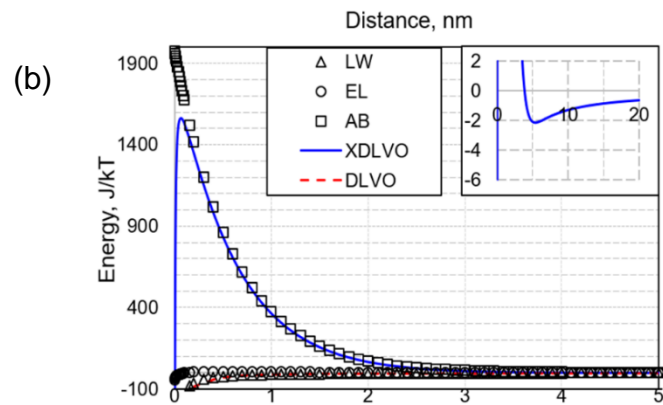
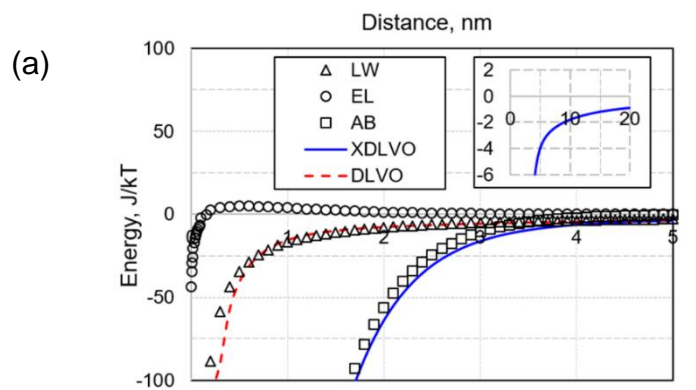


Figure 31. XDLVO energies of interaction of SiO₂ with Vaseline lip balm at pH 4.2 (a, b) and pH 7.2 (c, d) in dry (a, c) and hydrated (b, d) states. DLVO total energy is provided for reference.

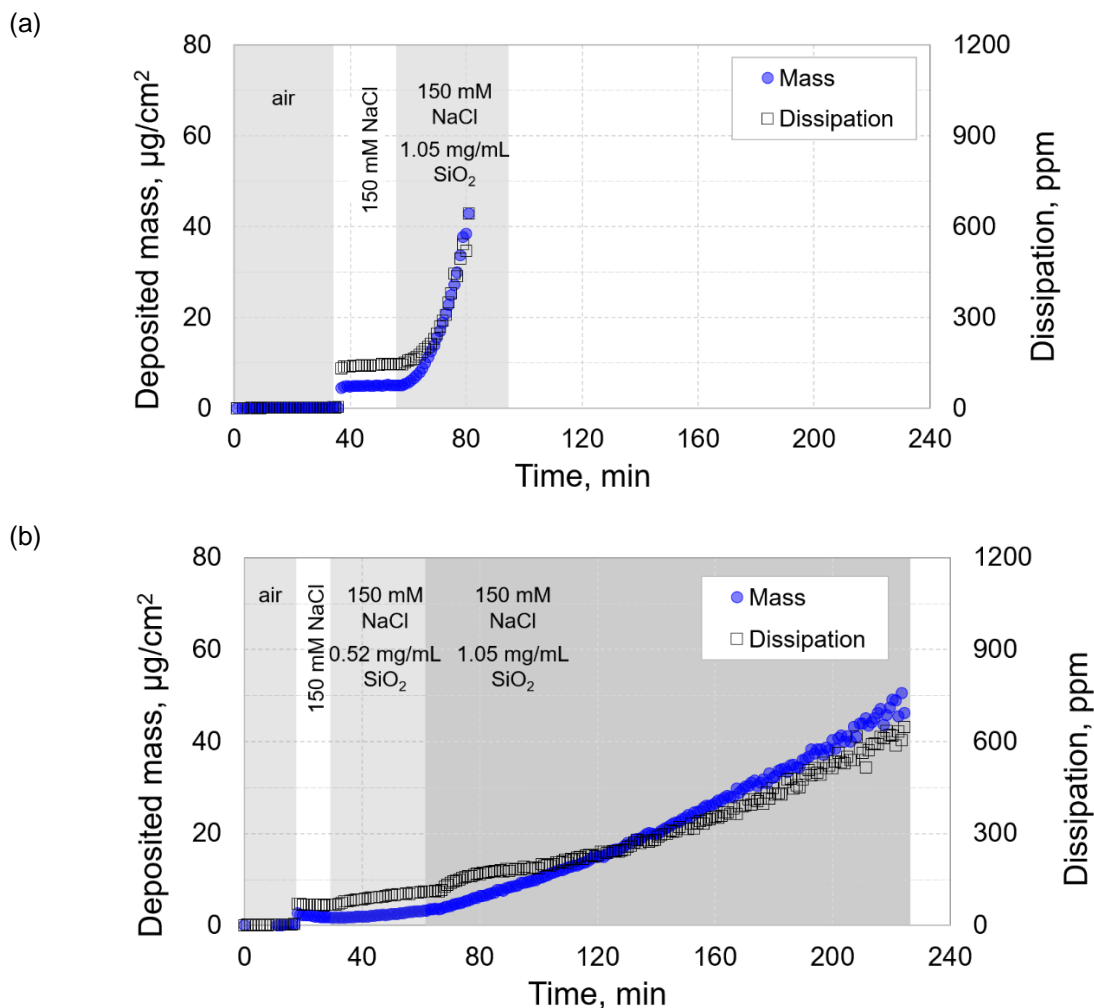


Figure 32. Deposition of SiO₂ colloids onto hydrated Burt's Bees lip balm under conditions when SiO₂ loading is either a) constant (1.05 mg/ml) or b) increases stepwise from 0.52 mg/ml to 1.05 mg/ml. In both tests deposition occurs from 150 mM NaCl electrolyte at pH 7.2. The mass values are calculated based on Sauerbrey equation (eq. (3)) with $n = 5$. The results for $n = 3$ are similar and shown in the main manuscript (Fig. 8).

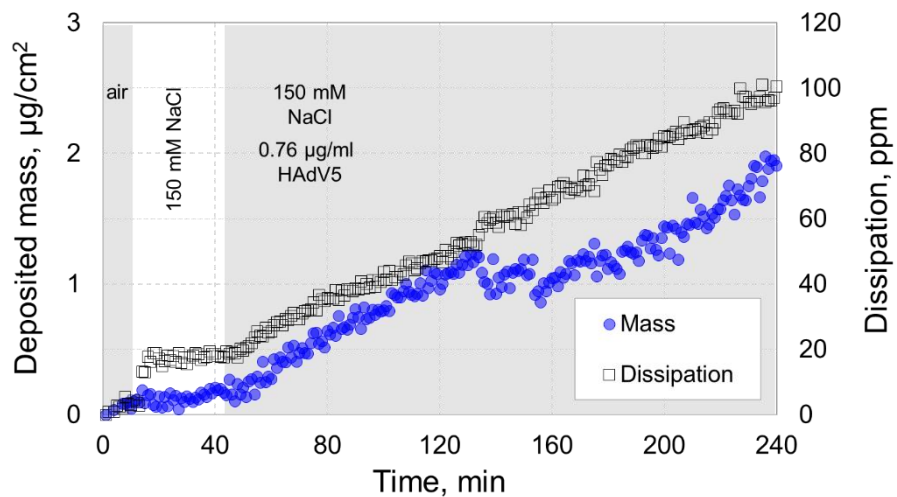


Figure 33. QCM-D measurements of the deposition of human adenovirus 5 onto hydrated Carmex lip balm from 150 mM NaCl electrolyte at pH 7.2. HAdV5 concentration in the QCM-D feed is $\sim 10^9$ GC/mL (~ 0.76 $\mu\text{g}/\text{mL}$). The mass values are calculated based on Sauerbrey equation (eq. (3)) with $n = 5$. The results for $n = 3$ are similar and shown in the main manuscript (Fig. 9).

REFERENCES

REFERENCES

- [1] B. Stephens, P. Azimi, M.S. Thoemmes, M. Heidarinejad, J.G. Allen, J.A. Gilbert, Microbial exchange via fomites and implications for human health, *Curr. Poll. Rep.* (2019) 1-16.
- [2] S.A. Ansari, S.A. Sattar, V.S. Springthorpe, G.A. Wells, W. Tostowaryk, Rotavirus survival on human hands and transfer of infectious virus to animate and nonporous inanimate surfaces, *J. Clin. Microbiol.* 26(8) (1988) 1513-1518.
- [3] S.A. Ansari, V.S. Springthorpe, S.A. Sattar, S. Rivard, M. Rahman, Potential role of hands in the spread of respiratory viral infections: Studies with human parainfluenza virus 3 and rhinovirus 14, *J. Clin. Microbiol.* 29(10) (1991) 2115-2119.
- [4] J.N. Mbithi, V.S. Springthorpe, J.R. Boulet, S.A. Sattar, Survival of hepatitis A virus on human hands and its transfer on contact with animate and inanimate surfaces, *J. Clin. Microbiol.* 30(4) (1992) 757-763.
- [5] T.R. Julian, J.O. Leckie, A.B. Boehm, Virus transfer between fingerpads and fomites, *J. Appl. Microbiol.* 109(6) (2010) 1868-1874.
- [6] A.K. Pitol, H.N. Bischel, T. Kohn, T.R. Julian, Virus transfer at the skin–liquid interface, *Environ. Sci. Technol.* 51(24) (2017) 14417-14425.
- [7] A.K. Pitol, H.N. Bischel, A.B. Boehm, T. Kohn, T.R. Julian, Transfer of enteric viruses adenovirus and coxsackievirus and bacteriophage MS2 from liquid to human skin, *Appl. Environ. Microbiol.* 84(22) (2018) e01809-18.
- [8] A.M. Wilson, K.A. Reynolds, M.P. Verhougstraete, R.A. Canales, Validation of a stochastic discrete event model predicting virus concentration on nurse hands, *Risk Anal.* 39 (2019) 1812-1824.
- [9] R. Gfatter, P. Hackl, F. Braun, Effects of soap and detergents on skin surface pH, stratum corneum hydration and fat content in infants., *Dermatology* 195 (1997) 258-262.
- [10] S.E. Stewart, M.D. Parker, A. Amézquita, T.L. Pitt, Microbiological risk assessment for personal care products, *Int. J. Cosmet. Sci.* 38(6) (2016) 634-645.
- [11] L. Jimenez, Microorganisms in the environment and their relevance to pharmaceutical processes, *Microbial contamination control in the pharmaceutical industry*, CRC Press 2004, pp. 19-32.
- [12] E. Neza, M. Centini, Microbiologically contaminated and over-preserved cosmetic products according Rapex 2008–2014, *Cosmetics* 3(1) (2016) 3.

- [13] M.O. Osungunna, B.B. Oluremi, A. Adetuyi, Bacteriological and antibiotic sensitivity patterns of bacterial isolates from creams and lotions hawked in Sagamu, Ogun State, Pak. J. Nutr. 9 (2010) 773-775.
- [14] P.A. Geis, R.T. Hennesy, Preservative development, CRC Press, Florida, 2000, pp. 143-161.
- [15] F.R. Reid, T.O. Wood, Pseudomonas corneal ulcer: the causative role of contaminated eye cosmetics, Arch. Ophthalmol. 97(9) (1979) 1640-1641.
- [16] M.D. Lundov, C. Zachariae, Recalls of microbiologically contaminated cosmetics in EU from 2005 to May 2008, Int. J. Cosmetic Sci. 30(6) (2008) 471-474.
- [17] J. Wang, A.B. Kay, J. Fletcher, M.K. Formica, T.E. McAlindon, Is lipstick associated with the development of systemic lupus erythematosus (SLE)?, Clin. Rheumatol. 27 (2008) 1183-1187.
- [18] The SCCS notes of guidance for the testing of cosmetic ingredients and their safety evaluation, 9th revision SCCS/1564/15 Scientific Committee on Consumer Safety Brussels, 2015.
- [19] B. Yuan, M. Pham, T.H. Nguyen, Deposition kinetics of bacteriophage MS2 on a silica surface coated with natural organic matter in a radial stagnation point flow cell, Environ. Sci. Technol. 42(20) (2008) 7628-7633.
- [20] M. Tong, Y. Shen, H. Yang, H. Kim, Deposition kinetics of MS2 bacteriophages on clay mineral surfaces, Colloids Surfaces B 92 (2012) 340-347.
- [21] H. Shi, I. Xagorarakis, K.N. Parent, M.L. Bruening, V.V. Tarabara, Elution is a critical step for recovering human adenovirus 40 from tap water and surface water by cross-flow ultrafiltration, Appl. Environ. Microbiol. 82(16) (2016) 4982-4993.
- [22] K. Wong, B. Mukherjee, A.M. Kahler, R. Zepp, M. Molina, Influence of inorganic ions on aggregation and adsorption behaviors of human adenovirus, Environ. Sci. Technol. 46(20) (2012) 11145-11153.
- [23] R. Lu, Q. Li, T.H. Nguyen, Random sequential adsorption of human adenovirus 2 onto polyvinylidene fluoride surface influenced by extracellular polymeric substances, J. Colloid Interface Sci. 466 (2016) 120-127.
- [24] D.K. Roper, S. Nakra, Adenovirus type 5 intrinsic adsorption rates measured by surface plasmon resonance, Anal. Biochem. 348(1) (2006) 75-83.
- [25] H.T.T. Dang, V.V. Tarabara, Virus deposition onto polyelectrolyte-coated surfaces: A study with bacteriophage MS2, J. Colloid Interface Sci. 540 (2019) 155-166.
- [26] ARMWG, Adenovirus Type 5 Reference Material (Product Information Sheet for VR-1516), in: A.T.C.C. (ATCC) (Ed.) 2010.

- [27] B.G. Huyghe, X. Liu, S. Sutjipto, B.J. Sugarman, M.T. Horn, H.M. Shepard, C.J. Scandella, P. Shabram, Purification of a type 5 recombinant adenovirus encoding human p53 by column chromatography, *Hum. Gene Ther.* 6(11) (1995) 1403-1416.
- [28] C. Boo, S. Lee, M. Elimelech, Z. Meng, S. Hong, Colloidal fouling in forward osmosis: Role of reverse salt diffusion, *J. Membr. Sci.* 390 (2012) 277-284.
- [29] S.R. Dasari, V.V. Goud, Comparative extraction of castor seed oil using polar and non polar solvents, *Int. J. Curr. Eng. Technol.* 1 (2013) 121-123.
- [30] H. Shi, V.V. Tarabara, Charge, size distribution and hydrophobicity of viruses: Effect of propagation and purification methods, *J. Virol. Methods* 256 (2018) 123-132.
- [31] C.J. van Oss, *Interfacial forces in aqueous media*, CRC Press 2006.
- [32] C.J. van Oss, R.F. Giese, The hydrophilicity and hydrophobicity of clay minerals, *Clay Clay Miner.* 43 (1995) 474-477.
- [33] E.V. Pasco, H. Shi, I. Xagorarakis, S.A. Hashsham, K.N. Parent, M.L. Bruening, V.V. Tarabara, Polyelectrolyte multilayers as anti-adhesive membrane coatings for virus concentration and recovery, *J. Membr. Sci.* 469 (2014) 140-150.
- [34] M. Pham, E.A. Mintz, T.H. Nguyen, Deposition kinetics of bacteriophage MS2 to natural organic matter: Role of divalent cations, *J. Colloid Interface Sci.* 338(1) (2009) 1-9.
- [35] M.C. Dixon, Quartz crystal microbalance with dissipation monitoring: enabling real-time characterization of biological materials and their interactions, *J. Biomol. Tech.* 19 (2008).
- [36] A. Armanious, M. Aeppli, R. Jacak, D. Refardt, T. Sigstam, T. Kohn, M. Sander, Viruses at solid-water interfaces: a systematic assessment of interactions driving adsorption, *Environ. Sci. Technol.* 50(2) (2015) 732-743.
- [37] H.T.T. Dang, Virus attachment to surfaces: Assessing relative contributions of electrostatic, van der Waals, and acid-base interactions. Ph.D. dissertation, Civil and Environmental Engineering, Michigan State University, 2018.
- [38] N.F. Steinmetz, E. Bock, R.P. Richter, J.P. Spatz, G.P. Lomonossoff, D.J. Evans, Assembly of multilayer arrays of viral nanoparticles via biospecific recognition: a quartz crystal microbalance with dissipation monitoring study, *Biomacromol.* 9(2) (2008) 456-462.
- [39] X. Huang, J. Xu, H.-F. Ji, G. Li, H. Chen, Quartz crystal microbalance based biosensor for rapid and sensitive detection of maize chlorotic mottle virus, *Anal. Method.* 6(13) (2014) 4530-4536.

- [40] L. Gutierrez, S.E. Mylon, B. Nash, T.H. Nguyen, Deposition and aggregation kinetics of rotavirus in divalent cation solutions, *Environ. Sci. Technol.* 44(12) (2010) 4552-4557.
- [41] G. Tiliket, G. Ladam, Q.T. Nguyen, L. Lebrun, Polyethylenimine surface layer for enhanced virus immobilization on cellulose, *Appl. Surf. Sci.* 370 (2016) 193-200.
- [42] G. Ross, *Essentials of human physiology*, Yearbook Medical Publishers Chicago, 1978.
- [43] G.W. Gary, J.C. Hierholzer, R.E. Black, Characteristics of noncultivable adenoviruses associated with diarrhea in infants: a new subgroup of human adenoviruses, *J. Clin. Microbiol.* 10(1) (1979) 96-103.
- [44] G. Winberg, G. Wadell, Structural polypeptides of adenovirus type 16 incomplete particles, *J. Virol.* 22(2) (1977) 389-401.
- [45] G. Sauerbrey, Verwendung von Schwingquarzen zur Wägung dünner Schichten und zur Mikrowägung, *Zeitschrift für physik* 155(2) (1959) 206-222.
- [46] B. Derjaguin, L. Landau, Theory of the stability of strongly charged lyophobic sols and of the adhesion of strongly charged particles in solutions of electrolytes, *Acta Physico Chimica URSS* 14 (1941).
- [47] E.J.W.O. Verwey, J. Th. G., *Theory of the stability of lyophobic colloids*, Elsevier, Amsterdam, 1948.
- [48] C. Dika, M.H. Ly-Chatain, G. Francius, J.F.L. Duval, C. Gantzer, Non-DLVO adhesion of F-specific RNA bacteriophages to abiotic surfaces: importance of surface roughness, hydrophobic and electrostatic interactions, *Colloids Surfaces A* 435 (2013) 178-187.
- [49] C.J. van Oss, M.K. Chaudhury, R.J. Good, Interfacial Lifshitz-van der Waals and polar interactions in macroscopic systems, *Chem. Rev.* 88 (1988) 927-941.
- [50] Y. Chen, L. Shen, R. Li, X. Xu, H. Hong, H. Lin, J. Chen, Quantification of interfacial energies associated with membrane fouling in a membrane bioreactor by using BP and GRNN artificial neural networks, *J. Colloid Interface Sci.* 565 (2020) 1-10.
- [51] J. Teng, L. Shen, Y. Xu, Y. Chen, X.-L. Wu, Y. He, J. Chen, H. Lin, Effects of molecular weight distribution of soluble microbial products (SMPs) on membrane fouling in a membrane bioreactor (MBR): Novel mechanistic insights, *Chemosphere* 248 (2020).
- [52] Y. Xing, A. Ellis, M. Magnuson, W.F. Harper, Adsorption of bacteriophage MS2 to colloids: Kinetics and particle interactions, *Colloids Surfaces A* 585 (2020) 124099.
- [53] J.A. Brant, A.E. Childress, Assessing short-range membrane–colloid interactions using surface energetics, *J. Membr. Sci.* 203(1-2) (2002) 257-273.

- [54] A.R. Fernandes, M.F. Dario, C.A.S. de Oliveira Pinto, T.M. Kaneko, A.R. Baby, M.V.R. Velasco, Stability evaluation of organic lip balm, *Braz. J. Pharmaceut. Sci.* 49 (2013) 293-299.
- [55] I. Foubert, I.V. Caeteren, K. Dewettinck, A. Huyghebaert, Differential scanning calorimetry as a means of predicting chocolate fat-blooming, in: N. Widlak, R. Hartel, S. Narine (Eds.), *Crystallization and solidification properties of lipids*, AOCS Press 2001, pp. 79-86.
- [56] S. Pan, N. Germann, Mechanical response of industrial benchmark lipsticks under large-scale deformations, *Acta Mechanica* 231 (2020) 3031-3042.
- [57] A.W. Adamson, A.P. Gast, *Physical Chemistry of Surfaces*, Wiley - Interscience 1997.
- [58] E.I. Trilisky, A.M. Lenhoff, Sorption processes in ion-exchange chromatography of viruses, *J. Chromatogr. A* 1142 (2007) 2-12.
- [59] J. Kim, M.J. Park, M. Park, H.K. Shon, S.-H. Kim, J.H. Kim, Influence of colloidal fouling on pressure retarded osmosis, *Desalination* 389 (2016) 207-214.
- [60] A. Zdziennicka, K. Szymczyk, B. Jańczuk, Correlation between surface free energy of quartz and its wettability by aqueous solutions of nonionic, anionic and cationic surfactants, *J. Colloid Interface Sci.* 340(2) (2009) 243-248.
- [61] S. Baliga, S. Muglikar, R. Kale, Salivary pH: A diagnostic biomarker, *J. Indian Soc. Periodont.* 17(4) (2013) 461.
- [62] L. Graetz, Ueber die Wärmeleitfähigkeit von Flüssigkeiten, *Annalen der Physik* 254(79) (1882).
- [63] W.M. Deen, *Analysis of Transport Phenomena*, Oxford University Press, New York, Oxford, 1998.
- [64] B.W. Robinson, E.H. Nickel, A useful new technique for mineralogy: the backscattered-electron/low vacuum mode of SEM operation, *Am. Mineral.* 64(11-12) (1979) 1322-1328.
- [65] R.C. Wilhoit, B.J. Zwolinski, *Handbook of vapor pressures and heats of vaporization of hydrocarbons and related compounds*, Thermodynamics Research Center, College Station, TX 1971.
- [66] V.B. Wigglesworth, The use of osmium in the fixation and staining of tissues, *Proc. R. Soc. London. B - Biol. Sci.* 147(927) (1957) 185-199.
- [67] W. Kern, The evolution of silicon wafer cleaning technology, *J. Electrochem. Soc.* 137(6) (1990) 1887-1892.

[68] B. Hutchins, Development of a reference material for characterizing adenovirus vectors, *Bioprocess. J.* 1(1) (2002) 25-28.

[69] S.L. Simek, FDA Perspectives on the use of Adenoviral Reference Material, 2002.

[70] ARMWG, Adenovirus Type 5 Reference Material (Product Information Sheet for VR-1516), in: A.T.C.C. (ATCC) (Ed.) 2010.

[71] E.I. Trilisky, A.M. Lenhoff, Sorption processes in ion-exchange chromatography of viruses, *J. Chromatogr. A* 1142 (2007) 2-12.

CHAPTER THREE

Virus adhesion to archetypal fomites: A study with human adenovirus and human respiratory syncytial virus

3.1 Abstract

Adhesion of two viruses – one enveloped (human respiratory syncytial virus, HRSV) and one non-enveloped (human adenovirus 5, HAdV5) – to four fomites (silica, nylon, stainless steel, polypropylene) was quantified and interpreted based on physicochemical properties of viruses and fomites. The selected fomites are tentatively identified as “archetypes” representing groups of materials distinctly different in mechanisms of their interfacial interactions. The surfaces are typified on the basis of their surface energy components including the dispersive (Lifshitz-van der Waals) component and two polar (electron donor and electron acceptor) components. Virus-fomite interactions are predicted using the extended Derjaguin-Landau-Verwey-Overbeek (XDLVO) theory and are experimentally assessed in tests with quartz crystal microbalance with dissipation (QCM-D). Polar interactions (manifested as hydrophobic attraction for all virus-fomite pairs but HAdV5/silica) governed virus attachment to fomites from a solution of high ionic strength typical for a respiratory fluid, while dispersive interactions played a relatively minor role. For both HAdV5 and HRSV, the areal mass density of deposited viruses correlated with the free energy of virus-fomite interfacial interaction in water, ΔG_{vwf} . The dependence of virus-fomite attachment probability on ΔG_{vwf} collapsed into one trend for both HAdV5 and HRSV pointing to the

possibility of using ΔG_{vwf} as a predictor of virus adhesion. Fomite rinsing with DI water resulted in a partial virus removal attributable to longer range repulsive electrostatic interactions. The proposed methodology can guide screening and selection of materials that discourage virus adhesion. The information on the efficiency of virus attachment to materials as a function of their surface energy components can help design anti-adhesive surfaces, develop surface cleaning solutions and protocols, and inform transport and fate models for viruses in indoor environments.

3.2 Introduction

Fomites are any inanimate surfaces that, when contaminated with pathogenic microorganisms, can serve as a means of transferring the pathogens to a new human host. There is growing evidence that fomites play an important role in the spread of viruses [1-3]. Higher probability of transfer is associated with fomites in indoor environments such as classrooms, hospitals, nursing homes, cruise ships, and restaurants and especially with surfaces that are frequently touched (e.g. doorknobs, refrigerator handles, dishcloths, faucets) or facilitate virus transmission through other uses (e.g. airducts, hospital linen) [3-11]. Personal protection equipment such as rubber gloves, N95 particulate respirators, surgical masks, gowns may also act as fomites for viral cross-infection [12]. Indoor airflow may enhance transport of virus and virus-laden particles, which could be sucked into the ventilation system through return vents [13].

The COVID-19 pandemic highlighted the importance of understanding the relative importance of a various pathways for pathogen transmission. While it appears that airborne transport is the dominant mechanism for the transmission of SARS-CoV-2, indirect transmission via fomites does contribute to the spread of this virus [14-18]. Indeed, viable SARS-CoV-2 virus has been found on many surfaces and objects contaminated by respiratory secretions or droplets expelled by infected individuals [19-26]. Even if the probability of transfer on a single touch is low, high persistence of viruses on a surface translates into a higher number of touches and a higher overall infection risk [26]. A number of studies have shown that respiratory pathogens are capable of surviving on fomites for extended periods of time - from hours to months [2, 27, 28]. While the knowledge of SARS-CoV-2 transmission mechanisms is still incomplete, fomites have been firmly established as a transfer route for many other viral pathogens of significant concern to human health including influenza virus [29, 30] and norovirus [31, 32]. There is a large and growing knowledge base on the persistence of viruses at various surface [33]; at the same time, physicochemical bases of virus attachment to and removal from surfaces under different conditions remain relatively unexplored [1, 33]. Given the operational definition of risk as a product of availability and infectivity, adhesion and removal studies are needed to quantify the contribution of surface-mediated transmission to the availability term – that is the likelihood that a particular fomite surface has an attached virus that can be detached and transmitted to a human host.

In their recent review, Castaño et al. [1] described how separate virus-fomite interactions are accounted by the classical DLVO and XDLVO theories. There have been many studies that applied XDLVO modeling to describe virus adhesion to various surfaces including membrane filters [34], iron oxide particles [35], personal care products [36], foods and food-contact surfaces [37], polyelectrolyte multilayers [38] and sand [39]. Experimental techniques used to study virus attachment to surfaces range from simple direct contact tests and traditional adsorption studies to record kinetics and isotherms of adsorption [37] to more complex methods such as those employing sensors based on surface plasmon resonance (SPR) [40] and quartz crystal microbalance [38, 41]. SPR is a powerful surface sensing technique especially suitable for studying interfacial kinetics and affinity characterization. SPR is sensitive to the vertical position of individual viruses and, coupled with microscopy, enables high-throughput imaging of single viruses [42]. Liu et al. recently employed plasmonic imaging technology to study the interfacial dynamics of SARS-CoV-2 pseudovirus (SARS-CoV-2 surrogate) adsorption on self-assembled monolayers with amino and carboxyl terminal groups from solutions including artificial saliva, artificial lung fluid and surface water [40]. SPR-based techniques are limited by the requirement of having a noble metal substrate to excite the plasmon resonance. Free of this constraint, QCM-D method has been used to explore virus adhesion to various surfaces while providing (through the dissipation data) additional information on the rheology of the adsorbed layers. Studied surfaces include silica [41], natural organic matter [43, 44], polyelectrolyte multilayers [38], household paints [45] and self-assembled monolayers [46]. Yet, to our knowledge neither XDLVO nor QCM-D prior studies had focused on

fomites with the specific goal of exploring virus adhesion to common indoor surfaces. The dearth of systematic knowledge in this area is likely due to the sheer diversity of fomites in terms of their chemical makeup, morphology and physicochemical properties of their surface. Viruses too, differ significantly in their size, charge, hydrophobicity and morphology. The broad range of possible deposition, attachment and resuspension scenarios adds to this complexity. Once viruses are attached, their survival on fomites depends on virus type, strain and inoculation titer; as a broad example, enteric viruses (which are mostly non-enveloped) are known to maintain their infectivity for longer than respiratory viruses (mostly enveloped). While a reductionist approach with its incremental accumulation of data based on studies of specific virus-fomite pairs is certainly possible, it would be desirable to identify a limited range of representative fomites, viruses and deposition conditions that can typify practically relevant scenarios and help reach generalizable conclusions.

The practical goal of the present work is to develop an approach for reducing the complexity of the broad range of surface chemistries and morphologies presented by fomites to a relatively small subset of “archetype” surfaces. An “archetype” is operationally defined as representing a set of surface properties that are characteristic of a distinct group of materials and define their adhesive behavior with respect to a virus of concern. The practical value of the approach is in facilitating both the selection of surfaces with desired virus adhesion characteristics and the design of surface cleaning solutions and protocols. With the premise that fomites can be grouped based on the values of their surface energy components, we select four specific materials - silica,

stainless steel, nylon, and polypropylene - and rationalize the selection using the van Oss theory, a three-component model for surface energy [47]. SiO₂ represents high surface energy metal oxides with a dominant electron donor component, nylon 6,6 typifies monopolar polymer with strong dispersive interactions, stainless steel is a pure metal coated by an oxide-rich passivation film with commensurate electron donor and electron acceptor components, while polypropylene represents low surface energy apolar polymers with weak dispersive interactions only.

The study employs two pathogenic microorganisms - human respiratory syncytial virus (HRSV) and human adenovirus 5 (HAdV5) - as representatives of enveloped and nonenveloped viruses, respectively. HRSV and HAdV5 are selected based on the high relevancy of both viruses for public health, demonstrated importance of fomites for their transmission, as well as for practical reasons (both are available commercially in high purity and titer). HAdV, a large nonenveloped virus [48, 49], is highly resistant to both monochloramine and UV irradiation [50] and can survive on fomites for many days [2]. HAdV is primarily spread by the fecal-oral and respiratory routes through person-to-person contact and fomite-mediated transfer [51, 52]. Adenoviruses can cause a range of clinical diseases, including respiratory, gastrointestinal, and conjunctival illness. HRSV, which features a distribution of sizes and morphologies (spherical or filamentous) [53], can cause severe disease, especially in children, the elderly and immunocompromised adults [54]. HRSV is primarily spread by large droplets and via fomites, and can survive on nonporous surfaces, skin, and gloves for many hours [55, 56]. The makeup of the solution from which deposition occurs affects the likelihood of

virus attachment. A large number of illnesses are associated with more than 150 different types of pathogenic respiratory viruses transmittable from bodily secretions to surfaces. Indeed, viruses deposit onto fomites either as a result of direct contact with an infected human or from respiratory droplets produced by such person. Given that both HRSV and HAdV5 are present in the human respiratory tract, the present study focuses on the latter transmission route and explores virus deposition from a high ionic strength electrolyte (150 mM NaCl) typical for respiratory fluid (9 g·L⁻¹, physiological concentration [57]). While the composition of respiratory fluid is complex and varies with individual's health status [58, 59], some aggregate characteristics such as pH and ionic strength can be captured in modeling studies.

The study explores the hypothesis that virus attachment to fomites in a high ionic strength solution is governed by hydrophobic interactions. To test the hypothesis, we use quartz crystal microbalance with dissipation (QCM-D) and QCM-D sensors with specialty coatings to experimentally determine attachment efficiency for HRSV and HAdV5 depositing onto four “archetypal” fomites that span a range of hydrophobicities. The experimental measurements are complemented by modeling based on the extended Derjaguin-Landau-Verwey Overbeek (XDLVO) theory. Experimental and modeling results are interpreted in terms of polar, dispersive, and electrostatic interactions between viruses and fomites.

3.3 Materials and Methods

3.3.1 Reagents, fomites, viruses

All chemical reagents were of high purity (>99%). NaCl, KCl, glycerol, sodium dodecyl sulfate (SDS), ethylene glycol (EG) and diiodomethane (DID) were purchased from Sigma Aldrich. QCM-D sensors coated with materials representing fomites – silica, nylon 6,6 (hereafter “nylon”), stainless steel (SS), and polypropylene (PP) – were purchased from Nanoscience. Deconex 11 (Fisher Scientific) was used as the cleaning solution for PP and nylon sensors (see Supplementary Material (SM)). Silica and SS sensors were cleaned with 2% SDS solution and Hellmanex II (Hellma GmbH & Co. KG), respectively.

Human adenovirus 5 (HAdV5) was purchased from American Type Culture Collection (ATCC® VR-1516™) [60]. The product is an aqueous suspension of HAdV5 in 20 mM TRIS, 25 mM NaCl, 2.5% glycerol (pH 8.0) [61] purified by single column chromatography [62]. HAdV5 is a non-enveloped dsDNA virus with an icosahedral nucleocapsid. Human respiratory syncytial virus (HRSV; strain: Long) was also purchased from ATCC (VR-26PQ™) [63]. The product is an aqueous suspension of HRSV in 50 mM Tris-HCl, 150 mM NaCl, 1 mM EDTA prepared by concentrating another HRSV stock (ATCC VR-26™) via sucrose cushion centrifugation [64]. HRSV is an ssRNA virus with a helical nucleocapsid surrounded by matrix protein and an envelope. Spherical and filamentous HRSV virions have been identified [53, 65, 66].

3.3.2 Virion characterization: Hydrodynamic size, ζ -potential, concentration

Electrophoretic mobility and hydrodynamic diameter of HRSV virions were measured by laser doppler micro-electrophoresis (Zetasizer Nano ZS, Malvern) and dynamic light scattering (DLS), respectively. The 1 mM KCl diluent used in these measurements was pre-filtered through 0.22 μm syringe filter. The charge and size of HAdV5 (ATCC[®] VR-1516[™]) were determined previously [36]. These measurement techniques capture averaged values of virus charge and size. While the electrical charge has a certain distribution over the virus surface, streaming potential is an aggregate estimate of the surface potential averaged over the surface. Similarly, DLS estimates particle's diffusion coefficient, which is then converted to particle size assuming that the particle is spherical. Yet viruses (including HAdV5 [36] and HRSV [53, 65, 67]) have complex morphology. The adopted approach where viruses are treated as spherical colloids with a chemically homogenous surface are justified as both XDLVO modeling (section 2.4) and interpretation of experimental data on virus adhesion obtained by QCM-D (sections 2.5 and 3.1) rely on these assumptions. As a complement to DLS measurements, both HRSV and HAdV5 were imaged using transmission electron microscopy (TEM, JEM-1400 Flash, Jeol, Nieuw-Vennep). TEM sample preparation and imaging procedures are described in SM, section S1. Virus concentration was measured by fluorometry (Qubit fluorometer, Invitrogen) with Qiagen DNA and RNA mini kits used to extract dsDNA from HAdV5 and ssRNA from HRSV. The ssRNA High Sensitivity and dsDNA

High Sensitivity modes were utilized for HRSV and HAdV5 genome quantification, respectively.

3.3.3 Quantifying surface energy of viruses and fomites

3.3.3.1 Approach

Hydrophobicity of a solid (s) can be quantified in terms of the free energy of its interfacial interaction with an identical material when immersed in water (w), ΔG_{sws} [47]. We applied this approach to evaluate hydrophobicity of viruses (v) and fomites (f) by computing ΔG_{vww} and ΔG_{fww} , respectively. The calculation relies on the knowledge of the solid's surface energy in terms of its three components: two Lewis acid-base (electron acceptor, γ_s^+ , and electron donor, γ_s^-) components and the Lifshitz-van der Waals component, γ_s^{LW} . The Lewis acid-base components are also described as *polar* while the Lifshitz-van der Waals component is often referred to as *dispersive* or *apolar*. The components can be determined by measuring contact angles (θ) of three probe liquids (l) with known γ_l^{LW} , γ_l^+ and γ_l^- on the surface of the solid and substituting these values into the Young-Dupré equation [68, 69]

$$(1 + \cos\theta)\gamma_l^{TOT} = 2 \left(\sqrt{\gamma_s^{LW}\gamma_l^{LW}} + \sqrt{\gamma_s^+\gamma_l^-} + \sqrt{\gamma_s^-\gamma_l^+} \right), \quad (1)$$

where γ_l^{TOT} is the total surface energy of the probe liquid:

$$\gamma^{tot} = \gamma^{LW} + \gamma^{AB} = \gamma^{LW} + 2\sqrt{\gamma^-\gamma^+}. \quad (2)$$

The free energy of solid-solid interfacial interaction in water is given by

$$\Delta G_{sws} = -2 \left(\sqrt{\gamma_s^{LW}} - \sqrt{\gamma_w^{LW}} \right)^2 - 4 \left(\sqrt{\gamma_s^+ \gamma_s^-} + \sqrt{\gamma_w^+ \gamma_w^-} - \sqrt{\gamma_s^+ \gamma_w^-} - \sqrt{\gamma_s^- \gamma_w^+} \right) \quad (3)$$

where γ_w^{LW} , γ_w^+ and γ_w^- are surface energy components of water. A positive value of ΔG_{sws} indicates a hydrophilic surface, while negative ΔG_{sws} corresponds to a hydrophobic surface. The absolute value of ΔG_{sws} indicates the degree of hydrophilicity (or hydrophobicity, when $\Delta G_{sws} < 0$) of the surface. As in the case with size and charge measurements, the determination of virus and fomite surface energies based on contact angles of probe liquids treats these surfaces as chemically homogeneous. Thus, the presence of hydrophobic or hydrophilic “patches” on a surface is not accounted for and energy values describe interaction of “equivalent” chemically homogenous surfaces.

3.3.3.2 Experiments

Contact angles of three probe liquids - DI water, glycerol, and DID - on fomite surfaces and HRSV lawns were measured using the sessile drop method (goniometer / tensiometer model 250, ramé-hart). Additional contact angle measurements with EG as the fourth probe liquid were done for the polypropylene surface. Virus lawns were formed by filtering virus stock suspensions through a polyethersulfone ultrafiltration membrane (50 kDa, Pall Life Sciences) to form a multilayer (> 5 monolayers) cake, or lawn, of virions [70]. Prior to recording contact angle values, the lawn was allowed to dry in air until the contact angle of water on the virus lawn stabilized. A separate set of measurements was performed to study the effect of pH and ionic strength on water contact angles on fomite surfaces. All measurements were performed in the air at the ambient temperature of 22 °C and the relative humidity of 47 %. The droplet volume

was 6 μl . Contact angle values were calculated by DROPImage Advanced software based on recorded droplet shapes.

3.3.4 Modeling virus-fomite interactions. Extended Derjaguin-Landau-Verwey-Overbeek theory

The interactions between colloidal and surfaces can be predicted by XDLVO theory.

The theory describes the total energy of interaction U_{vwf}^{XDLVO} between a spherical particle (representing a virus (v)) and a flat surface (representing a fomite (f)) in water (w) as a sum (see eq. (7)) of Lifshitz-van der Waals (LW), U_{vwf}^{LW} , electrostatic double layer (EL), U_{vwf}^{EL} , and Lewis acid-base (AB), U_{vwf}^{AB} , energies expressed as follows:

$$U_{vwf}^{LW}(d) = -\frac{Aa}{6d} = 2\pi d_0^2 \frac{a}{d} \Delta G_{d_0}^{LW} \quad (4)$$

$$U_{vwf}^{EL}(d) = \pi \varepsilon_r \varepsilon_0 a \left[2\psi_v \psi_f \ln \left(\frac{1 + e^{-\kappa d}}{1 - e^{-\kappa d}} \right) + (\psi_v^2 + \psi_f^2) \ln(1 - e^{-2\kappa d}) \right] \quad (5)$$

$$U_{vwf}^{AB}(d) = 2\pi a \lambda \Delta G_{d_0}^{AB} \exp \left(\frac{d_0 - d}{\lambda} \right) \quad (6)$$

$$U_{vwf}^{XDLVO} = U_{vwf}^{LW} + U_{vwf}^{EL} + U_{vwf}^{AB} \quad (7)$$

where a is the virus radius, d is the virus-fomite minimal interfacial separation distance,

$A = -12\pi d_0^2 \Delta G_{d_0}^{LW}$ is the Hamaker constant, ε_r is the relative dielectric permittivity of

water (for water at 25 °C, $\varepsilon_r \approx 78.3$), ε_0 is the dielectric permittivity of vacuum ($\varepsilon_0 =$

$8.854 \times 10^{12} \text{ C} \cdot \text{V}^{-1} \cdot \text{m}^{-1}$), ψ_v and ψ_s are surface potentials of the virus and fomite,

respectively, κ is the inverse Debye screening length, λ is the characteristic delay length

of AB interactions in water ($\lambda = 0.6 \text{ nm}$), and d_0 is the minimum separation distance (d_0

= 0.158 nm) due to Born repulsion. Surface potentials ψ_v and ψ_f are commonly approximated by ζ -potentials (ζ_v and ζ_f). Values of $\Delta G_{d_0}^{LW}$ and $G_{d_0}^{AB}$ in eq. (4) and eq. (6) are given by:

$$\Delta G_{d_0}^{LW} = 2 \left(\sqrt{\gamma_v^{LW}} - \sqrt{\gamma_w^{LW}} \right) \left(\sqrt{\gamma_w^{LW}} - \sqrt{\gamma_f^{LW}} \right) \quad (8)$$

$$\Delta G_{d_0}^{AB} = 2 \sqrt{\gamma_w^+} \left(\sqrt{\gamma_f^-} + \sqrt{\gamma_v^-} - \sqrt{\gamma_w^-} \right) + 2 \sqrt{\gamma_w^-} \left(\sqrt{\gamma_f^+} + \sqrt{\gamma_v^+} - \sqrt{\gamma_w^+} \right) - 2 \sqrt{\gamma_f^+ \gamma_v^-} - 2 \sqrt{\gamma_f^- \gamma_v^+} \quad (9)$$

The free energy of virus-fomite interfacial interaction in water, ΔG_{vwf} , is

$$\Delta G_{vwf} = \Delta G_{d_0}^{LW} + \Delta G_{d_0}^{AB} \quad (10)$$

Note that eq. (3) can be obtained from eqs. (8 - 10) by substituting subscripts v and f for s . Lewis acid-base interactions are also referred to as electron donor/electron acceptor or polar interactions. Hydrophobic attraction and hydrophilic repulsion (i. e. hydration pressure) are two types of polar interactions [47].

Virion size, surface charge and surface energy components as well as surface charge and surface energy components of each of the four fomites were used as inputs to the XDLVO model. In its description of the energy of sphere-plate interaction energy, the model assumes that both surfaces are smooth. The effect of surface roughness can be taken into account by adding the sphere-asperity term to the calculation of the total interaction energy [71, 72]. Applied to the calculation of the energy of interaction between household paint coatings and human adenovirus 40 (a virus similar to HAdV5), this approach showed that the presence of ~ 27 nm asperities on paint-coated QCM-D

sensors had only a minor effect (~ 10% change in the total energy) [38]. Based on the manufacturer's data, the root mean square surface roughness of QCM-D sensors is < 1 nm for stainless steel and silica and ~ 3.5 nm for nylon and polypropylene [73] – well below the 27 nm value for which XDLVO predictions were only weakly affected.

Most data were obtained in experiments as described in sections 2.2 and 2.3. Size and charge of HAdV5 were determined in our earlier study and used in the present work [36]. Values of the ζ -potential of the four fomites as a function of pH were adopted from literature (Zemljic et al. [74] for PP, Hedberg et al. [75] for SS, Zhang et al. [76] for nylon, and Wang et al. [36] for silica).

3.3.5 QCM-D studies of HAdV5 and HRSV attachment to fomites

3.3.5.1 Approach: Quantifying virus-fomite attachment efficiency

To accurately assess the mass flux of viruses towards the QCM-D sensor surface one needs to solve the Graetz problem of diffusion-limited transport to a flat plate from a crossflow [77, 78]. Given the complexity of the QCM-D chamber geometry and the need to add surface reaction (describing the finite probability of virus attachment to the sensor surface), the solution would need to be numerical. Instead, we propose a simple model that describes the rate of virus deposition (ng/min) onto QCM-D sensor surface as

$$\frac{dm_v}{dt} = \alpha_{vf} j_m A_s \quad (11)$$

where α_{vf} (unitless) is the virus-fomite attachment efficiency, A_s (cm²) is surface area of the sensor and j_m (ng·cm⁻²·min⁻¹) is the mass flux of viruses towards the sensor. We define mass transfer coefficient, k (m·s⁻¹), as follows:

$$j_m = k(C_b - C_s) \quad (12)$$

where C_b and C_s are virus concentrations in the bulk of the flow and at the sensor surface, respectively. For early stages of deposition $C_s \ll C_b$, the sensor is mostly virus-free and the rate of virus deposition is approximately constant:

$$\frac{dm_v}{dt} \approx \alpha_{vf} k C_b A_s \quad (13)$$

The linearity of the deposition rate dependence on concentration was confirmed in tests with different C_b (see SM, Fig. 12). Because the rate of mass transfer across the viscos

sublayer at the QCM-D sensor surface depends on virus diffusivity, mass transfer coefficient, k , needs to be determined for each virus separately.

3.3.5.2 QCM-D experiments

The QCM-D E4 system (Biolin Scientific) was used to quantify the deposition of viruses onto sensor surfaces. Prior to measurement, QCM-D sensors were cleaned (see SM, section S4) and then mounted into the flow chamber to determine their resonance frequency in air. QCM-D tests were carried out at 25 °C in a continuous flow mode (0.15 ml/min) using a digital peristaltic pump (IPC, four channels, ISMATEC). The sensors were first equilibrated with DI water (pH 5.8), then with 0.22 μm filtered NaCl electrolyte (pH 5.8) and only after the vibration frequency stabilized were challenged with a virus suspension. Procedures performed to avoid air bubble formation on the surface of hydrophobic PP sensors are described in SM, section S2. QCM frequency and dissipation were recorded every 1 min. The frequency shifts were fitted into the Sauerbrey equation [79] to compute the change in areal mass density, Δm ($\text{ng}\cdot\text{cm}^{-2}$):

$$\Delta m = -\frac{C\Delta f}{n} \quad (14)$$

where C is the mass sensitivity constant ($C = 17.7 \text{ ng}\cdot\text{Hz}^{-1}\cdot\text{cm}^{-2}$), n is the overtone number and Δf is the frequency shift (Hz). All virus suspensions used in QCM-D tests were prepared by diluting the virus stock in a background electrolyte pre-filtered through a 0.22 μm filter. Background electrolytes were either 150 mM NaCl (pH 5.8) or 1 mM NaCl (pH 4.1 in tests with HAdV5 and pH 3.8 in tests with HRSV). The 150 mM NaCl solution was used in most tests with all 8 fomite-virus pairs. The 1 mM NaCl was used

in additional tests with HAdV5/PP and HRSV/PP pairs to simulate conditions of $\alpha_{vf} = 1$ (see SM, section S6). Prior to use in QCM-D experiments, virus suspensions were vortexed for 15 s to ensure a uniform dispersion of virions.

After ~ 60 min of QCM-D measurement, the sample chamber and tubing were flushed with the background electrolyte followed by DI water (pH 5.8). Each sensor was used in 5 to 7 different QCM-D experiments and cleaned after each test. To ascertain that cleaning did not affect the hydrophobicity of the sensor coatings, contact angles of three probe liquids were re-measured after multiple cycles of QCM-D tests and cleaning (see SM; Tables 4 – 6).

3.4 Results and Discussion

3.4.1 Virus concentration, size, charge and hydrophobicity

The concentrations of HAdV5 and HRSV in stock suspensions were verified by fluorometry (Qubit, Invitrogen) and found to be somewhat different from the values given by ATCC for these specific lots. The measured concentrations were 3.45×10^{11} GC/ml for HAdV5 (lower than ATCC-reported 5.8×10^{11} GC/ml [61]) and 2.65×10^{10} GC/ml for HRSV (higher than ATCC-reported 1.7×10^{10} GC/ml [64]). Based on the measured values of the hydrodynamic size (see below) and the approximate virion density, the corresponding mass concentrations of HAdV5 and HRSV in the feed suspensions were estimated to be 28 ng/mL and 12 ng/mL.

The hydrodynamic diameter, d_h , of HAdV5 was ~ 102 nm as determined by DLS in our previous study [36]. This size is derived using Stokes-Einstein equation (eq. (15)) based on the measured value of HAdV5 diffusivity, $D = 4.27 \times 10^{-12}$ ($\text{m}^2 \cdot \text{s}^{-1}$).

$$D = \frac{k_B T}{3\pi\mu d_h} \quad (15)$$

The difference between HAdV5 diameter values estimated from TEM images (~ 90 nm, Figures 10G and 10H) and measured by DLS is likely due to the presence of fibers on the HAdV5 surface [39, 48], which slow down diffusion.

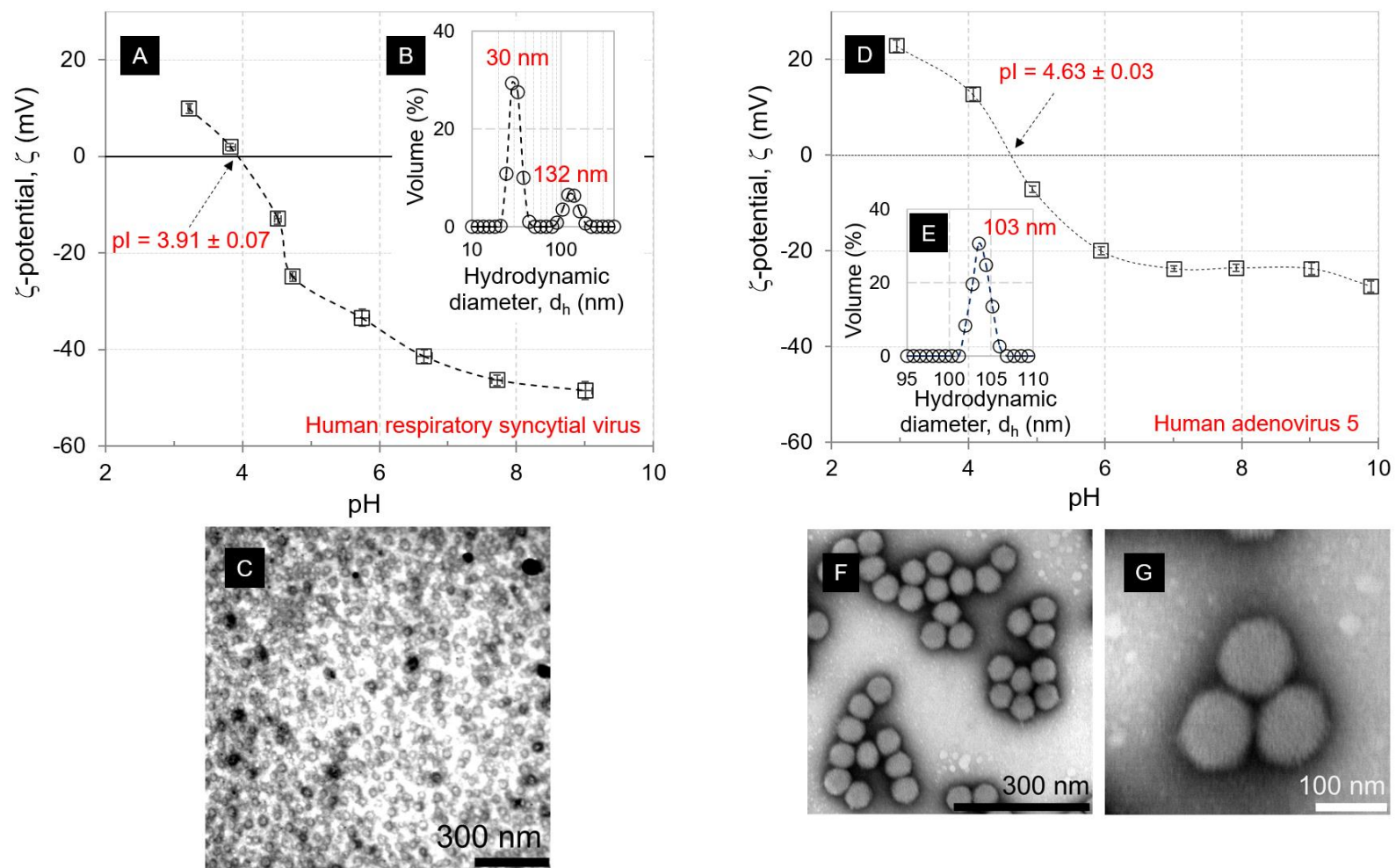


Figure 34. ζ -potential as a function of pH (A, D), size distribution (B, E), and TEM images (C, F, G) of HRSV (A-C) and HAdV5 (D-G). In A, B, D and E, lines are added to guide the eye. Charge and size values for HAdV5 (D, E) are adopted from our earlier report [36]. Additional TEM images are shown in SM, Figure 42.

Table 8. Contact angle of probe liquids, surface energy parameters (γ^{LW} , γ^+ , γ^- , γ^{AB} , γ^{tot}) and the free energy of interfacial interaction in water (ΔG_{sws}) of four fomites (clean, before use) and two viruses. Error estimates were obtained by propagating experimental errors in measured contact angles through the calculation of surface energy components (eqs (1) and (2)) and ΔG_{sws} (eq. (3)). Additional contact angle measurements were performed for the four fomites using 150 mM NaCl solution at pH 5.8; the contact angle data and calculated surface energy values are given in SM (Table 11).

Parameter	Fomites				Viruses		
	Silica	Nylon	Stainless steel	Polypropylene	HAdV5 ^B	HRSV ^C	
Contact angle	H ₂ O ^A	12.1 ± 0.9	50.1 ± 1.4	60.7 ± 1.9	100.5 ± 1.5	72.3 ± 0.4	73.5 ± 2.6
	Glycerol	14.7 ± 1.5	50.5 ± 1.0	31.4 ± 0.8	89.4 ± 1.6	70.5 ± 1.2	63.6 ± 1.3
	DID	31.4 ± 2.6	12.4 ± 0.9	50.2 ± 1.5	58.6 ± 2.9	28.5 ± 1.0	45.2 ± 2.0
	EG	n/a	n/a	n/a	77.5 ± 1.8	n/a	n/a
Surface energy (mJ·m ⁻²)	γ^{LW}	43.6 ± 1.1	49.6 ± 0.2	34.2 ± 0.8	29.4 ± 1.7	36.1 ± 1.9	36.9 ± 1.1
	γ^+	2.2 ± 0.2	0.02 ± 0.02	6.8 ± 0.5	0	0	0.4 ± 0.2
	γ^-	44.5 ± 0.7	26.9 ± 2.1	7.4 ± 1.5	0.5 ± 0.2	14.9 ± 1.2	9.0 ± 2.6
	γ^{AB}	19.7 ± 0.6	1.4 ± 0.4	14.2 ± 1.6	0	0	3.8 ± 1.1
	γ^{tot}	63.3 ± 1.2	51.0 ± 0.4	48.4 ± 1.8	29.4 ± 1.7	36.1 ± 1.9	40.7 ± 1.5
	ΔG_{sws}	15.7 ± 1.1	- 8.5 ± 3.9	- 25.5 ± 2.9	- 88.9 ± 2.5	- 27.7 ± 1.1	- 40.2 ±

Notes: ^A DI water, pH 5.8; ^B Wang et al. [36]; ^C Contact angle measurements were performed on top of a multilayer lawn of viruses assembled, by filtration, on the surface of a hydrophilic ($\Delta G_{sws} = 18.9 \text{ mJ}\cdot\text{m}^{-2}$) polyethersulfone ultrafiltration membrane.

In addition, drying-induced shrinkage of virions during negative staining may have decreased the diameters observed in TEM images [80]. A similar discrepancy between DLS- and TEM-derived sizes was also reported for HAdV40 [81]. For the HRSV suspension, the volume-based particle size distribution obtained by DLS (Fig. 10B; note the logarithmic size scale) was bimodal with a larger peak at $\sim 30 \text{ nm}$ and a smaller peak at $\sim 132 \text{ nm}$, indicating varied particle size or morphology of HRSV [53, 65, 67]. Given that volume-based distributions are sensitive to the presence of larger particles, the small intensity of the 132 nm peak points to their low abundance. Still, because deconvolution of DLS scattered light frequency data assumes monodisperse scatterers, multimodal distributions should be treated with caution as quantitatively inaccurate. In such case, direct visualization by TEM is especially valuable. TEM imaging showed the preponderance of smaller and spherical HSRV virions (Fig. 10C) although larger and irregularly shaped virions were also occasionally observed. The latter observation is consistent with earlier reports of HRSV polymorphism [53, 65, 67].

Based on the measured values of HRSV electrophoretic mobility as a function of pH (Fig. 41), the isoelectric point (pI) of HRSV was estimated to be 3.91 ± 0.07 .

Electrophoretic mobilities were converted to ζ -potentials (Fig. 10A) using Ohshima equation [82] (see SM, section A5, Table 10). The Ohshima approach was used

because for HRSV in 1 mM KCl, $\kappa a \approx 6.4$, making neither Smoluchowski expression (valid when $\kappa a \gg 1$) nor Hückel expression (valid when $\kappa a \ll 1$) applicable. At pH 5.8, which has been reported to fall within the pH range typical for human respiratory fluid [83], the ζ -potential of HRSV is -33.9 ± 2.6 mV. The electrophoretic mobility of HAdV5 was measured earlier [36]; the pI of HAdV5 is 4.6 ± 0.03 while ζ -potential at pH 5.8 is -18.2 ± 0.1 mV (Fig. 10D).

Hydrophobicity of adenoviruses is responsible for their low recoveries from water [84-86] presumably in relation to virus loss to surfaces during sample handling (e. g. storage, transfer, sample concentration) [81]. The high negative values of ΔG_{sws} reported for HAdV40 (-30.4 mJ·m⁻² [81]) and HAdV5 (-27.7 mJ·m⁻² [36]) confirm their hydrophobicity. The propensity of these viruses to attach to surfaces also implies a higher likelihood of fomite-mediated transfer. In the present work, HRSV was determined to be even more hydrophobic (than HAdV5 and HAdV40) with ΔG_{sws} of -40.2 mJ·m⁻². In terms of surface energy components, the hydrophobicity of HAdV40, which is a monopolar virus ($\gamma^+ = 0$; Table 3), was due to the small value of the only non-zero component of virus-water polar interactions, $\sqrt{\gamma_s^- \gamma_w^+}$, when compared to the polar interaction between water molecules, $\sqrt{\gamma_w^+ \gamma_w^-}$ (see eq. (3)). The latter term represents the hydrogen bonding energy of the cohesion of water. To our knowledge the present study is the first report of HRSV surface energy and, more generally, of HRSV hydrophobicity.

3.4.2 Fomite hydrophobicity

In the order from most hydrophilic to most hydrophobic, the four fomites ranked as follows: silica > nylon > SS > PP, with $\Delta G_{f_{wf}}$ values of 15.7, - 8.5, -25.5, and - 88.9 $\text{mJ}\cdot\text{m}^{-2}$, respectively (Table 3). These estimates were computed based on contact angles measured using DI water at pH 5.8 as one of the probe liquids. For PP, $\sqrt{\gamma_s^+}$ took on a small negative value; this is a common observation for monopolar or near-monopolar materials where an experimental error prevents solving eq. (1) to determine surface tension components of the solid [87]. In this study, we assumed that γ_s^+ for PP is zero and computed γ_l^- using a graphical approach described by McCafferty [88] (see SM, section S8).

Surfaces in contact with aqueous solutions are most hydrophobic at pH near the pI of the surface. Indeed, isoelectric points can be determined by contact angle titration [89]. Cuddy et al. [90] performed such measurements for several common QCM-D sensors (Al_2O_3 , Au, SiO_2 , Ag, Ti). Because pH of the deposition and cleaning solutions can vary, it is important to evaluate hydrophobicity of fomites at different pH. The pH dependence of $\Delta G_{f_{wf}}$ for each fomite is shown in Fig. 11. The trends closely followed those of water contact angles (Fig. 44). For all four fomites the dependence of $\Delta G_{f_{wf}}$ on pH was a curve with a minimum. The dependence was strongest for stainless steel, which was considerably hydrophobic ($\Delta G_{f_{wf}} = - 24.2 \text{ mJ}\cdot\text{m}^{-2}$) near its pI but became hydrophilic ($\Delta G_{f_{wf}} > 0$) at $\text{pH} \lesssim 2.1$ and $\text{pH} \gtrsim 8.4$. Hydrophobicity of nylon, PP, silica and SS peaked at pH of $\sim 2.5, 2.6, 3.9$ and 4.0 respectively. The estimate for silica is in good

agreement with the pI value determined for silica-coated QCM-D sensors by Cuddy et al. [90].

Virga et al. [91] showed that the contact angle of an aqueous electrolyte is a stronger function of pH for higher ionic strength electrolytes. For the solutions employed in this work (DI water, 1 mM NaCl, 150 mM NaCl), the effects of the ionic strength of the contact angle (Fig. 44) and, by extension, hydrophobicity (Fig. 11) were not statistically significant. It was also assumed that the dependence of the surface tension of the aqueous solution on its ionic strength and pH was insignificant. Indeed, for the electrolyte used in the present work (150 mM NaCl) the effect was reported to be small: $\sim 2 \text{ mJ}\cdot\text{m}^{-2}$ increase over the surface tension of DI water [92].

3.4.3 Quantifying virus-fomite interactions. Four archetypal fomites

Table 4 presents values of ΔG_{vwf} and its dispersive and polar constituents ($\Delta G_{d_0}^{LW}$ and $\Delta G_{d_0}^{AB}$, see eqs (8-10)) for all eight virus-fomite pairs. The net interfacial interaction is attractive ($\Delta G_{vwf} < 0$) for all pairs except HAdV5/silica. A detailed analysis of ΔG_{vwf} in terms of surface energy components (i. e. relative contributions of various terms in eqs. (8) and (9)) can identify surface properties responsible for the strength, or weakness, of the overall interaction. Potentially, such analysis can help with the selection of surfaces resisting virus adhesion as well as the optimal makeup of surface cleaning solutions.

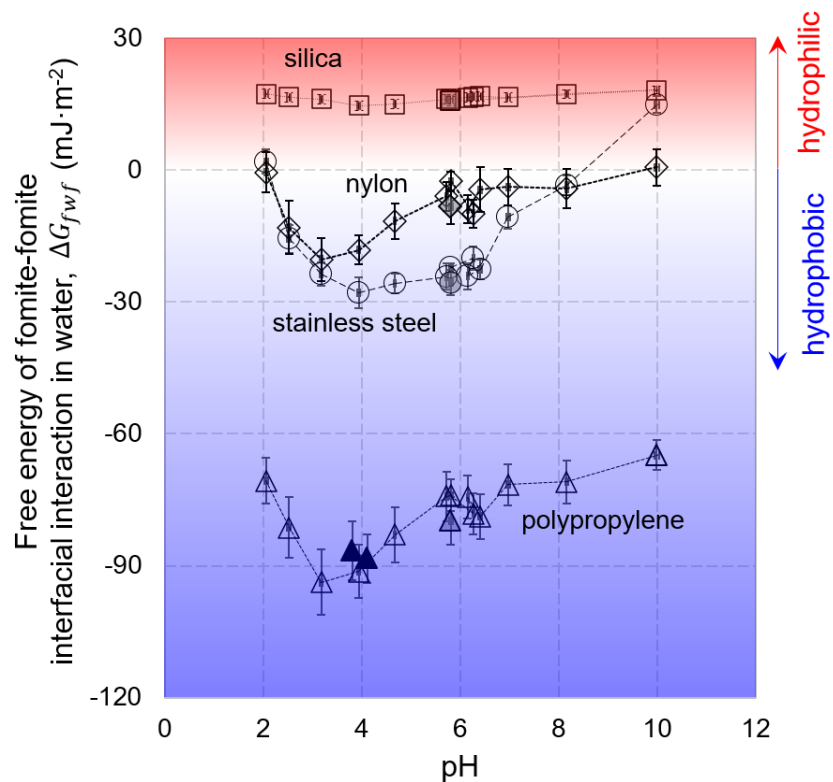


Figure 35. Free energy of interfacial interaction in water (ΔG_{fwf}) of four fomites as a function of pH. Depending on the type of aqueous solution used as a probe liquid, values are shown using either empty symbols (150 mM NaCl at pH 5.8; Table 10) or gray symbols (DI water at pH 5.8; Table 3) or black symbols (1 mM NaCl water at pH 3.8 and 4.1; Table 14).

Table 9. Free energy of virus-fomite interfacial interaction in water, ΔG_{vwf} , and its dispersive ($\Delta G_{d_0}^{LW}$) and polar ($\Delta G_{d_0}^{AB}$) components, for eight different virus-fomite pairs. Standard deviations were obtained by propagating experimental errors in measured contact angles (Table 3) through the calculation of surface energy parameters (eqs. (1) and (2)) and ΔG_{vwf} (eqs. (8), (9), and (10)).

Virus	Fomite	Interaction energy (mJ·m ⁻²)		
		$\Delta G_{d_0}^{LW}$	$\Delta G_{d_0}^{AB}$	ΔG_{vwf}
Human respiratory syncytial virus	Silica	- 5.5 ± 0.4	- 0.4 ± 3.2	- 5.8 ± 3.2
	Nylon	- 6.7 ± 0.4	- 19.0 ± 1.8	- 25.7 ± 1.9
	Stainless steel	- 3.3 ± 0.3	- 30.6 ± 3.3	- 33.9 ± 3.2
	Polypropylene	- 2.1 ± 0.5	- 59.1 ± 4.6	- 61.3 ± 4.6
Human adenovirus 5	Silica	- 5.2 ± 0.6	7.9 ± 1.1	2.7 ± 1.3
	Nylon	- 6.4 ± 0.8	- 10.4 ± 0.0	- 16.7 ± 0.8
	Stainless steel	- 3.2 ± 0.4	- 29.4 ± 0.8	- 32.5 ± 0.9
	Polypropylene	- 2.0 ± 0.5	- 56.0 ± 0.0	- 58.0 ± 0.5

A common feature for all four fomites and the two viruses studied in this work is that their γ^{LW} component is higher than that of water ($\gamma_w^{LW} = 21.8 \text{ mJ}\cdot\text{m}^{-2}$); as a result, for none of the virus-fomite pairs the conditions ($\gamma_f^{LW} < \gamma_w^{LW} < \gamma_v^{LW}$ or $\gamma_v^{LW} < \gamma_w^{LW} < \gamma_f^{LW}$) necessary for dispersive interaction to be repulsive ($\Delta G_{d_0}^{LW} > 0$; eq. (8)) were fulfilled. Thus, for both HAdV5 and HRSV their dispersive interactions with each of the four fomites were attractive. Notably, some common materials such as PTFE ($\gamma_w^{LW} = 18.6$

mJ·m⁻²; see Table 2.3 in the book by Kinloch [93]) would have repulsive dispersive interactions with HAdV5 and HRSV in water.

In several other respects, the four selected fomites differed. In what follows, the differences are described and presented as the basis for considering the four fomites as typifying distinct groups of materials (i. e. as “archetypes”).

1. *Silica* is characterized by a large electron donor component of its surface tension such that $\gamma_f^- \gg \gamma_f^+$. Silica’s polar interactions with HAdV5 are repulsive due to hydration of both silica and virus surfaces (large $\gamma_f^- \gamma_w^+$ and $\gamma_v^- \gamma_w^+$ terms in eq. (9)). Repulsive polar interactions ($\Delta G_{d_0}^{AB} > 0$) are referred to as *hydration pressure*. For the HAdV5/silica pair, hydration pressure overcomes water cohesion given by $\gamma_w^- \gamma_w^+$ so that even in the presence of attractive dispersive forces ($\Delta G_{d_0}^{LW} < 0$), the overall interaction is a mild repulsion ($\Delta G_{vwf} > 0$).
2. *Nylon* is less polar than silica. A near-monopolar surface ($\gamma_f^+ \cong 0$), nylon also has a smaller γ_f^- . As a result, the electron-donor attraction between nylon and viruses is weaker than water cohesion leading to $\Delta G_{d_0}^{AB} < 0$. Attractive polar interactions ($\Delta G_{d_0}^{AB} < 0$) are referred to as *hydrophobic attraction*. In case of nylon, the attraction is further enhanced due to the high (the highest among the four fomites) dispersive component of nylon’s surface tension, γ_f^{LW} .
3. *Stainless steel* surface has a substantial electron acceptor component such that $\gamma_f^+ \cong \gamma_f^-$. This gives stronger polar interactions with viruses (i. e. higher $\gamma_f^+ \gamma_v^-$ and

$\gamma_f^- \gamma_v^+$). Notably, these terms are independent of the properties of the continuous phase.

4. *Polypropylene* is an apolar material ($\gamma_f^+ \cong 0$; $\gamma_f^- \cong 0$). Because the dispersive component of PP's surface tension, γ_f^{LW} , is close to that of water (29.4 vs 21.8 mJ·m⁻²; Table 3), dispersive interactions of PP with any virus are also weak (eq. (8)). For viruses such that $\gamma_v^{LW} > \gamma_w^{LW}$ (which is the case for both HRSV and HAdV5), the dispersive interactions are attractive. As a result, hydrophobic attraction is the dominant mechanism of virus interaction with PP surface.

Many common materials are monopolar or nearly so with γ_f^+ very close to zero [94]. For such materials, substituting eq. (8) and eq. (9) into eq. (10), and posing $\Delta G_{vwf} = 0$, gives the following relationship between γ_f^- and γ_f^{LW} :

$$\gamma_f^- = \left[\frac{\sqrt{\gamma_v^{LW} \gamma_w^{LW}} + \sqrt{\gamma_f^{LW} \gamma_w^{LW}} - \sqrt{\gamma_v^{LW} \gamma_f^{LW}} - \gamma_w^{LW} - 2\sqrt{\gamma_w^- \gamma_w^+} + \sqrt{\gamma_w^- \gamma_v^+} + \sqrt{\gamma_w^+ \gamma_v^-}}{\sqrt{\gamma_v^+} - \sqrt{\gamma_w^+}} \right]^2 \quad (16)$$

In the 2D space with γ_f^- and γ_f^{LW} as coordinates, eq. (16) corresponds to the boundary separating all monopolar materials into those that have an overall attractive interaction ($\Delta G_{vwf} < 0$) and those having an overall repulsive interaction ($\Delta G_{vwf} > 0$) with a given colloid. Figure 12 illustrates such boundary for the case when the colloid is HRSV². Both the monopolar PP and the near-monopolar nylon (Table 3) interact with HRSV favorably.

² In his book "Interfacial Forces in Aqueous Media", van Oss pointed out that electron donor-only monopolar ($\gamma_s^+ = 0$) surfaces with $\gamma_s^{LW} = 40$ mJ·m⁻² ("a typical value for most biological and many other organic materials") are hydrophilic when their γ_s^- is above 28.3 mJ·m⁻². In effect, this comment referred to a specific point on the $\Delta G_{sws} = 0$ curve on a graph similar to Fig. 3 but drawn for ΔG_{sws} .

Note that ΔG_{vwf} does not account for electrostatic interactions, which, under appropriate conditions (see section 3.5), can create a substantial primary barrier and prevent adhesion. Such graph constructed for a given virus with known surface tension components would allow screening of various candidate materials and selecting ones with desirable adhesive properties vis-à-vis the virus.

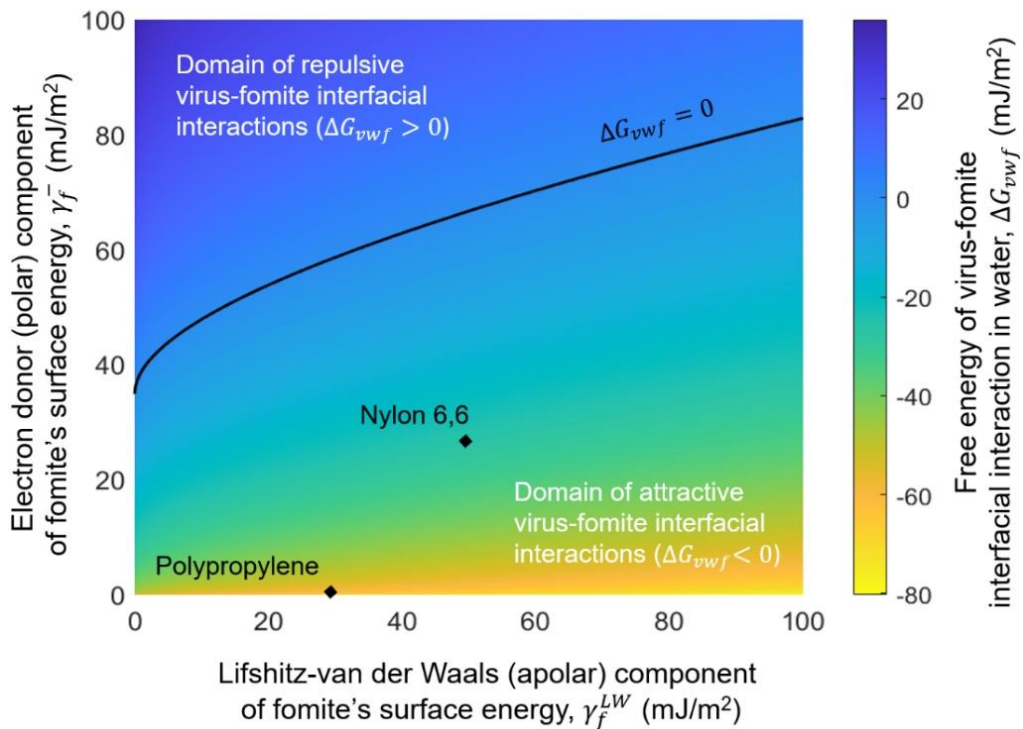


Figure 36. Free energy, ΔG_{vwf} , of interfacial interaction of HRSV with *monopolar* fomites ($\gamma_f^+ = 0$) in DI water. The solid line corresponds to $\Delta G_{vwf} = 0$ (i. e. solution of eq. (16)).

3.4.4 Virus adhesion to fomites: QCM-D measurements

3.4.4.1 Model of mass transfer in QCM-D chamber. Assumptions

Virus transport to the QCM-D sensor surface can be viewed as a two-step process – long range transport from the bulk of the flow to the surface followed by a collision event, which may or may not result in an attachment. The attachment efficiency, α_{vf} , is defined as the probability that a collision results in attachment. The QCM-D part of the present work is designed to determine α_{vf} values so that they can be related to the energy of virus-fomite interactions. In the simple mass transfer model given by eq. (13), the long-range transport of a virus and short-range virus-fomite interactions are described by k and α_{vf} , respectively. The linearity of eq. (13) was tested and confirmed ($R^2 > 0.99$) in a subset of QCM-D tests with HAdV5 and SS (see SM, Fig. 43). Further, it was assumed that deposited virions formed a laterally homogeneous film. In reality, the deposited layer is laterally heterogeneous, consisting of discrete virions with a solvation shell contributing to the QCM-D signal to different extents at different coverages. The use of the Sauerbrey equation is justified, however, in view of the near-overlapping time dependencies of $\Delta f_n/n$ for different harmonics (see section 3.4.3) and a relatively weak dissipation signal $\Delta D_n/(\Delta f_n/n) \ll 4 \times 10^{-7} \text{ Hz}^{-1}$ [41, 95].

3.4.4.2 Quantifying mass transfer in QCM-D chamber: Mass transfer coefficients for HAdV5 and HRSV and size of depositing virions

Based on dm_v/dt values measured in tests with PP under conditions of attractive electrostatic interactions (i. e. assuming $\alpha_{vf} = 1$; Fig. 49a, Fig. 49c), eq. (13) predicted the mass transfer coefficient, k , for HRSV and HAdV5 to be 5.97×10^{-9} (m/s) and 1.87×10^{-9} (m/s), respectively. The value of k for HAdV5 together with HAdV5 diffusion coefficient measured by DLS (section 3.1) can be used to estimate the effective thickness of the mass transfer boundary layer in the QCM-D chamber:

$$\delta \approx \frac{D}{k} \quad (17)$$

The thickness of boundary layer is defined by the hydrodynamics of the flow in the chamber and should be the same for both viruses. Given the very narrow size distribution for the HAdV5 stock (Fig. 10E) and, therefore, a more accurate D estimate for this virus, eq. (17) was applied to HAdV5 to predict $\delta \approx 2.3$ mm. This value of δ together with the value of k for HRSV can be used to predict the effective hydrodynamic diameter of HRSV based on Stokes-Einstein equation. Combining eq. (15) and eq. (17) gives:

$$d_h = \frac{k_B T}{3\pi\mu k \delta} \quad (18)$$

Eq. (18) predicts HRSV hydrodynamic diameter of 32 nm, which is an almost exact match to the higher peak in the size distribution for this virus (Fig. 10B). We conclude that the smaller size fraction of HRSV is the morphological subset of HRSV virions that predominantly deposit on the QCM-D sensor surface. While the polydispersity of HRSV

(Fig. 10B) confounds a direct application of size data in mass transfer calculations for this virus, the above analysis shows that QCM-D signal is due to the deposition of virions from the smaller size fraction of the HRSV population.

3.4.4.3 Virus deposition onto fomites. Virus-fomite attachment efficiency, α_{vf}

Figure 13 shows a QCM-D dataset recorded in experiments on virus deposition from 150 mM NaCl solution. Representative QCM-D results (both frequency and dissipation signals) from tests with all virus-fomites pairs are given in SM (Figures 50 – 57). During the virus deposition stage, the dissipation signal increased monotonously, with a relatively constant deposition rate, dm_v/dt , indicating early stages of the deposition process, far from the jamming limit. Indeed, based on the areal mass density and virion size, the surface coverage was below 4 % for HRSV and below 1 % for HAdV.

Three additional observations in QCM-D tests require a commentary. First, changes in the QCM-D signal in response to changes of the background solution (from DI to 150 mM and back) were not immediate. The transient period is due to a finite retention time within the QCM-D chamber. The lower bound on the retention time in the tubing and the QCM-D chamber is ~ 1.5 min; the estimate considers QCM-D chamber as an ideal completely mixed flow reactor so that the actual retention time should be higher.

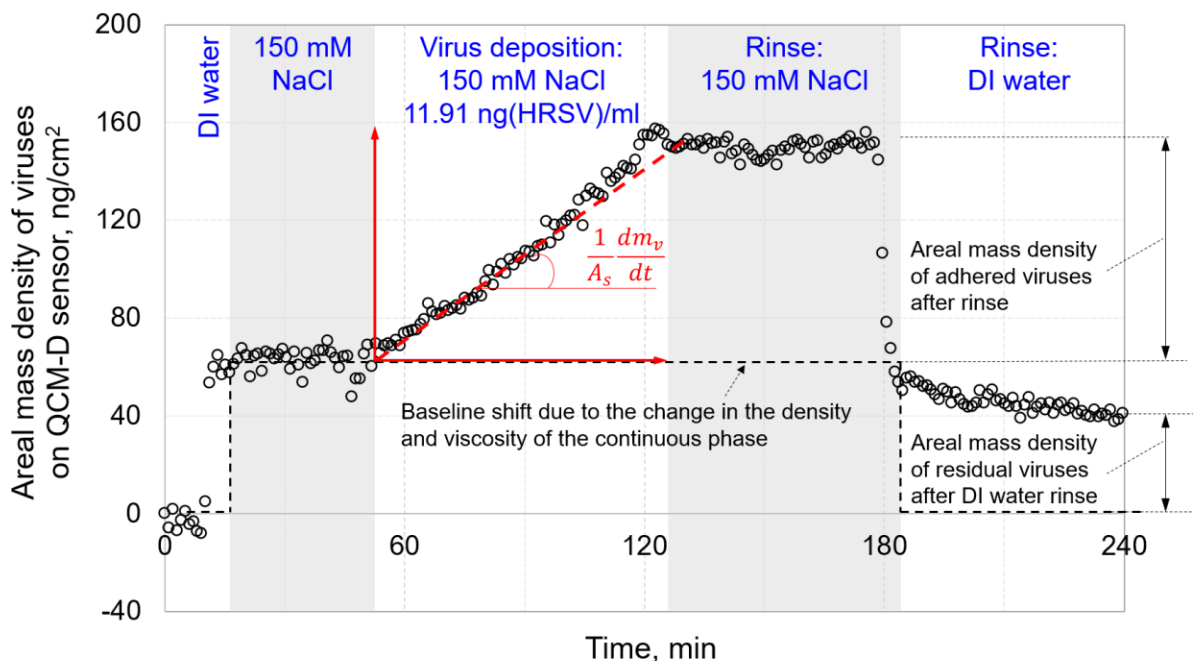


Figure 37. Example QCM-D data set: deposition of HRSV on stainless steel. Representative QCM-D data for all virus-fomite pairs and deposition conditions are given in SM (Figures 50 – 57). All calculations based on the QCM-D data were performed using the signal for the 5th overtone ($n = 5$ in eq. (14)). The reason for choosing the 5th harmonic was that the signals for the 3rd and 1st harmonics were unstable, likely due to their high sensitivity to mounting stress caused by the O-rings holding the sensor within the QCM-D chamber [96].

Second, averaged over all 24 QCM-D experiments (8 virus-fomite pairs, triplicate tests), the frequency shift due to the change of the solution from DI water to 150 mM NaCl was 20.9 ± 4.0 Hz. This was smaller than the shift predicted by the Kanazawa-Gordon equation (64.6 Hz; see eq. (S1)) based on the density and viscosity of the two solutions at 20 °C [97, 98]. The discrepancy may be due to a limited sensitivity of the sensors or a variation in the density of the quartz sensor. Third, the high reproducibility of dm_v/dt values for each condition indicated that the limited reuse of QCM-D sensors (for cleaning protocols see SM, section S4) had little impact on virus adhesion. This is

consistent with results of t-testing, which showed that sensor surface energy, $\Delta G_{f_{wf}}$, remained stable ($p > 0.1$) after repeated usage-cleaning cycles (Tables 12 and 13 vs Table 11).

Figure 14 shows values of the attachment efficiency computed based on dm_v/dt slopes in QCM-D tests with various virus-fomite pairs. For both HAdV5 and HRSV, more favorable interfacial interaction (quantitatively expressed in terms of ΔG_{vwf}) corresponded to a higher probability of attachment. Remarkably, normalization by C_b (a step in the computation of α_{vf}), made the α_{vf} vs ΔG_{vwf} dependencies for both viruses collapse into one trend, pointing to the possibility of using of ΔG_{vwf} as a predictor of virus adhesion. Whether this result holds true for other viruses and fomites warrants further testing.

As described in section 2.5.1, the determination of α_{vf} relies on quantifying the mass transfer coefficient, k , which is based on tests performed under conditions of highly favorable virus-fomite interaction with $\alpha_{vf} = 1$. To model this scenario, QCM-D tests were performed with polypropylene as the most hydrophobic of the four fomites (to maximize hydrophobic attraction U_{vwf}^{AB}), and under conditions when the electrostatic interactions are favorable ($U_{vwf}^{EL} < 0$) and strongest. The latter conditions were achieved by a) adjusting pH to be within the pH range bracketed by the pI values of polypropylene and the virus in question (see SM, section S6) and b) switching to low ionic strength electrolyte (1 mM NaCl) to minimize screening of attractive electrostatic interactions.

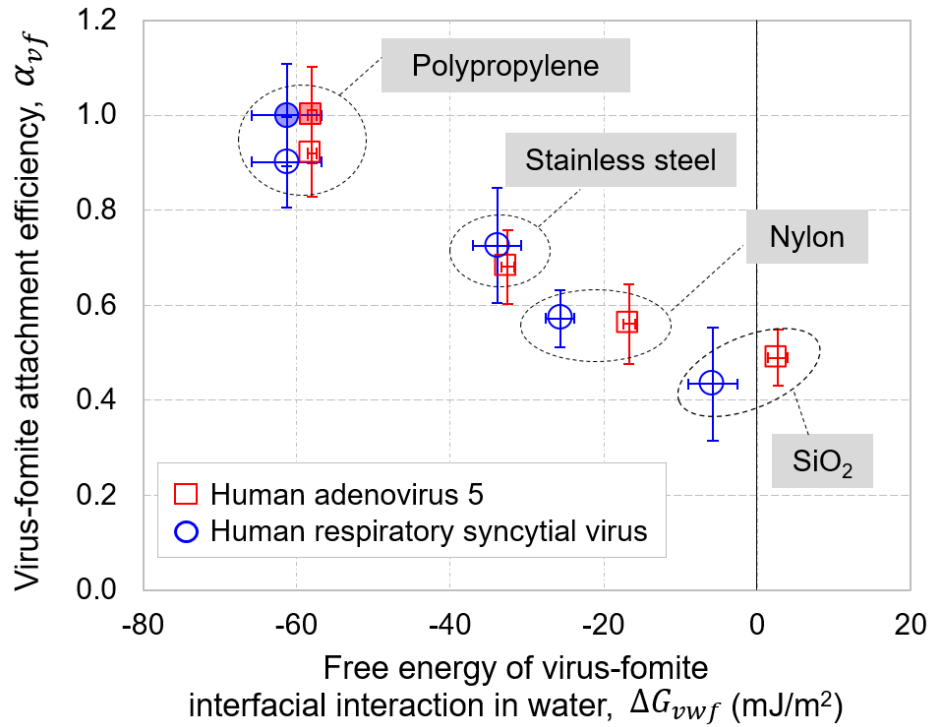


Figure 38. Virus-fomite attachment efficiency as a function of the free energy of virus-fomite interaction in water. Empty symbols correspond to tests with 150 mM NaCl electrolyte as the deposition solution. Filled symbols correspond to tests with virus deposition onto polypropylene from 1 mM NaCl at pH 4.1 for HAdV5 and at pH 3.8 for HRSV where virus-fomite electrostatic interaction is favorable and at its maximum absolute value. (See SM, section S6 for the algorithm used to select these pH values.).

Figure 15 gives examples of two QCM-D datasets that correspond to the least hydrophobic fomite-virus pair (silica and HAdV5 with $\Delta G_{f_{wf}}$ of 15.7 and - 27.7 mJ·m⁻², respectively) and the most hydrophobic one (HRSV and PP with $\Delta G_{f_{wf}}$ of - 40.2 and - 88.9 mJ·m⁻², respectively). As mentioned earlier, one simplification behind the presented approach is that the deposited layer is assumed to be laterally homogeneous. We note that this assumption provides a conservative estimate on the difference between hydrophilic and hydrophobic fomites in terms of their adhesiveness. The contribution of the solvent to the QCM-D signal should be higher for attached particles

with a larger shell of associated solvent, especially at lower coverages [95], such as those (< 4%) that occurred in our QCM-D tests. Thus, we expect that due to the higher contribution of the solvation shell, the values of α_{vf} are overpredicted for more hydrophilic virion-fomite pairs; therefore, the contrast between PP and silica should be more pronounced than what is apparent from Fig. 14.

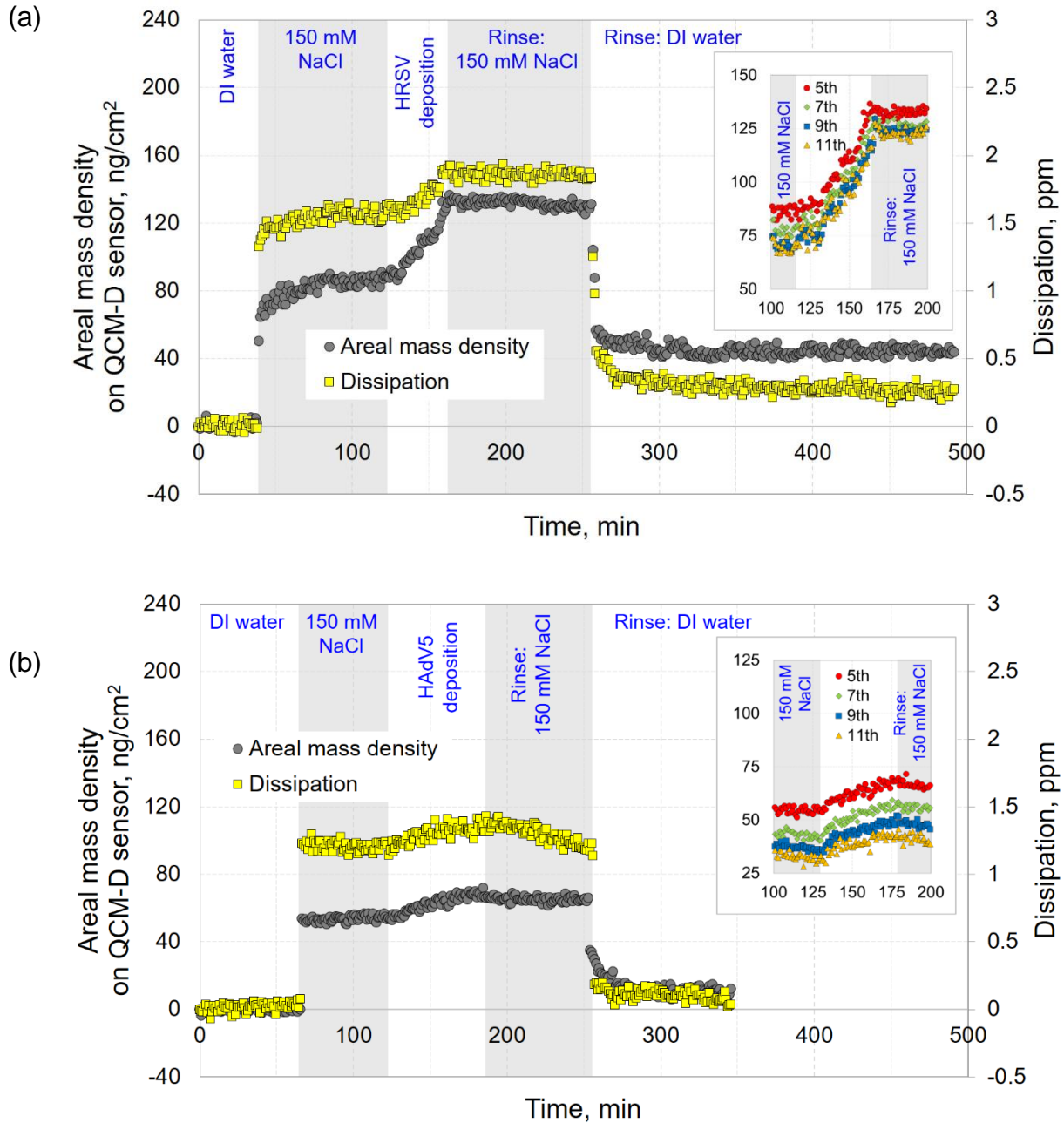


Figure 39. Mass and dissipation QCM-D data for the deposition of a) HRSV on polypropylene and b) HAdV5 on silica. Insets illustrate areal mass density values computed based on 5th, 7th, 9th, and 11th harmonics of the QCM-D signal.

3.4.5 XDLVO predictions

Virus properties required as inputs to XDLVO model included virus size as well as surface energy and ζ -potential of viruses and fomites. The ζ -potential of the four fomites as a function of pH was obtained from literature [36, 74, 75]. There was a significant variation in the reported values of ζ -potential of stainless steel [75, 99, 100] likely due to different degrees of passivation of the surface. While pure metals have very high surface energy, fast oxidation in air passivates the surface and minimizes its energy through the formation of a metal oxide bilayer. The passive film on the stainless steel surface consists of an inner sub-layer with segregated chromium oxide and an outer sublayer enriched in iron oxyhydroxide [101-103]. For XDLVO simulations, we adopted surface charge data reported by Hedberg et al. [75].

For both viruses, the XDLVO model predicted attractive interactions with nylon, SS and PP at all virus-fomite separation distances (Figures 16a, 45a, 45c, 46a, 47a, 47c, 48a) due to strong hydrophobic attraction. The XDLVO energy of interaction between silica and each of the two viruses featured a primary maximum and a secondary minimum. For HAdV5/silica (Fig. 16c), the corresponding energy values were 200 kT and - 3.0 kT; the reason for the very high primary energy barrier was the strong repulsive Lewis acid-base interaction between HAdV5 and silica (“hydration pressure”) as indicated by the positive value of $\Delta G_{d_0}^{AB}$ ($\sim 7.9 \text{ mJ}\cdot\text{m}^{-2}$; Table 4). For HRSV/silica (Fig. 48c), the primary maximum was much lower (21 kT) while the secondary minimum was shallower ($- 2.3 \text{ kT}$). The repulsive electrostatic interaction between HRSV and silica results in slightly

repulsive total interaction even though LW and AB interactions are both attractive ($\Delta G_{d_0}^{LW} = -5.5 \text{ J}\cdot\text{m}^{-2}$, $\Delta G_{d_0}^{AB} \approx -0.4 \text{ J}\cdot\text{m}^{-2}$; Table 4). During DI water rinse, there was always an energy barrier for all virus-fomite pairs except for the condition of $\alpha_{vf} = 1$. In XDLVO simulations describing the DI rinse, the ionic strength of the solution was assumed to be 10^{-5} M .

In XDLVO energy profiles corresponding to the conditions of DI water rinse (Fig. 16b, Fig 16d), the energy barriers were observed in all the cases at longer distance ($> 5 \text{ nm}$) except for HAdV5/silica, where barrier was located at the distance of $\sim 0.4 \text{ nm}$. The appearance of energy barriers is due to the increased importance of repulsive electrostatic interactions. In high ionic strength solution, the electrostatic interaction is limited due to the compression of the electric double layer, making the U_{vwf}^{EL} decrease much faster with distance. With the lowering of the ionic strength, this restriction disappears, making U_{vwf}^{EL} higher at longer distance. This is consistent with QCM-D results showing a much more effective removal of viruses when switching from 150 mM rinse to DI water rinse.

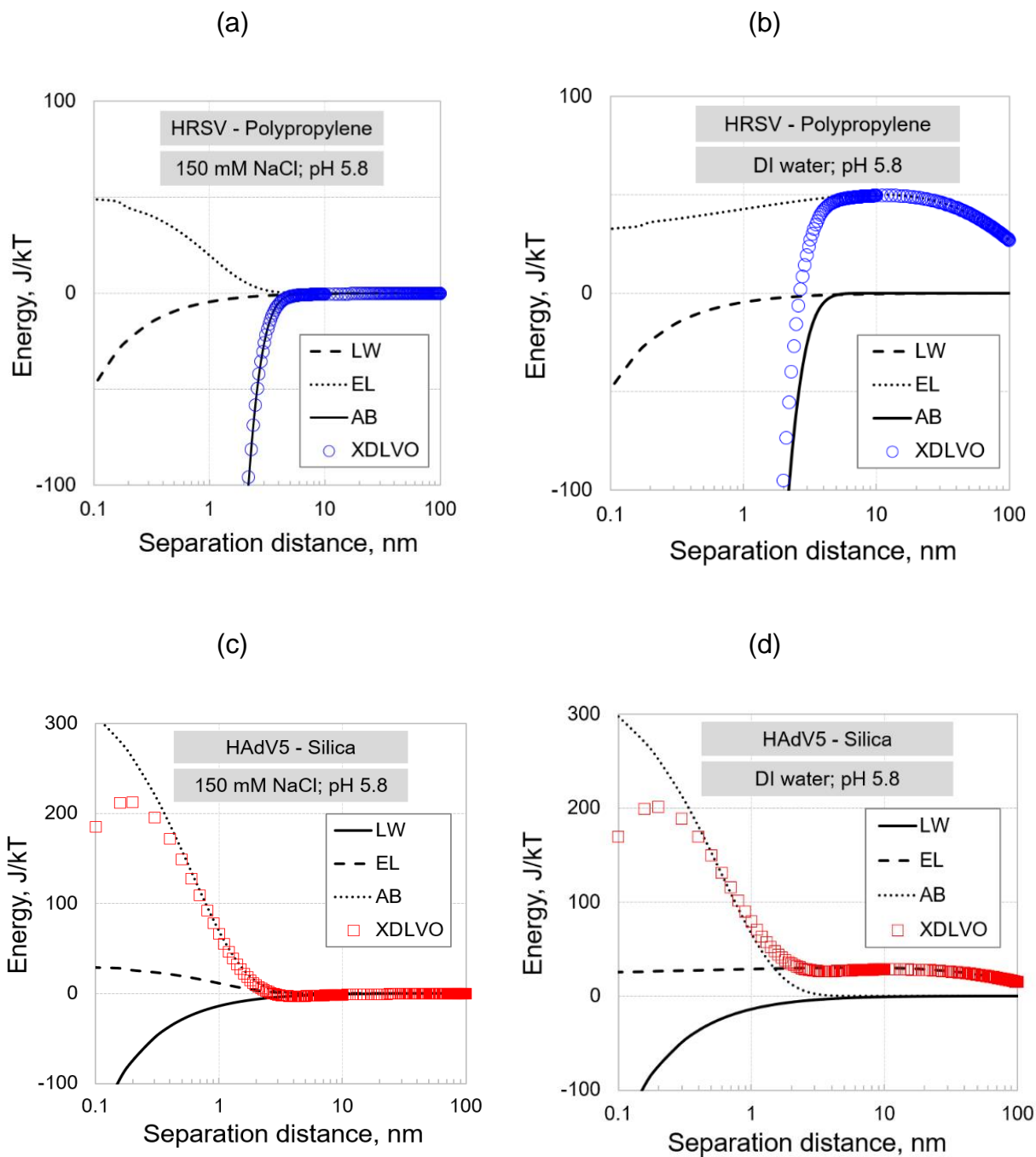


Figure 40. XDLVO total energy of interactions during virus deposition (a, c) and cleaning (b, d) stages of QCM-D experiments. The results are for HRSV interaction with polypropylene (a, b) and HAdV5 interaction with silica (c, d).

While outside of the scope of the present work, testing non-polar liquids as cleaning agents for virus removal is also of interest.

The XDLVO modeling complements interfacial energy analysis (Table 4) by providing insights into the relative importance of electrostatic interactions as a function of ionic strength. Accounting for classical DLVO (LW, EL) as well as polar (AB) interactions, the model predicts that at lower ionic strengths a solution with an appropriate pH deters adhesion and can help resuspend attached viruses. Separation distances that correspond to primary maxima (barriers for irreversible adhesion) and secondary minima (loci for possible reversible adhesion) correspond to a fraction of a virus diameter. Thus, for solution chemistries that discourage adhesion, a very minor disturbance in a virus' position at the surface may lead to detachment. While almost no removal of viruses was observed by flowing 150 mM NaCl solution after virus deposition, removal of 28.8% on average was possible after switching to DI water as the rinsing solution. These findings are also consistent with the results reported by Liu et al who employed SPR imaging to study adsorption of SARS-CoV-2 pseudovirus onto model surfaces [40]. Under conditions when the virus and the surface carried the charge of the same sign, adsorption was stronger at a higher ionic strength where the repulsive electrostatic interactions are screened out.

In general, anti-adhesion surfaces should have high positive value of the interfacial free energy of its interaction with a virus, ΔG_{vwf} (see Fig. 12). Consistent with XDLVO

modelling results, QCM-D data show that for both HAdV and HRSV, the efficiency of their attachment to fomites is correlated with ΔG_{vwf} . For a virus with known surface tension parameters, this knowledge can be used to select surfaces with as high ΔG_{vwf} as practically possible to deter virus adhesion. The proposed approach can also guide the selection of surface cleaning solutions and protocols. When the virus and surface carry electrical charges of the same sign, a cleaning solution with low ionic strength will allow for electrostatic repulsion. Whereas if the virus and surface are oppositely charged, cleaning solution with a high ionic strength can screen out attractive electrostatic interactions. Both strategies should promote virus detachment.

3.5 Conclusions

The present work considers interactions of two human enteric viruses – one enveloped (HRSV) and one non-enveloped (HAdV5) – with four fomites (silica, nylon, stainless steel, polypropylene). The selected fomites are tentatively identified as “archetypes” representing surfaces that are distinctly different in mechanisms of their interfacial interactions. The surfaces are typified on the basis of their surface energy components:

- Archetype 1 (e. g. silica) is characterized by a large electron donor component such that $\gamma_f^- \gg \gamma_f^+$. For these surfaces, hydration pressure can overcome water cohesion to result in an overall repulsion of viruses.
- Archetype 2 (e. g. nylon) is less polar than archetype 1 and has high dispersive component, γ_f^{LW} . A near-monopolar surface ($\gamma_f^+ \cong 0$), archetype 2 also has a smaller

γ_f^- . As a result, the electron-donor attraction between archetype 2 and viruses is weaker than water cohesion leading to hydrophobic attraction that is further enhanced due to dispersive forces.

- Archetype 3 (e. g. stainless steel) has a substantial electron acceptor component such that $\gamma_f^+ \cong \gamma_f^-$. This gives stronger polar interactions with viruses (i. e. higher $\gamma_f^+ \gamma_v^-$ and $\gamma_f^- \gamma_v^+$).
- Archetype 4 (e. g. polypropylene) is an apolar material ($\gamma_f^+ \cong 0$; $\gamma_f^- \cong 0$) with the dispersive component, γ_f^{LW} , close to that of water. Hydrophobic attraction is the dominant mechanism of virus interaction with such surfaces.

Areal mass density on the fomite surface is found to correlate with the free energy of virus-fomite interfacial interaction in water, ΔG_{vwf} . For both HAdV5 and HRSV, more negative ΔG_{vwf} values correspond to higher virus-fomite attachment efficiencies.

Moreover, α_{vf} vs ΔG_{vwf} dependencies for HAdV5 and HRSV collapse into one trend pointing to the possibility of using ΔG_{vwf} as a predictor of virus adhesion. Virus deposition from 150 mM NaCl electrolyte is defined by polar interactions. Under conditions of low ionic strength, however, electrostatic forces emerge as a dominant interaction at a longer range.

Through the analysis of relative contributions of separate surface tension components to the energy of interfacial interaction, the study describes a possible approach to the selection of surfaces with desired adhesion properties. The methodology helps fill the

knowledge gap on virus adhesion to fomites – an important component of models on virus transport and fate in built environments. The study can help guide screening and selection of materials that discourage virus adhesion, design of anti-adhesive surfaces, as well as development of surface cleaning solutions and protocols.

Acknowledgements

This material is based upon work supported in part by the U.S. National Science Foundation under Grant OISE-1952438 and in part by the Research Council of Norway under project #310074. We are grateful to Dr. Wei Zhang (Department of Plant, Soil and Microbial Sciences, Michigan State University) for making available the Malvern Zetasizer Nano-ZS instrument in his laboratory as well as to Dr. Irene Xagorarakis and Brijen Miyani (Department of Civil and Environmental Engineering, Michigan State University) for providing training on the procedures for RNA and DNA extraction.

Nomenclature

α_{vf}	virus-fomite attachment efficiency
γ_l^{LW}	Lifshitz-van der Waals component of the surface energy of probe liquid
γ_s^{LW}	Lifshitz-van der Waals component of the surface energy of solid
γ_w^{LW}	Lifshitz-van der Waals component of the surface energy of water
γ_l^+	electron acceptor component of the surface energy of probe liquid
γ_s^+	electron acceptor component of the surface energy of solid
γ_w^+	electron acceptor component of the surface energy of water
γ_l^-	electron donor component of the surface energy of probe liquid
γ_s^-	electron donor component of the surface energy of solid
γ_w^-	electron donor component of the surface energy of water
δ	effective diffusion distance
ε_r	relative dielectric permittivity of water
ε_0	dielectric permittivity of vacuum
ζ	ζ -potential
θ	contact angle
κ	inverse Debye screening length (also referred to as Hückel parameter)
λ	(=0.6 nm) the decay length for Lewis acid-base interaction in water
μ	dynamic viscosity
ψ_v	surface potential of a virus
ψ_f	surface potential of a fomite

A	Hamaker constant
A_s	surface area of the QCM sensor
a	virus radius
C	QCM sensor mass sensitivity constant
C_b	virus concentration in the bulk of the flow
C_s	virus concentration at the sensor surface
D	diffusion coefficient
d	virus-fomite minimal separation distance
d_h	hydrodynamic diameter
d_0	minimum separation distance due to Born repulsion
k	mass transfer coefficient
k_B	Boltzmann's constant
E_{max}	primary maximum in the total XDLVO energy of interaction
E_{min}	secondary minimum in the total XDLVO energy of interaction
Δf	QCM vibration frequency shift
ΔG_{fwf}	free energy of interfacial interaction of two identical fomites in water
ΔG_{sww}	free energy of interfacial interaction of two identical solids in water
ΔG_{vww}	free energy of interfacial interaction of two identical viruses in water
ΔG_{vwf}	free energy of virus-fomite interfacial interaction in water
j_m	mass flux of virus towards the QCM sensor

m	areal mass density
n	QCM vibration overtone number
U_{slv}^{XDLVO}	total XDLVO energy of interaction between a sphere and a plate
U_{vwf}^{LW}	energy of Lifshitz-van der Waals interaction between a sphere and a plate
U_{vwf}^{EL}	energy of electrostatic interaction between a sphere and a plate
U_{vwf}^{AB}	energy of Lewis acid-base interaction between a sphere and a plate
T	absolute temperature

APPENDIX

APPENDIX

A1. Transmission electron microscopy of HAdV5 and HRSV

In correlation with using dynamic light scattering as a method to measure the particle size, transmission electron microscopy can also be used to determine particle size, shape, and chemical makeup. TEM provides the primary particle size (exact particle diameter) in comparison to the hydrodynamic diameter, obtained using DLS, which tends to be larger. If agglomeration of the particles is present, larger particle size distributions or multi-model particle size distributions will most likely occur using DLS. TEM is the preferred method for determining the primary particle size of dilute colloidal dispersions [104]. In order to avoid exposure of lab personnel and the public by accidentally released viruses during handling of HAdV5 and HRSV, efficient and feasible safety precautions should be addressed. Virus sample inactivation was performed to guarantee biosafety. The inactivation procedures must not only inactivate the virus, but also preserve their morphology. In diagnostic negative staining EM, Formaldehyde (FA) at a concentration of 2% to 4% is commonly used because it stabilizes biological structures [105]. In our study, 37% FA was added in the virus suspension to reach a final concentration of 3.7% of FA. The mixture was vortexed for 15 s and then incubated in 25 °C for 12 h as suggested by Moeller et al. [105]. To prepare specimen for TEM imaging, one drop of purified virus stock was applied to a carbon-coated formvar grid. The virus sample was incubated on the grid for 5 min and the washed away by drops of water. Uranyl acetate (1%) was then used to stain the grid, and excess stain was removed with filter paper. The grid was air-dried prior to TEM

imaging. Images were recorded using JEM-1400 Flash (Jeol, Nieuw-Vennep, Tokyo). High accelerating voltages give higher resolution, but less contrast, and can result in greater specimen damage. For these reasons, studies of biological samples tend to employ low accelerating voltages (60 kV to 100 kV), while studies of inorganic materials, which often require higher resolution, usually employ an accelerating voltage of 200 kV. In this study, 100 kV accelerating voltage was utilized.

A2. QCM-D experiments: Avoiding air bubbles in tests with hydrophobic sensors

When an aqueous solution is brought into contact with a dry hydrophobic surface of a QCM-D sensor, air bubbles tend to form on the surface confounding QCM-D measurements [106-108]. Accordingly, in tests with hydrophobic PP sensors, we adopted a different protocol to establish a baseline. All sample solutions (except virus suspensions) were first sonicated for at least 30 min in the air, and then degassed in a vacuum desiccator. Virus suspensions were degassed in a vacuum desiccator but not sonicated. An Erlenmeyer flask was filled with solution so there was no head space. The sample solution was kept in the vacuum desiccator for at least 15 s and was immediately sealed with parafilm after being taken out of the vacuum desiccator to avoid re-aeration. The QCM-D tubing was inserted into the solution through a parafilm cover. Further, before each QCM-D test, the PP sensors were flowed first with ethanol for at least 2 h at 0.1 ml/min [106] and then with the DI water for at least 60 min while QCM frequency was recorded. No significant frequency changes during this time indicated absence of air bubbles. Finally, the baseline was established with DI water at

0.15 ml/min flow rate. The rest of the procedure was the same as with hydrophilic (SiO₂,) and less hydrophobic (nylon-6,6, SS) sensors.

A3. QCM-D experiments: Accounting for the effect of liquid viscosity and density

The effect of fluid's viscosity and density on QCM-D sensor vibration frequency when switching from DI water to the electrolyte solutions (150 mM NaCl) was accounted for using eq. (S1), which is commonly attributed to Kanazawa and Gordon [109, 110]. (See Revyakine et al. [111] for references to earlier reports where the equation appears). The relationship expresses the change in the oscillation frequency of a quartz crystal in contact with a fluid as a function of materials parameters of the fluid and the quartz:

$$\Delta f = - \sqrt{f_0^3 \frac{\eta_L \rho_L}{\pi \mu_Q \rho_Q}} \quad (\text{S1})$$

where $\mu_Q = 2.974 \times 10^{11} \text{ g} \cdot \text{cm}^{-1} \cdot \text{s}^{-2}$ ($2.974 \times 10^{10} \text{ Pa}$) and $\rho_Q = 2.648 \text{ g} \cdot \text{cm}^{-3}$ are the shear modulus and density of quartz, respectively; $f_0 = 25 \text{ MHz}$ is the nominal vibration frequency of the dry quartz crystal at the 5th harmonic, η_L and ρ_L are the absolute viscosity and density of the liquid respectively [109, 110]. For pure water at 25 °C, η_L and ρ_L are $0.89 \times 10^{-3} \text{ Pa} \cdot \text{s}$ and $0.997 \text{ g} \cdot \text{cm}^{-3}$, respectively. For 150 mM NaCl solution at 25 °C, η_L and ρ_L are $0.9 \times 10^{-3} \text{ Pa} \cdot \text{s}$ [112] and $1.003 \text{ g} \cdot \text{cm}^{-3}$ [113], respectively.

A4. QCM-D experiments: Cleaning protocols

Protocol for cleaning QCM-D tubing

After the test with viruses, the fluid path (including both tubing and QCM-D chamber) was first disinfected with bleach using the following steps:

- 1) Priming the fluid path with deionized water.
- 2) Flushing the fluid path with a 0.625% NaOH solution. The solution was prepared by diluting commercial bleach (12.5% NaOH) with DI water.
- 3) Pausing the priming sequence.
- 4) After 30 min of leaving the fluid path filled with the bleach solution and no pumping, priming the fluid path using DI water to remove the remaining bleach solution from the tubing and into the waste container.

After disinfection, the fluid path was cleaned to remove any virions possibly remaining on the inner surfaces of the tubing and the QCM-D chamber. The procedure included the following steps:

- 1) Flushing the fluid path with a 2% SDS solution
- 2) Pausing the priming sequence.
- 3) After 30 min of leaving the fluid path filled with the SDS solution and no pumping, resume flushing and prime the fluid path using deionized water to remove the remaining SDS solution from the tubing and into the waste container.

Protocols for cleaning stainless steel and silica sensors

The cleaning protocol for stainless steel sensor included the following seven steps:

1. Immersing in 1% Hellmanex II for 12 h at room temperature.
2. Rinsing with DI water.
3. Drying with nitrogen gas.
4. Sonicating in 99% ethanol for 10 min.
5. Rinsing with DI water.
6. Drying with nitrogen gas.
7. Treating with UV and O₃ (Bioforce UV-Ozone Cleaner) for 60 min.

The cleaning protocol for SiO₂ sensor (Qsx 303) included the following five steps:

1. Treating with Bioforce UV-Ozone Cleaner for 10 min.
2. Sonicating in 2% SDS aqueous solution for 60 min.
3. Rinsing with DI water.
4. Drying with nitrogen gas.
5. Treating with UV and O₃ (Bioforce UV Ozone Cleaner) for 60 min.

Protocols for cleaning polypropylene and nylon sensors

The manufacturer does not provide the standard cleaning protocols for polypropylene and nylon-6,6 sensors. The cleaning procedure for these two types of sensors was designed based in part on that for polystyrene and included the following five steps:

1. Immersing in 1% Deconex 11 solution for 60 min at room temperature.
2. Rinsing with DI water and keep immersed in DI water for 2 h.

3. Rinsing with 99% ethanol.
4. Drying with nitrogen gas.

A5. Determination of ζ -potential based on measured electrophoretic mobility

Experimentally determined values of HRSV electrophoretic mobility as a function of pH (Fig. 41) were converted to ζ -potential values, using an expression derived by Ohshima [114]:

$$\mu = \frac{2 \varepsilon_r \varepsilon_0}{3 \eta} \zeta \left[1 + \frac{1}{2 \left[1 + \frac{2.5}{\kappa a [1 + 2e^{-\kappa a}]} \right]^3} \right] \quad (\text{S2})$$

where κ (nm^{-1}) is the Hückel parameter (κ^{-1} (nm) is the Debye screening length), η is the viscosity of the electrolyte where viruses are suspended, and a is the radius of the virus. Equation (S2) provides an accurate ($< 1\%$ error) estimate of ζ -potential for any value of κa . For HRSV in 1 mM KCl, $\kappa a \approx 6.4$, making neither Smoluchowski expression (assumes $\kappa a \gg 1$) nor Hückel expression (assumes $\kappa a \ll 1$) for the relationship between ζ and μ applicable. The Ohshima equation was employed in our earlier study to determine ζ -potential of HAdV5 [115].

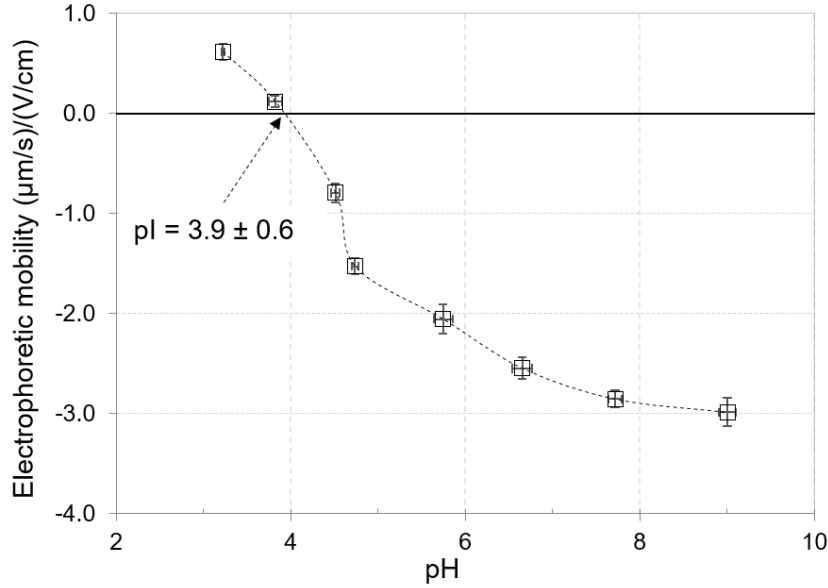


Figure 41. Electrophoretic mobility of HRSV virions as a function of pH. Table 10 lists mobility and zeta potentials as functions of pH in a tabular format.

A6. Algorithm for selecting the pH value where electrostatic interactions between a virus and a fomite surface are most attractive

To determine the pH when E_{vwf}^{EL} is most attractive, a few pH values were first selected between isoelectric point (pI) of virus and PP to ensure the attraction of U_{vwf}^{EL} . For example, the pIs of HAdV5 and PP were 4.6 and 3.8 respectively, so 3.9, 4.0, 4.1, 4.2, 4.3, 4.4, 4.5 were selected. Then the E_{vwf}^{EL} at these pH were calculated and compared. The pH at which the U_{vwf}^{EL} reaches the highest value was selected for these QCM-D tests. In eq. (5), $\ln\left(\frac{1+e^{-\kappa d}}{1-e^{-\kappa d}}\right)$ is positive for all distances, $(\psi_v^2 + \psi_f^2) \ln(1 - e^{-2\kappa d})$ is negative for all distances, Thus, for $U_{vwf}^{EL}(d)$ to be highly negative (virus-fomite attraction), the $\psi_v\psi_f$ should be highly negative.

$$U_{vwf}^{EL}(d) = \pi \varepsilon_r \varepsilon_0 a \left[2\psi_v \psi_f \ln \left(\frac{1 + e^{-\kappa d}}{1 - e^{-\kappa d}} \right) + (\psi_v^2 + \psi_f^2) \ln(1 - e^{-2\kappa d}) \right] \quad (5)$$

Based on the U_{vwf}^{EL} calculated, 4.1 and 3.85 was selected as the experimental pH for HAdV5-PP and HRSV-PP respectively.

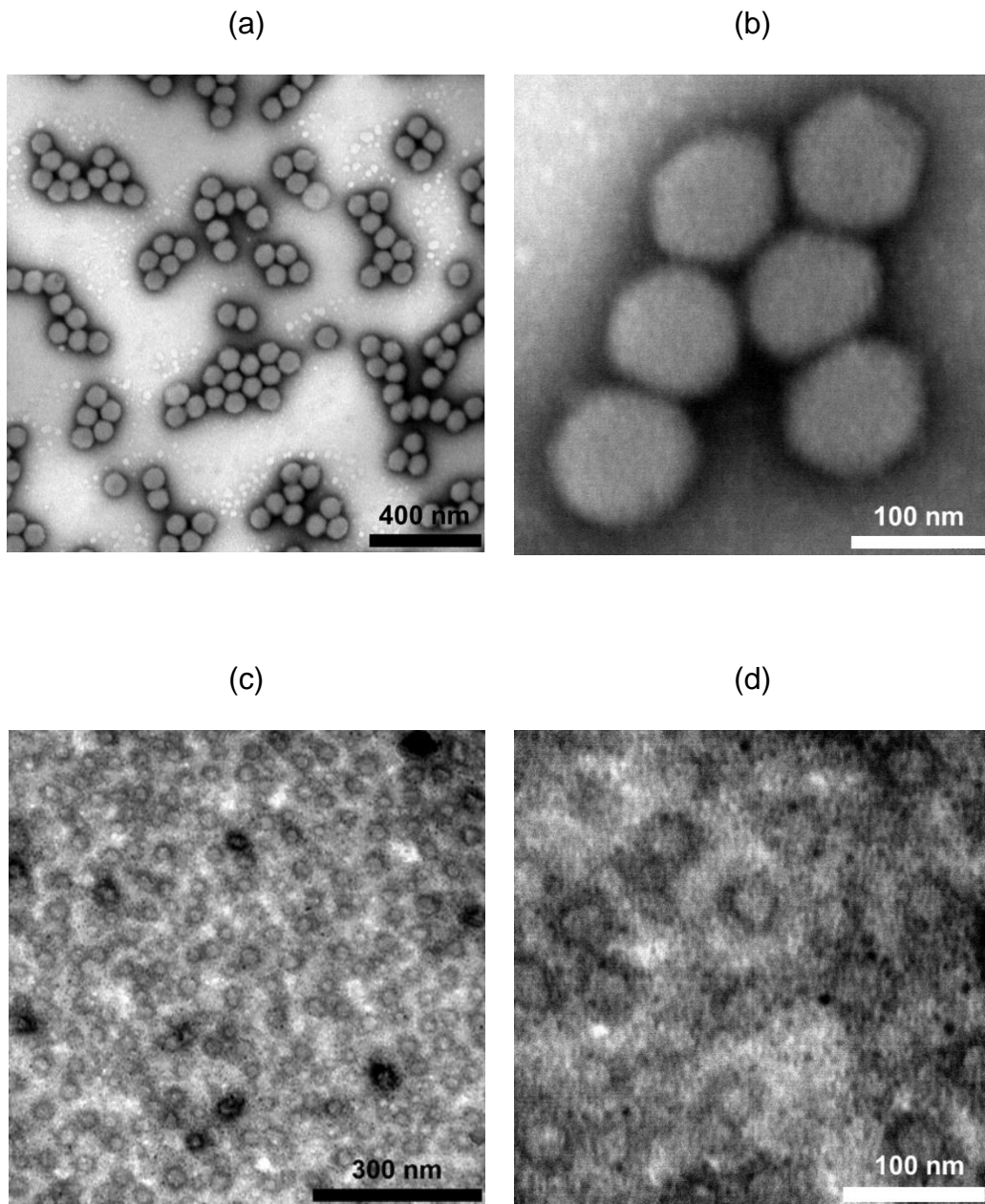


Figure 42. TEM images of (a, b) HAdV5 virions and (c, d) HRSV virions.

A7. Verification of linearity of the concentration dependence of virus mass flux to the sensor

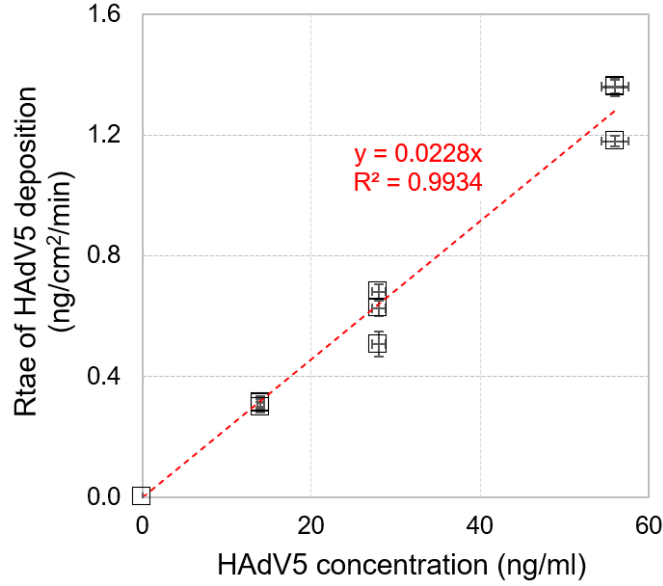


Figure 43. Rate of HAdV5 deposition on stainless steel QCM-D sensors ($\frac{dm_v}{dt}$) as a function of HAdV5 concentration in the feed suspension (C_b). The intermediate value of C_b and deposition conditions are the same as in all other QCM-D tests. Solution is 150 mM NaCl. The observed linearity validates the assumption behind eq. (3): $\frac{dm_v}{dt} \approx \alpha_{vf} k C_b A$.

A8. Computing surface tension components for polypropylene

Eq. (1) was recast as

$$\frac{(1 + \cos\theta)\gamma_l^{TOT} - 2\sqrt{\gamma_s^{LW}\gamma_l^{LW}}}{2\sqrt{\gamma_l^-}} = \sqrt{\gamma_s^+} + \sqrt{\frac{\gamma_l^+}{\gamma_l^-}}\sqrt{\gamma_s^-} \quad (S3)$$

and γ_s^- was determined from the slope of a linear dependence of the left-hand side of eq. (S3) on $\sqrt{\gamma_l^+/\gamma_l^-}$ with the intercept ($\sqrt{\gamma_s^+}$) set to zero. To improve the reliability of the prediction, additional contact angle measurements with EG, a probe liquid with a high $\sqrt{\gamma_l^+/\gamma_l^-}$ ratio, were performed.

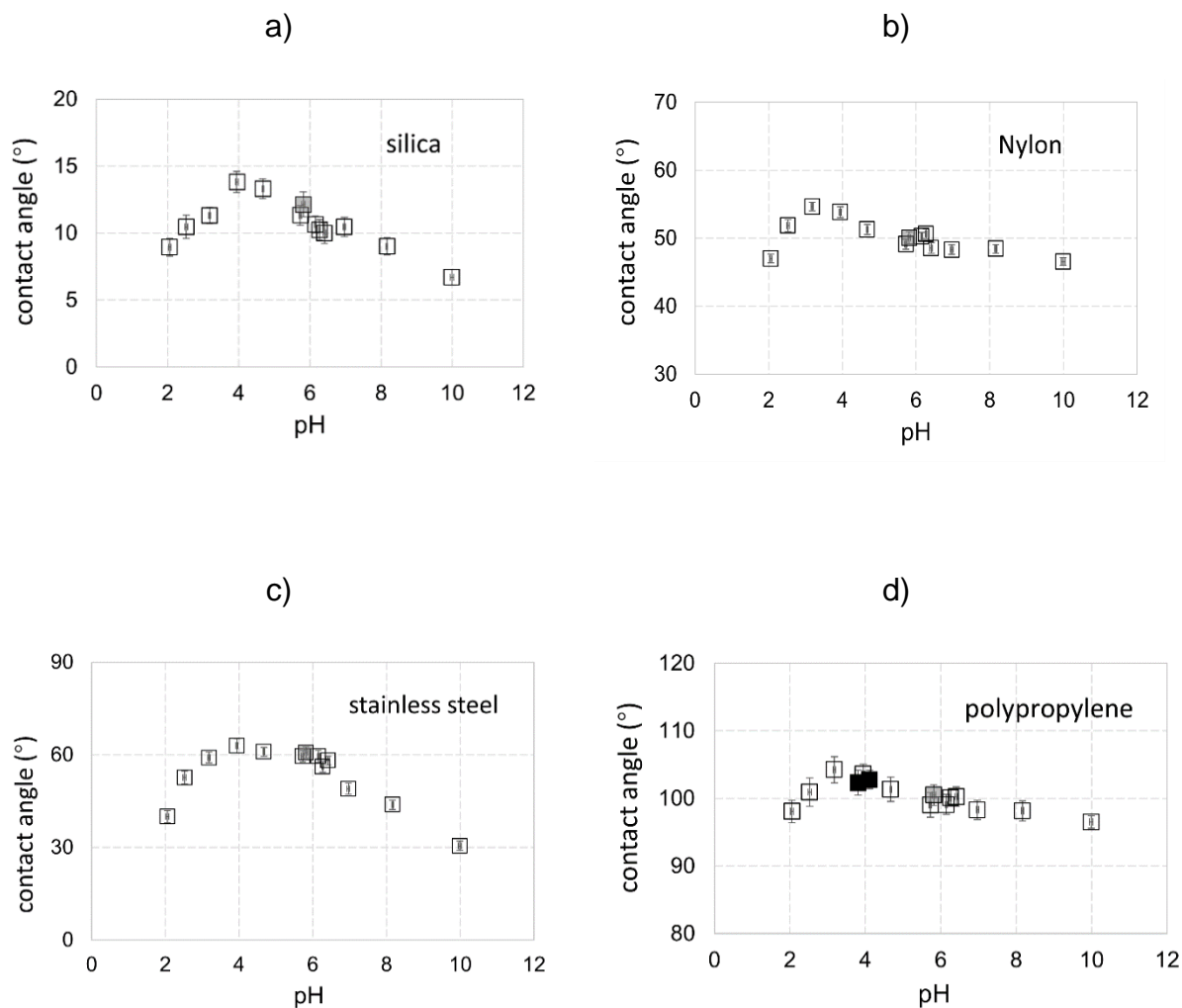


Figure 44. Contact angle of four fomites: a) silica, b) nylon, c) stainless steel, d) polypropylene, as a function of pH. Depending on the type of aqueous solution used, values are shown using either empty symbols (150 mM NaCl at pH 5.8) or gray symbols (DI water at pH 5.8) or black symbols (1 mM NaCl at pH 3.8 and 4.1).

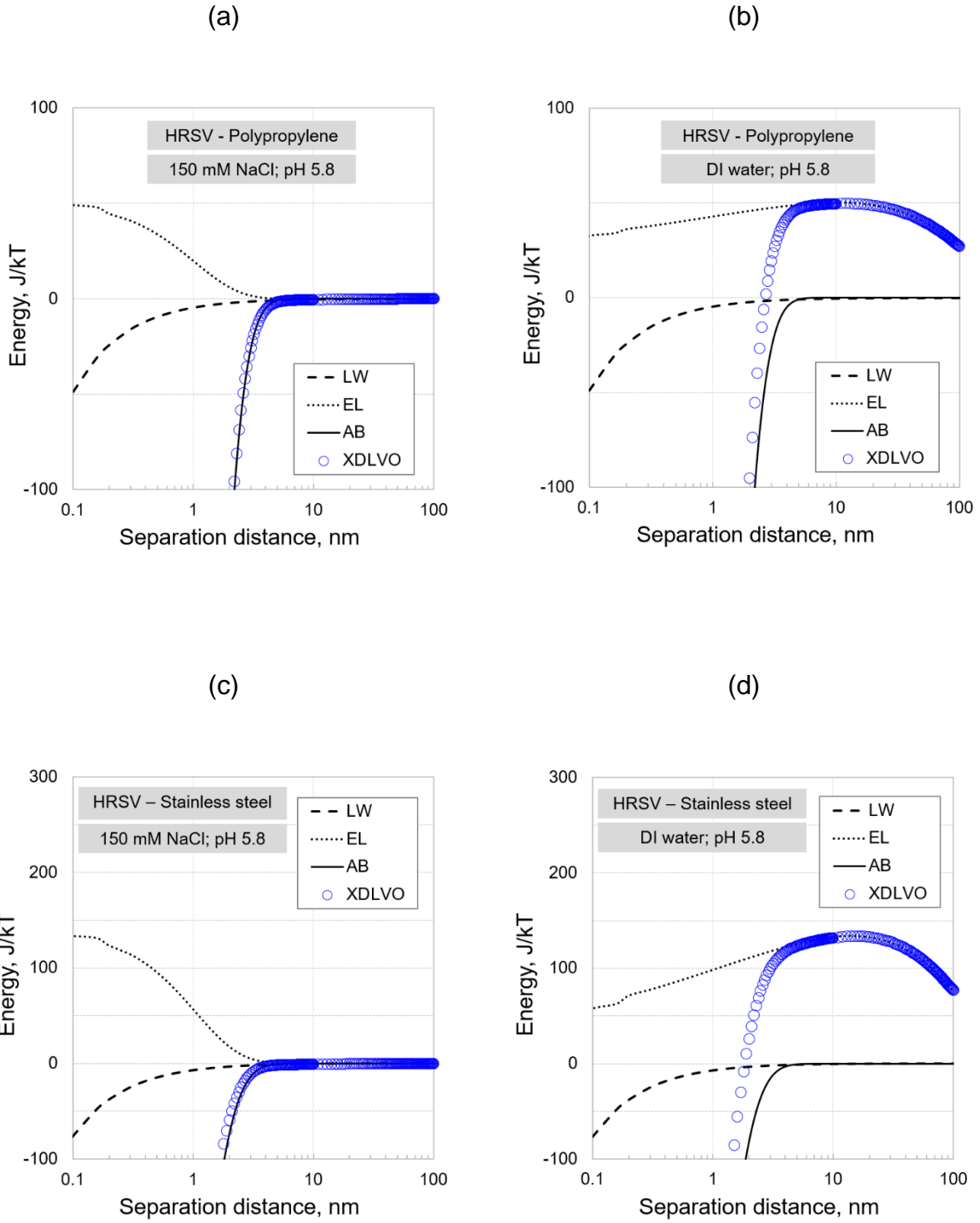


Figure 45. XDLVO total energy of interactions during virus deposition (a, c) and cleaning (b, d) stages of QCM-D experiments. The results are for HRSV interaction with polypropylene (a, b) and stainless steel (c, d).

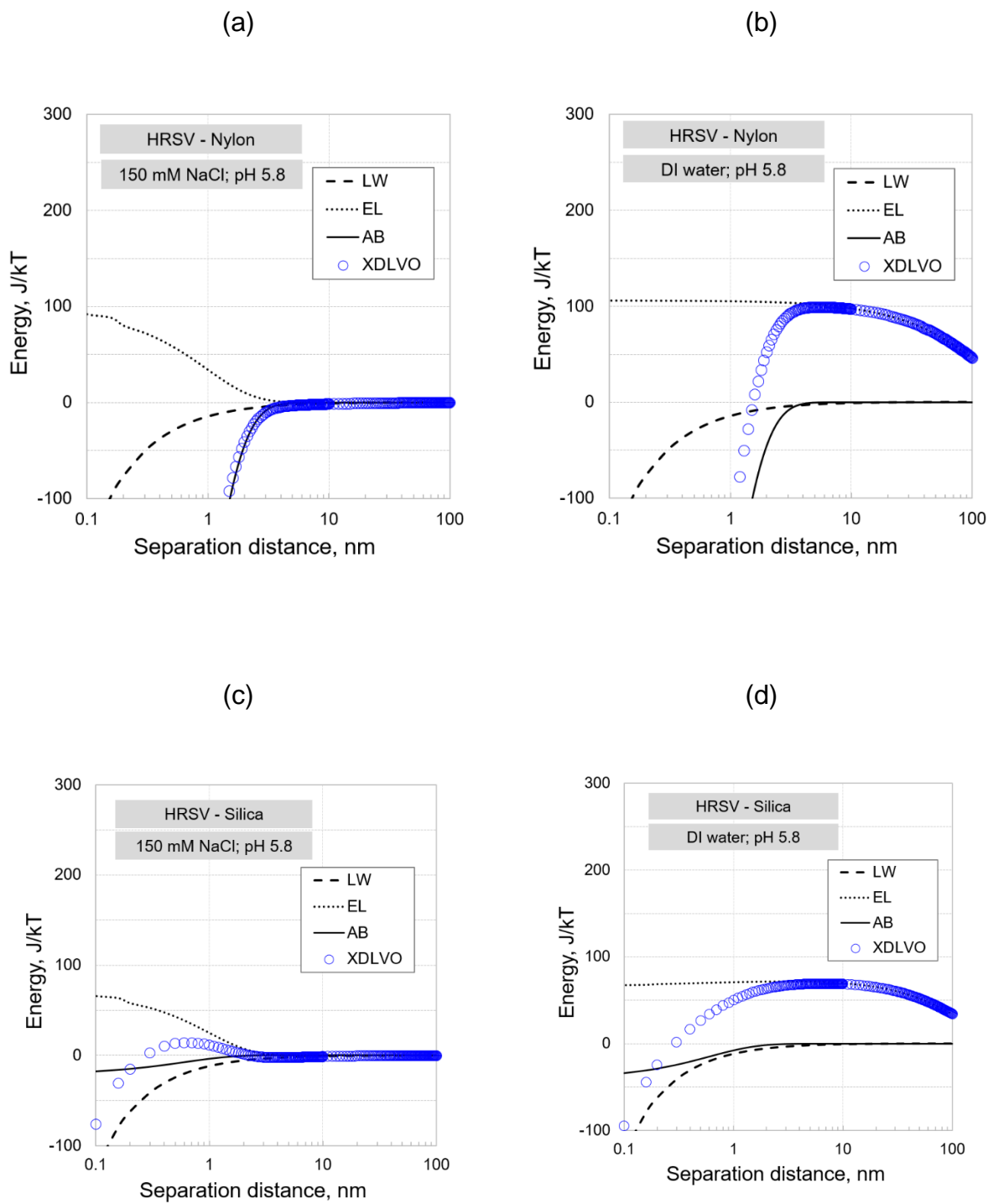


Figure 46. XDLVO total energy of interactions during virus deposition (a, c) and cleaning (b, d) stages of QCM-D experiments. The results are for HRSV interaction with nylon (a, b) and silica (c, d).

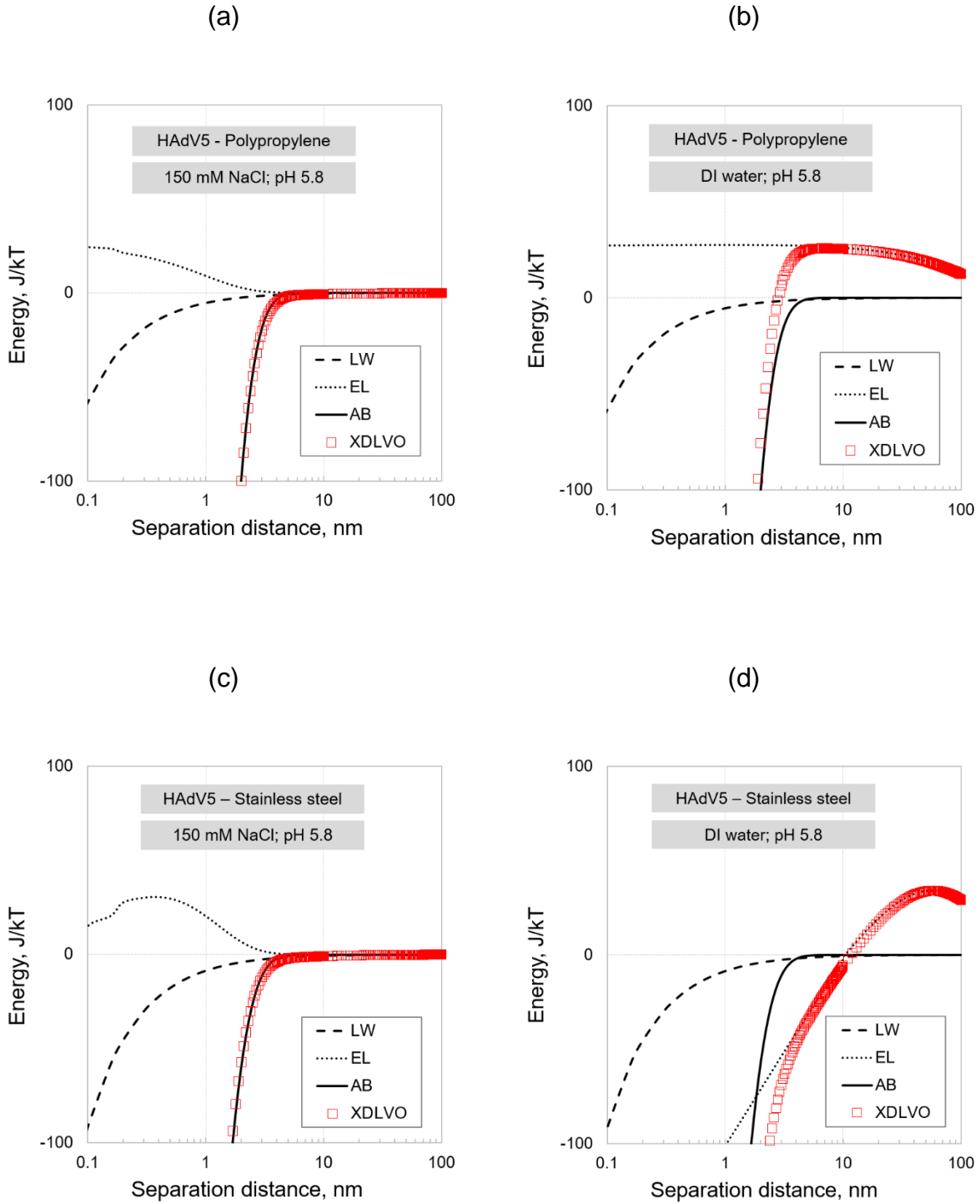


Figure 47. XDLVO total energy of interactions during virus deposition (a, c) and cleaning (b, d) stages of QCM-D experiments. The results are for HAdV5 interaction with polypropylene (a, b) and stainless steel (c, d).

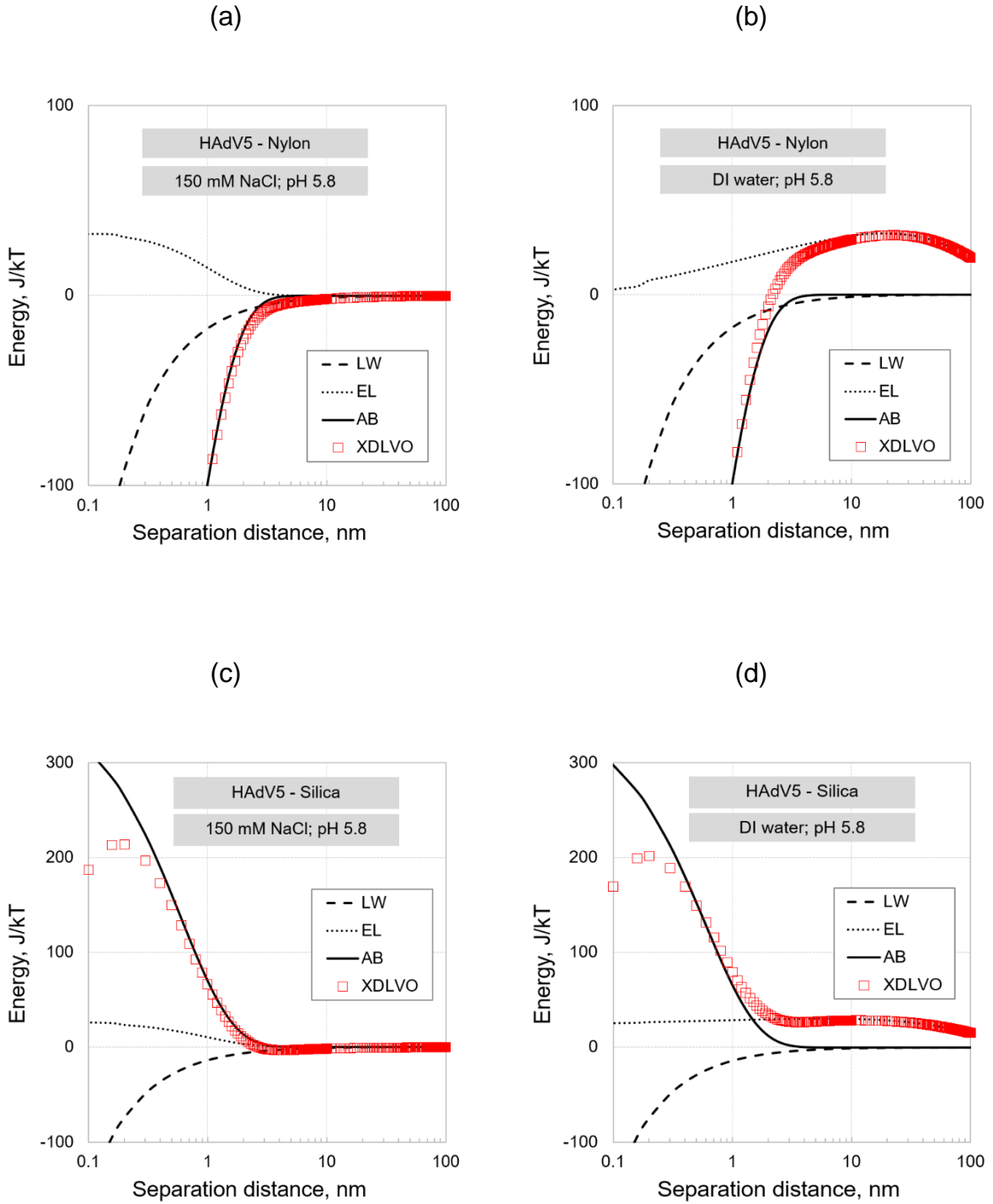


Figure 48. XDLVO total energy of interactions during virus deposition (a, c) and cleaning (b, d) stages of QCM-D experiments. The results are for HAdV5 interaction with nylon (a, b) and silica (c, d).

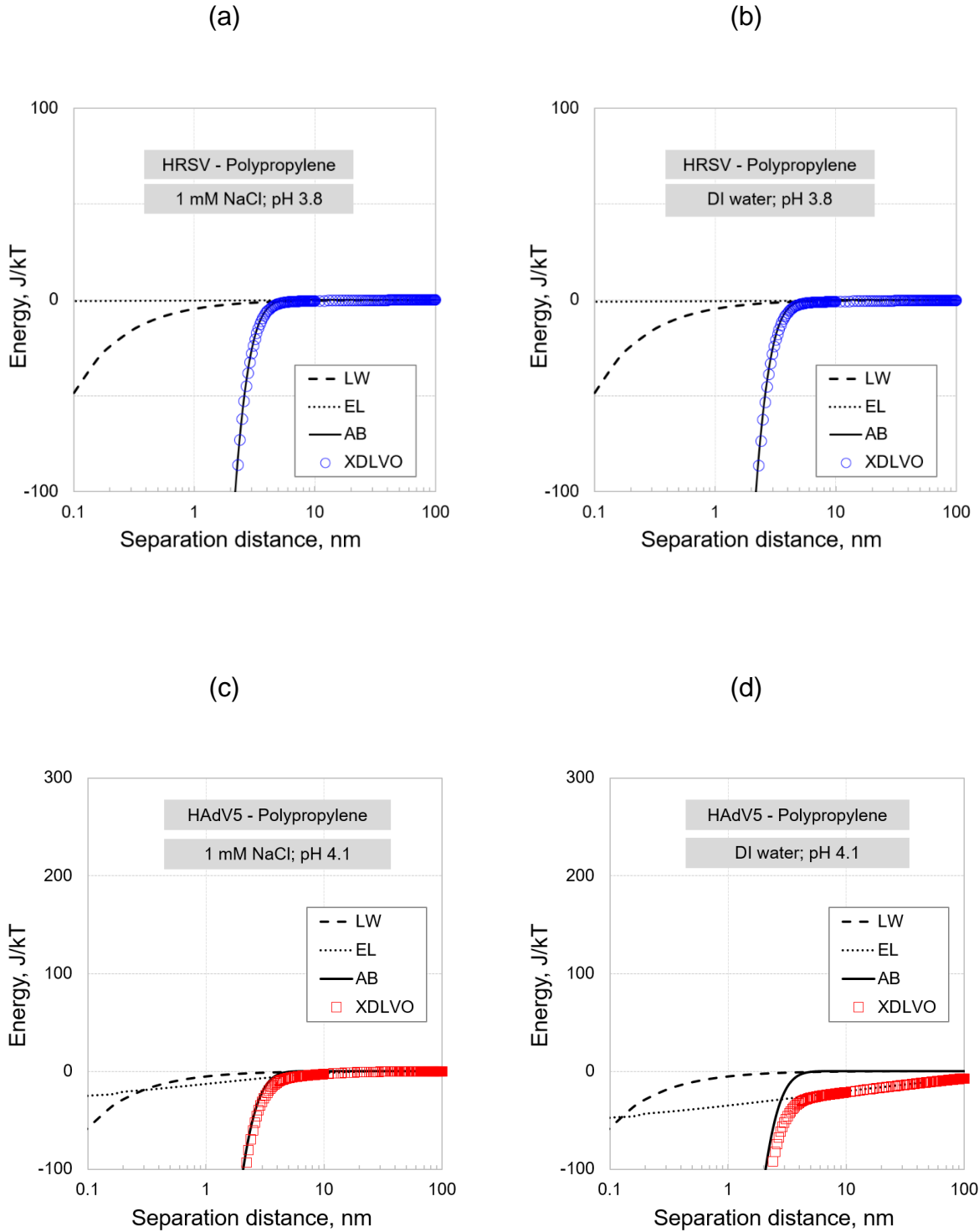


Figure 49. XDLVO total energy of interactions during virus deposition (a, c) and cleaning (b, d) stages of QCM-D experiments. The results are for HRSV (a, b) and HAdV5 (c, d) interaction with polypropylene. Conditions correspond to $\alpha_{vf} = 1$.

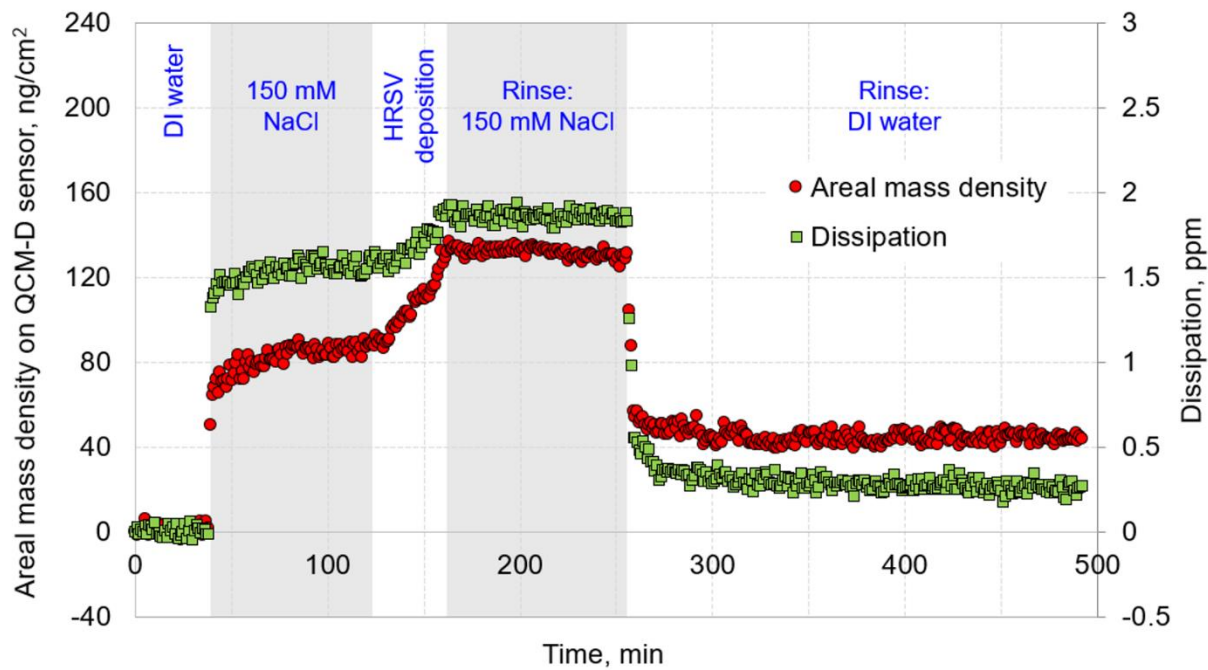


Figure 50. Example QCM-D data set: deposition of HRSV on polypropylene. The data are based on the 5th harmonic of the QCM-D signal.

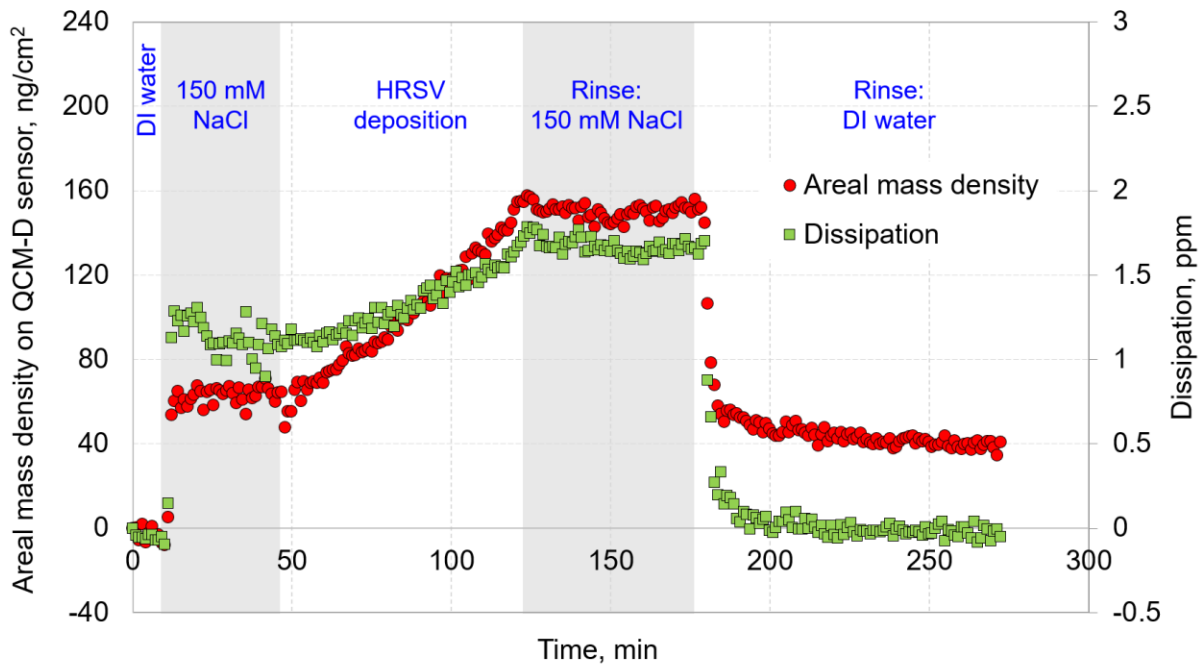


Figure 51. Example QCM-D data set: deposition of HRSV on stainless steel. The data are based on the 5th harmonic of the QCM-D signal.

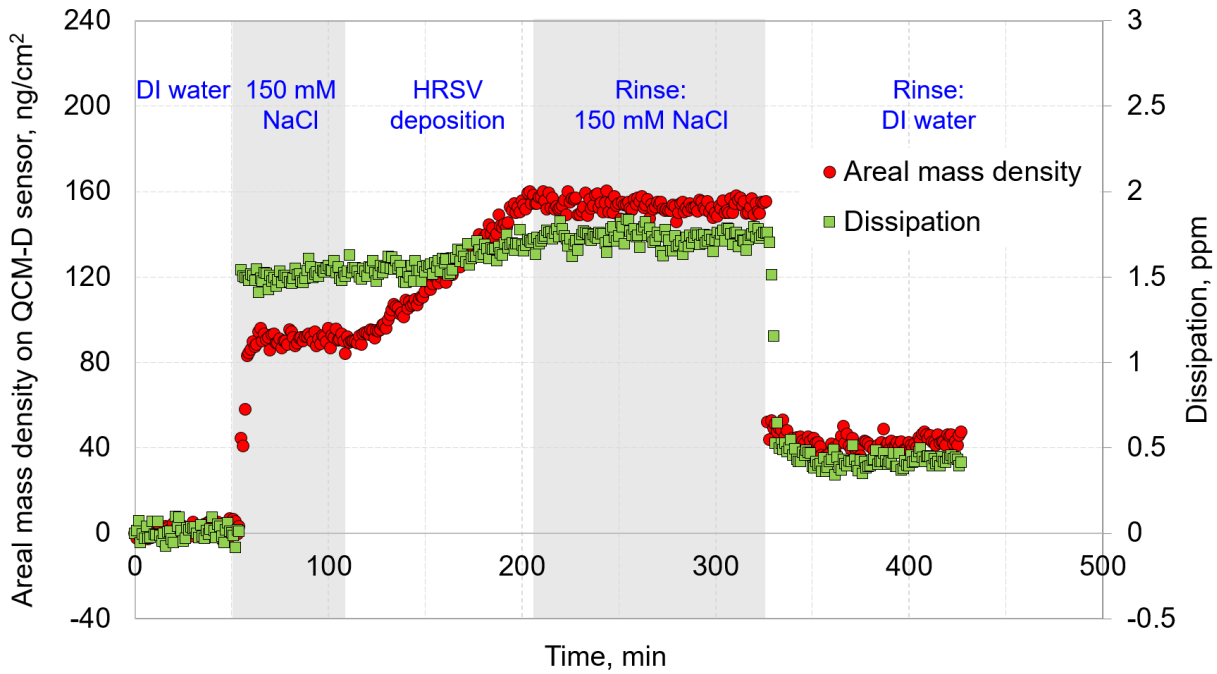


Figure 52. Example QCM-D data set: deposition of HRSV on nylon. The data are based on the 5th harmonic of the QCM-D signal.

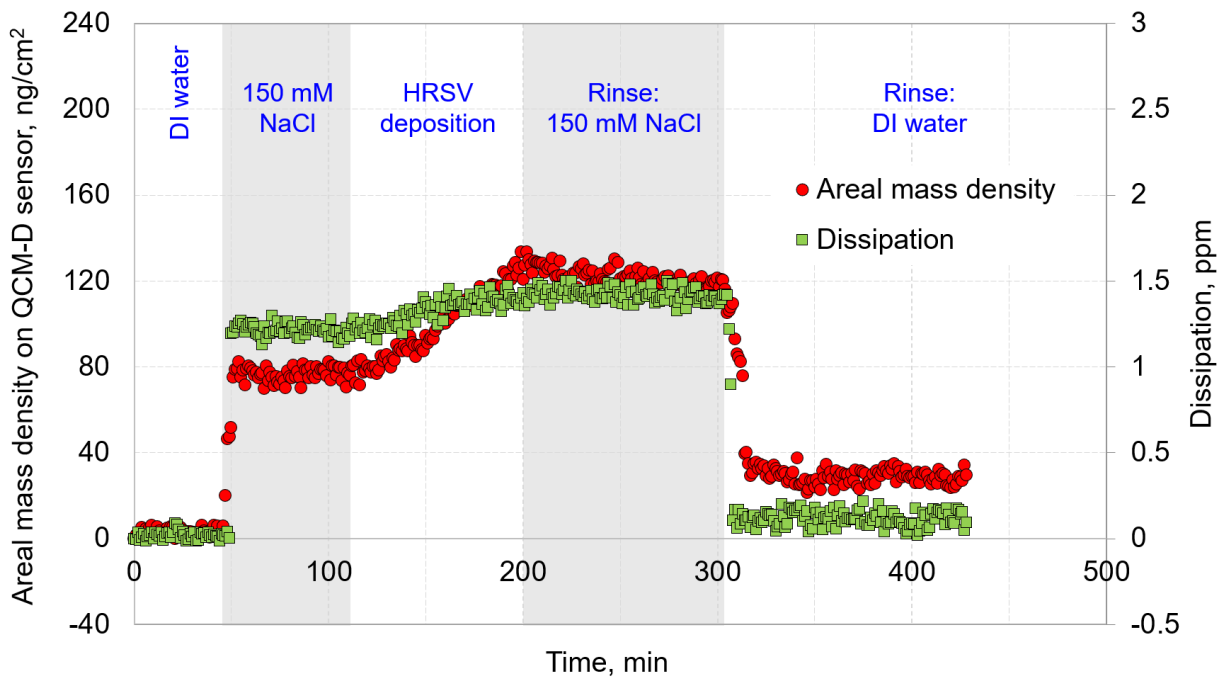


Figure 53. Example QCM-D data set: deposition of HRSV on silica. The data are based on the 5th harmonic of the QCM-D signal.

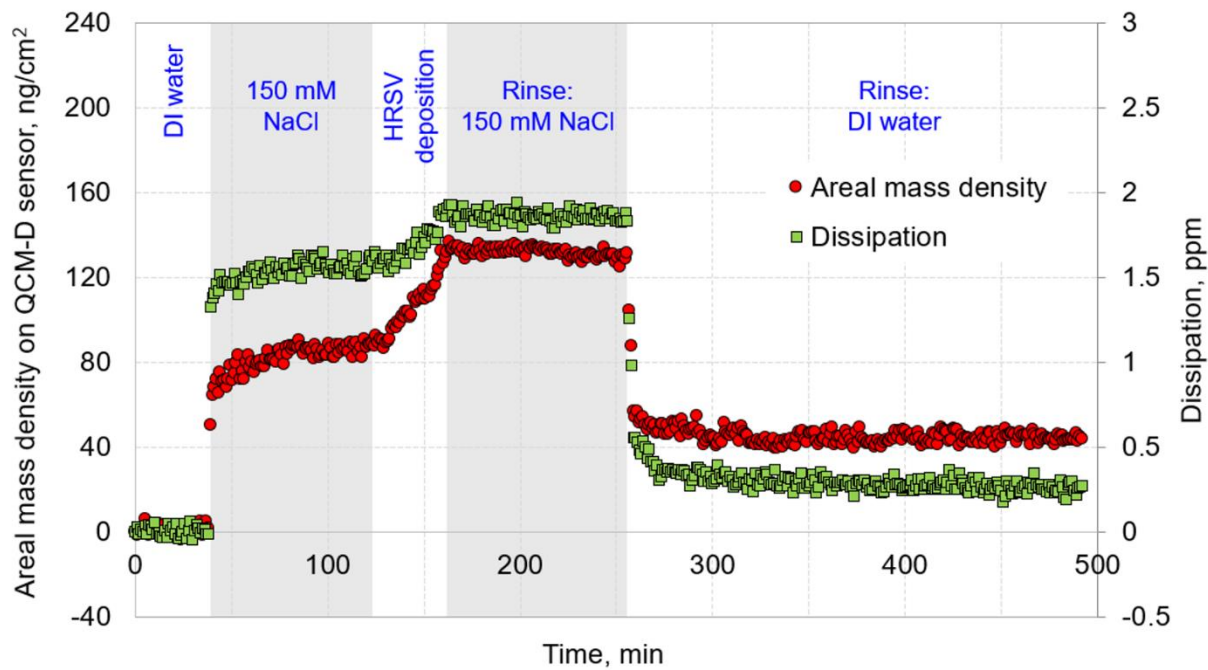


Figure 54. Example QCM-D data set: deposition of HAdV5 on polypropylene. The data are based on the 5th harmonic of the QCM-D signal

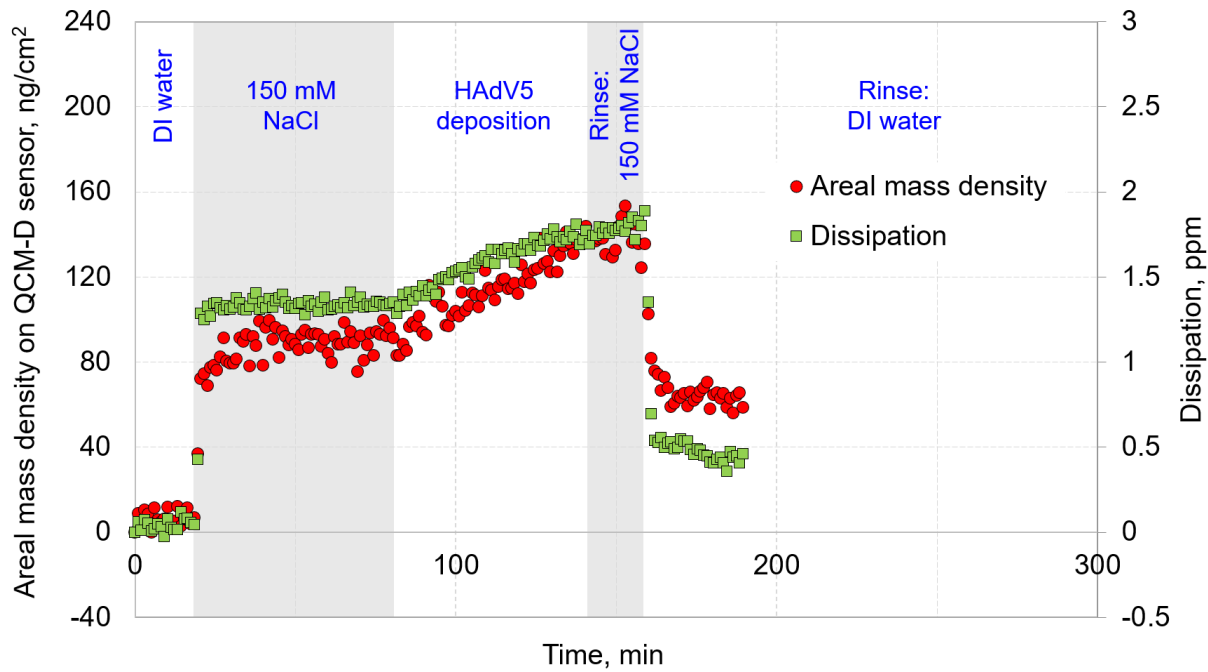


Figure 55. Example QCM-D data set: deposition of HAdV5 on stainless steel. The data are based on the 5th harmonic of the QCM-D signal.

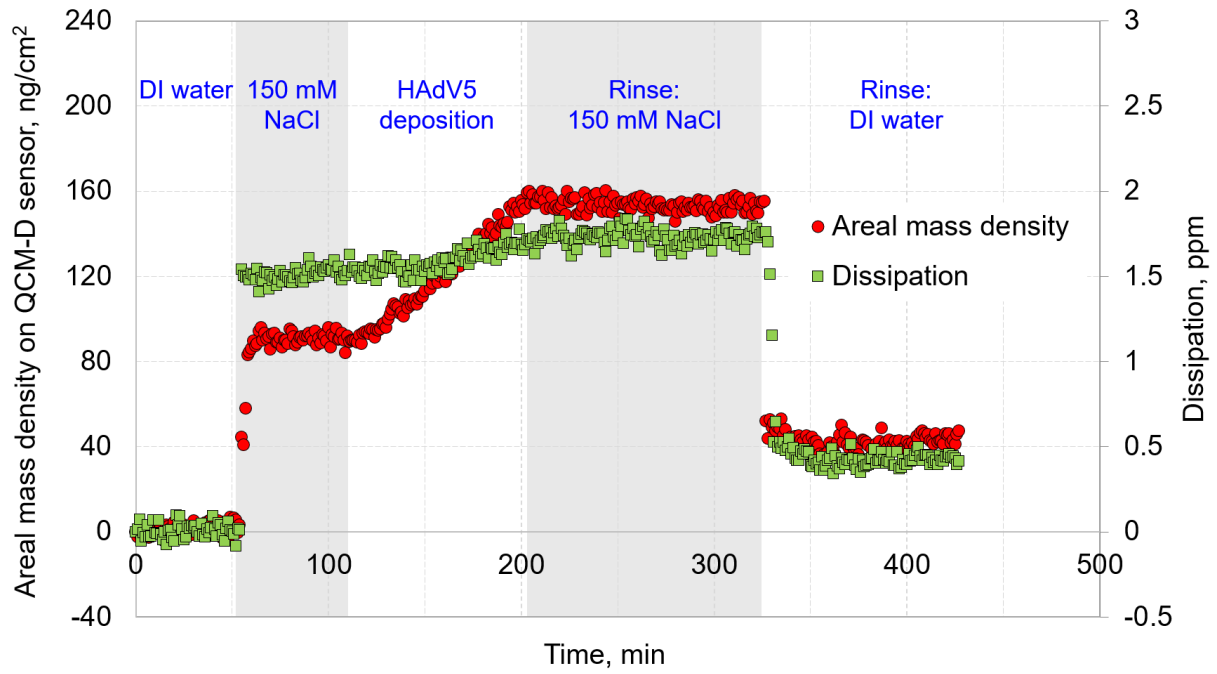


Figure 56. Example QCM-D data set: deposition of HadV5 on nylon. The data are based on the 5th harmonic of the QCM-D signal

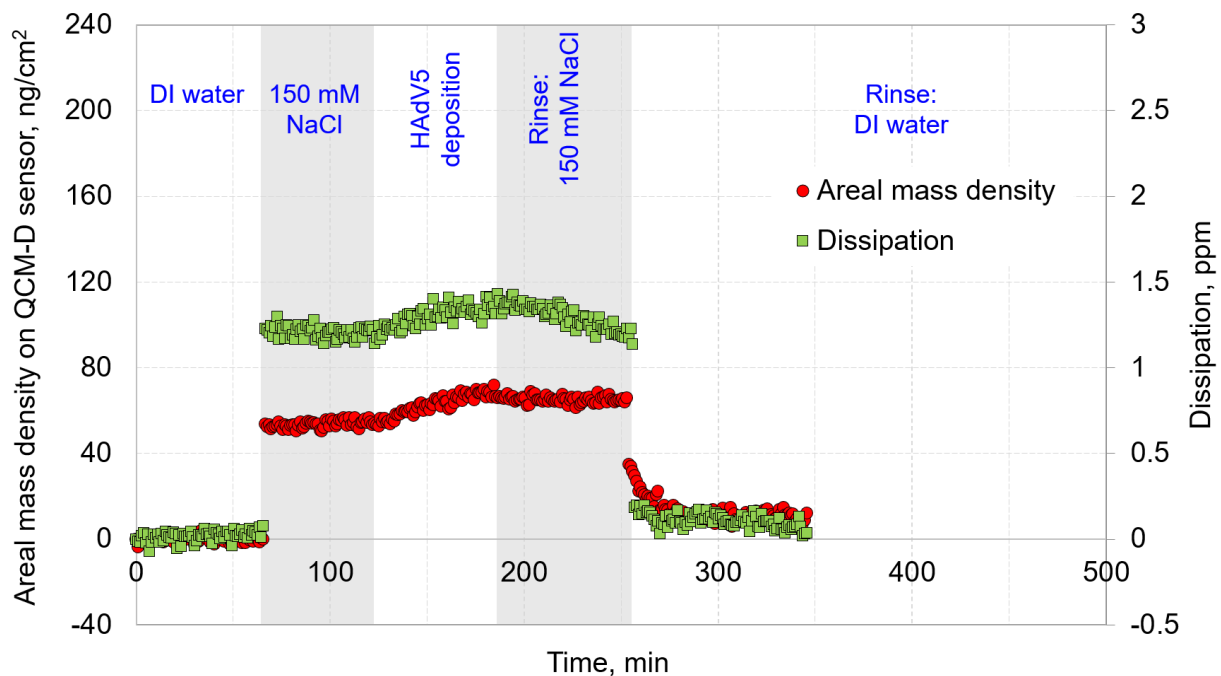


Figure 57. Example QCM-D data set: deposition of HAdV5 on silica. The data are based on the 5th harmonic of the QCM-D signal.

Table 10. ζ -potential values computed using Ohshima's expression (eq. (S1)) based on measured electrophoretic mobilities of HRSV as a function of pH.

pH	Mobility ($\mu\text{m/s}/(\text{V/cm})$)	ζ -potential (mV)
3.22 ± 0.02	0.613 ± 0.079	10.0 ± 1.3
3.82 ± 0.07	0.119 ± 0.059	1.9 ± 1.0
4.51 ± 0.05	-0.793 ± 0.092	-12.9 ± 1.5
4.74 ± 0.04	-1.527 ± 0.079	-24.8 ± 1.3
5.74 ± 0.11	-2.054 ± 0.143	-33.4 ± 2.3
6.65 ± 0.11	-2.546 ± 0.107	-41.4 ± 1.7
7.71 ± 0.08	-2.852 ± 0.086	-46.4 ± 1.4
9.00 ± 0.10	-2.985 ± 0.142	-48.6 ± 2.3

Table 11. Contact angle of probe liquids, surface energy parameters (γ^{LW} , γ^+ , γ^- , γ^{AB} , γ^{tot}) and the free energy of interfacial interaction in water (ΔG_{sws}) of four fomites (clean, before use). Surface energies are calculated based on contact angles of 150 mM NaCl instead of DI water. Corresponding surface energy values calculated based on contact angles of DI water are given in Table 3. Error estimates were obtained by propagating experimental errors in measured contact angles through the calculation of γ (eq. (1)) and ΔG_{sws} (eq. (3)).

Notes: ^A pH 5.8; ^B The data are the same as those reported in Table 3.

Parameter		Fomites			
		Silica	Nylon	Stainless steel	Polypropylene
Contact angle	150 mM NaCl ^A	11.3 ± 1.0	47.8 ± 0.7	59.0 ± 0.8	99.0 ± 0.7
	Glycerol ^B	14.7 ± 1.5	50.5 ± 1.0	31.4 ± 0.8	89.4 ± 1.6
	DID ^B	31.4 ± 2.6	12.4 ± 0.9	50.2 ± 1.5	58.6 ± 2.9
	EG ^B	n/a	n/a	n/a	77.5 ± 1.8
Surface energy (mJ/m ²)		43.6 ± 1.1	49.6 ± 0.2	34.2 ± 0.8	29.4 ± 1.7
		2.2 ± 0.2	0.003 ± 0.008	6.5 ± 0.4	0
		44.9 ± 0.7	30.1 ± 1.2	8.8 ± 0.7	0.7 ± 0.2
		19.7 ± 0.6	0.59 ± 0.15	15.1 ± 0.8	0
		63.3 ± 1.2	50.2 ± 0.22	49.3 ± 1.1	29.4 ± 1.7
		16.1 ± 1.1	- 2.6 ± 2.3	- 23.6 ± 1.4	- 85.9 ± 2.8

Table 12. Contact angle of probe liquids, surface energy parameters (γ^{LW} , γ^+ , γ^- , γ^{AB} , γ^{tot}) and the free energy of interfacial interaction in water (ΔG_{sws}) of four fomites (after use and subsequent cleaning; see section S4 for the description of cleaning protocols). Error estimates were obtained by propagating experimental errors in measured contact angles through the calculation of γ (eq. (1)) and ΔG_{sws} (eq. (3)).

Notes: ^A pH 5.8; ^B The data are the same as those reported in Table 3.

Parameter		Fomites			
		Silica	Nylon	Stainless steel	Polypropylene
Contact angle	H ₂ O ^A	14.9 ± 1.6	51.6 ± 2.1	63.1 ± 1.2	102.4 ± 2.3
	Glycerol	24.4 ± 2.7	47.5 ± 2.3	37.2 ± 1.3	91.0 ± 0.6
	DID	37.6 ± 2.0	15.7 ± 1.9	45.3 ± 1.6	59.7 ± 1.2
	EG	n/a	n/a	n/a	78.1 ± 1.5
Surface energy (mJ/m ²)		40.8 ± 1.0	48.9 ± 0.5	36.9 ± 0.8	28.8 ± 0.7
		1.8 ± 0.3	0.14 ± 0.13	4.9 ± 0.5	0
		48.0 ± 1.9	25.5 ± 2.1	6.9 ± 1.1	0.38 ± 0.14
		18.5 ± 1.1	3.7 ± 0.7	11.7 ± 1.1	0
		59.3 ± 1.5	52.7 ± 0.9	48.6 ± 1.4	28.8 ± 0.7
		22.0 ± 2.3	- 10.9 ± 3.8	- 31.3 ± 2.5	- 90.5 ± 2.3

Table 13. Contact angle of probe liquids, surface energy parameters (γ^{LW} , γ^+ , γ^- , γ^{AB} , γ^{tot}) and the free energy of interfacial interaction in water (ΔG_{sws}) of four fomites (after use and subsequent cleaning; see section S4 for the description of cleaning protocols). Surface energies are calculated based on contact angles of 150 mM NaCl instead of DI water. Error estimates were obtained by propagating experimental errors in measured contact angles through the calculation of γ (eq. (1)) and ΔG_{sws} (eq. (3)).

Notes: ^A pH 5.8; ^B The data are the same as those reported in Table 11.

Parameter		Fomites			
		Silica	Nylon	Stainless steel	Polypropylene
Contact angle	150 mM NaCl ^A	12.7 ± 1.1	47.5 ± 0.7	62.0 ± 1.6	101.7 ± 1.9
	Glycerol ^B	24.4 ± 2.7	47.5 ± 2.3	37.2 ± 1.3	91.0 ± 0.6
	DID ^B	37.6 ± 2.0	15.7 ± 1.9	45.3 ± 1.6	59.7 ± 1.2
	EG ^B	n/a	n/a	n/a	78.1 ± 1.5
Surface energy (mJ/m ²)		40.8 ± 1.0	48.9 ± 0.5	36.9 ± 0.8	28.8 ± 0.7
		1.7 ± 0.3	0.09 ± 0.10	4.7 ± 0.5	0
		49.3 ± 1.7	28.2 ± 2.0	7.9 ± 1.4	0.47 ± 0.16
		18.4 ± 1.1	3.2 ± 0.7	12.2 ± 1.3	0
		59.2 ± 1.4	52.1 ± 0.8	49.1 ± 1.6	28.8 ± 0.7
		23.5 ± 2.1	- 5.9 ± 3.6	- 29.8 ± 3.1	- 89.1 ± 2.3

Table 14. Contact angle of probe liquids, surface energy parameters (γ^{LW} , γ^+ , γ^- , γ^{AB} , γ^{tot}) and the free energy of interfacial interaction in water (ΔG_{sws}) of polypropylene at pH 4.1 and 3.8.

pH	Contact angle			Surface energy (mJ/m ²)					
	1 mM NaCl	Glycerol	DID	γ^{LW}	γ^+	γ^-	γ^{AB}	γ^{tot}	ΔG_{sws}
4.1	102.8 ± 1.4	91.0 ± 0.6	59.7 ± 1.2	29.4 ± 1.7	0 ± 0	0.23 ± 0.09	0 ± 0	29.4 ± 1.7	-93.4 ± 1.9
3.8	102.3 ± 1.9	91.0 ± 0.6	59.7 ± 1.2	29.4 ± 1.7	0 ± 0	0.28 ± 0.11	0 ± 0	29.4 ± 1.7	-92.5 ± 2.2

REFERENCES

REFERENCES

- [1] N. Castaño, S. Cordts, M.K. Jalil, K. Zhang, S. Koppaka, A. Bick, R. Paul, S.K. Tang, Fomite transmission, physicochemical origin of virus–surface interactions, and disinfection strategies for enveloped viruses with applications to SARS-CoV-2, *ACS Omega* (2021). <https://doi.org/10.1021/acsomega.0c06335>
- [2] S.A. Boone, C.P. Gerba, Significance of fomites in the spread of respiratory and enteric viral disease, *Appl. Environ. Microbiol.* 73(6) (2007) 1687-1696. <https://doi.org/10.1128/aem.02051-06>
- [3] B. Stephens, P. Azimi, M.S. Thoemmes, M. Heidarinejad, J.G. Allen, J.A. Gilbert, Microbial exchange via fomites and implications for human health, *Curr. Poll. Rep.* (2019) 1-16. <https://doi.org/10.1007/s40726-019-00123-6>
- [4] F. Pancic, D.C. Carpenter, P.E. Came, Role of infectious secretions in the transmission of rhinovirus. , *J. Clin. Microbiol.* 12 (1980) 567-571. <https://dx.doi.org/10.1128/JCM.12.4.567-571.1980>
- [5] A.A. Chughtai, S. Stelzer-Braid, W. Rawlinson, G. Pontivivo, Q. Wang, Y. Pan, D. Zhang, Y. Zhang, L. Li, C.R. MacIntyre, Contamination by respiratory viruses on outer surface of medical masks used by hospital healthcare workers, *BMC Infect. Dis.* 19(1) (2019). <https://doi.org/10.1186/s12879-019-4109-x>
- [6] M.Z. Hassan, K. Sturm-Ramirez, M.Z. Rahman, K. Hossain, M.A. Aleem, M.U. Bhuiyan, M.M. Islam, M. Rahman, E.S. Gurley, Contamination of hospital surfaces with respiratory pathogens in Bangladesh, *PLOS One* 14(10) (2019) e0224065. <https://doi.org/10.1371/journal.pone.0224065>
- [7] E.K. Kurgat, J.D. Sexton, F. Garavito, A. Reynolds, R.D. Contreras, C.P. Gerba, R.A. Leslie, S.L. Edmonds-Wilson, K.A. Reynolds, Impact of a hygiene intervention on virus spread in an office building, *Int. J. Hyg. Environ. Health* 222(3) (2019) 479-485. <https://doi.org/10.1016/j.ijheh.2019.01.001>
- [8] J.M.L. Brotherton, V.C. Delpech, G.L. Gilbert, S. Hatzi, P.D. Paraskevopoulos, J.M. McNulty, A large outbreak of influenza A and B on a cruise ship causing widespread morbidity, *Epidemiol. Infect.* 130(2) (2003) 263-271. <https://doi.org/10.1017/s0950268802008166>
- [9] S. Xiao, Y. Li, T.-W. Wong, D.S.C. Hui, Role of fomites in SARS transmission during the largest hospital outbreak in Hong Kong, *PLOS One* 12(7) (2017). <https://doi.org/10.1371/journal.pone.0181558>
- [10] S.F. Dowell, J.M. Simmerman, D.D. Erdman, J.-S.J. Wu, A. Chaovavanich, M. Javadi, J.-Y. Yang, L.J. Anderson, S. Tong, M.S. Ho, Severe acute respiratory

syndrome coronavirus on hospital surfaces, *Clin. Infect. Dis.* 39(5) (2004) 652-657.
<https://doi.org/10.1086/422652>

[11] A.J. Prussin II, J.A. Belser, W. Bischoff, S.T. Kelley, K. Lin, W.G. Lindsley, J.P. Nshimiyimana, M. Schuit, Z. Wu, K. Bibby, L.C. Marr, Viruses in the Built Environment (VIBE) meeting report, *Microbiome* 8 (2020) 1. <https://doi.org/10.1186/s40168-019-0777-4>

[12] H. Sakaguchi, K. Wada, J. Kajioka, M. Watanabe, R. Nakano, T. Hirose, H. Ohta, Y. Aizawa, Maintenance of influenza virus infectivity on the surfaces of personal protective equipment and clothing used in healthcare settings, *Environmental Health and Preventive Medicine* 15(6) (2010) 344-349. <https://doi.org/10.1007/s12199-010-0149-y>

[13] F. Cui, X. Geng, O. Zervaki, D.D. Dionysiou, J. Katz, S.-J. Haig, M. Boufadel, Transport and fate of virus-laden particles in a supermarket: Recommendations for risk reduction of COVID-19 spreading, *J. Environ. Eng.* 147(4) (2021) 04021007.
[https://doi.org/10.1061/\(ASCE\)EE.1943-7870.0001870](https://doi.org/10.1061/(ASCE)EE.1943-7870.0001870)

[14] A.K. Pitol, T.R. Julian, Community transmission of SARS-CoV-2 by fomites: Risks and risk reduction strategies, *Environ. Sci. Technol. Lett.* 8 (2021) 263-269.
<https://dx.doi.org/10.1021/acs.estlett.0c00966>

[15] A. Meiksin, Dynamics of COVID-19 transmission including indirect transmission mechanisms: A mathematical analysis, *Epidemiol. Infect.* 148 (2020) e257.
<https://doi.org/10.1017/s0950268820002563>

[16] L. Owen, K. Laird, The role of textiles as fomites in the healthcare environment: a review of the infection control risk, *PeerJ* 8 (2020) e9790.
<https://doi.org/10.7717/peerj.9790>

[17] A. Brlek, Š. Vidovič, S. Vuzem, K. Turk, Z. Simonović, Possible indirect transmission of COVID-19 at a squash court, Slovenia, March 2020: Case report, *Epidemiol. Infect.* 148 (2020) e120. <https://doi.org/10.1017/s0950268820001326>

[18] Z. Zhang, L. Zhang, Y. Wang, COVID-19 indirect contact transmission through the oral mucosa must not be ignored, *J. Oral Pathology Med.* 49(5) (2020) 450-451.
<https://doi.org/10.1111/jop.13019>

[19] T. Yamagishi, M. Ohnishi, N. Matsunaga, K. Kakimoto, H. Kamiya, K. Okamoto, M. Suzuki, Y. Gu, M. Sakaguchi, T. Tajima, S. Takaya, N. Ohmagari, M. Takeda, S. Matsuyama, K. Shirato, N. Nao, H. Hasegawa, T. Kageyam, I. Takayama, S. Saito, K. Wada, R. Fujita, H. Saito, K. Okinaka, M. Griffith, A.E. Parry, B. Barnetson, J. Leonard, Environmental sampling for severe acute respiratory syndrome coronavirus 2 during a COVID-19 outbreak on the Diamond Princess cruise ship, *J. Infect. Dis.* 222(7) (2020) 1098-1102. <https://doi.org/10.1093/infdis/jiaa437>

[20] S.W.X. Ong, Y.K. Tan, P.Y. Chia, T.H. Lee, O.T. Ng, M.S.Y. Wong, K. Marimuthu, Air, surface environmental, and personal protective equipment contamination by severe

acute respiratory syndrome coronavirus 2 (SARS-CoV-2) from a symptomatic patient, *JAMA* 323(16) (2020) 1610-1612. <https://doi.org/10.1001/jama.2020.3227>

[21] B. Pastorino, F. Touret, M. Gilles, X. de Lamballerie, R. Charrel, Prolonged infectivity of SARS-CoV-2 in fomites, *Emerg. Infect. Dis.* 26(9) (2020) 2256-2257. <https://dx.doi.org/10.3201/eid2609.201788>

[22] Z.-D. Guo, Z.-Y. Wang, S.-F. Zhang, X. Li, L. Li, C. Li, Y. Cui, R.-B. Fu, Y.-Z. Dong, X.-Y. Chi, Aerosol and surface distribution of severe acute respiratory syndrome coronavirus 2 in hospital wards, Wuhan, China, 2020, *Emerg. Infect. Dis.* 26(7) (2020) 1583-1591. <https://doi.org/10.3201/eid2607.200885>

[23] P.Y. Chia, K.K. Coleman, Y.K. Tan, S.W.X. Ong, M. Gum, S.K. Lau, X.F. Lim, A.S. Lim, S. Sutjipto, P.H. Lee, Detection of air and surface contamination by SARS-CoV-2 in hospital rooms of infected patients, *Nature Comm.* 11(1) (2020) 1-7. <https://doi.org/10.1038/s41467-020-16670-2>

[24] N. Van Doremalen, T. Bushmaker, D.H. Morris, M.G. Holbrook, A. Gamble, B.N. Williamson, A. Tamin, J.L. Harcourt, N.J. Thornburg, S.I. Gerber, Aerosol and surface stability of SARS-CoV-2 as compared with SARS-CoV-1, *New Engl. J. Med.* 382(16) (2020) 1564-1567. <https://doi.org/10.1056/NEJMc2004973>

[25] Transmission of SARS-CoV-2: implications for infection prevention precautions: Scientific Brief, 09 July 2020, World Health Organization, 2020.

[26] A.P. Harvey, E.R. Fuhrmeister, M. Cantrell, A.K. Pitol, J.M. Swarthout, J.E. Powers, M.L. Nadimpalli, T.R. Julian, A.J. Pickering, Longitudinal monitoring of SARS-CoV-2 RNA on high-touch surfaces in a community setting, *Environ. Sci. Technol. Lett.* 8(2) (2021) 168-175. <https://doi.org/10.1021/acs.estlett.0c00875>

[27] F.X. Abad, C. Villena, S. Guix, S. Caballero, R.M. Pintó, A. Bosch, Potential role of fomites in the vehicular transmission of human astroviruses, *Appl. Environ. Microbiol.* 67(9) (2001) 3904-3907. <http://dx.doi.org/10.1128/AEM.67.9.3904-3907.2001>

[28] A. Kramer, I. Schwebke, G. Kampf, How long do nosocomial pathogens persist on inanimate surfaces? A systematic review, *BMC Infect. Dis.* 6(1) (2006) 130. <https://doi.org/10.1186/1471-2334-6-130>

[29] A. Chabrelie, J. Mitchell, J. Rose, D. Charbonneau, Y. Ishida, Evaluation of the influenza risk reduction from antimicrobial spray application on porous surfaces, *Risk Anal.* 38(7) (2018) 1502-1517. <https://doi.org/10.1111/risa.12952>

[30] B. Killingley, J. Nguyen-Van-Tam, Routes of influenza transmission, *Influenza Other Resp.* 7 (2013) 42-51. <https://doi.org/10.1111/irv.12080>

[31] R.A. Canales, K.A. Reynolds, A.M. Wilson, S.L. Fankem, M.H. Weir, J.B. Rose, S. Abd-Elmaksoud, C.P. Gerba, Modeling the role of fomites in a norovirus outbreak, *J.*

- Occup. Environ. Hyg. 16(1) (2019) 16-26.
<https://doi.org/10.1080/15459624.2018.1531131>
- [32] E.L. Jones, A. Kramer, M. Gaither, C.P. Gerba, Role of fomite contamination during an outbreak of norovirus on houseboats, *Int. J. Environ. Health Res.* 17(2) (2007) 123-131. <https://doi.org/10.1080/09603120701219394>
- [33] M.O. Aydogdu, E. Altun, E. Chung, G. Ren, S. Homer-Vanniasinkam, B. Chen, M. Edirisinghe, Surface interactions and viability of coronaviruses, *J. R. Soc. Interface* 18 (2021). <https://doi.org/10.1098/rsif.2020.0798>
- [34] B. Michen, F. Meder, A. Rust, J. Fritsch, C. Aneziris, T. Graule, Virus removal in ceramic depth filters based on diatomaceous earth, *Environ. Sci. Technol.* 46(2) (2012) 1170-1177. <https://doi.org/10.1021/es2030565>
- [35] J.-A. Park, S.-B. Kim, DLVO and XDLVO calculations for bacteriophage MS2 adhesion to iron oxide particles, *J. Contam. Hydrol.* 181 (2015) 131-140.
<https://doi.org/10.1016/j.jconhyd.2015.01.005>
- [36] X. Wang, R. Şengür-Taşdemir, İ. Koyuncu, V.V. Tarabara, Lip balm drying promotes virus attachment: Characterization of lip balm coatings and XDLVO modeling, *J. Colloid Interface Sci.* 581 (2021) 884-894. <https://doi.org/10.1016/j.jcis.2020.07.143>
- [37] I. Samandoulgou, I. Fliss, J. Jean, Adhesion of norovirus to surfaces: Contribution of thermodynamic and molecular properties using virus-like particles, *Food Environ. Virol.* (2021). <https://doi.org/10.1007/s12560-021-09471-3>
- [38] H.T.T. Dang, V.V. Tarabara, Virus deposition onto polyelectrolyte-coated surfaces: A study with bacteriophage MS2, *J. Colloid Interface Sci.* 540 (2019) 155-166.
<https://doi.org/10.1016/j.jcis.2018.12.107>
- [39] K. Wong, B. Mukherjee, A.M. Kahler, R. Zepp, M. Molina, Influence of inorganic ions on aggregation and adsorption behaviors of human adenovirus, *Environ. Sci. Technol.* 46(20) (2012) 11145-11153. <https://doi.org/10.1021/es3028764>
- [40] Y.-N. Liu, Z.-T. Lv, S.-Y. Yang, X.-W. Liu, Optical tracking of the interfacial dynamics of single SARS-CoV-2 pseudoviruses, *Environ. Sci. Technol.* 55 (2021) 4115-4122. <https://dx.doi.org/10.1021/acs.est.0c06962>
- [41] A. Armanious, M. Aeppli, R. Jacak, D. Refardt, T. Sigstam, T. Kohn, M. Sander, Viruses at solid-water interfaces: a systematic assessment of interactions driving adsorption, *Environ. Sci. Technol.* 50(2) (2015) 732-743.
<https://doi.org/10.1021/acs.est.5b04644>
- [42] X.L. Zhou, Y. Yang, S. Wang, X.W. Liu, Surface plasmon resonance microscopy: From single-molecule sensing to single-cell imaging, *Angew. Chem., Int. Ed.* 59(5) (2020) 1776-1785. <https://doi.org/10.1002/anie.201908806>

- [43] B. Yuan, M. Pham, T.H. Nguyen, Deposition kinetics of bacteriophage MS2 on a silica surface coated with natural organic matter in a radial stagnation point flow cell, *Environ. Sci. Technol.* 42(20) (2008) 7628-7633. <https://doi.org/10.1021/es801003s>
- [44] M. Pham, E.A. Mintz, T.H. Nguyen, Deposition kinetics of bacteriophage MS2 to natural organic matter: Role of divalent cations, *J. Colloid Interface Sci.* 338(1) (2009) 1-9. <https://doi.org/10.1016/j.jcis.2009.06.025>
- [45] H.T.T. Dang, V.V. Tarabara, Attachment of human adenovirus onto household paints, *Colloids Surf. B* 204 (2021). <https://doi.org/10.1016/j.colsurfb.2021.111812>
- [46] X. Huang, J. Xu, H.-F. Ji, G. Li, H. Chen, Quartz crystal microbalance based biosensor for rapid and sensitive detection of maize chlorotic mottle virus, *Anal. Methods* 6(13) (2014) 4530-4536. <https://doi.org/10.1039/C4AY00292J>
- [47] C.J. Van Oss, *Interfacial forces in aqueous media*, CRC Press, 2006.
- [48] G.R. Nemerow, P.L. Stewart, V.S. Reddy, Structure of human adenovirus, *Curr. Opin. Virol.* 2(2) (2012) 115-121. <https://doi.org/10.1016/j.coviro.2011.12.008>
- [49] C. San Martín, Latest insights on adenovirus structure and assembly, *Viruses* 4(5) (2012) 847-877. <https://doi.org/10.3390/v4050847>
- [50] K. Sirikanchana, J.L. Shisler, B.J. Marinas, Effect of exposure to UV-C irradiation and monochloramine on adenovirus serotype 2 early protein expression and DNA replication, *Appl. Environ. Microbiol.* 74(12) (2008) 3774-3782. <https://doi.org/10.1128/aem.02049-07>
- [51] S. Jing, J. Zhang, M. Cao, M. Liu, Y. Yan, S. Zhao, N. Cao, J. Ou, K. Ma, X. Cai, Household transmission of human adenovirus type 55 in case of fatal acute respiratory disease, *Emerg. Infect. Dis.* 25(9) (2019) 1756. <https://doi.org/10.3201/eid2509.181937>
- [52] G. La Rosa, M. Fratini, S.D. Libera, M. Iaconelli, M. Muscillo, Viral infections acquired indoors through airborne, droplet or contact transmission, *Ann. Ist. Super. Sanità* 49 (2013) 124-132. https://doi.org/10.4415/ANN_13_02_03
- [53] L. Liljeroos, M.A. Krzyzaniak, A. Helenius, S.J. Butcher, Architecture of respiratory syncytial virus revealed by electron cryotomography, *PNAS* 110(27) (2013) 11133-11138. <https://doi.org/10.1073/pnas.1309070110>
- [54] A.R. Falsey, E.E. Walsh, Respiratory syncytial virus infection in adults, *Clin. Microbiol. Rev.* 13(3) (2000) 371-384. <https://doi.org/10.1128/CMR.13.3.371>
- [55] C.B. Hall, R.G. Douglas Jr, Modes of transmission of respiratory syncytial virus, *J. Pediatr.* 99(1) (1981) 100-103. [https://doi.org/10.1016/S0022-3476\(81\)80969-9](https://doi.org/10.1016/S0022-3476(81)80969-9)

- [56] C.B. Hall, R.G. Douglas Jr, J.M. Geiman, Possible transmission by fomites of respiratory syncytial virus, *J. Infect. Dis.* 141(1) (1980) 98-102.
<https://doi.org/10.1093/infdis/141.1.98>
- [57] E.P. Vejerano, L.C. Marr, Physico-chemical characteristics of evaporating respiratory fluid droplets, *J. R. Soc. Interface* 15(139) (2018) 20170939.
<https://doi.org/10.1098/rsif.2017.0939>
- [58] B.K. Walsh, D.J. Mackey, T. Pajewski, Y. Yu, B.M. Gaston, J.F. Hunt, Exhaled-breath condensate pH can be safely and continuously monitored in mechanically ventilated patients, *Respir. Care* 51(10) (2006) 1125-1131.
- [59] R.M. Effros, K.W. Hoagland, M. Bosbous, D. Castillo, B. Foss, M. Dunning, M. Gare, W. Lin, F. Sun, Dilution of respiratory solutes in exhaled condensates, *Am. J. Respir. Crit. Care Med.* 165(5) (2002) 663-9. <https://doi.org/10.1164/ajrccm.165.5.2101018>
- [60] ATCC Product Sheet. Human adenovirus 5 (ATCC® VR1516™).
- [61] ATCC Certificate of Analysis. Adenovirus type 5 Reference Material.
- [62] ATCC Product Information Sheet for VR-1516™.
- [63] ATCC Product Sheet. Human respiratory syncytial virus, High titer (ATCC® VR-26PQ™).
- [64] ATCC Certificate of Analysis. Human respiratory syncytial virus, High titer (Strain: Long).
- [65] Z. Ke, R. Dillard, T. Chirkova, F. Leon, C. Stobart, C. Hampton, J. Strauss, D. Rajan, C. Rostad, J. Taylor, H. Yi, R. Shah, M. Jin, T. Hartert, R. Peebles, B. Graham, M. Moore, L. Anderson, E. Wright, The morphology and assembly of respiratory syncytial virus revealed by cryo-electron tomography, *Viruses* 10(8) (2018) 446.
<https://doi.org/10.3390/v10080446>
- [66] C. Griffiths, S.J. Drews, D.J. Marchant, Respiratory syncytial virus: infection, detection, and new options for prevention and treatment, *Clin. Microbiol. Rev.* 30(1) (2017) 277-319. <https://doi.org/10.1128/cmr.00010-16>
- [67] G. Kiss, J.M. Holl, G.M. Williams, E. Alonas, D. Vanover, A.W. Lifland, M. Gudheti, R.C. Guerrero-Ferreira, V. Nair, H. Yi, B.S. Graham, P.J. Santangelo, E.R. Wright, Structural analysis of respiratory syncytial virus reveals the position of M2-1 between the matrix protein and the ribonucleoprotein complex, *J. Virol.* 88(13) (2014) 7602-7617.
<https://doi.org/10.1128/jvi.00256-14>
- [68] C.J. van Oss, M.K. Chaudhury, R.J. Good, Interfacial Lifshitz-van der Waals and polar interactions in macroscopic systems, *Chem. Rev.* 88(6) (1988) 927-941.
<https://doi.org/10.1021/cr00088a006>

- [69] M.E. Schrader, Young-Dupre revisited, *Langmuir* 11 (1995) 3585-3589.
<https://doi.org/10.1021/la00009a049>
- [70] H. Shi, V.V. Tarabara, Charge, size distribution and hydrophobicity of viruses: Effect of propagation and purification methods, *J. Virol. Methods* 256 (2018) 123-132.
<https://doi.org/10.1016/j.jviromet.2018.02.008>
- [71] E.M.V. Hoek, G.K. Agarwal, Extended DLVO interactions between spherical particles and rough surfaces, *J. Colloid Interface Sci.* 298 (2006) 50-58.
<https://doi.org/10.1016/j.jcis.2005.12.031>
- [72] X. Huang, S. Bhattacharjee, E.M.V. Hoek, Is surface roughness a "Scapegoat" or a primary factor when defining particle - substrate interactions?, *Langmuir* 26 (2010) 2528-2537. <https://doi.org/10.1021/la9028113>
- [73] Nanoscience Instruments (personal communication).
- [74] L.F. Zemljič, O. Plohl, A. Vesel, T. Luxbacher, S. Potrč, Physicochemical characterization of packaging foils coated by chitosan and polyphenols colloidal formulations, *Int. J. Mol. Sci.* 21(2) (2020) 495. <https://doi.org/10.3390/ijms21020495>
- [75] Y. Hedberg, X. Wang, J. Hedberg, M. Lundin, E. Blomberg, I.O. Wallinder, Surface-protein interactions on different stainless steel grades: effects of protein adsorption, surface changes and metal release, *J. Mater. Sci.: Mater. Med.* 24(4) (2013) 1015-1033.
<https://doi.org/10.1007/s10856-013-4859-8>
- [76] X. Zhang, R. Bai, Adsorption behavior of humic acid onto polypyrrole-coated nylon 6, 6 granules, *J. Mater. Chem.* 12(9) (2002) 2733-2739.
<https://doi.org/10.1039/B201364A>
- [77] L. Graetz, Ueber die Wärmeleitungsfähigkeit von Flüssigkeiten, *Annalen der Physik* 254 (79) (1882) 79-94. <https://doi.org/10.1002/andp.18822540106>
- [78] W.M. Deen, *Analysis of Transport Phenomena*, Oxford University Press, 1998.
- [79] G. Sauerbrey, Verwendung von Schwingquarzen zur Wägung dünner Schichten und zur Mikrowägung, *Zeitschrift für Physik* 155(2) (1959) 206-222.
<https://doi.org/10.1007/BF01337937>
- [80] J.-L. Putaux, A. Buléon, R. Borsali, H. Chanzy, Ultrastructural aspects of phytoglycogen from cryo-transmission electron microscopy and quasi-elastic light scattering data, *Int. J. Biol. Macromol.* 26(2) (1999) 145-150.
[https://doi.org/10.1016/S0141-8130\(99\)00076-8](https://doi.org/10.1016/S0141-8130(99)00076-8)
- [81] H. Shi, I. Xagorarakis, K.N. Parent, M.L. Bruening, V.V. Tarabara, Elution is a critical step for recovering human adenovirus 40 from tap water and surface water by cross-flow ultrafiltration, *Appl. Environ. Microbiol.* 82(16) (2016) 4982.
<https://doi.org/10.1128/AEM.00870-16>

- [82] H. Ohshima, A simple expression for Henry's function for the retardation effect in electrophoresis of spherical colloidal particles, *J. Colloid Interface Sci.* 168(1) (1994) 269-271. <https://doi.org/10.1006/jcis.1994.1419>
- [83] H. Fischer, J.H. Widdicombe, Mechanisms of acid and base secretion by the airway epithelium, *J. Membr. Biol.* 211(3) (2006) 139-150. <https://doi.org/10.1007/s00232-006-0861-0>
- [84] N. Albinana-Gimenez, P. Clemente-Casares, B. Calgua, J.M. Huguet, S. Courtois, R. Girones, Comparison of methods for concentrating human adenoviruses, polyomavirus JC and noroviruses in source waters and drinking water using quantitative PCR, *J. Virol. Methods* 158(1) (2009) 104-109. <http://dx.doi.org/10.1016/j.jviromet.2009.02.004>
- [85] C. Gibbons, R. Rodriguez, L. Tallon, M. Sobsey, Evaluation of positively charged alumina nanofibre cartridge filters for the primary concentration of noroviruses, adenoviruses and male-specific coliphages from seawater, *J. Appl. Microbiol.* 109(2) (2010) 635-641. <https://doi.org/10.1111/j.1365-2672.2010.04691.x>
- [86] H. Shi, E.V. Pasco, V.V. Tarabara, Membrane-based methods of virus concentration from water: a review of process parameters and their effects on virus recovery, *Environ. Sci. Water Res. Technol.* 3 (2017) 778-792. <https://doi.org/10.1039/C7EW00016B>
- [87] G. Hwang, C.-H. Lee, I.-S. Ahn, B.J. Mhin, Determination of reliable Lewis acid-base surface tension components of a solid in LW-AB approach, *J. Ind. Eng. Chem.* 17 (2011) 125-129. <https://doi.org/10.1016/j.jiec.2010.12.009>
- [88] E. McCafferty, Acid-base effects in polymer adhesion at metal surfaces, *J. Adhes. Sci. Technol.* 16(3) (2002) 239-255. <https://doi.org/10.1163/156856102317295478>
- [89] L.-K. Chau, M.D. Porter, Surface isoelectric point of evaporated silver films: Determination by contact angle titration, *J. Colloid Interface Sci.* 145(1) (1991) 283-286. [https://doi.org/10.1016/0021-9797\(91\)90121-N](https://doi.org/10.1016/0021-9797(91)90121-N)
- [90] M.F. Cuddy, A.R. Poda, L.N. Brantley, Determination of isoelectric points and the role of pH for common quartz crystal microbalance sensors, *ACS Appl. Mater. Interf.* 5 (2013) 3514-3518. <https://doi.org/10.1021/am400909g>
- [91] E. Virga, E. Spruijt, W.M. de Vos, P.M. Biesheuvel, Wettability of amphoteric surfaces: The effect of pH and ionic strength on surface ionization and wetting, *Langmuir* 34 (2018) 15174-15180. <https://doi.org/10.1021/acs.langmuir.8b02875>
- [92] P.K. Weissenborn, R.J. Pugh, Surface tension of aqueous solutions of electrolytes: Relationship with ion hydration, oxygen solubility, and bubble coalescence, *J. Colloid Interface Sci.* 184 (1996) 550-563. <https://doi.org/10.1006/jcis.1996.0651>
- [93] A.J. Kinloch, *Adhesion and Adhesives: Science and Technology*, Springer, 1987.

- [94] C.J. van Oss, M.K. Chaudhury, R.J. Good, Monopolar surfaces, *Adv. Colloid Interface Sci.* 28 (1987) 35-64. [https://doi-org.proxy1.cl.msu.edu/10.1016/0001-8686\(87\)80008-8](https://doi-org.proxy1.cl.msu.edu/10.1016/0001-8686(87)80008-8)
- [95] I. Reviakine, D. Johannsmann, R.P. Richter, Hearing what you cannot see and visualizing what you hear: Interpreting quartz crystal microbalance data from solvated interfaces, *Anal. Chem.* 83(23) (2011) 8838-8848. <https://doi.org/10.1021/ac201778h>
- [96] M. Rodal, How are QCM results influenced by the lateral distribution of the measured layer? *Surface Science Blog*, Biolin Scientific, 2019. <https://www.biolinscientific.com/blog/how-are-qcm-results-influenced-by-the-lateral-distribution-of-the-measured-layer>. (Accessed April 9 2021).
- [97] K.K. Kanazawa, J.G. Gordon, Frequency of a quartz microbalance in contact with liquid, *Anal. Chem.* 57(8) (1985) 1770-1771. <https://doi.org/10.1021/ac00285a062>
- [98] K.K. Kanazawa, J.G. Gordon, The oscillation frequency of a quartz resonator in contact with liquid, *Anal. Chim. Acta* 175 (1985) 99-105. [https://doi.org/10.1016/S0003-2670\(00\)82721-X](https://doi.org/10.1016/S0003-2670(00)82721-X)
- [99] L. Boulangé-Petermann, A. Doren, B. Baroux, M.-N. Bellon-Fontaine, Zeta potential measurements on passive metals, *J. Colloid Interface Sci.* 171(1) (1995) 179-186. <https://doi.org/10.1006/jcis.1995.1165>
- [100] S. Wu, S. Altenried, A. Zogg, F. Zuber, K. Maniura-Weber, Q. Ren, Role of the surface nanoscale roughness of stainless steel on bacterial adhesion and microcolony formation, *ACS Omega* 3(6) (2018) 6456-6464. <https://doi.org/10.1021/acsomega.8b00769>
- [101] G. Okamoto, Passive film of 18-8 stainless steel structure and its function, *Corrosion Sci.* 13 (1973) 471-489. [https://doi.org/10.1016/0010-938X\(73\)90031-0](https://doi.org/10.1016/0010-938X(73)90031-0)
- [102] N. Sato, M. Cohen, The kinetics of anodic oxidation of iron in neutral solution: II The initial stages, *J. Electrochem. Soc.* 111 (1964) 512-522. <https://doi.org/10.1149/1.2426171>
- [103] L. Boulangé-Petermann, C. Jullien, P.E. Dubois, T. Benezech, C. Faille, Influence of surface chemistry on the hygienic status of industrial stainless steel, *Biofouling* 20(1) (2004) 25-33. <https://doi.org/10.1080/08927010410001655542>
- [104] G.C. Laine, Characterization of and controlling morphology of ultra-thin nanocomposites, University of Kentucky, 2013.
- [105] L. Moeller, L. Schuenadel, A. Nitsche, I. Schwebke, M. Hanisch, M. Laue, Evaluation of virus inactivation by formaldehyde to enhance biosafety of diagnostic electron microscopy, *Viruses* 7(2) (2015) 666-679. <https://doi.org/10.3390/v7020666>

- [106] N.I. Rabiah, Y. Sato, A. Kannan, W. Kress, F. Straube, G.G. Fuller, Understanding the adsorption and potential tear film stability properties of recombinant human lubricin and bovine submaxillary mucins in an in vitro tear film model, *Colloid Surface B* 195 (2020) 111257. <https://doi.org/10.1016/j.colsurfb.2020.111257>
- [107] H. Seo, M. Yoo, S. Jeon, Influence of nanobubbles on the adsorption of nanoparticles, *Langmuir* 23(4) (2007) 1623-1625. <https://doi.org/10.1021/la062763r>
- [108] X.H. Zhang, Quartz crystal microbalance study of the interfacial nanobubbles, *Phys. Chem. Chem. Phys.* 10(45) (2008) 6842-6848. <https://doi.org/10.1039/b810587a>
- [109] K.K. Kanazawa, J.G. Gordon, The oscillation frequency of a quartz resonator in contact with liquid, *Anal. Chim. Acta* 175 (1985) 99-105. [https://doi.org/10.1016/S0003-2670\(00\)82721-X](https://doi.org/10.1016/S0003-2670(00)82721-X)
- [110] K.K. Kanazawa, J.G. Gordon, Frequency of a quartz microbalance in contact with liquid, *Anal. Chem.* 57(8) (1985) 1770-1771. <https://doi.org/10.1021/ac00285a062>
- [111] I. Reviakine, D. Johannsmann, R.P. Richter, Hearing what you cannot see and visualizing what you hear: Interpreting quartz crystal microbalance data from solvated interfaces, *Anal. Chem.* 83(23) (2011) 8838-8848. <https://doi.org/10.1021/ac201778h>
- [112] H. Ozbek, Viscosity of aqueous sodium chloride solutions from 0 to 150 C, American Chemical Society 29th Southeast Regional Meeting, Tampa, FL, 1977.
- [113] G.M. Iliescu, C. Vasile, Caracteristici termofizice ale produselor alimentare, Editura Tehnică, 1982.
- [114] H. Ohshima, A simple expression for Henry's function for the retardation effect in electrophoresis of spherical colloidal particles, *J. Colloid Interface Sci.* 168(1) (1994) 269-271. <https://doi.org/10.1006/jcis.1994.1419>
- [115] H. Shi, I. Xagorarakis, K.N. Parent, M.L. Bruening, V.V. Tarabara, Elution is a critical step for recovering human adenovirus 40 from tap water and surface water by cross-flow ultrafiltration, *Appl. Environ. Microbiol.* 82(16) (2016) 4982. <https://doi.org/10.1128/AEM.00870-16>

CHAPTER FOUR

PVDF membrane ageing due to chemical cleaning: Understanding the evolution of membrane-foulant interactions

4.1 Abstract

This study investigates the surface chemistry evolution of polyvinylidene fluoride (PVDF) under the effect of intermittent Humic acid (HA) fouling and sodium hypochlorite (NaClO) cleaning. The surface physicochemical evolutions of aged membranes are characterized based on surface energy calculation. The membrane ageing tests show that NaClO cleaning have opposite effect on pristine PVDF membrane and pristine PVDF/PVP membrane. Specifically, NaClO cleaning enhances the hydrophilicity of PVDF membrane but hydrophobicity of PVDF/PVP membrane. Static fouling-cleaning tests show that the surface energy of the membrane floats between a lower value after each cleaning stage and a higher value after each fouling stage. More experiments will be performed, including FTIR and XPS analysis, to help interpret the surface energy change from molecular level.

4.2 Introduction

Membrane processes are being increasingly used in drinking water treatment due to their effectiveness to remove many contaminants in raw water as well as their low cost. Polyvinylidene fluoride (PVDF) is widely used as the base polymer for many membranes due to its high hydrophobicity, chemical resistance, and excellent mechanical strength. However, pure PVDF membranes are highly hydrophobic, making them more susceptible to fouling in water treatment [1]. In this sense, hydrophilic additives which have hydroxyl, amine, or carboxylic acid groups are often blended into PVDF, which enhance the filtration performance of these membranes [2, 3]. Yet these polymeric additives may leach out from the membrane due to their relatively small sizes and their affinity to the water.

Indeed, membrane fouling is one of the critical challenges in the successful application of membrane processes. Fouling arises from interactions between a membrane and various components present in the raw water [4]. Natural organic matter (NOM), such as humic acid, is ubiquitous in surface water – a common source of raw water for drinking water treatment plants. NOM is one of the major membrane foulants as documented in research literature and reports from professional practice community [4-7]. Humic acid fouling is a complex phenomenon which involves both reversible and irreversible processes [4].

Chemical cleaning is necessary to remove irreversible pollution. There are several categories of cleaning chemicals including surfactants, oxidants, acids, and chelating agents. Among them, sodium hypochlorite (NaClO) is one of the most commonly used cleaning reagents because of its low price and effectiveness against organic foulants [8]. However, chemical agents can cause damage to the membrane [9]. Numerous studies have shown that changes in the characteristics of aged membranes were due to the oxidation or decomposition of the hydrophilic additives in blended PVDF membranes [1]. The evolution of hydrophilicity of aged PVDF membranes was extensively studied [8, 10]. However, there are no unified conclusions obtained on the evolution of the intrinsic characteristics of PVDF membranes when cleaned with NaClO solutions [10].

In this study, humic acid (Sigma-Aldrich) was chosen as the model organic foulant. This humic acid has been thoroughly characterized and used in numerous membrane fouling studies [4, 11, 12]. Humic acid (HA) is representative of natural organic matter, a common component in surface water where it is present in both dissolved and suspended fractions. HA is a complex and heterogeneous combination of many macromolecules. The fouling potential of HA during membrane filtration of surface waters varies greatly depending on the solution chemistry and membrane properties [13].

The study explores the hypothesis that a layer of residual foulants offers increasing protection of the membrane polymer against bleach as it develops on the membrane surface.

4.3 Experimental

4.3.1 Reagents and materials

The humic acid sodium salt (HA), polyvinylpyrrolidone (PVP) powder, NaClO (10%), Dimethylformamide (DMFA), glycerol, ethylene glycol (EG) and diiodomethane (DID) were purchased from Sigma Aldrich. Polyvinylidene fluoride (PVDF) powder (Solef 1015, Solvay) and DMFA was used in PVDF membrane preparation (See Supplementary Materials (SM), section S1). QCM-D sensors coated with PVDF were purchased from Nanoscience.

4.3.2 Chemical cleaning study of membranes

The cleaning agent used in the study is 1% NaClO (pH 12). Pristine membranes were kept in NaClO solution or DI water for 5, 10, 20, 30, 50, 60, 80, 100 hours. The contact angles of four probe liquids (water, glycerol, DID, EG) on the PDVF membrane were measured at the end of each cleaning period. The surface energy and surface tension components were calculated and plotted as a function of CT values.

4.3.3 Static fouling-cleaning test of membranes

Prior to static fouling-cleaning tests, 100 mg/ml HA solution was prepared and maintained at a pH of 7. The ionic strength (IS) of HA was kept at 15 mM. The following two steps were continuously performed for several cycles of fouling (HA for 24 hours) and cleaning (1% NaClO for 5 hours). The solution was stirred during the whole process to keep its homogeneity.

4.3.4 Quantifying surface energy of PVDF membrane

The hydrophobicity of membrane was quantified

$$(1 + \cos\theta)\gamma_l^{TOT} = 2 \left(\sqrt{\gamma_s^{LW}\gamma_l^{LW}} + \sqrt{\gamma_s^+\gamma_l^-} + \sqrt{\gamma_s^-\gamma_l^+} \right), \quad (1)$$

where γ_l^{TOT} is the total surface energy of the probe liquid:

$$\gamma^{tot} = \gamma^{LW} + \gamma^{AB} = \gamma^{LW} + 2\sqrt{\gamma^-\gamma^+}. \quad (2)$$

The free energy of solid-solid interfacial interaction in water is given by

$$\Delta G_{sws} = -2 \left(\sqrt{\gamma_s^{LW}} - \sqrt{\gamma_w^{LW}} \right)^2 - 4 \left(\sqrt{\gamma_s^+\gamma_s^-} + \sqrt{\gamma_w^+\gamma_w^-} - \sqrt{\gamma_s^+\gamma_w^-} - \sqrt{\gamma_s^-\gamma_w^+} \right) \quad (3)$$

where γ_w^{LW} , γ_w^+ and γ_w^- are surface energy components of water. A positive value of ΔG_{sws} indicates a hydrophilic surface, while negative ΔG_{sws} corresponds to a hydrophobic surface. The absolute value of ΔG_{sws} indicates the degree of hydrophilicity (or hydrophobicity, when $\Delta G_{sws} < 0$) of the surface.

Contact angles of four probe liquids (DI water, glycerol, DID, and EG) were measured using the sessile drop method (goniometer/tensiometer model 250, ramé-hart). The droplet volume was 6 μl . All measurements were performed in the air at the room temperature of 22 $^{\circ}\text{C}$ and the relative humidity of 46 %. Contact angle values were calculated by DROPPimage Advanced software based on droplet shapes recorded by camera.

4.3.5 Quantification of HA-membrane interactions

The free energy of virus-PVDF interfacial interaction in water ΔG_{vwm} , is calculated as follows:

$$\Delta G_{d_0}^{LW} = 2 \left(\sqrt{\gamma_v^{LW}} - \sqrt{\gamma_w^{LW}} \right) \left(\sqrt{\gamma_w^{LW}} - \sqrt{\gamma_m^{LW}} \right) \quad (8)$$

$$\Delta G_{d_0}^{AB} = 2 \sqrt{\gamma_w^+} (\sqrt{\gamma_m^-} + \sqrt{\gamma_v^-} - \sqrt{\gamma_w^-}) + 2 \sqrt{\gamma_w^-} (\sqrt{\gamma_m^+} + \sqrt{\gamma_v^+} - \sqrt{\gamma_w^+}) - 2 \sqrt{\gamma_m^+ \gamma_v^-} - 2 \sqrt{\gamma_m^- \gamma_v^+} \quad (9)$$

$$\Delta G_{vwm} = \Delta G_{d_0}^{LW} + \Delta G_{d_0}^{AB} \quad (10)$$

4.4 Results

4.4.1 Impact of NaClO cleaning on membrane characteristics

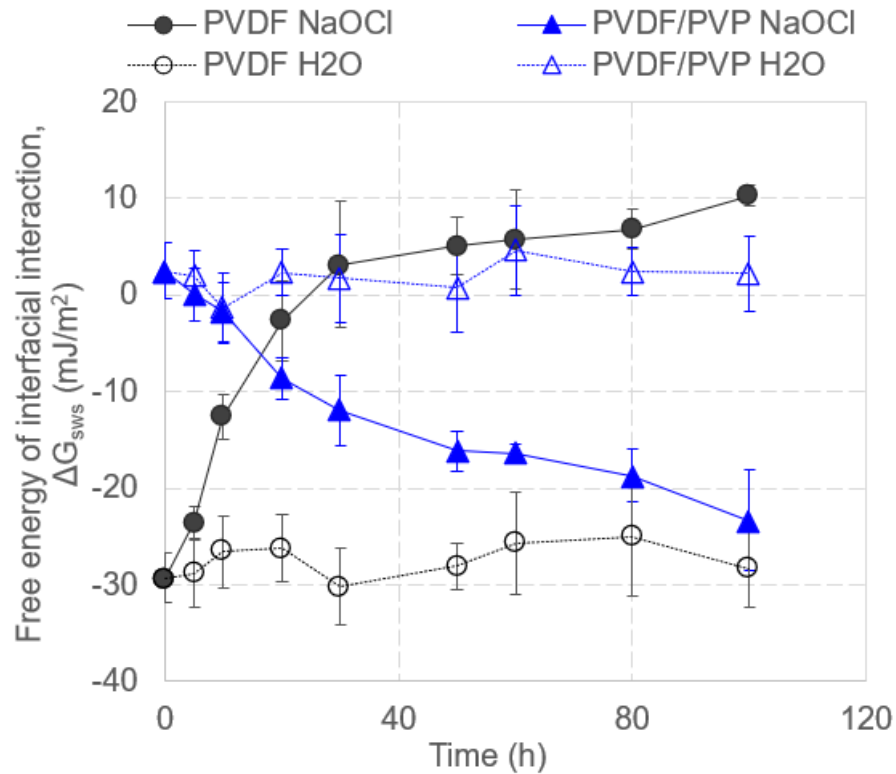


Figure 58. Free energy of interfacial interaction in water (ΔG_{sws}) of membrane as a function of cleaning time (cleaning agent: 1% NaClO).

From Fig. 58, one can observe that DI water has no influence on the surface energy of PVDF and PVDF/PVP membrane. Fig. 58 also shows that pristine PVDF membrane is hydrophobic ($\Delta G_{sws} = -29.3 \text{ mJ/m}^2$), and PVP causes an increase in hydrophilicity of as-

cast membrane ($\Delta G_{sws} = 2.5 \text{ mJ/m}^2$ for PVDF/PVP membrane). Fig. 58 shows that NaClO cleaning increases the hydrophilicity of pristine PVDF membrane. This is consistent with one previous study, in which PVDF membrane is also shown to become more hydrophilic with NaClO cleaning [14]. One possible explanation of this hydrophilicity increase is the formation of carbonyl groups in PVDF polymeric structure. For PVDF/PVP membrane, Fig. 58 shows that extended ageing in NaClO makes the PVDF/PVP membrane more hydrophobic, presumably because the increase in hydrophobicity caused by PVP leaching overcame the increase in hydrophilicity due to the formation of carbonyl group. This result is consistent with the study conducted by Ren [10].

4.4.2 Static fouling and cleaning cycles

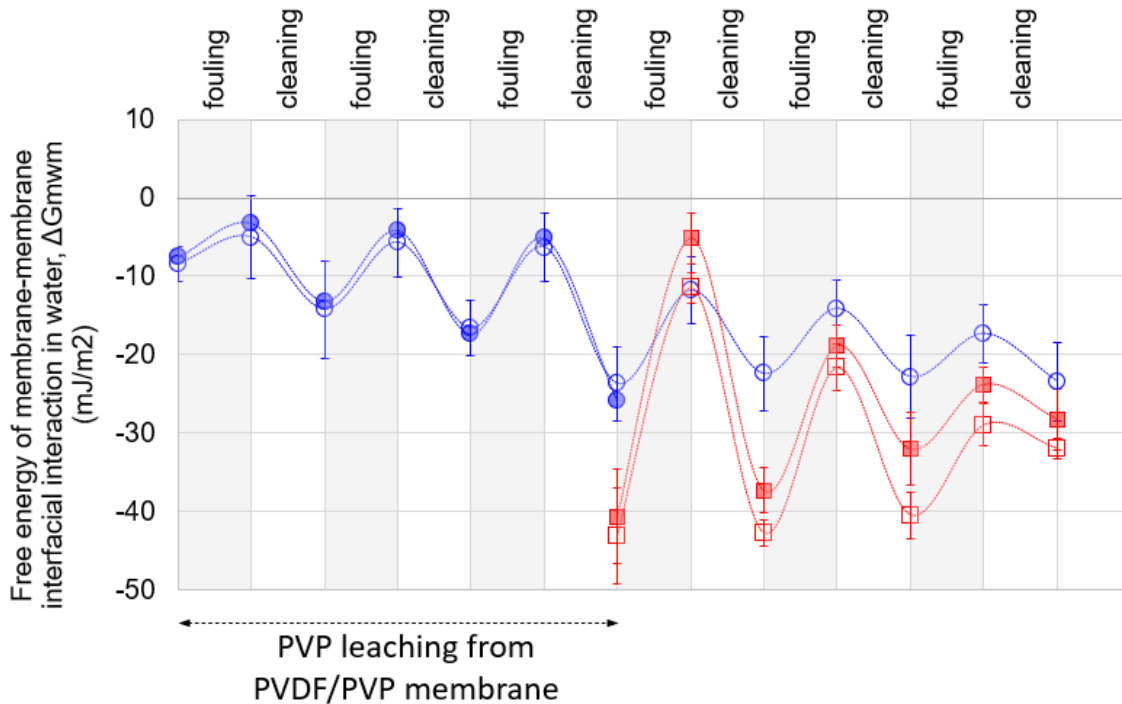


Figure 59. Free energy of interfacial interactions (ΔG_{mwm}) of PVDF (red) and PVDF/PVP (blue) membrane as a function of fouling and cleaning cycles. The solid and empty symbols refer to replicated tests.

Fig. 59 shows that surface energy of the membrane floats between a lower value after each cleaning stage and a higher value after each fouling stage. The asymptotic value corresponds to the chemically irreversible layer of foulants that is conditioned by consecutive exposures to foulants and is comprised by the adsorbed foulant fraction that is hard to oxidize further. The hydrophilicity of PVDF and PVDF/PVP membrane are enhanced after each fouling may be attributed to the hydrophilic nature of humic acid. PVDF/PVP membrane became more hydrophobic after three cycles of fouling-cleaning compared to the pristine membrane, as presented in Fig. 59. This hydrophobicity

increase may be due to the leaching of PVP from PVDF/PVP membrane. After the third cycles of fouling-cleaning, PVDF/PVP membrane is still less hydrophobic than pristine PVDF membrane, suggesting the existence of residual PVP in the membrane. However, for the rest of the fouling-cleaning cycles, PVDF and PVDF/PVP membrane have similar trends of surface energy change, as shown in Fig. 59, which may indicate that after three cycles most PVP was leached out from PVDF/PVP membrane so PVDF structure change prevails over PVP leaching as a factor responsible for the overall change in membrane surface energy.

4.5 Discussion

In this study, reagent grade NaClO (10%, Sigma Aldrich) is used as the cleaning agent. Some wastewater treatment facilities such as Traverse City Regional Wastewater Treatment Plant, citric acid and NaClO are used for maintenance cleaning. Therefore, more research is needed to study the effect of citric acid and NaClO cleaning on the surface chemistry of PVDF membrane. Also, the fouling solution used in this study is humic acid sodium salt (Sigma Aldrich), which is a standard humic acid. In general, the raw water, which treated by municipal water treatment plant, usually contains various components apart from humic acid. These components will have potential influence on the kinetics of membrane fouling and cleaning. Future study is needed to study the surface chemistry evolution of PVDF when raw water is involved.

Furthermore, both PVDF and PVDF/PVP membranes used in this study were made in the lab. In WWTPs, however, commercial membranes are more commonly used in the filtration systems. Commercial membranes are usually modified with coatings or blended with additives to enhance the membrane performance and mechanical strength. Typically, the chemical components of these coatings or additives are not known since they belong to the intellectual properties of manufacturers.

Lastly, the concentration of NaClO selected in this study (1%) is much higher than that in Traverse city WWTPs (0.036%). The purpose of choosing this concentration (C) is to accelerate the ageing effect, so that reasonable cleaning time (T) can be selected to reach the same CT value as Traverse city WWTPs.

4.6 Conclusions

From the data collected so far, one can tentatively conclude that a firmly attached humic acid layer may be formed on membrane surface after a few cycles of fouling and cleaning. This humic acid layer can protect the membrane from being further aged by NaClO. This study is still in progress. More experiment including FTIR, XPS analysis will be performed to investigate the change of functional groups on the surface of membrane. FTIR and XPS analysis will help understand the evolution of this humic acid layer from molecular level. This study can help understand the adsorption kinetics of humic acid on PVDF membrane as well as the NaClO cleaning effect on PVDF membrane fouled with humic acid.

APPENDIX

APPENDIX

S1. PVDF and PVDF/PVP membrane preparation

The PVDF and PVDF/PVP membranes were prepared using phase inversion method by immersion precipitation. The preparation procedure is as follows:

Table 15. The amount of each ingredient to make 50 g 15% solution of PVDF and PVDF/PVP in DMFA.

	PVDF	DMFA	PVP
PVDF membrane	7.5 g	45 ml	0
PVDF/PVP membrane	7.5 g	43.4 ml	1.5 g

1. Preparation of PVDF and PVDF/PVP solution: certain amount of PVDF, PVP and DMFA (density $\rho = 0.9445 \text{ g/cm}^3$) were added in a beaker. The polymer solution was stirred and heated until complete dissolution. The solution must not boil, otherwise it will take additional time to remove bubbles.
2. Degassing of the polymer solution: The polymer solution was degassed using a vacuum desiccator (Wheaton) and a vacuum pump (model UN726 FTP, KNF NEUBERGER).
3. Casting of membranes: The membrane was casted using an automatic film applicator (Elcometer 4340) with a molding knife (Elcometer 3570) on a glass

plate. Homogenous polymer solution was poured into the molding knife. A uniform layer of polymer on the surface of the glass plate was made.

4. Immersion precipitation: Immersing the glass with a layer of polymer solution into precipitating bath (stage of coagulation) for 5 min at 20 °C. In our study, DI water was used as the coagulant.

The membranes were stored in the DI water at room temperature prior to use.

REFERENCES

REFERENCES

- [1] S.Z. Abdullah, P.R. Bérubé, Assessing the effects of sodium hypochlorite exposure on the characteristics of PVDF based membranes, *Water research* 47(14) (2013) 5392-5399.
- [2] D. Musale, S. Kulkarni, Fouling reduction in poly (acrylonitrile-co-acrylamide) ultrafiltration membranes, *Journal of membrane science* 111(1) (1996) 49-56.
- [3] N. Hilal, O.O. Ogunbiyi, N.J. Miles, R. Nigmatullin, Methods employed for control of fouling in MF and UF membranes: a comprehensive review, *Separation Science and Technology* 40(10) (2005) 1957-2005.
- [4] W. Yuan, A.L. Zydney, Humic acid fouling during ultrafiltration, *Environmental Science & Technology* 34(23) (2000) 5043-5050.
- [5] I.H. Suffet, M. Patrick, *Aquatic humic substances: influence on fate and treatment of pollutants*, 1988.
- [6] V. Lahoussine-Turcaud, M.R. Wiesner, J.-Y. Bottero, Fouling in tangential-flow ultrafiltration: the effect of colloid size and coagulation pretreatment, *Journal of Membrane Science* 52(2) (1990) 173-190.
- [7] Y. Kaiya, Y. Itoh, K. Fujita, S. Takizawa, Study on fouling materials in the membrane treatment process for potable water, *Desalination* 106(1-3) (1996) 71-77.
- [8] Q. Wang, H. Zeng, Z. Wu, J. Cao, Impact of sodium hypochlorite cleaning on the surface properties and performance of PVDF membranes, *Applied Surface Science* 428 (2018) 289-295.
- [9] X. Gan, T. Lin, F. Jiang, X. Zhang, Impacts on characteristics and effluent safety of PVDF ultrafiltration membranes aged by different chemical cleaning types, *Journal of Membrane Science* 640 (2021) 119770.
- [10] L. Ren, S. Yu, H. Yang, L. Li, L. Cai, Q. Xia, Z. Shi, G. Liu, Chemical cleaning reagent of sodium hypochlorite eroding polyvinylidene fluoride ultrafiltration membranes: Aging pathway, performance decay and molecular mechanism, *Journal of Membrane Science* 625 (2021) 119141.
- [11] A.I. Schäfer, L.D. Nghiem, N. Oschmann, Bisphenol A retention in the direct ultrafiltration of greywater, *Journal of Membrane Science* 283(1-2) (2006) 233-243.
- [12] C.Y. Tang, Y.-N. Kwon, J.O. Leckie, Fouling of reverse osmosis and nanofiltration membranes by humic acid—effects of solution composition and hydrodynamic conditions, *Journal of Membrane Science* 290(1-2) (2007) 86-94.

[13] L.D. Nghiem, D. Vogel, S. Khan, Characterising humic acid fouling of nanofiltration membranes using bisphenol A as a molecular indicator, *Water research* 42(15) (2008) 4049-4058.

[14] Y. Zhang, J. Wang, F. Gao, Y. Chen, H. Zhang, A comparison study: The different impacts of sodium hypochlorite on PVDF and PSF ultrafiltration (UF) membranes, *Water research* 109 (2017) 227-236.

CHAPTER FIVE

Conclusions and future work

Conclusions on individual projects are provided at the end of corresponding Chapters. This Chapter lists several overarching conclusions drawn from the entirety of the work.

Overall, this dissertation considers the interactions of various viruses to various fomites (personal care products, silica, nylon, stainless steel, polypropylene) as well as the interactions of natural organic matter foulants to PVDF membrane. The methodology proposed in this study helps fill the knowledge gap on virus adhesion to fomites – an important component of models on virus transport and fate in the built environment. The proposed approach can help guide screening and selection of materials that discourage virus adhesion, design of anti-adhesive surfaces, as well as development of surface cleaning solutions and protocols.

Virus adhesion can be affected by various variables including the characteristics of virus (particle size, zeta potential, hydrophobicity, etc.), characteristics of fomites (surface charge, hydrophobicity, surface roughness, etc.), and environmental conditions (ionic strength, pH, temperature, etc.). This dissertation considers three types of interactions between virus and fomites: van der Waals interaction, electrostatic interaction, and acid-base (or hydrophobic) interaction. However, other forces (apart from the three mentioned above) can play a role. For instance, steric repulsions and specific interactions with divalent cations were shown as important for controlling rotavirus

deposition [1]. Steric effects caused by irregular topographies of the virus (e.g., protein loops that protrude from the capsid into solution) and the deposition surface may affect adhesion [2-4].

This dissertation considers virus adhesion to surfaces with static properties. Yet, surface characteristics can change over time due to environmental influences or intrinsic evolution. For example, in water treatment plants, the surface chemistry of membrane filters evolve due to fouling and cleaning. As another example, fomite surfaces undergo changes through repeated use: for instance, doorknob surface can change its roughness and attain a coat of oxides and/or foulants over an extended period of usage, which can affect their interaction with pathogens of interest. More research is needed to understand such changes and they affect virus adhesion to surfaces.

One important direction for future research is on the design of surfaces with tailored properties to control adhesion. Due to their size and unique functionalities, nanomaterials are of particular interest in this regard. As a part of my future work, I intend to use Janus particles to develop novel coatings to prevent bacterial and protein fouling as well as the interactions of lipids and proteins in biomembranes. Janus particles are particles containing at least two different chemical compounds, and this chemical asymmetry gives Janus particles two or more different properties [5]. Biofouling is of great concern in numerous applications ranging from biosensors to biomedical implants and devices, and from food packaging to industrial and marine

equipment [6]. Janus nanoparticles have strong adsorption force, orientation, and surface activity on the interface, which may reduce the interfacial tension of foulants and materials [7].

Another research area that is of great interest for the design of surfaces with controlled adhesion properties is to use machine learning to predict material characteristics based on their molecular structure. Design of new membrane materials has been guided mostly by experience and intuition. Synthesis of new polymeric materials and testing of permeability is time-consuming and expensive. Machine learning (ML) models can be selected and trained on the experimental database to correlate polymer chemical structure and their surface properties. The information obtained from the modeling can guide the design of new polymer compositions with target characteristics (resistance to virus adhesion, antifouling, etc.).

REFERENCES

REFERENCES

- [1] L. Gutierrez, S.E. Mylon, B. Nash, T.H. Nguyen, Deposition and aggregation kinetics of rotavirus in divalent cation solutions, *Environmental science & technology* 44(12) (2010) 4552-4557.
- [2] B. Yuan, M. Pham, T.H. Nguyen, Deposition kinetics of bacteriophage MS2 on a silica surface coated with natural organic matter in a radial stagnation point flow cell, *Environmental science & technology* 42(20) (2008) 7628-7633.
- [3] S.L. Penrod, T.M. Olson, S.B. Grant, Deposition kinetics of two viruses in packed beds of quartz granular media, *Langmuir* 12(23) (1996) 5576-5587.
- [4] J.A. Redman, S.B. Grant, T.M. Olson, M.E. Hardy, M.K. Estes, Filtration of recombinant Norwalk virus particles and bacteriophage MS2 in quartz sand: importance of electrostatic interactions, *Environmental science & technology* 31(12) (1997) 3378-3383.
- [5] X. Li, L. Chen, D. Cui, W. Jiang, L. Han, N. Niu, Preparation and application of Janus nanoparticles: Recent development and prospects, *Coordination Chemistry Reviews* 454 (2022) 214318.
- [6] I. Banerjee, R.C. Pangule, R.S. Kane, Antifouling Coatings: Recent Developments in the Design of Surfaces That Prevent Fouling by Proteins, Bacteria, and Marine Organisms, *Advanced Materials* 23(6) (2011) 690-718.
<https://doi.org/https://doi.org/10.1002/adma.201001215>.
- [7] L. Yang, J. Xu, J. Wang, F. Lang, B. Liu, Z. Yang, Responsive Single-Chain/Colloid Composite Janus Nanoparticle, *Macromolecules* 53(6) (2020) 2264-2270.
<https://doi.org/10.1021/acs.macromol.0c00109>.